



HAL
open science

Data mining and volcanic eruption forecasting

Anaïs Boué

► **To cite this version:**

Anaïs Boué. Data mining and volcanic eruption forecasting. Volcanology. Université Grenoble Alpes, 2015. English. NNT: 2015GREAU007 . tel-01560889

HAL Id: tel-01560889

<https://theses.hal.science/tel-01560889>

Submitted on 12 Jul 2017

HAL is a multi-disciplinary open access archive for the deposit and dissemination of scientific research documents, whether they are published or not. The documents may come from teaching and research institutions in France or abroad, or from public or private research centers.

L'archive ouverte pluridisciplinaire **HAL**, est destinée au dépôt et à la diffusion de documents scientifiques de niveau recherche, publiés ou non, émanant des établissements d'enseignement et de recherche français ou étrangers, des laboratoires publics ou privés.

THÈSE

Pour obtenir le grade de

DOCTEUR DE L'UNIVERSITÉ DE GRENOBLE

Spécialité : **Sciences de la Terre, de l'Univers et de l'Environnement**

Arrêté ministériel : 7 août 2006

Présentée par

Anaïs Boué

Thèse dirigée par **Philippe Lesage**

préparée au sein de l'**Institut des Sciences de la Terre**
et de l'**école doctorale Terre Univers Environnement**.

Data mining and volcanic eruption forecasting

Thèse soutenue publiquement le **30 avril 2015**,
devant le jury composé de :

Dr. Christopher Kilburn

Principal research fellow, University College London, United Kingdom,
Rapporteur

Dr. Francois Beauducel

Physicien, IPGP, Paris, France, Rapporteur

Dr. Jean-Robert Grasso

Physicien, ISTerre, Grenoble, France, Examineur

Pr. Anne Mangeney

Professeur, IPGP, Université Paris VII, France, Examineur

Pr. Jean-Luc Got

Professeur, ISTerre, Université Savoie-Mt Blanc, France, Examineur

Dr. Philippe Lesage

Maître de conférence, ISTerre, Université Savoie-Mt Blanc, France,
Directeur de thèse



Résumé

L'intégration de méthodes de prédiction des éruptions volcaniques dans une stratégie de surveillance globale peut être un outil d'aide à la décision précieux pour la gestion des crises, si les limites des méthodes utilisées sont connues. La plupart des tentatives de prédiction déterministes des éruptions volcaniques et des glissements de terrain sont effectuées avec la méthode FFM (*material Failure Forecast Method*). Cette méthode consiste à ajuster une loi de puissance empirique aux précurseurs de sismicité ou de déformation des éruptions. Jusqu'à présent, la plupart des travaux de recherche se sont attachés à faire des prédictions *a posteriori*, basées sur la séquence complète de précurseurs, mais le potentiel de la méthode FFM pour la prédiction en temps réel, en n'utilisant qu'une partie de la séquence, n'a encore jamais été évaluée. De plus, il est difficile de conclure quant-à la capacité de la méthode pour prédire les éruptions volcaniques car le nombre d'exemples publiés est très limité et aucune évaluation statistique de son potentiel n'a été faite jusqu'à présent. Par conséquent, il est important de procéder à une application systématique de la FFM sur un nombre important d'éruptions, dans des contextes volcaniques variés.

Cette thèse présente une approche rigoureuse de la FFM, appliquée aux précurseurs sismiques des éruptions volcaniques, développée pour une application en temps réel. J'utilise une approche Bayésienne basée sur la théorie de la FFM et sur un outil de classification automatique des signaux ayant des mécanismes à la source différents. Les paramètres d'entrée de la méthode sont les densités de probabilité des données, déduites de la performance de l'outil de classification. Le paramètre de sortie donne la distribution de probabilité du temps de prédiction à chaque temps d'observation précédant l'éruption. Je détermine deux critères pour évaluer la fiabilité d'une prédiction en temps réel : l'étalement de la densité de probabilité de la prédiction et sa stabilité dans le temps. La méthode développée ici surpasse les applications classiques de la FFM, que ce soit pour des applications en *a posteriori* ou en temps réel, en particulier parce que l'information concernant l'incertitude sur les données est précisément prise en compte.

La classification automatique des signaux sismo-volcaniques permet une application systématique de cette méthode de prédiction sur des dizaines d'années de données pour des contextes volcaniques andésitiques, au volcan Colima (Mexique) et au volcan Mérapi (Indonésie), et pour

un contexte basaltique au Piton de la Fournaise (La Réunion, France). Le traitement de longues séries temporelles que permet cette approche s'apparente à de la fouille de données. Je quantifie le nombre d'éruptions qui ne sont pas précédées de précurseurs, ainsi que les crises sismiques qui ne sont pas associées à des épisodes volcaniques. Au total, 64 séquences de précurseurs sont étudiées et utilisées pour tester la méthode de prédiction des éruptions développée dans cette thèse. Ce travail permet de déterminer dans quelles conditions la FFM peut être appliquée avec succès et de quantifier le taux de réussite de la méthode en temps réel et en *a posteriori*. Seulement 62% des séquences précurseurs étudiées dans cette thèse sont utilisables dans le cadre de la FFM et la moitié du nombre total d'éruptions sont prédites *a posteriori*. En temps réel, seulement 36% du nombre total d'éruptions auraient pu être prédites. Cependant, ces prédictions sont précises dans 83% des cas pour lesquels les critères de fiabilités sont satisfaites. Par conséquent, il apparaît que l'on peut avoir confiance en la méthode de prédiction en temps réel développée dans cette thèse mais que la FFM semble être applicable en temps réel uniquement si elle est intégrée dans une stratégie de prédiction plus globale. Cependant, elle pourrait être potentiellement utile combinée avec d'autres méthodes de prédictions et supervisée par un observateur. Ces résultats reflètent le manque de connaissances actuelles concernant les mécanismes pré-éruptifs.

Abstract

Eruption forecasting methods are valuable tools for supporting decision making during volcanic crises if they are integrated in a global monitoring strategy and if their potentiality and limitations are known. Many attempts for deterministic forecasting of volcanic eruptions and landslides have been performed using the material Failure Forecast Method (FFM). This method consists in adjusting an empirical power law on precursory patterns of seismicity or deformation. Until now, most of the studies have presented hindsight forecasts, based on complete time series of precursors, and do not evaluate the method's potential for carrying out real-time forecasting with partial precursory sequences. Moreover, the limited number of published examples and the absence of systematic application of the FFM makes it difficult to conclude as to the ability of the method to forecast volcanic eruptions. Thus it appears important to gain experience by carrying out systematic forecasting attempts in various eruptive contexts.

In this thesis, I present a rigorous approach of the FFM designed for real-time applications on volcano-seismic precursors. I use a Bayesian approach based on the FFM theory and an automatic classification of the seismic events that do not have the same source mechanisms. The probability distributions of the data deduced from the performance of the classification are used as input. As output, the method provides the probability of the forecast time at each observation time before the eruption. The spread of the posterior probability density function of the prediction time and its stability with respect to the observation time are used as criteria to evaluate the reliability of the forecast. I show that the method developed here outperforms the classical application of the FFM both for hindsight and real-time attempts because it accurately takes the uncertainty of the data information into account.

The automatic classification of volcano-seismic signals allows for a systematic application of this forecasting method to decades of seismic data from andesitic volcanoes including Volcán de Colima (Mexico) and Merapi volcano (Indonesia), and from the basaltic volcano of Piton de la Fournaise (Reunion Island, France). This approach allows for analysing large temporal series of data, similarly to data mining. The number of eruptions that are not preceded by precursors is quantified, as well as the number of seismic crises that are not followed by eruptions. Then, I use 64 precursory sequences and apply the forecasting method developed in this thesis. I thus determine in which conditions the FFM can be successfully applied and I quantify the

success rate of the method in real-time and in hindsight. Only 62% of the precursory sequences analysed in this thesis were suitable for the application of FFM and half of the total number of eruptions are successfully forecast in hindsight. In real-time, the method allows for the successful predictions of only 36% of the total of all eruptions considered. Nevertheless, real-time predictions are successful for 83% of the cases that fulfil the reliability criteria. Therefore, we can have a good confidence on the method when the reliability criteria are met, but the deterministic real-time forecasting tool developed in this thesis is not sufficient in itself. However, it could potentially be informative combined with other forecasting methods and supervised by an observer. These results reflect the lack of knowledge concerning the pre-eruptive mechanisms.

Remerciements

L'aboutissement de cette thèse fut un parcours périlleux et semé d'embûches, depuis le moment où j'ai pris connaissance du sujet. Je voulais étudier la prédiction des éruptions volcaniques utilisant la FFM, coûte que coûte. Malheureusement, les financements de thèse sont chers. C'est en premier lieu grâce à mon directeur de thèse, Philippe Lesage, que j'ai pu y arriver. Il m'a soutenu pour l'obtention d'un financement auprès d'AXA Research Funds et a cru en moi jusqu'au bout. Je le remercie donc pour son soutien.

Je tiens particulièrement à remercier Bernard Valette qui a sauvé les meubles, m'a permis de me raccrocher aux branches et m'a soutenu durant le mois d'Août 2014 lorsque j'errais seule dans les couloirs sombres du labo, stressée par les échéances.

Un grand merci à mes proches collaborateurs de l'Université de Grenade (Espagne) pour m'avoir initiée durant un mois à l'outil de classification automatique que j'utilise dans cette thèse. En particulier, je tiens à remercier Guillermo Cortés pour sa patience et son investissement qui m'ont permis de prendre relativement rapidement en main cet outil un peu difficile d'utilisation. Et merci aussi pour sa relecture du Chapitre 2 de ce manuscrit. Merci à tout le reste de l'équipe: Carmen Benitez, Isaac Alvàrez, Luz García, Angél de la Torre, Jesus Ibanez.

J'ai eu la chance de rencontrer les deux personnes qui ont été mes principales sources d'inspiration pendant cette thèse: Chistopher Kilburn et Ian Main. Ils ont pris le temps de discuter et de m'expliquer certains points clés pendant les conférences. Merci à Chris pour son investissement dans notre projet de post-doc et à Ian pour son intéressante et complète review de mon article.

Je tiens évidemment à remercier mon jury de thèse: Christopher Kilburn, François Beauducel, Anne Mangeney, Jean-Robert Grasso et Jean-Luc Got.

Je tiens à exprimer ma gratitude à Raúl Arámbula et Miguel Gonzàles-Amuezca pour avoir répondu à mes questions au tout début de la thèse et pour leur accueil hyper chaleureux à Colima. De plus, grâce à eux et aux organisateurs de la conférence COV7, j'ai pu survoler el Volcán de Colima sí ! Et puisque je suis passée de l'autre côté de l'Atlantique, j'en profite pour remercier mes collègues de la Ciudad de Mexico. Tout d'abord le CENAPRED pour m'avoir aménagé un coin de bureau pour me permettre la récupération des données du Popocatepetl

REMERCIEMENTS

(qui m'ont bien embêtée et qui n'apparaîtront pas dans ce manuscrit, soit dit en passant), mais tout particulièrement Thalia Reyes pour son amitié et sa bonne humeur. Le Mexique m'a aussi permis de rencontrer Zack Spica et Denis Legrand, avec qui j'ai eu la chance de partager de supers moments, autant sur le point scientifique que personnel.

Ces trois ans et demi de thèse se sont déroulés avec plaisir dans l'ambiance chaleureuse que m'a apportée la 'ISTerre-Chambéry-Family'. Tout d'abord merci à tous les permanents de l'équipe volcans qui ont toujours été à l'écoute et disponibles, autant du côté scientifique que personnel, au labo, au Japon ou en Indonésie sur les flancs du Mérapi. Je suis heureuse d'avoir partagé de très bon moments avec Pascale Bascou qui m'a sorti la tête de la rédaction aux moments opportuns, et à toutes les autres personnes du bâtiment Belledonne. Les copains... je commence par ceux qui m'ont supportée (dans tous les sens du terme) à Chambé: Thomas-bisous-bisous-le-mec-sympa, Laure-Brigitte, Camille-Jorjita, Léa-mini-pousse-Giroud, Carlos, Sirel, Fabien-Fabio, Joaquin, Marceau-Marcel, Margueritte-Jojo... et un big up à Hervé pour ses massages incroyables qui m'ont probablement sauvée dans les pires moments ! Merci à Aurore-Georgette mon petit Kinder surprise pour les moments incroyables qu'on a passé au Kamchatka, ton soutien et ton aide dans ma décision de regarder les données du Piton, et ta disponibilité scientifique et personnelle...

Je remercie aussi les amis de toujours pour leur soutien de près ou de loin, et pour être toujours là après cette dernière année de silence radio. Je remercie d'abord tout particulièrement Karim qui a corrigé ma thèse. Ensuite, les ours des montagnes grenobloises: Flo, Julie, Pierre, Estelle, Magalie, Sylvain, ma filleule Roxy et sa soeur qui ont trouvé mon schéma de volcan bien moche, ainsi qu'Anne-So et Julie R. Merci à Marlénours et Matt pour les colis surprises qui tombent à pic. Merci aux malouins Fleur, Tony, Camille, Lucie, Hélène et Fanch, Lucile, Marine... Et enfin, je tiens à remercier mes potes ERASMUS pour leur soutien des 4 coins du monde.

L'aboutissement de ce travail de recherche et plus généralement de ces études a été rendu possible grâce au soutien permanent de ma famille. Mes parents m'ont toujours poussée à tenter de réaliser mon rêve, bien que les perspectives d'emploi dans la recherche soient minces. Je remercie mon modèle et super frangin Yvonnick pour son humour, son intelligence, son soutien et surtout pour m'avoir redonné de l'énergie dans les moments difficiles (et merci aussi à Fannette !). Merci aux cousins-grande-tante Pouchot-Thireau du grand Ouest ou de La Réunion pour avoir suivi mes aventures avec intérêt. Enfin, je tiens à remercier mes grands-parents qui m'ont permis d'arriver au bout de ce cycle. Mes grand-pères auraient probablement été fiers de cet aboutissement. Je remercie Mamie Chantal (et J.P.) qui a probablement été un de mes meilleurs soutiens, et je tiens à dédier cette thèse à ma chère mamie Simone qui nous a quittée un an trop tôt et à qui je dois tout.

Pour finir, cette thèse n'aurait jamais été possible sans François. Son amour, son soutien, sa motivation, ses nombreuses relectures de mon manuscrit ont créé un cocktail indispensable

à cet aboutissement. Ma reconnaissance envers son investissement afin que je touche mon rêve du bout du doigt est infinie, et mon amour pour lui va bien au delà de la puissance d'une Plinienne.

Acknowledgements

The outcome of this thesis were a precarious route full of pitfalls, from the moment where I discovered this PhD subject. I wanted to study volcanic eruption forecasting using the FFM and I was going to do anything to reach this goal. Unfortunately, PhD fundings are not numerous. I could obtain fundings thank to my supervisor, Philippe Lesage. He supported me to apply for AXA Research Funds PhD grants and believed in me until the end. I particularly acknowledge him for his constant support.

I wish to particularly thank Bernard Valette who helped me a lot and saved me in the worse moments, and particularly when I was alone in front of my laptop in the cold and shadow laboratory, stressed by the deadlines.

I acknowledge my close collaborators from the University of Granada (Spain) for their investment in teaching me the functioning of automatic classification tool. I particularly thank Guillermo Cortés for his patience and his investment that allowed me to learn very quickly the functioning of the recognition tool. I also thank him for having read the Chapter 2. I thank the rest of the team: Carmen Benitez, Isaac Álvarez, Luz García, Angel de la Torre, Jesus Ibanez.

I had the chance to meet the two persons who were my main source of inspiration during this thesis: Chistopher Kilburn et Ian Main. They took some time to discuss and explain me some key points of this work during conferences. I particularly thank Chris for his investment in our post-doc project and Ian for his fruitful review of the article.

Of course, I thank my PhD committee for giving a bit of their precious time: Christopher Kilburn, François Beauducel, Anne Mangeney, Jean-Robert Grasso and Jean-Luc Got.

I express my gratitude to Raúl Arambula and Miguel Gonzales-Amuesca because they answered my questions at the beginning of my PhD, and because of their warm welcome in Colima. Moreover, thank to them and the COV7 organizers, I could fly over Volcán de Colima, sí! Now that I came on the other side of the Atlantic ocean, I wish to thank my colleagues from Mexico City. First, I thank the CENAPRED for giving me an office in which I could gather Popocatepetl data (that bothered me during this thesis and will not appear in this manuscript by the way), but also particularly Thalia Reyes for her friendship and her happiness. I could also met Zack Spica and Denis Legrand with whom I had the chance to spend some good times,

ACKNOWLEDGEMENTS

from a scientific and personal point of view.

These three years were spent in a warm mood thank to the 'ISTerre-Chambéry-Family'. First, I thank all the permanent researchers of the team 'volcans' who were always free and kind, in a scientific and personal point of view, in the lab, in Japan or in Indonesia on the flank of Merapi volcano. Also, I would like to thank Pascale Bascou for helping me thinking about something else than the thesis when I needed, and the other persons of the corridor. Friends... I start the acknowledgements with those who supported me in Chambéry: Thomasbisous-bisous-le-mec-sympa, Laure-Brigitte, Camille-Jorjita, Léa-mini-pousse-Giroud, Carlos, Sirel, Fabien-Fabio, Joaquin, Marceau-Marcel, Margueritte-Jojo... and more particularly thank to Hervé for his massages that probably saved me in the worse moments ! Thank you Aurore-Georgette little Kinder of mine for the incredible moments spent in Kamchatka, and for your support when I took the decision to study the Piton de la Fournaise at the last moment, and for your scientific and personal availability.

I thank my other friends for their support, from far or from close, and for being here even after this year of silence. I particularly thank Karim for reading the manuscript. Then, I thank my little mountain bears from Grenoble : Flo, Julie, Pierre, Estelle, Magalie, Sylvain, my goddaughter and her sister who thought my schematics of volcano were ugly. Thank you Marlène and Matt for your surprise that arrived just on time. Thank you to friends from St Malo: Fleur, Tony, Camille, Lucie, Hélène, Lucile, Marine. And finally I thank all my ERASMUS friends who supported me from every sides of the world.

The outcome of this work and more generally of these studies were being possible thank to the permanent support of my family. My parents always pushed me to try to realise my dream, even if there are no many job perspectives. I thank my model and big brother Yvonnick for his sense of humour, his intelligence, his support and for giving me new energy when I needed. Finally, I thank my grand-parents who allowed me to reach the end of this cycle of my life. My grand-fathers would have probably been proud of this outcome. I thank my grand-mothers who have probably been my main supports, and I dedicate this thesis to my other grand-mother who passed away one year too early.

Finally, this thesis would not have been possible without my boyfriend François. His love, his support, his motivation, his non-official hat of co-supervisor, and his numerous readings of my manuscript was an essential cocktail for this outcome. My acknowledgement towards his investments for allowing me to touch the dream is infinite, and my love goes far beyond the power of a Plinian eruption.

Preamble

Forecasting natural disasters is one of the main challenges of today's research because they bear direct consequences on our lives and affect the world's economic equilibrium. Although volcanic eruptions are not the deadliest natural disaster, large populations living nearby active volcanoes make this issue of paramount importance. In addition, volcanic eruptions may result in significant economic losses, as for example during the eruption of Eyafjallajökull volcano (Iceland, 2010) that paralysed the European air traffic. Being part of advances that can directly benefit to populations through collaborations developed with volcanic observatories is the main motivation of this thesis. This work objectively illustrates the complexity of forecasting volcanic eruption.

There are two main research fields on the issue of volcanic eruption forecasting. First, there is a probabilistic approach that consists in learning from the past to evaluate the chance of an eruption to happen in the future. This approach is mainly used for long-term hazard mitigation and to build hazard maps. In this thesis, I focus on deterministic eruption forecasting, i.e. attempting to accurately forecast the precise date of incoming eruptions. In case of an emergency, populations have to know when and for how long they will have to evacuate. Giving the date of incoming eruptions is a valuable and concrete information, easily understandable for populations and decision makers. However, eruptions are inherently difficult to forecast, because of the complexity of the mechanisms involved in volcanic processes. Moreover, the current understanding of volcanic processes is still in its infancy since a direct access to the inside of active volcanoes is not possible. Fortunately, most magma movements occurring prior to eruptions trigger detectable changes in the surrounding environment, these are called *precursors*. Some of these precursors, in particular pre-eruptive seismicity, have been empirically described with power-law models, which asymptote can be extrapolated and interpreted as the time of eruption. This method is called the material Failure Forecast Method (FFM), and published examples seem to work out very well... in hindsight (i.e. when considering the entire precursory sequence until the eruption). In fact, the application of this method is not always straightforward because some eruptions are not preceded by precursors. In this case the deterministic forecasting method cannot be applied. Furthermore, some observables sometimes feature a power law pattern without any incoming eruption: in this case, if an eruption is

predicted, people would have to leave their homes for no reason. In other cases the precursory observable display a pattern that is not necessarily well described by a power-law. Should we trust the prediction made with the power law in this case? Moreover, in the real world, the measurement of the precursory observables before volcanic eruptions always contains some uncertainties, thus eruption predictions will never be accurate. How to properly quantify these uncertainties and how will it impact the uncertainty of the forecasts? Finally, all seismic events are not necessarily precursors of eruptions. Can we classify the seismic signals and isolate the most relevant ones in order to improve observations and thus eruption forecasts? This thesis provides new tools to answer these questions, through the real-time adaptation of the existing deterministic forecasting method, and the systematic evaluation of its performance.

Outline of the manuscript

The manuscript is organised as follows: in Chapter 1, I first present the different precursors of volcanic eruptions and I focus on seismo-volcanic precursors in particular. Then, I introduce the basics and necessary concepts of seismo-volcanology. I present the different types of seismo-volcanic signals, each one being associated with a particular source mechanism. Although most of these mechanisms are still being debated, their presentation is necessary to understand the precursory behaviour of each class of events. Finally, the different eruption forecasting methods are presented in order to introduce the challenges faced by the community of volcanology. Once the reader is familiar with volcano-seismic signals and the challenges of forecasting volcanic eruptions, I present in Chapter 2, the automatic classification tool I use to separate the different types of signals. This voice recognition tool, based on Hidden Markov Models (HMM), is very efficient to classify years of seismic records. This part is the heart of this PhD thesis insofar as, in addition to classifying a large number of seismic events, it allows for calculating the uncertainty on the count of seismic data which is necessary for the Bayesian inversion presented in the following chapters. The seismic signals being classified, it is possible in Chapter 3 to analyse whether some of these classes are precursors of the eruptions encountered for the studied volcanoes: Colima (Mexico), Merapi (Indonesia) and Piton de la Fournaise (Reunion Island, France). This analysis enables the quantification of eruptions that are not preceded by precursors or volcano-seismic activity unrelated to visible eruptions. When the precursory activities are identified, and in particular the power-law patterns of precursors, the FFM for deterministic eruption predictions can be applied. We will see in Chapter 4 that the typical use of the FFM is only possible for describing the precursory patterns or carrying out eruption forecasts in hindsight, but its application for real-time forecasting is limited. We consequently propose a new real-time application of the FFM using a Bayesian inversion. In Chapter 5, the method is tested on the precursory activity of the above-mentioned volcanoes to determine how reliable the FFM is for real-time forecasting.

Finally, I discuss the prediction results made in real-time and in hindsight. In particular,

a detailed discussion is addressed about the possible applicability in observatories as well as about the physical mechanisms that could explain the precursory behaviour of the different precursors. The latter point will lead to the perspectives of this PhD dissertation.

When skimming the manuscript, the reader should keep in mind that the main objective of this thesis is to answer the following question: What is the potential of the FFM for real-time forecasting ?

Contents

Résumé	3
Abstract	5
Remerciements	7
Acknowledgements	11
Preamble	13
1 Introduction	21
1.1 Volcanic eruptions processes	23
1.1.1 Pre-eruptive mechanisms	24
1.1.2 Precursors of volcanic eruptions	26
1.2 Classes of seismo-volcanic signals	31
1.2.1 Volcano-Tectonic (VT) earthquakes	31
1.2.2 Long-Period (LP) earthquakes	33
1.2.3 Hybrid or multiphase events (MP)	35
1.2.4 Volcanic Tremor	36
1.2.5 Explosions	38
1.2.6 Surface events: rockfalls, lahars and pyroclastic flows	38
1.2.7 Other recorded signals	39
1.3 Volcanic eruptions forecasting	40
1.3.1 Probabilistic approach	41
1.3.2 Deterministic approach: The material Failure Forecast Method (FFM)	43
Objectives of the thesis	46
2 Automatic classification of seismo-volcanic signals	49
2.1 Introduction	50
2.2 Hidden Markov model Tool Kit: HTK	51
2.2.1 Introduction to Hidden Markov Models (HMM)	51

2.2.2	Recognition principle	53
2.2.3	Training phase	54
2.2.4	Summary	56
2.3	Manual database	57
2.3.1	Building the manual database	58
2.3.2	Statistical evaluation	60
2.3.2.1	Closed test	61
2.3.2.2	Blind test	62
2.4	Recognition results	64
2.5	Conclusions on the VSR, advantages and limitations	67
3	Seismic precursors of volcanic eruptions: three case studies	69
3.1	Introduction	70
3.2	Piton de la Fournaise (La Réunion island, France)	71
3.2.1	Volcanic activity and precursors	72
3.2.2	Precursory seismic patterns of effusive eruptions	77
3.3	Merapi volcano (Indonesia)	80
3.3.1	Precursors of the explosion of the 26 of October 2010	81
3.4	Volcán de Colima (Mexico)	85
3.4.1	Volcanic activity and precursors	87
3.4.2	Precursory patterns of vulcanian explosions	97
3.5	Summary and partial conclusions	100
4	Methodology for real-time eruption prediction using the FFM	103
4.1	Introduction	104
4.2	Modeling the evolution of seismicity prior to failure: the FFM	106
4.2.1	The FFM theory	106
4.2.2	Physical interpretations of the FFM	107
4.2.2.1	Physical interpretation of VT acceleration patterns	108
4.2.2.2	Physical interpretation of LP acceleration patterns	112
4.2.3	Critical analysis of the FFM	114
4.2.3.1	The inverse linear regression method	114
4.2.3.2	FFM with variable α	116
4.2.4	The FFM for real-time predictions	117
4.3	Bayesian inversion of seismic rates prior eruptions	119
4.3.1	Formulation	119
4.3.1.1	General Bayesian inversion	119
4.3.1.2	Least-square criterion	123
4.3.2	Data information	124

4.3.2.1	Computation of seismic event rates uncertainty	125
4.3.2.2	Cumulative vs non-cumulative data	126
4.3.2.3	Choice of tuning parameters	127
4.3.2.4	Impact of the structure of the data uncertainty on the model parameters estimation	129
4.4	Partial conclusions on the methodology	134
5	Real-time applications of the FFM	135
5.1	Introduction	135
5.2	Real-time predictions	137
5.2.1	Testing the forecasting method on textbook cases	137
5.2.1.1	Application on VT precursors: Piton de la Fournaise and Mer- api volcanoes	137
5.2.1.2	Application on LP precursors: Volcán de Colima	142
5.2.2	Complex cases for real-time applications	143
5.2.2.1	Acceleration-deceleration patterns	144
5.2.2.2	Multiple acceleration patterns	147
5.2.2.3	Too short precursory sequences	150
5.2.3	Comparison with results of the literature	153
5.3	Systematic application and statistical performance	156
5.3.1	Global applicability of the method	156
5.3.2	Accuracy of the method when applicable	162
5.3.2.1	Accuracy of real-time forecasts	162
5.3.2.2	Accuracy of hindsightforecasts	164
5.4	Partial conclusions on the application of the FFM for real-time forecasting . . .	166
6	Discussion and general conclusions	169
6.1	Discussion	170
6.1.1	Limitations of the real-time forecasting method	170
6.1.2	LP precursory patterns of vulcanian explosions	174
6.1.3	VT precursory patterns of eruptions	175
6.1.4	Applicability of the FFM in volcano observatories	175
6.2	Conclusions	177
6.3	Perspectives	178
Appendix A Comparison of the automatic classification with the OVPF cata- logue		183
Appendix B Catalogues of volcanic seismicity at Volcán de Colima		185

Appendix C Results of real-time predictions with complicated precursory patterns	191
C.1 Short duration precursory patterns	192
C.2 Multiple precursory patterns	197
C.3 Other patterns	204
Appendix D Publication Boué <i>et al.</i> (2015), <i>Journal of Geophysical Research</i>	209
Bibliography	229

Chapter 1

Introduction

Contents

1.1	Volcanic eruptions processes	23
1.1.1	Pre-eruptive mechanisms	24
1.1.2	Precursors of volcanic eruptions	26
1.2	Classes of seismo-volcanic signals	31
1.2.1	Volcano-Tectonic (VT) earthquakes	31
1.2.2	Long-Period (LP) earthquakes	33
1.2.3	Hybrid or multiphase events (MP)	35
1.2.4	Volcanic Tremor	36
1.2.5	Explosions	38
1.2.6	Surface events: rockfalls, lahars and pyroclastic flows	38
1.2.7	Other recorded signals	39
1.3	Volcanic eruptions forecasting	40
1.3.1	Probabilistic approach	41
1.3.2	Deterministic approach: The material Failure Forecast Method (FFM)	43
	Objectives of the thesis	46

Volcanoes are as fascinating as dangerous. About one in ten people live around one of Earth's 1,500 active volcanoes (Simkin and Siebert, 1994). Even though only a fraction of these volcanoes erupt in any given year, the potential volcanic hazard that represent dormant volcanoes is not negligible. Volcanic eruptions are not frequent but they are very dangerous for populations because very difficult to predict.

One of the deadliest volcanic eruption occurred in La Montagne Pelée (Martinique, France) killing about 30,000 persons in 1902. More recently, the volcano Nevado del Ruiz (Columbia) killed about 23,000 people in 1985. Since deadly eruptions do not occur very often, volcanic risk is easily neglected by populations leaving nearby volcanoes. However, the recent eruptions of Mount Ontake (Japan) in September 2014 and Eyjafjallajökull (Iceland) in 2010 revived the interest of forecasting volcanic eruptions both in the aim of saving lives and of preventing economic losses.

A total of $91,000 \pm 10,000$ deaths have been listed between 1900 and 2008 as having been caused by volcanic eruptions (Doocy et al., 2013). Moreover, the risk of catastrophic losses from future eruptions is significant given the current population growth, the proximity of major cities to volcanoes, and the possibility of larger eruptions. Thus, the development of strategies for eruption forecasting is one of the most important issues in today's volcanology. Many questions arise when dealing with volcanic eruption forecasting. Authorities and populations need to be aware of the spatial and temporal impacts of the eruption: when, where, how long, of which kind will be the eruption, and who will be affected. This thesis will provide new clues as to answering the all-important question of eruption forecasting and whether it is possible to carry out deterministic predictions in real-time.

Fortunately, volcanic eruptions are sometimes preceded by precursors, i.e. detectable signs of magma movements. Some of these precursors are used since the 19th century to forecast volcanic eruptions. Indeed, Luigi Palmieri started monitoring Mt Vesuvius in 1856, making it possible to observe seismic precursors of the 1861 eruption (Gasparini et al., 1992). The most recent successful example of eruption prediction occurred in 2010 before the eruption of Merapi volcano (Indonesia). This prediction, mostly based on seismic precursors, led to the evacuation of hundreds of thousands of people. About 350 fatalities were reported but 10,000 to 20,000 lives were saved thanks to the evacuation. Although many processes are still being debated, volcanic eruption forecasting based on precursory seismicity is promising. However, precursors are sometimes missing or very difficult to interpret due to the limited knowledge on pre-eruption processes.

Volcano-seismology is the study of volcano-related earthquakes in the order to better understand volcanic processes. It is a wide research field and this thesis particularly focusses on the different types of volcanic earthquakes, and how they can be used for eruption forecasting. New technologies now make it possible to study large number of cases in order to enhance our knowledge on the precursory seismic activity. The large amount of available seismic data

requires automating the pre-processing of the stream of seismic records for an efficient and rapid analysis.

In this Chapter, I briefly explain the possible processes leading to eruptions. I will review and explain the different types of precursory activity for historical eruptions. Abnormal (i.e. higher than the usual background activity) volcano-seismic activity is one of the most widespread precursors of volcanic eruptions. I therefore present the different classes of volcanic earthquakes with their associated source mechanisms. Furthermore, the characteristics of the signals will be presented so the reader becomes familiar with the classification of seismo-volcanic signals, which is at the heart of this thesis. Finally, I will explain how it is possible to use precursory seismicity to perform deterministic forecasts of volcanic eruptions.

1.1 Volcanic eruptions processes

A volcanic eruption is the sudden discharge of volcanic material (such as gas, lava, magma fragments or ash) at the surface of the Earth. The nature of the extracted materials depends on the magma composition and on the physical and chemical conditions occurring within the conduit during magma transport. Different types of eruptions are observed on Earth depending on the tectonic setting. Vulcanian eruptions occur at andesitic-dacitic strato-volcanoes located above subduction zones. They consist in the alternation of viscous lava flows generally forming a plug and short-lived explosions lasting minutes to hours. Plinian eruptions are rare but more powerful than vulcanian explosions. They can last hours to days and their ash plume can reach altitudes of up to 45 km in the atmosphere. These two types of eruptions are of the deadliest kind as they are violent and often located in densely populated areas (Indonesia, Japan, South and Central America).

Effusive eruptions refer to very fluid lava flows forming shield volcanoes in hot spot tectonic settings, such as Hawaii or Piton de la Fournaise. It also describes the extrusion of the viscous lava domes of andesitic-dacitic volcanoes. If the rising magma does not reach the Earth's surface, it remains at a simple intrusion stage and can be seen as an aborted eruption. Andesitic-dacitic volcanoes usually alternate between effusive and explosive phases. This transition is not yet well understood but an effusive eruption sometimes leads to explosive phases depending on the magma composition, its gas contents and the emitted volume (Melnik and Sparks, 1999). This thesis particularly focusses on vulcanian eruptions that are the most dangerous volcanic events for populations, but also on effusive phases in the context of andesitic-dacitic and basaltic volcanoes.

1.1.1 Pre-eruptive mechanisms

Volcanic eruptions involve mass transport processes from depth to the surface through a network of fractures that can be either dykes and/or magma conduits. It is the most efficient way for the magma to make its way towards the surface through the cold surrounding rock (Rubin, 1995). In the crust, geological discontinuities can create favourable conditions for magma accumulation in the form of magma chambers (Lister, 1990b,a; Hill et al., 2002) as shown in Figure 1.1A. For the magma body to further migrate, it must exert a pressure that is high enough to break the surrounding wallrock of the magma chamber (Lister, 1990b). This overpressure is induced by buoyancy, refilling of magma from depth or crystallisation of the magma body. Once created, a crack can propagate (Figure 1.1B) making it possible for the magma to follow this new pathway towards the surface (Kilburn, 2003). Degassing is the main driving force behind most volcanic phenomena. The separation of gas and melt phases leads to the formation of bubbles, whose presence decreases the magma density, enhances its buoyancy and favours its ascent (Wilson and Head, 1981).

When a magma reaches the surface, it can flow rapidly down the crater if its viscosity is low enough in the case of basaltic eruptions, or very slowly in andesitic-dacitic type eruptions. Alternatively, the magma will seal the magmatic conduit (lava plug) if it is too viscous to flow (Figure 1.1C). A lava dome is a plug that can be seen at the surface. These three classic effusion phases can then be interspersed with episodes of explosions (Figure 1.1D).

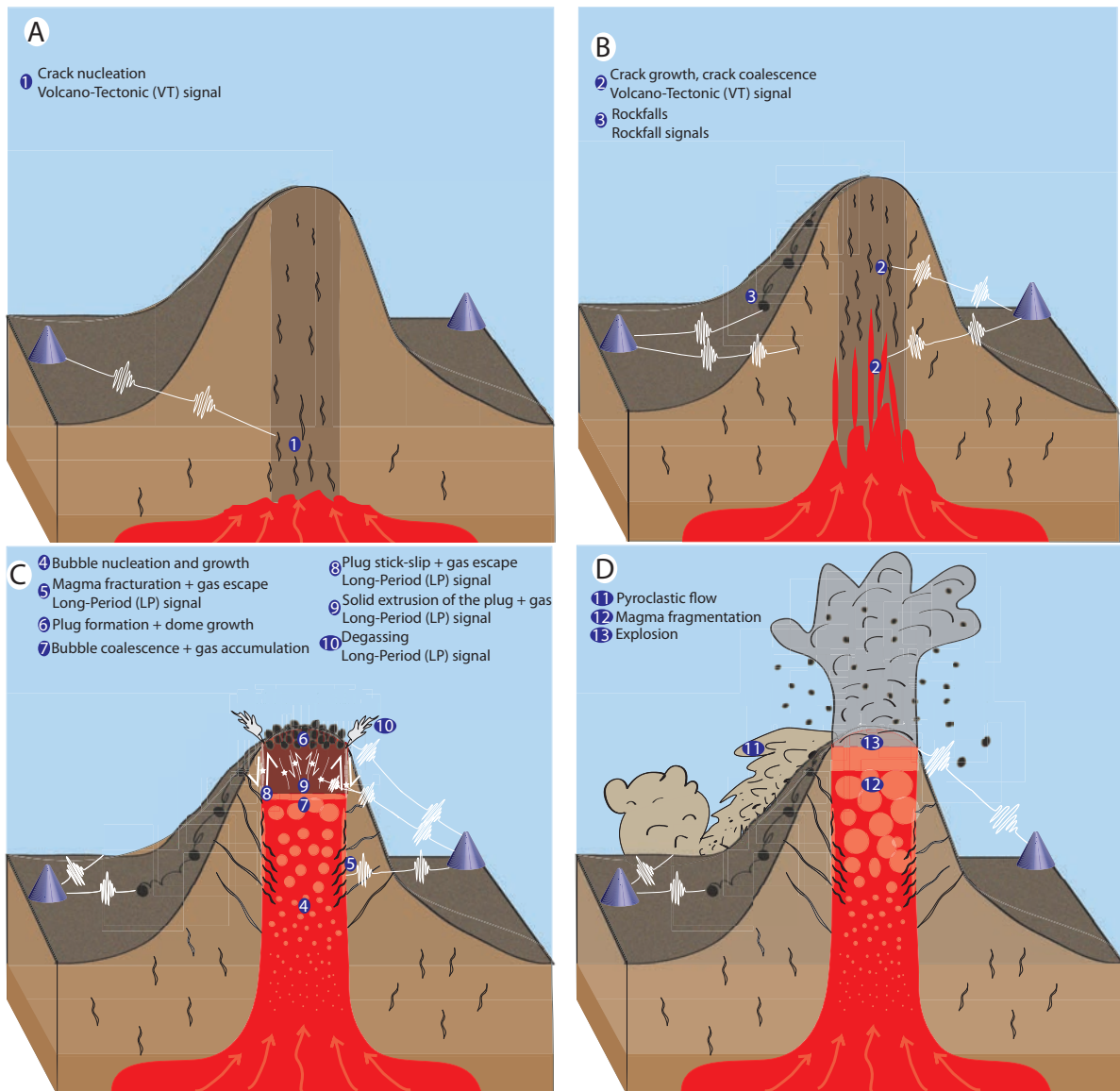


Figure 1.1: General overview of pre-eruption processes for andesitic-dacitic volcanoes. Blue cones represent the seismic stations. (A) Magma rises up and stress increases, leading to the nucleation of cracks in the surrounding rock. (B) The surrounding rocks damage. The cracks already created during stage (A) extend and eventually coalesce, allowing the magma to rise further. (C) Magma can migrate towards the surface. While the magma rises, bubbles nucleate and grow, and magma crystallises. Favourable conditions for magma fracturing at the conduit wall. A plug seals the conduit at the top of the edifice because of crystallisation, degassing and cooling. The conduit pressure builds up. The plug slips when the pressure of the conduit exceeds the plug strength. Degassing at the surface occurs through the fractures. This stage is accompanied by rockfalls. (D) A rapid decompression of the conduit leads to magma fragmentation and an explosion, eventually followed by pyroclastic flows.

There are different types of explosions depending mainly on the physical and chemical properties of the magma. The physical properties of magmas are strongly dependent on its temperature, melt composition, water content, and on the amount of gas and crystals (Melnik and Sparks, 1999; Sparks, 2003). It is thus very complicated to know whether a magmatic intrusion will lead to a lava flow or to the formation of a plug and if an explosive phase will occur. Basaltic-type eruptions involve low viscosity magmas, leading to spectacular lava flows and sometimes strombolian explosions or fire fountains, depending on the amount of gas in the magma (Sigurdsson et al., 2000). Even though these explosions are spectacular, they are usually not as hazardous as vulcanian or Plinian explosions. Vulcanian or Plinian explosions eventually occur once the conduit becomes sealed by viscous magma. In this case, the conduit can be subjected to overpressures (Hammer et al., 1999; Belousov et al., 2002; Druitt et al., 2002; Taddeucci et al., 2004; Cashman and McConnell, 2005) caused by buoyancy forces, degassing or crystallisation (Figure 1.1C). Vulcanian explosions (Figure 1.1D) are the results of a sudden decompression of this over-pressured magmatic conduit, through the fragmentation of continuous magmas (Alidibirov and Dingwell, 1996; Sparks, 1978; Mader, 1998; Cashman et al., 2000). Magma fragmentation greatly enhances the release of dissolved gases. Decompression of the conduit can be caused by the collapse of a part of a volcanic edifice such as Mt St Helens (P.W. Lipman, 1981), the rapid ascent of volatile saturated magmas or the sudden unplugging of a sealed volcanic vent. These types of explosions can eject volcanic materials (Figure 1.1D) as high as 20 km in the atmosphere (Sigurdsson et al., 2000). They can also eject bombs as far as 5 km away from the vent (Sigurdsson et al., 2000) or pyroclastic flows traveling to distances of 10 to 20 km (Gilbert and Sparks, 1998).

Explosions can also occur without the presence of a plug. When a magma encounters water, a phreato-magmatic fragmentation can be triggered, leading to a so-called phreato-magmatic explosion.

Effusive and explosive eruptions always involve fluid movements in the edifice (magma, gases or hydrothermal fluids). Following and understanding these movements would greatly help predict volcanic eruptions. However, the difficulty of making direct observations of the processes occurring in the magma conduit limits our understanding of magmatic processes. We consequently need to monitor these movements through indirect means and identify the reliable precursors of volcanic eruptions.

1.1.2 Precursors of volcanic eruptions

Prior to the occurrence of an eruption, signs of magma motion towards the surface such as degassing, deformations or seismic activity can be monitored. Anomalous variations of these signals are interpreted as precursors of an incoming volcanic eruption.

Each volcano may have its particular pre-eruptive behaviour, depending on magma com-

position, conduit shape or external environment (presence of a hydrothermal system, weather conditions, stability of the edifice). As a consequence, each precursor has to be interpreted individually from one volcano to another. Some precursors can appear to be very informative of an incoming eruption at a particular volcano, while it will not necessarily be the case for another. For one given volcano, the more types of precursors are combined, the more volcanologists can learn about an imminent eruption. An ideal monitoring would require recording all geophysical precursors. However, it is not always possible for observatories to have of all instruments at their disposal. They therefore have to choose among the most relevant set of instruments. Some precursors require expensive tools to be monitored, while other are very difficult to follow continuously because they require field work.

Gases. Magma degassing is one of the essential components of eruption dynamics. Recording magma degassing can allow for monitoring magma rising in the volcanic conduit. A magma is initially rich in components such as sulfur (SO_2) and carbon dioxide (CO_2). These gases have low solubilities in magma, they are therefore progressively lost during degassing while more soluble gases such as water (H_2O) are retained. Thus, if there is no new injection of magma, SO_2 and CO_2 fluxes are expected to decrease as a function of time while H_2O is expected to increase. The rock permeability and its variation can also modify the gas fluxes. However, SO_2 and CO_2 will increase if there is new injection of magma from depth. Degassing can be monitored at fumaroles and hot springs, assuming that they reflect direct degassing of the magma through the edifice fractures (Figure 1.1B-C). Even if such precursors are useful indicators of incoming eruptions, their monitoring is particularly difficult because it usually requires field work sometimes close from the vent. Remote sensing techniques (from the ground or using satellites) circumvent this problem but the results are usually more difficult to interpret and the number of studied gas species limited. An other major issue for forecasting applications is that data sampling is not even and its frequency can vary from weeks to months in the case of manual gas sampling. For example at Merapi volcano, high levels of CO_2 , increase in CO_2/SO_2 and H_2S/SO_2 recorded in fumarole gas samples have been observed before the major eruption of November 2010 (Surono et al., 2012). Surono et al. (2012) suggested a deep degassing source associated with an input of fresh magma before the eruption. Airborn and stream data carried out before the 2009 eruption of Redoubt Volcano are consistent with upflow of a CO_2 -rich magmatic gas for at least 5 months prior to eruption Werner et al., 2012). Other examples of CO_2 and SO_2 increases have been observed before the 1998 eruption of Volcán de Colima (Zobin et al., 2002) or at Mount St Helens (USA) in 1980 (Berlo et al., 2004). The interpretation of gas emission is however not always straightforward since SO_2 flux increase is not always observed before eruptions, probably because of gas-water or gas-rock-water reactions that reduce SO_2 fluxes (e.g. Werner et al., 2011 or Symonds et al., 2001). Recent improvements include the use of UV spectrometers (e.g. mini DOAS) or other remote sensing techniques.

Deformation. Pressure increase in the magma chamber induce magma transfers which in turn produces stress and strain variations in the edifice, eventually leading to some degree of deformation of the volcano. Changes to the surface of a volcano provide clues about what is going on inside the volcanic edifice. Most volcano deformation can only be detected and measured with precise surveying techniques.

Satellites of the Global Positioning System (GPS) continuously transmit their positions to ground-based receivers through radio signals. Knowing the travel time of these signals, the receivers can then compute the satellite-receiver distance at a certain time and thus its position on Earth. This method is widely used, as for instance to monitor the increasing deformation of Augustine volcano before the 2006 eruption (Cervelli et al., 2006) or to measure the accelerating displacement of Merapi lava dome before its collapse in January 2001 (Beauducel et al., 2006). Beauducel et al. (2006) also located known fractures with the help of dense GPS measurements.

Recording changes in the slope angle of the ground of a volcanic edifice is another method for volcano deformation measurements. These measurements are carried out with tiltmeters. This is one of the oldest and simplest methods for monitoring deformation caused by magma movements. Continuous tilt monitoring has been observed to be a good precursor of eruptions generally related to the rise of magma and formation of dikes and eruptive fissures at Sicilian volcanoes (Gambino et al., 2014) or at Piton de la Fournaise volcano (Peltier et al., 2011).

Interferometric Synthetic Aperture Radar (InSAR) is a microwave imaging system provided by satellites. The differences in the waves' phases of two different images allows for generating surface deformation maps. Contrary to GPS or tiltmeters that provide measurements at specific points, InSAR provides spatially complete ground deformation maps in the direction of the satellite position. Despite obvious advantages of this method (cloud penetrating and day and night operational capabilities), the main limitation is the non-negligible cost of each image and the sampling intervals of several days. A complete review of SAR applications has been recently published by Pinel et al. (2014). So far, SAR has been mainly used to characterize processes posterior to volcanic eruptions and thus rather helped for the understanding of volcanic processes rather than forecasts potential eruptions. It is however worth noting that SAR data have been used for hazard mitigation during the 2010 eruption at Merapi volcano (Surono et al., 2012). Limitations in the application of SAR data for long-term forecasting volcanic eruptions have been underlined by Chaussard et al. (2013), who studied ground deformation at different volcanoes of the Mexican volcanic belt as well as Indonesian volcanoes like Agung or Merapi. Chaussard et al. (2013) observed that some eruptions are preceded by increasing deformation of the edifice while others are not, or some deformation is observed without volcanic activity. They hypothesize that closed volcanic systems display precursory inflation reflecting pressure increase in the magma chamber. If this pressure reaches a critical threshold, then it can lead to an eruption. However, the volcanoes identified as open volcanic systems dare not incline to pressurize before eruptions.

Electronics Distance Measurement (EDM) is another possibility for measuring volcano deformation. EDM calculates the distance between the transmitter and the reflector by using the phase shift between the emitted and received electromagnetic wave. By encompassing measurements carried out at different times and on different lines, deformations can be estimated. This method has been used to measure the increasing deformation of Merapi volcano before the eruption of November 2010 (Surono et al., 2012), for instance.

Models can be adjusted to volcano deformation data, in order to infer the magma chamber depth, chamber geometry or chamber pressure which are valuable informations for a better understanding of pre-eruptive processes and thus for forecasting volcanic eruptions. Simple models based on a spherical magma chamber approximation have been proposed (Mogi model, Mogi, 1958), as well as ellipsoidal approximations (Segall, 2010) for example. A wide variety of models and their applications at various volcanoes are reviewed in Segall (2013).

Gravity anomalies. The interpretation of ground deformation can be difficult as it can reflect either deep (magma chamber) and/or shallow magma injection (dike, sill). Because the injection of magma can locally change the density of the ground, measurements of gravity anomalies is a complementary observation of deformation. Gravity variations can be related both to density changes, to mass transfers, or to altitude changes. Basaltic volcanoes are expected to produce increase in gravity since the magma chamber fills before eruptions. In contrast, andesitic volcanoes are expected to produce a decrease in gravity before eruptions because of the accumulation of gas in the conduit before eruptions. Gravity measurement can either be carried out in discrete or continuous. A drawback of discrete gravity surveys is the lack of information between successive surveys (from a week to a year) as well as the surveys irregularities. Therefore, continuous gravity measurements have been developed. Discrete gravity anomalies correlated with increasing deformation have been observed by Williams-Jones and Rymer (2002) at Rabaul (Papua New-Guinea) and Krafla volcanoes (Iceland), by Yokoyama (1989) at Sakurajima (Japan) in 1982, by Rymer and Brown (1984) at Poás volcano (Costa Rica) or by Eggers (1983) before the Pacaya (Guatemala) 1980 eruption. Carbone and Greco (2007) demonstrated the potential of both discrete and continuous microgravity measurements to forecast volcanic eruptions at Mt Etna. Sainz-Maza et al. (2014) interpreted the spatial and temporal evolution of gravity before El Hierro eruption (Spain) as a lateral migration of magma.

Thermal anomalies. Injection of magma from depth, magma coming to the surface, gas escaping through fractures, and lava flow emplacement can give rise to heat transfer to the surface. Thus, thermal anomalies can be directly or indirectly measured at the surface and used as valuable information of an upcoming eruption. Thermal measurements can be done from the ground and from space. Thermal measurements directly in the ground give temperatures at a

single point but cannot cover large regions. To circumvent these problems, the growing access to remote sensing data during the last decades has been exploited to thermally monitor volcanic activity. For example, Marchese et al. (2012) a posteriori used Moderate Resolution Imaging Spectroradiometer (MODIS) data to show the occurrence of pre-eruptive thermal anomalies at Mt. Asama, before the two main vulcanian eruptions of 2004. Because different remote sensing techniques were developed, Murphy et al. (2013) proposed to carry out a thermal analysis at four different volcanoes, using both Moderate Resolution Imaging Spectroradiometer (MODIS) and the Advanced Spaceborne Thermal Emission and Reflection Radiometer (ASTER). They show that MODIS provides a higher temporal resolution (daily) than ASTER but a lower spatial resolution (1 km for MODIS and 90m for ASTER). Combining both methods, they could identify a thermal precursor to lava flows at Kliuchevskoi while no precursory behaviour of ground temperature was observed for the other target volcanoes. For the moment, remote sensing techniques are still developing and the number of examples of precursory thermal activity of volcanic eruptions is still too low to conclude about the utility of these techniques for real-time monitoring. Moreover, the sampling frequency would only allow for detecting long term thermal precursors.

Seismicity. Finally, the most studied and widespread type of precursor remains the seismic activity. Increase of enhanced seismic activity has been reported before most of historical eruptions (McNutt, 1996). In many published cases, it seems that the precursory seismic activity shows acceleration patterns that can be used as a robust precursor of volcanic eruptions (McNutt, 1996). Precursory seismicity can be represented either in terms of number of events, in terms of energy, or with the Real Time Seismic Amplitude/Energy Measurement, which is the average amplitude/energy calculation of the seismic signal (RSAM, Endo and Murray, 1991; RSEM, De La Cruz-Reyna and Reyes-Davila, 2001). For example, an acceleration of the root mean square of the energy of seismic events has been reported several days before the 2010 eruption at Merapi volcano (Budi-Santoso et al., 2013). An acceleration of the energy of seismic events was also very clear a few days before the 1990 eruption of Redoubt volcano (Alaska, Cornelius and Voight, 1994) and before the 1991 explosive eruption at Mount Pinatubo (Philippines, Cornelius and Voight, 1996). An acceleration of the amplitude of seismic signals was showed by Ortiz et al. (2003) few days before low magnitude vulcanian explosions at Villarica volcano (Chile). Alternatively, Lesage and Surono (1995) reported an acceleration of the number of seismic events a few days before the 1990 eruption of Kelud volcano (Indonesia) and Traversa et al. (2011) observed some hours of acceleration in the number of volcanic earthquakes before vulcanian explosions at Ubinas volcano (Peru). However, seismic precursors do not always occur before eruptions, such as in the 2002-2003 eruptive period at Popocatepetl volcano (Quezada-Reyes et al., 2013). These non-exhaustive examples of precursory seismicity before the eruptions of different volcanoes show a wide variability of the precursory duration of seismic signals as well as a variability in the type of observed seismic precursor. In the literature,

the precursory patterns of amplitude or energy takes into account the whole seismic signal and most of them count the number of seismic events without classification. Nevertheless, volcano-seismicity records feature many different seismic classes, depending on their source: fracturing of the volcanic edifice, magma degassing, magma fracturing, rockfalls, regional earthquakes or explosions (Figure 1.1). Thus, the different classes of precursory seismicity can potentially provide various different informations on the evolution of the magma intrusion. A classification of the different classes of signal has to be carried out to better interpret the precursory signs of unrest, which is what I propose in this thesis. The minimal equipment of an observatory generally includes a seismometer so the forecasting method based on seismicity developed in this thesis can be distributed to most observatories. In this context, we are only able to work with one station. For all these reasons, I mainly focus on analysing precursory behaviour of seismic signals before eruptions.

1.2 Classes of seismo-volcanic signals

Different types of volcanic seismicity are observed at volcanoes. Each class of signals gives different kinds of informations on the volcanic processes occurring and some of these signals are sometimes not related to volcanic activity. Consequently, analysing the precursory patterns of the different classes of events separately is particularly important to accurately monitor a volcano. The description of the signals' characteristics is important to understand the automatic classification tool presented in Chapter 2. This section presents the signals that are encountered at the volcanoes studied in this thesis.

Among the different classes of events presented in this section, the Volcano-Tectonic (VT), Long-Period (LP) and tremor events are the most interesting in terms of predictive potential because they are all closely related to magma movements before eruptions. More precisely, the source mechanism of VT is now well-known, which is not the case for tremors and LP events. A description of the signal's characteristics and the source mechanism is proposed for each class but I will put the emphasis on LP and tremor events.

1.2.1 Volcano-Tectonic (VT) earthquakes

Description

These signals are characterised by sharp impulsive onsets corresponding to the first arrival of the P-wave, followed by S-waves. When a VT occurs at great depth, the delay between P and S waves is larger. The frequency content of these signals is approximately comprised between 1 Hz and 15 Hz (Lahr et al., 1994). In the spectrograms it has a typical exponential decrease through time in the coda (Figure 1.2). These events last several tens of seconds.

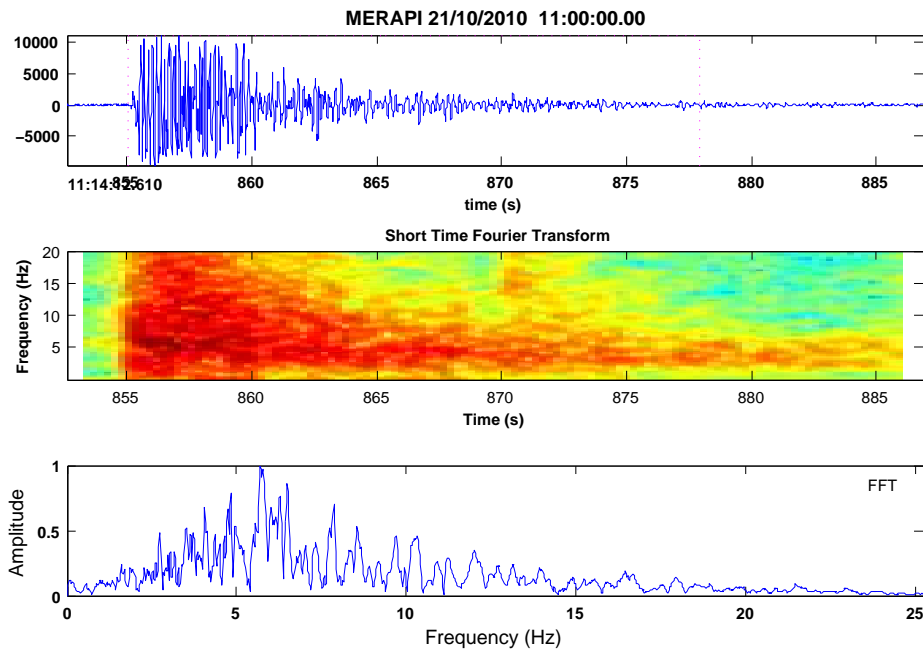


Figure 1.2: Example of a VT event, from Merapi volcano (Indonesia). From top to bottom: VT waveform, spectrogram of the signal, spectrum of the signal.

Mechanisms

The source mechanism of VT events is similar to that of tectonic earthquakes, this is why they are called Volcano-Tectonic events. The difference lies in the source of stress which is driven by magmatic intrusions rather than large scale tectonic movements. The first sign of volcanic unrest is usually seen through the response of the surrounding rock to the stress changes induced by rising magmas at depth. The surrounding rock is damaged and deformed through the creation of fractures (Figure 1.1A), by re-opening of pre-existing cracks, or by frictional slip. If the stress induced by the magma is sufficient, these cracks can propagate and coalesce to open a new magmatic pathway (Figure 1.1B, Kilburn, 2003, 2012). When a crack opens or propagates, an elastic wave is generated by a rapid release of the energy accumulated during stress loading. This signal corresponds to a VT event that propagates through the Earth towards the seismic station where it is recorded, as represented in Figure 1.1A-B. This class of seismic signals usually abnormally increases at the beginning of volcanic unrest because of the accumulation of damage in the edifice.

1.2.2 Long-Period (LP) earthquakes

Description

Long-Period events (Figure 1.3) last several seconds and are characterised by an emergent P-wave and no visible S-waves before the surface wave arrival. They are called Long-Period (LP) because of their relatively low frequency content between 1 Hz and 5 Hz. The depth of LP events depends on the volcano, but they are usually described as shallow events. Even if there is a general common description to recognise LP events, many different waveforms are observed (two examples are shown in Figure 1.3) probably reflecting different source mechanisms but also different volcanic structures (Bean et al., 2008). Indeed, volcanic structure (i.e. hydrothermal systems or geology) can greatly affect the waveform and the spectral content of the travelling wave between its source and the seismic station (Bean et al., 2008).

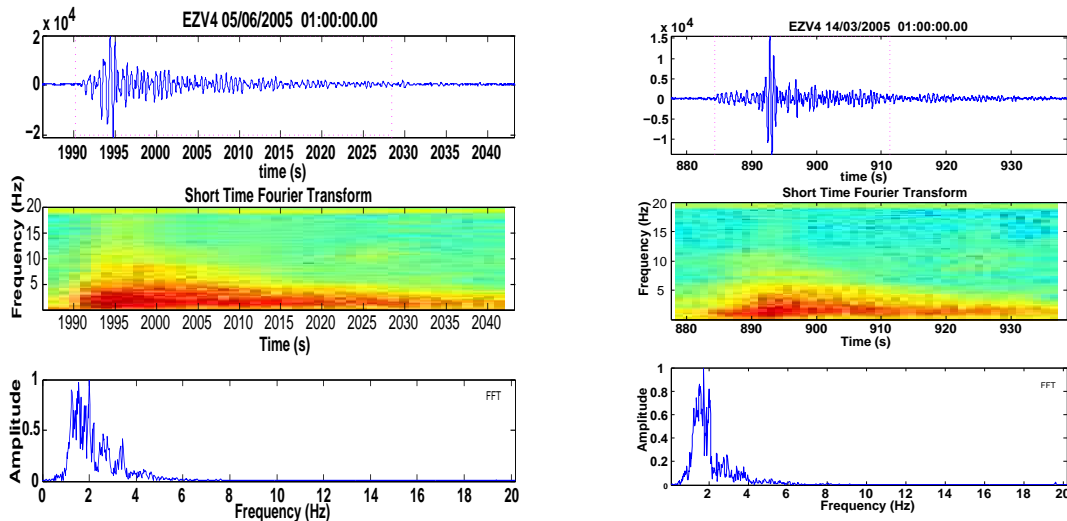


Figure 1.3: Examples of LP events, from Colima volcano (Mexico). From top to bottom: LP waveforms, spectrogram of the signals, spectrum of the signals.

Mechanisms

Unlike VT events, the LP source mechanism is a very controversial subject, so this review might not be exhaustive. For a more exhaustive review see Chouet and Matoza (2013).

By inducing stress changes large enough to open and propagate new cracks, the magma creates its own way towards the surface (Figure 1.1C). Fluid movements are thought to produce Long-Period events (LP). Proposed source mechanisms fall into two categories (Chouet and Matoza, 2013): (1) the resonance of fluids (magma or gas) in fractures and (2) fracturing and slip of the ascending magma as it solidifies against the wall of a feeding conduit (Figure 1.1C).

Resonance. Early models focussed on explaining the low frequencies of tremors and have been adapted to explain the low frequencies of LP events. The fluid-driven crack model is one of the most commonly accepted mechanism (Chouet, 1986, 1988, 1992). If an excitation is produced in a fluid-filled crack, the elastic waves are trapped in the crack and reflect from one tip to another. A similar analysis has been carried out to model the resonance in a magmatic conduit (Neuberg et al., 2000; Jousset et al., 2003). All these models describe rather well the features of the waveforms and the spectral content of LP events, however they do not address the trigger mechanisms of LP events.

Magmatic-hydrothermal interactions. When magma rises up, it can enter in contact with water if it encounter a hydrothermal system. It is one of the first proposed mechanism to explain LP events (Chouet, 1985). It was first observed at Old Faithful Geyser that LP events were created by ground water boiling (Leet, 1988; Kieffer, 1984; Kedar et al., 1996, 1998). Leet (1988) suggested that this boiling process could be the explanation of shallow volcanic tremor. This mechanism has further been used to explain the source mechanisms of LP events at specific volcanoes (e.g., Chouet et al., 1994; Morrissey and Chouet, 1997; Kumagai. et al., 1995; Matoza and Chouet, 2010).

Magmatic degassing. Many studies on magmatic degassing as a source of LP events focussed on basaltic volcanoes. For andesitic-dacitic type volcanoes, Cruz and Chouet (1997) noticed that very small exhalations were accompanied by LP events at Galeras volcano (Colombia). These small jets escaped from a visible crack located on the dome. Since degassing and LP events are correlated, magma degassing is one of the probable mechanism for the generation of LP. This source mechanism is also similar to the model proposed by Lesage et al. (2006) explaining harmonic tremors and small explosions.

Brittle failure of melt. Geological observations (Tuffen et al., 2003; Tuffen and Dingwell, 2005), laboratory experiments (Tuffen et al., 2008; Lavallée et al., 2012) and models of magma conduit (Neuberg et al., 2006; Goto, 1999) suggest that, in the case of a viscous magma intrusion, LP events can be generated by brittle fracturing of the magma due to large strain rates close to the conduit wall. Magma fracturing occurs when reaching a certain critical strain rate (Lavallée et al., 2008, 2011). We can consider that a LP event is produced each time this critical strain level is reached. The strain rate of the magma depends on its composition and ascent rate. A viscous magma associated with an accelerating ascent rate are probably the most favorable conditions leading to magma fracturing. Gonnermann and Manga (2012), Melnik et al. (2005) and Papale (1999) analysed the parameters leading to ascent rates and viscosity evolution for different depths. Many parameters (gas content, crystal contents, density of the magma) contribute to increase the viscosity and the ascent rate in an exponential

manner, forcing the magma to accelerate and thus increasing the horizontal stress gradient from the center of the conduit to the wall, creating the conditions leading to magma fracturing at the conduit walls.

Stick-slip of a plug. Stick-slip motion of a dome (Iverson et al., 2006) is another mechanism proposed for the source of LP events. When magma rises in the conduit, the upper part of the magma column solidifies because of the increased crystal and bubble contents. Iverson et al. (2006) made the hypothesis that this solid-plug eventually sticks and slip on the conduit walls, creating low intensity and regular LP events. Stick-slip mechanisms have been proposed by Ruina (1983) and Dieterich (1994) in natural rock systems under changes in applied stress to explain tectonic earthquake mechanisms. This model can be extrapolated to the behaviour of a solid plug stuck in a conduit. A solid plug slips when the pressure in the magma conduit exceeds the friction force of the plug on the conduit wall, otherwise it sticks. A similar mechanism applied to a single fault has been used by Dmitrieva et al. (2013) to explain the behaviour of LP events merging to a gliding tremor at Redoubt volcano (see Section 1.2.4 for the description of a gliding tremor).

Tuffen et al. (2008), carried out laboratory experiments to reproduce the same conditions as dome building eruptions and concluded that shear faulting can develop at the conduit wall and within the lava dome itself, eventually leading to gas escape at the surface. It is expected that when shear faulting occurs, it triggers a seismic wave that can resonate if the fault is filled by fluids. This hypothesis is supported by the laboratory experiments of Benson et al. (2008, 2010).

1.2.3 Hybrid or multiphase events (MP)

Description

Hybrid events consist in an impulsive high-frequency onset and a low frequency coda. In this thesis, hybrid events are mainly observed at Merapi volcano (called MP events). Multiphase (MP) events are similar to hybrid events in the classification of McNutt (1996). These MP events have an emergent onset and their frequencies are usually between 3 Hz and 9 Hz (Figure 1.4).

Mechanism

Hybrid events are interpreted as a brittle failure creating a wave that is trapped and resonates in a fluid-filled crack (Lahr et al., 1994). It is an extension of the fluid-filled resonator of Chouet (1996) for LP events, but with a triggering mechanism represented by the failure of a crack

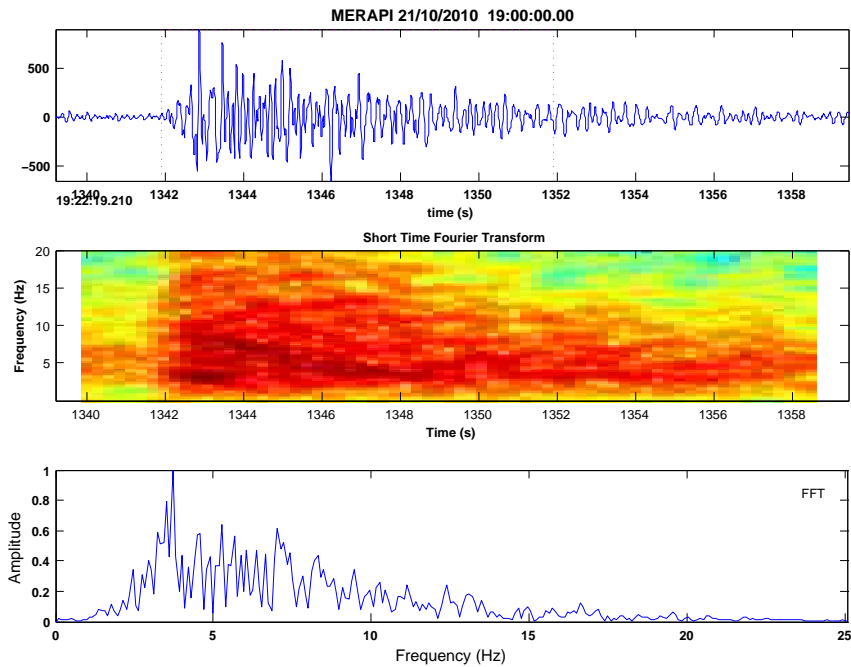


Figure 1.4: Example of a MP event, from Merapi volcano (Indonesia). From top to bottom: MP waveform, spectrogram of the signal, spectrum of the signal.

similarly to VT events. Note that this mechanism can also occur for magma failure, stick-slip motion of the plug or its solid extrusion provoking shear faults.

MP events at Merapi volcano are complex and very shallow earthquakes. MP are thought to result from shear stress variations within the viscous magma along the conduit (Beauducel et al., 2000), as they are correlated with deformation and rockfalls (Ratdomopurbo and Poupinet, 2000; Figure 1.1C).

1.2.4 Volcanic Tremor

A tremor is a sustained seismic vibration that can last minutes to several days. Tremors can be either volcanic or non-volcanic (e.g. slow slip events in subduction zones, glaciers or iceberg movements). Volcanic tremors can occur at active volcanoes or hydrothermal systems.

Description

Various types of tremors are reported in the literature and only the main categories are presented in this section. The characteristics of tremor signals are very close to those of LP events, with a difference in duration. Spasmodic tremors (Figure 1.5a) are characterised by a waveform with an emergent onset and frequencies comprised between 1 Hz and 5 Hz. Harmonic

tremors (Figure 1.5b) have an emergent onset and a low frequency content but the frequencies are harmonics, i.e. each frequency is a multiple of the fundamental frequency. These tremors can also become gliding tremors (Figure 1.6) when the harmonic frequencies vary in time, such as those observed at Redoubt volcano by Dmitrieva et al. (2013). Monochromatic tremors can also be observed. They feature only one dominant frequency. Finally, pulsative tremors are similar to a regular repetition of LP events (Figure 1.5c). It has been observed that pulsative tremors can merge in a spasmodic tremor leading to the hypothesis that some LPs are closely related to tremor mechanisms.

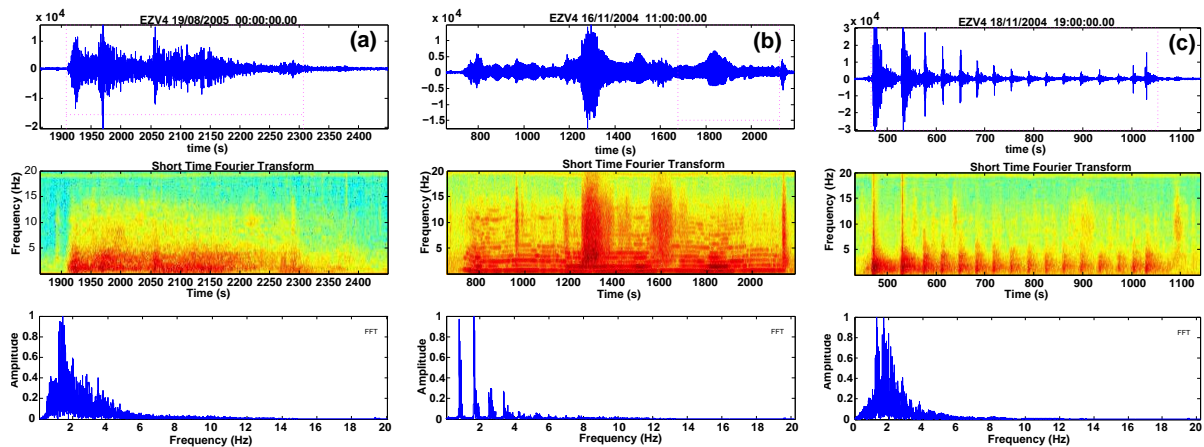


Figure 1.5: Examples of volcanic tremors, from Colima volcano (Mexico). (a) Spasmodic tremor. (b) Harmonic tremor. (c) Pulsative tremor. From top to bottom: tremor waveforms, spectrogram of the signals, spectrum of the signals.

Mechanism

It is not yet clear whether there is a link between LP events and tremors, but LP events merging into tremor such as in the case of Mt St Helens (Neuberg et al., 2000) lead to believe that some LP mechanisms are closely linked with some types of volcanic tremors (Figure 1.1C). Thus, source mechanisms proposed for LPs also stand for tremor mechanisms. In addition, Julian (1994) proposed a model of self-sustained oscillations in the magmatic conduit. This model is based on the coupling of an elastic conduit wall with the magma column. The idea is that an increase in the magma flow velocity will produce movements of the walls inward and outward depending on the variability of fluid pressure. However, Rust et al. (2008) and Dunham and Ogden (2012) both led to the conclusion that this tremor source mechanism is probably not the most relevant, partly due to unrealistic magma flow conditions of the model of Julian (1994).

1.2.5 Explosions

Explosions encompass a wide range of phenomena, from the small exhalation to the vulcanian explosion or the catastrophic Plinian explosion.

Explosion signals (Figure 1.6) are characterised by low frequencies and are usually followed by rockfalls or tremors. Shock waves are sometimes recorded as the first arrival of the explosion, making the explosion signal easily recognisable on the seismic record. Explosion signals are sometimes saturated when they are of very high intensity, thus artificially including high frequencies in the spectrogram.

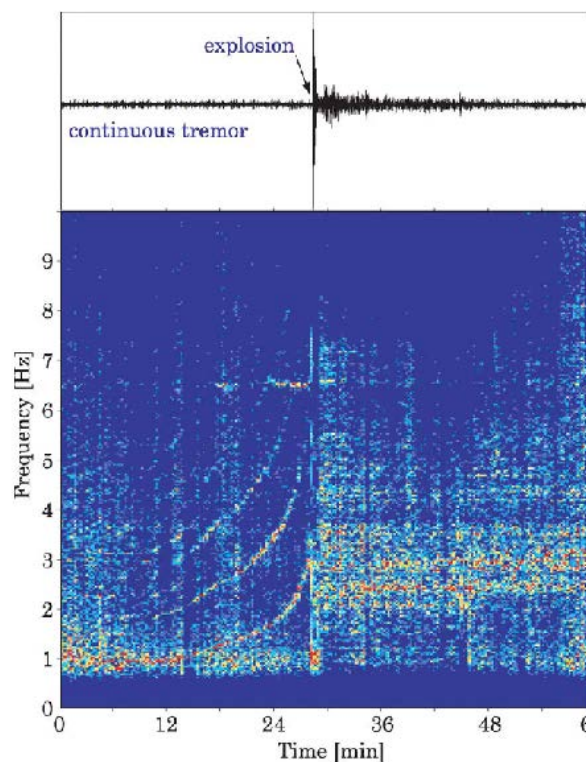


Figure 1.6: Example of an explosion signal preceded by a gliding tremor, from Soufriere Hills (Jousset et al., 2003). From top to bottom: Signal waveform, spectrogram of the signal.

Explosion mechanisms were described in Section 1.1.1 (Figure 1.1C-D). However, smaller explosions, called exhalations, can also be recorded. They consist of intense surface degassing.

1.2.6 Surface events: rockfalls, lahars and pyroclastic flows

When a magma reaches the surface in the form of a lava dome or of a lava flow, it usually causes rockfalls either in the crater or rolling down the flanks (Figure 1.1C). Even without the presence of magma, volcano flank can be unstable and landslides or rockfalls can be recorded at any time (Figure 1.1B). Rockfalls are easily recognisable on the seismic record (Figure 1.7, left).

Their onsets are emergent and their waveforms are cigar-shaped. Rockfalls can last several tens of seconds depending on the distance travelled by the rocks. Their frequency content is spreads up to 20 Hz.

Pyroclastic flows can be triggered by the partial collapse of a dome or subsequent to the column collapse following an explosion (Figure 1.1D). A pyroclastic flow is an avalanche of very hot gases, ash and blocks that can travel down the flanks of a volcano to distances of 10 to 20 km and at velocities as high as hundreds of kilometers per hour (Gilbert and Sparks, 1998). Signals are similar to rockfalls signal with a longer duration (up to several minutes).

Finally, lahars are mud flows made of water and ash. The water can either have a meteoric or a glacial origin such as in Iceland, where volcanoes are covered by an icecap that can melt. Lahars are usually very destructive and do not necessary travel very fast down the flanks of the volcano. Their signals (Figure 1.7, right) are also characteristic as they resemble rockfall signals with a much larger duration sometimes lasting a few hours.

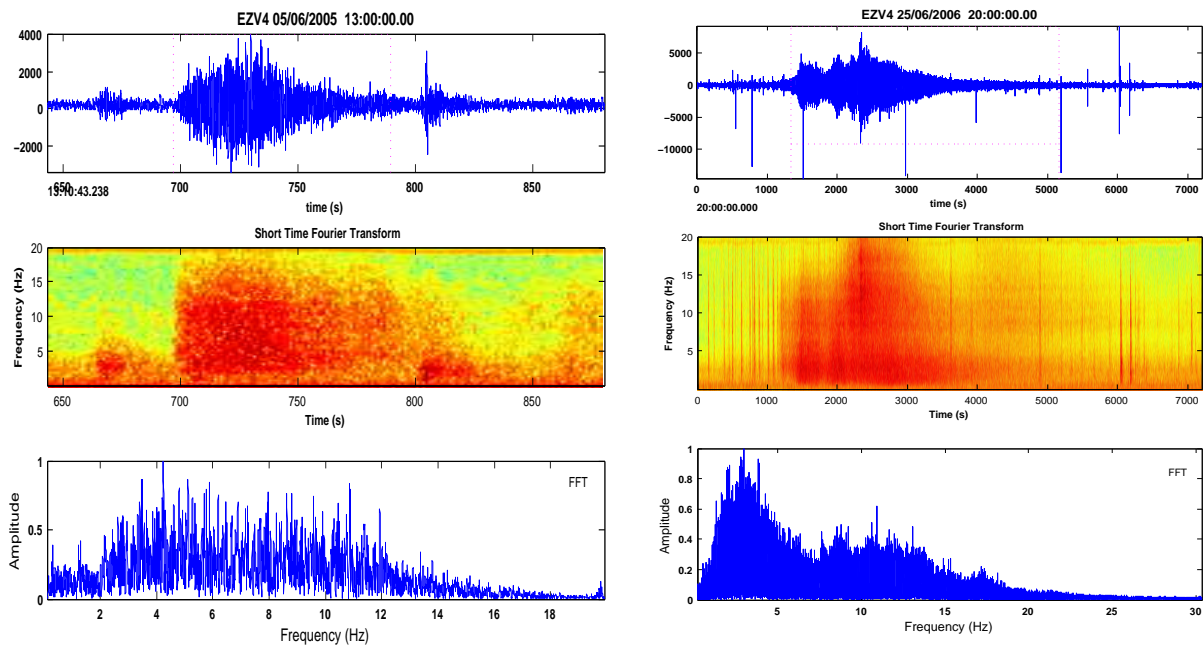


Figure 1.7: Example of surface events, from Colima volcano (Mexico). Left: rockfall. Right: Lahar. From top to bottom: Rockfall and lahar waveforms, spectrogram of the signals, spectrum of the signals.

1.2.7 Other recorded signals

In regions that are tectonically very active, regional earthquakes are usually recorded at volcano seismic stations. Their signals (Figure 1.8) have the same characteristics as VT events with a delay between the P- and S-waves that is usually much longer. Moreover, they can last

up to several minutes depending on the magnitude and on the distance of the station from the source of the earthquake. The contributing energy of these signals can be of great importance in comparison with volcanic signals. It is thus important to separate this class of signals from the volcanic classes.

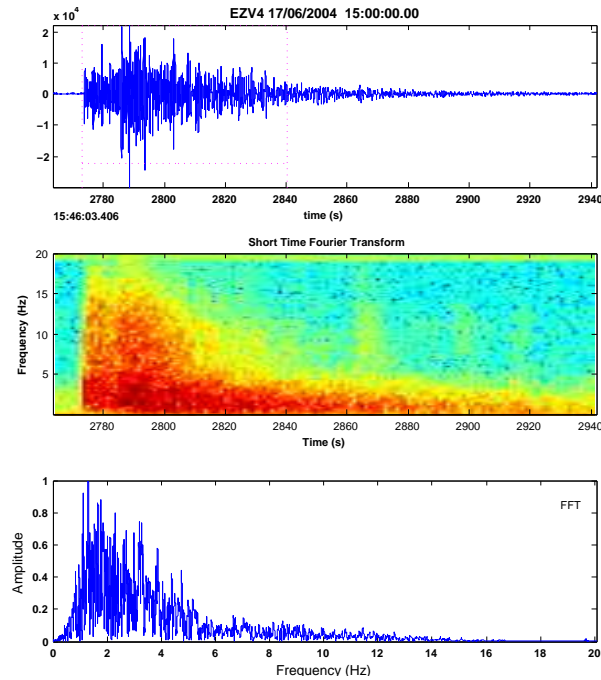


Figure 1.8: Example of a regional tectonic event, from Colima volcano (Mexico). From top to bottom: Signal waveform, spectrogram of the signal, spectrum of the signal.

Seismic stations can also record human activity, helicopters or thunderstorms. Moreover, spikes due to a malfunction of the station are also usually recorded. These signals must be removed from the dataset.

As a conclusion, seismic precursors can be very informative but it is necessary to analyse them separately because each class of signal does not provide the same information on the volcanic processes. In the next section, I will show how this precursory activity has been used to forecast volcanic eruptions until now.

1.3 Volcanic eruptions forecasting

Volcanic eruption forecasting is very challenging because of the non-linearity of pre-eruptive mechanisms (Melnik and Sparks, 1999; Sparks, 2003). However, it is possible to observe, interpret and model the consequences of the magma movements through the analysis of historical data and of the different precursory patterns. These analyses eventually allows inferring a possible time of a subsequent eruption.

The first step of eruption forecasting is to identify the practical needs of the authorities for the potential evacuation of populations in case of a volcanic crisis, but also to prevent economic losses. In this perspective, short-term to long-term forecasting have to be considered. Short-term forecast (i.e. shorter than inter eruptive time, from hours to days) are particularly informative for population evacuation and useful to prevent economic losses (e.g. air traffic). This time scale is realistic and meaningful for populations. However, scientists have to be very careful on the uncertainty of the predictions and the probability that an eruption can actually occur to be convincing towards authorities and indirectly towards population. The most important aspect of short-term forecasting methods is the reduction of uncertainties. On the other hand, long-term forecasts (i.e. larger than inter-eruptive time, from month to decades) are particularly informative to evaluate if a volcano can be considered extinct after a long repose interval. They are also used to evaluate the risk of an eruption occurring at a particular place and thus to inform the populations and decision makers about the objective risks of leaving in these areas.

Scientists investigate both forecasting time scales through probabilistic and deterministic methods, which are complementary and necessary to develop useful and realistic forecasting tools. The main issue regarding these methods is the limited amount of data, which seriously undermine the statistical relevance and the objective efficiency of the forecasting tools because (1) the unsuccessful forecasting results are usually easily discarded and not published, and (2) the number of cases studied is too low to conclude as to the efficiency of the forecasting tools.

1.3.1 Probabilistic approach

Probabilistic methods are based on the historical activity of a particular volcano. They have been investigated for short-term and long-term eruption forecasts. Two main approaches can be identified: pattern recognition techniques, used to define alert periods, and probabilistic evaluation of the occurrence of an eruption of a certain size in the next years. Pattern recognition techniques are useful for short-term forecasts and population evacuation, and probabilistic approaches for hazard management, mainly in a long-term perspective. Finally, these two techniques can be combined in Bayesian event trees (Marzocchi. et al., 2008) for the probabilistic evaluation of all possible eruptive scenarii, in the long and short-term perspectives.

Pattern recognition methods consist in the identification of precursory pattern from the geophysical precursors described in Section 1.1.2. A system of alert is triggered when a certain threshold of the mean level of a parameter is reached. These methods provide the probability of an eruption to occur within an endless alarm period (Mulargia et al., 1991, 1992; Grasso and Zialapin, 2004). These methods are convenient because it uses information from geophysical observables without the need of any physical model (Mulargia et al., 1991). This technique has been used to determine reliable eruption precursors for eruption alarm periods (Schmid

et al., 2012). It has also been used on Ubinas volcano (Peru) by Traversa et al. (2011) on precursory patterns of LP increase prior to vulcanian explosions. Their prediction results show 63% of explosions forecast and 58% of false alarms. The advantage of the pattern recognition methods is the objective analysis of the continuous record and its statistical relevance. Indeed, it is easily automatable and hence many different eruptive sequences can be processed in an objective manner. However, the required amount of available eruptive sequences is a limitation because numerous eruptive sequences are not systematically observed for every volcano.

The probabilistic evaluation of eruption occurrences consists in studying the cyclicity pattern of inter-eruptive times (Connor et al., 2003). For one volcano, the duration between consecutive eruptions are listed and investigated as far as possible in the history of the volcano. They are represented in the form of histograms on which statistical distributions are then adjusted. Given a duration between the present time and the last eruption, and based on the statistical distribution that best describes the duration distribution of inter-eruptive times for the volcano of interest, it is possible to give the probability that an eruption of a given Volcanic Explosivity Index (VEI, Newhall and Self, 1982) occurs within a given time interval. For example, Dzierma and Wehrmann (2010) evaluate the chance of an eruption of $VEI > 2$ within the next ten years at Llaima volcano to 100%, for Villarica and Nevado de Chillán from 40 to 100% and for Osono volcano at 20%. These methods are very informative for hazard management, for instance to control demographic development in areas exposed to volcanic risks. However each volcano seems to follow a different statistical distribution (Watt et al., 2007) and requires a large amount of reported eruptions for the prediction to be statistically significant. Unfortunately, the required informations are not always accurately known or sometimes the number of listed eruptions is too low because the observation window is small compared to recurrence times.

Both of these probabilistic methods have been used in Bayesian event trees (Newhall and Hobblitt, 2002) in the hope of estimating the probability of occurrence of a volcanic eruption. Given as many informations as possible such as theoretical models, *a priori* beliefs, monitoring measurements or geological data, it is possible to evaluate the probability of an eruption to occur. In this perspective, all scenarii can be explored (Marzocchi. et al., 2008). It has a useful application for both short and long-term forecasts and the userfriendly interface makes it an operational tool for observatories (Marzocchi. et al., 2008; Marzocchi and Bebbington, 2012; Sobradelo et al., 2014). Every observatory with the required data can thus estimate the probability of a particular eruptive scenario in time and space. However, the construction of a Bayesian event tree also requires a good and complete knowledge of the past and present behaviour of the volcano of interest.

The statistical relevance of probabilistic methods makes them reliable tools for hazard mitigation both in time and space (i.e. hazard maps, infrastructure investments, evacuation protocols). Although pattern recognition techniques are informative, they lead to endless alarm

periods with no indication on the likelihood of an eruption at a precise date. The methodological improvement of deterministic forecasting, both for real-time and hindsight purposes, has so far been neglected except by a few authors (Smith and Kilburn, 2010; Bell et al., 2011, 2013). Consequently, this thesis focuses on the improvement of deterministic eruption forecasting.

1.3.2 Deterministic approach: The material Failure Forecast Method (FFM)

The development of deterministic approaches for the prediction of eruptions is a complementary tool for decision-makers. Deterministic forecasting aims at determining the date of a potential eruption instead of an endless alarm period. Efforts towards deterministic forecasting of eruption and landslides have been made for more than thirty years. Fukuzuno (1985) started to use an empirical power law to model the patterns of surface displacements prior to slope failure. Later on, Voight (1988) proposed a general materials failure law to characterise patterns of deformation and acoustic emissions prior to rock failure. This approach is referred to as the material Failure Forecast Method (FFM, Figure 1.9) and has been widely used to describe precursory phenomena for landslides, rock failure or volcanic eruptions, or to process deterministic predictions in hindsight. However, its potential for real-time volcanic eruption forecasts has only been evaluated recently (Bell et al., 2011, 2013). The latter point is the main objective of this thesis.

The precursory seismicity can be quantified by its energy, by the number of recorded events per unit time or by the mean level of the seismic signal. Many observations showed that the acceleration in the number, energy or level of seismic signals or acoustic emissions prior to eruptions, landslides or rock failure can be described by the empirical FFM relating the rate of change of a given precursor $\dot{\Omega}$ (e.g. deformation or seismicity) to its acceleration $\ddot{\Omega}$ (Fukuzuno, 1985; Voight, 1988, 1989) as

$$\ddot{\Omega} = A\dot{\Omega}^\alpha, \quad (1.1)$$

where the coefficients α and A are empirical constants that determine how the rate $\dot{\Omega}$ changes with time. When it exists, the vertical asymptote of the function $\dot{\Omega}(t)$, i.e. the time when the observable rate $\dot{\Omega}$ is virtually infinite, is commonly interpreted as the opening of a crack that is, for volcanoes, the opening of the magma conduit towards the surface, leading to an eruption. In the aim of using the FFM for eruption forecasting, we first need to adjust the FFM model to observables like the seismicity or ground displacement prior to volcanic eruptions, as shown in Figure 1.9. This fitting procedure corresponds to an inverse problem, where the model parameters (including the prediction date) have to be determined. I am consequently interested in how to formulate this inverse problem. First of all, the most adapted models have to be chosen among different solutions of the differential equation (1.1), keeping in mind that the most important parameter to determine is the eruption time. Then, the selected data will be discussed. We chose to analyse the seismic activity because it is one of the most relevant and

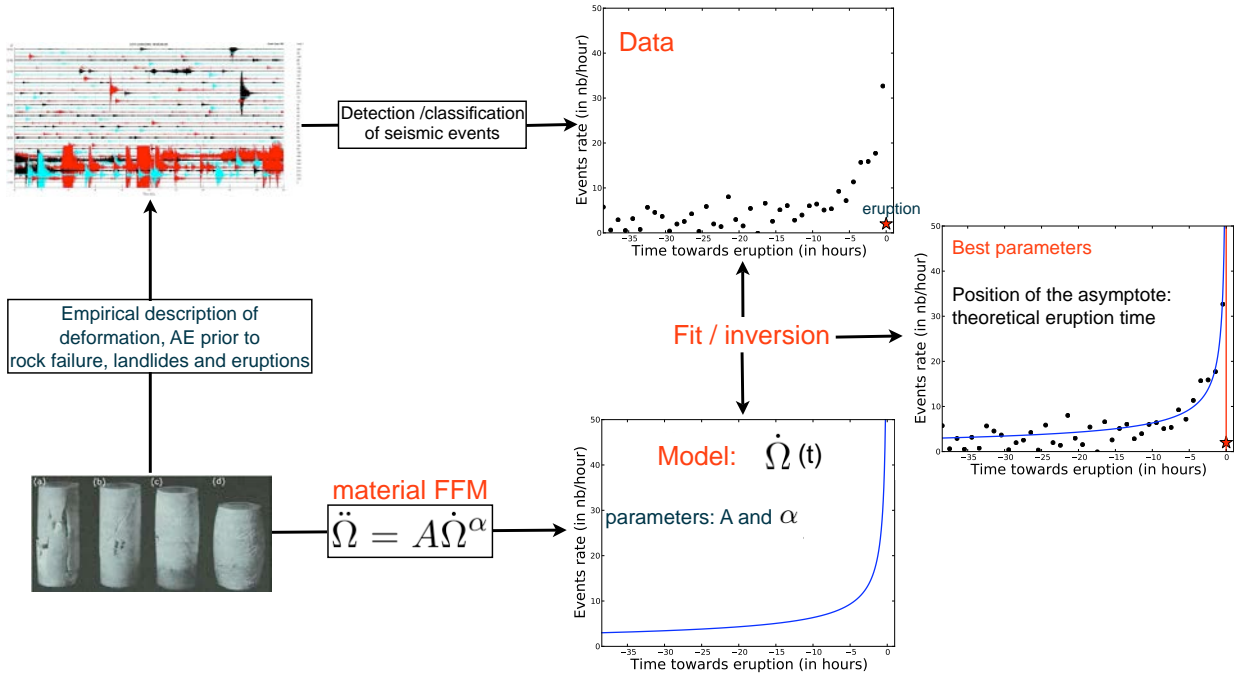


Figure 1.9: Schematic diagram of *a posteriori* deterministic eruption prediction in hindsight, based on the material Failure Forecast Method (FFM). The output of the method gives the time of the asymptote of the law, i.e. the theoretical time of eruption (red vertical line in the right panel). The rock samples picture (bottom left panel) is taken from laboratory experiments of Paterson (1958) and the helicorder (top left) is the seismic activity prior to a vulcanian explosion at Colima volcano (Mexico) in 2005.

useful precursor as it is supposed to be directly linked with magma rising from depth (McNutt, 1996). Finally, the way to solve the inverse problem has to be tackled seriously in order to obtain reliable input values for the model parameters and their uncertainties.

Most studies on volcanic eruption forecasting use the FFM to describe the whole sequence of acceleration and carry out hindsight forecasting of the date of eruption (see Ortiz et al., 2003; Voight, 1988; Cornelius and Voight, 1995; Kilburn and Voight, 1998; Chastin and Main, 2003; Arámbula-Mendoza et al., 2011; De La Cruz-Reyna and Reyes-Davila, 2001). The common application of the FFM consists in setting the exponent $\alpha = 2$ which corresponds to a hyperbolic law. This is the easiest way of using the FFM because in this case, the inverse of $\dot{\Omega}$ decreases linearly with time and fitting the inverse of the data can be achieved by simple linear regression. Although this method provides good results for hindsight analysis of laboratory failure experiments, landslides and eruptions (Cornelius and Voight, 1994; Murray and Ramirez Ruiz, 2002; Carniel et al., 2006), the correlation coefficients obtained for the linear regression are low in most of the studies. This suggests that the value $\alpha = 2$ is not always appropriate for explaining the observed data. Moreover, experimental evidences show that the exponent α may take values different from 2. For instance, Cornelius and Scott (1993) found α

values between 1.47 and 2.12 for laboratory experiments on rock damaging. Voight (1989) deduced values of $1.74 < \alpha < 2.01$ from experiments on metals, $1.9 < \alpha < 2.1$ for experimentally deformed soils, and $2.0 < \alpha < 2.2$ for landslides. Cornelius and Scott (1993) and Voight and Cornelius (1991) found most values in the range $[1.0, 2.0]$, with typical values near 1.5 for precursory phenomena at Mount St. Helens (USA) from 1980 to 1986. Finally, Smith and Kilburn (2010) found that α takes values of up to 3.30 for the 1991 Mount Pinatubo eruption (Philippines). Consequently, the assumption $\alpha = 2$ appears to be too simplistic and poorly reliable as the precursory patterns of accelerations already studied all seems to be different from one to another. Furthermore, its physical basis is not well established and does not take the natural variability of α values into account. Even though some successful hindsight eruption forecasts were carried out using the FFM with variable α values (Cornelius and Scott, 1993; Cornelius and Voight, 1994; Smith and Kilburn, 2010), the number of published examples is still too limited to conclude about the best way of using FFM for eruption forecasting. The latter point is another aspect that will be developed in this thesis. Thank to automatic processing tools, I apply the forecasting method to as many examples as possible, in the spirit of data mining. The science of data mining consists in extracting knowledge or typical patterns from a large amount of data, with the use of automatic methods. It has been developed in the last decades with the development of computer sciences that now allows for recording and processing large quantities of data. Data mining is widely used in astronomy for cataloguing pictures of sky objects or in marketing to analyse customers catalogues for example (Fayyad et al., 1996). This thesis will carry out seismic data mining, through automatic classification of decades of seismic records. The aim is to identify precursory patterns of each class of volcano-seismic precursor and to systematically apply the FFM, in order to compute the success rate of the forecasting method developed. My methodology will thus be applied objectively on the studied volcanoes, as all eruptive sequences will be analysed.

In addition, the common application of the FFM as practiced in the literature suffers from other issues:

1. The seismic observables used as precursors usually mix together numerous types of seismic events that are associated to different physical mechanisms at the source. For instance, when the observable is the mean level of the seismic signal, described by the Real-time Seismic Amplitude/Energy Measurement (RSAM/RSEM, Endo and Murray, 1991; De La Cruz-Reyna and Reyes-Davila, 2001), it can include all signals that are not related to damage processes within the volcano (Ortiz et al., 2003; De La Cruz-Reyna and Reyes-Davila, 2001). Therefore, in order to clearly identify precursory sequences associated with a single physical process described by a power-law and thus be able to carry out precise predictions, it is of paramount importance to process the different classes of events separately. In this perspective, the Spectral Seismic Amplitude/Energy Measurement (SSAM/SSEM; Stephens et al., 1994) can be used as observable. It is obtained

by calculating the level of the signal in various spectral bands which can correspond to different types of events. The use of SSAM/SSEM (Tarraga et al., 2006; Cornelius and Scott, 1993) instead of RSAM/RSEM provides more suitable precursory sequences and better results of eruption prediction using the FFM. However different classes of signals are still mixed if they have energies in the same frequency ranges.

2. Whether to use cumulative or non-cumulative data in FFM application has only been addressed in few studies (Bell et al., 2013). However, this point is in debate in the framework of accelerating moment release before earthquakes (Hardebeck et al., 2008). A discussion will be carried out to determine which form of the data is the most adapted for the use of FFM.
3. Although the uncertainty of the predicted time of eruption would be a highly valuable information for decision-makers during crises, the errors on the eruption forecast are not calculated in most of the studies or they are roughly approximated. The first step in calculating these errors reliably is to estimate the uncertainty on the observables.
4. Real-time predictions address a less constrained inverse problem than hindsight forecasts because they deal with partial datasets that end at the time at which the prediction is done. Voight and Cornelius (1991) and Cornelius and Voight (1994) question whether forecasts would be possible some times before the eruption, using incomplete sequences of precursors. For a real-time application of the FFM, they propose to update the forecasts at given time intervals and they find that the predictions tend to converge towards the eruption date some time before the eruption, using the FFM with $\alpha = 2$. More recently, Smith and Kilburn (2010), Bell et al. (2013) and Budi-Santoso et al. (2013) applied similar approaches. They represented the prediction time t_f as a function of the observation time t_{obs} advancing towards the eruption. In Budi-Santoso et al. (2013), who used the FFM with $\alpha = 2$, it is clear that the predicted time of eruption stabilises close to the eruption date several days before the onset of the eruption. However, this is not clear in Smith and Kilburn (2010) and Bell et al. (2013) where the FFM with variable α was used. In the latter cases, it is not straightforward to know how reliable the predictions are in real-time situations.

Objectives and outline of the thesis

The aim of this thesis is to determine a reliable and accurate manner of using the FFM for eruption forecasting and to evaluate its potential for real-time applications. To achieve this goal, I will proceed as follows:

1. I classify the different classes of volcano-seismic events as a function of their source mechanisms, presented in Chapter 1. The classification is carried out with an automatic

classification tool, allowing to rapidly identify the precursory sequences in an exhaustive way. This automatic classification tool is presented in Chapter 2.

2. In Chapter 3, I analyse separately the precursory classes of seismicity for two andesitic volcanoes (Volcán de Colima in Mexico and Merapi volcano in Indonesia) and one basaltic volcano (Piton de la Fournaise in France) and identify the classes that can be used for deterministic eruption forecasting. Furthermore, I quantify the number of seismic crises that do not lead to an eruption.
3. I define two criteria to decide whether the predictions made with the FFM are reliable in real-time: the stability of the predictions as a function of time and their associated uncertainties. This development is discussed in Chapter 4.
4. I point out the limits in the classical applications of the FFM, showing that real-time eruption forecasting would not be possible based on the reliability criteria defined in Chapter 4. Instead, I develop an original Bayesian approach to find the model parameters, allowing for a relevant evaluation of the uncertainty of the time of prediction and a greater stability of the predictions as a function of time than with the classical applications of the FFM. This main methodological improvement is developed in Chapter 4.
5. Chapter 5 is dedicated to the application of the method proposed in Chapter 4. I first describe typical case studies to highlight the potential and limitations of the method. I then present a systematic application of the method on all encountered precursory patterns in the aim of evaluating the statistical performance of the forecasting method, both for real-time and hindsight applications.

Chapter 2

Automatic classification of seismo-volcanic signals

Contents

2.1	Introduction	50
2.2	Hidden Markov model Tool Kit: HTK	51
2.2.1	Introduction to Hidden Markov Models (HMM)	51
2.2.2	Recognition principle	53
2.2.3	Training phase	54
2.2.4	Summary	56
2.3	Manual database	57
2.3.1	Building the manual database	58
2.3.2	Statistical evaluation	60
2.3.2.1	Closed test	61
2.3.2.2	Blind test	62
2.4	Recognition results	64
2.5	Conclusions on the VSR, advantages and limitations	67

2.1 Introduction

Classification of volcano-seismic signals is of paramount importance to separate signals that are associated to different source mechanisms. It enables to accurately identify precursory patterns of each type of signals. Until now, most of the studies take into account the whole seismic signal, which can potentially perturb or hide useful precursory patterns.

Moreover, the methodological developments of the FFM for real-time forecasting proposed in this thesis will have to be tested for a great number of eruptions to determine their statistical performance. In addition, I aim to diversify the observed precursors and eruption contexts to point out the limits of the predictions made with volcano-seismic precursors. These objectives are accomplished through the automatic recognition of volcano-seismic signals.

The automatic recognition of seismic events is very useful for observatories, when hundreds of events can be recorded within few hours. First, it avoids a tedious and slow task processed by the observers. Second, it objectively discriminates the classes of events while sometimes a unique event can be labelled in different ways by different observers. Automatic recognition thus guaranties the homogeneity of the catalogues of seismicity. Third, it can sometimes classify low energy events that would have not been manually classified by humans. Fourth, the statistical tests carried out to evaluate the efficiency of automatic recognition tool give a direct access to the uncertainty of the catalogues generated.

Event detection algorithms have been developed since many years and with various techniques (Withers, 1998). However, a proper classification of the detected events is only developed since few years. Neural networks (Del Pezzo et al., 2003; Scarpetta et al., 2005; Langer and Falsaperla, 2003) and self organizing maps (Esposito et al., 2008) have been used to automatically classify volcano-seismic events at Vesuvius, Phlegrean Fields and Stromboli Volcanoes (Italy). Orhberger (2001) automatically classified the events at Merapi Volcano (Indonesia) using Hidden Markov Models (HMM). However, this method could not be used to detect and discriminate seismic events in continuous recording systems and in real-time because it requires a pre-processing of the data before each classification. Benítez et al. (2007) were the first to adapt the HMM-based classification for continuous recognition and built a Volcano Seismic Recognition system (VSR). Cortés et al. (2009) and Cortés et al. (2014) kept on improving this efficient recognition tool.

This thesis took advantage of the collaboration with the University de Granada (Spain) to use this HMM-based automatic recognition tool (or Volcano Seismic Recognition system, VSR). Even though the HMM-based automatic classification tool has not been developed in the present thesis, the expertise developed in manual labelling led to close collaborations for the improvement of the tool. The algorithm used has been developed by Guillermo Cortés (University of Granada, Spain) and "the TSTC@UGR group" (Teoría de la Señal y Sistemas Telemáticos - TSTC e Instituto Andaluz de Geofísica IAG @ UGR). A complete understanding

of the system functioning is required to be able to run it properly and obtain satisfactory recognition results.

In this Chapter, some generalities about Hidden Markov Models (HMM) are first introduced to understand how they can be used for volcano-seismic signals recognition. The system is built on a training phase that uses a manual database of events. The basic concepts and tips for building a manual database are thus explained in a second section. In this second section, I also explain how the statistical tests are processed in the aim to improve the manual database and to estimate the success rate of the recognition. In a third part, the recognition results obtained on continuous records of Volcán de Colima are then analysed, in the aim to point out the limits of the method. Finally, I draw some conclusions on the system used in this study by pointing out advantages, drawbacks and some perspectives of research on HMM-based recognition.

All the examples considered in this Chapter are taken from the manual database built for Volcán de Colima, but the results obtained for the other target volcanoes are available in Chapter 3.

2.2 Hidden Markov model Tool Kit: HTK

The recognition system I use has been extended from the speech-based Hidden Markov Models Toolkit (HTK, Young et al., 2006). HTK was used in other areas as audio-visual speech, sign language and optical character recognition. It was finally adapted for Volcano Seismic Recognition by Benítez et al., 2007; Ibanez et al., 2009; Cortés et al., 2014. In this part, I introduce the theory of Hidden Markov models for automatic classification. For more specific details, see Rabiner (1989); Juang and Rabiner (1991) and Young et al. (2006).

2.2.1 Introduction to Hidden Markov Models (HMM)

A Markov chain is a series of random variables X_t ($t \in \mathbb{N}$) which models the evolution of a random system where X_t is the state of the system at instant t . Markov chains follow the Markov property: the future evolution of the dynamic system depends only on the present X_t value and not on the past values. In other words, X_{t+1} depends on X_t but is independent of (X_0, \dots, X_{t-1}) , so $P(X_{t+1} = x | X_0, \dots, X_t) = P(X_{t+1} = x | X_t)$. A Markov chain is characterised by a transition matrix A containing the probabilities of transition a_{ij} from state x_i to state x_j with $\sum_j a_{ij} = 1$, and by the initial matrix π which is the probability of the system to be at the state x_n at the initial time $t = 0$. Figure 2.1 represents a classical left to right Markov chain, defined by five states and a Markov model $\lambda = (\pi, A)$, with π the initial matrix and A the transition matrix. In this example, the entry state can only be the state x_1 because the initial probability has been set to 1 for the state x_1 and to 0 for the other states. Some transitions from one state to another are possible, while other ones are not, like the transition from state x_2

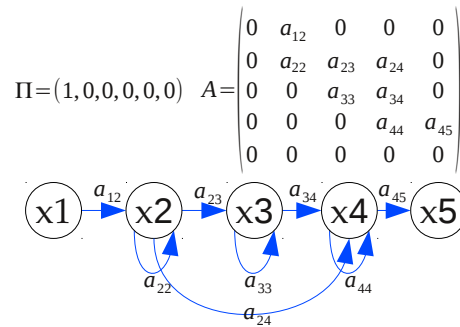


Figure 2.1: Example of a Markov chain with a left-to-right architecture, composed of 5 states and of initial (π) and transition (A) matrices. The allowed transitions are represented by the blue arrows and the entry state is obligatory the state 1.

to state x_1 for example, because $a_{21} = 0$. The architecture of a Markov model (i.e. number of states and initial and transition matrices) has to be adapted to a given problem. The initial and transition probabilities are calculated based on the experience that we have on the system. For example, a Markov model can be built to predict the evolution of our favourite cat’s behaviour given that it is in a certain state. From the experience we have on the cat’s habits, three states can be defined: sleeping (x_1), eating (x_2), playing (x_3). Moreover, we know that a cat sleeps more than other activities so the initial transition matrix can be $\pi = (0.8, 0.1, 0.1)$ for example. Finally, we know by experience that after sleeping, the cat is likely to play, after what it may eat and sleep again, which gives the transition probabilities from one state to the others so the transition matrix can be built. Now it is thus possible to calculate the probability for the cat to follow the state sequence $\mathbf{X} = \{\text{eating, sleeping, sleeping, playing}\}$ knowing that it is currently in the state sleeping.

Taking the example of the simple left to right model of Figure 2.1, it is possible to evaluate the probability to have the state sequence $\mathbf{X} = x_1, x_2, x_4, x_5$ given the model $\lambda = \{\pi, A\}$ as

$$P(\mathbf{X}|\lambda) = \pi_1 a_{12} a_{23} a_{24} a_{45} \tag{2.1}$$

Markov chains are simple because one observation corresponds to one state. However, it is not always the case as for example in speech recognition. In this case, the observations are the voice signals but the number of states is unknown and the number of observations emitted in one state is aleatory. This is simply due to the different manners of pronouncing one word, depending on the accent and on the voice of the persons. Consequently, one word can have different spectral contents as a function of time and from one person to another. It can also last longer or shorter depending on the persons’ way of speaking. In this case the state sequence \mathbf{X} in the Markov chain is thus *hidden*, leading to the use of Hidden Markov Models (HMM). When the system is in the state x_n , it produces an observable data o_t at the time t . The probabilities $b_n(o_t)$ that the system produces an observation o_t given that it is in the state x_n

are put together in a so-called observation matrix B , with $\sum_t b_n(o_t) = 1$. A HMM λ is thus defined by three parameters: $\lambda = \{A, B, \pi\}$.

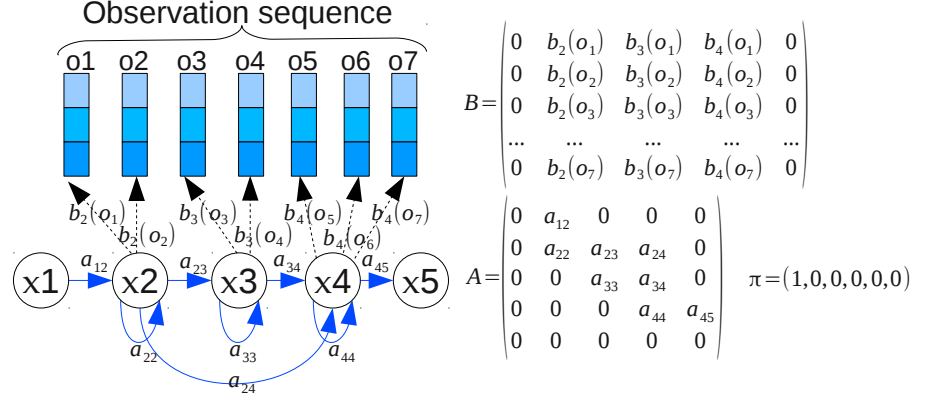


Figure 2.2: Example of a hidden Markov chain of model $\lambda = \{A, B, \pi\}$. The states are supposed to be hidden so we only dispose of the observation sequence. Because the transition from one state to itself is allowed, there is the possibility of observing two or more observations that correspond to the same state. Each blue stick represents an observation vector and each different square is a characteristic of the vector.

Figure 2.2 is an example of HMM architecture, that represents the HMM of the observation sequence $\mathbf{O} = \mathbf{o}_1, \mathbf{o}_2, \dots, \mathbf{o}_7$, which can be a seismic signal. In the model represented in Figure 2.2 the corresponding states are going from state 2 to state 4. States 1 and 5 are used to link this model to previous and further seismic signals. The system moves along the state sequence $\mathbf{X} = x_1, x_2, x_2, x_3, x_3, x_4, x_4, x_4, x_5$ in order to generate the observation sequence $\mathbf{O} = \mathbf{o}_1, \mathbf{o}_2, \dots, \mathbf{o}_7$. Each observation corresponds to an observation vector with different features about the spectral content of the signal. Given the model λ , the probability $P(\mathbf{O}, \mathbf{X}|\lambda)$ to generate the observations \mathbf{O} by the state sequence \mathbf{X} is calculated as

$$P(\mathbf{O}, \mathbf{X}|\lambda) = \pi_1 a_{12} b_2(\mathbf{o}_1) a_{22} b_2(\mathbf{o}_2) a_{23} b_3(\mathbf{o}_3) a_{33} b_3(\mathbf{o}_4) \dots a_{44} b_4(\mathbf{o}_7) a_{45} \quad (2.2)$$

In the case of volcano-seismic signal, each HMM represents one class of signal. However, in practice, the observation sequence \mathbf{O} and the HMM are the only information which is known and the state sequence \mathbf{X} is hidden (not known). This is why we call these models Hidden Markov Models.

2.2.2 Recognition principle

Let us consider that each seismic signal is represented by an observation sequence $\mathbf{O} = \mathbf{o}_1, \mathbf{o}_2, \mathbf{o}_t, \dots, \mathbf{o}_T$ where \mathbf{o}_t is the seismic signal vector observed at time t . The seismic signal

recognition problem can be seen as the following optimisation problem

$$\lambda^* = \operatorname{argmax}_c \{P(\lambda_c | \mathbf{O})\} \quad (2.3)$$

where λ_c is the HMM of the c^{th} class of signal among a set of classes $\mathbf{c} = VT, LP, T, \dots, C$. In other words, we want to maximize the probability to have the event of class c knowing the observation sequence \mathbf{O} . The model λ^* that maximises this probability is the class of events which is the most likely to be under consideration, given the observation \mathbf{O} . The probability can be computed using Bayes' theorem as

$$P(\lambda_c | \mathbf{O}) = \frac{P(\mathbf{O} | \lambda_c) P(\lambda_c)}{P(\mathbf{O})} \propto P(\mathbf{O} | \lambda_c) \quad (2.4)$$

with $P(\lambda_c) = \text{constant}$ is assumed to be the same for all classes and $P(\mathbf{O}) = \text{constant}$ since every observation is expected to have the same probability to occur. Consequently, the probability that a signal belongs to a class of events given an observation sequence only depends on the likelihood $P(\mathbf{O} | \lambda_c)$. The system thus aims to maximize $P(\mathbf{O} | \lambda_c)$. This probably is computed just as equation (2.2), with the difference that the state sequence X is not known, so the likelihood is computed over all possible state sequences $\mathbf{X} = X_1, X_2, \dots, X_T$ as

$$P(\mathbf{O} | \lambda) = \sum_{\mathbf{X}} a_{X_1, X_2} \prod_{t=1}^T b_n(\mathbf{o}_t) a_{X_t, X_{t+1}} \quad (2.5)$$

The computation of equation (2.5) requires a huge computation cost. For example, disposing of a model composed of N states and an observation sequence of size T , there are N^T possible state sequences. The alternative way for the computation of equation (2.5) is the use of a recursive forward algorithm (Bahl et al., 1983; Baum et al., 1970) and the so-called Viterbi algorithm (see Viterbi, 1967 for more details).

The next section will explain how it is possible to extract a HMM λ for each class of seismic events, during the *training phase*.

2.2.3 Training phase

A primary step in both training and recognition phases is the initialisation stage, i.e. the extraction of feature vectors from the raw seismic signal to produce the sequence of observations $\mathbf{O} = \mathbf{o}_1, \mathbf{o}_2, \dots, \mathbf{o}_T$. To do so, the seismic signal is divided in regular overlapped windows which duration can be set according to the user. Each of these windows is transformed into an observation feature vector \mathbf{o}_t with a parametrization corresponding to the energy content in the different frequency bands $\Delta f_1, \Delta f_2, \Delta f_3, \dots$, called filter bank. I do not detail this aspect here, see Benítez et al. (2007) for more details.

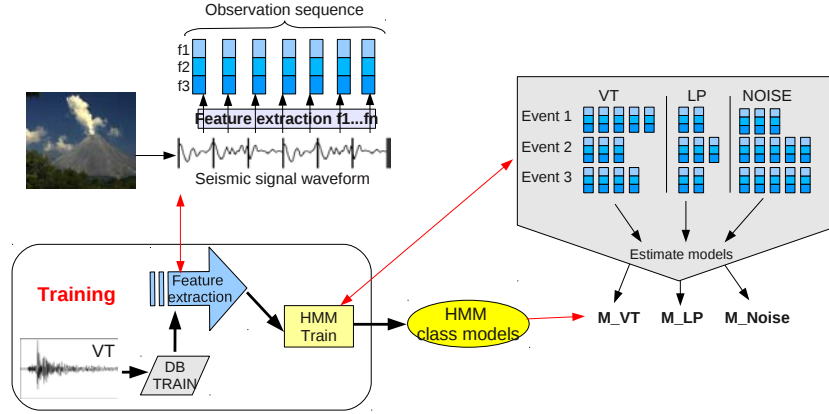


Figure 2.3: Schematic diagram explaining the training phase. A database of events is available for each class of signals (DB train). Each of these signals are transformed in a serie of feature vectors during the feature extraction. Then all the observation sequences in each class are used to build the Markov models of the target classes (in this example M_{VT} , M_{LP} , M_{noise}). The outputs of this phase are thus the HMM for each class of events.

Each HMM is constructed based on a database of events that have been manually classified (see Section 2.3). Thus a bunch of events is available for each class of seismo-volcanic signals. Given this set of training examples for one class of events, the parameters of the HMM $\lambda = \{A, B, \pi\}$ of this class can be constructed. We have to keep in mind that one HMM is constructed for one class of volcano-seismic events. This step is illustrated Figure 2.3.

One of the first steps required for the VSR is to carry out the training phase is to set the architecture of the Markov Models that can be adapted to each class of signals depending on their mean duration and spectral variability:

1. The topology of the Markov chain: in the case of voice or seismic events recognition, the classical left-to-right topology is always adopted (as in Figure 2.2).
2. The number of states.
3. The number of components in the probability density functions used for the Gaussian Mixtures Models (GMM). One state has one GMM. A GMM is an estimation of the distribution of aleatory variables (representing the observations) modelled by the sum of several Gaussians for each state. Then it is necessary to estimate the mean and variance of each Gaussian that composes the mixture model with the forward algorithm (Bahl et al., 1983; Baum et al., 1970).

Given the set of signals for each class, transformed then in sequences of observation \mathbf{O} through the parametrization step and the architecture of the HMM, we estimate the values of the model parameters that best explain the observations in the training phase. Assuming a GMM-like probability density function and given an observation vector o_t , the output probability of the observation o_t in the state j can be evaluated as

$$b_j(\mathbf{o}_t) = \sum_{m=1}^M c_{jm} \mathcal{N}(\mathbf{o}_t; \mu_{jm}, \mathcal{C}_{jm}) \quad (2.6)$$

where \mathcal{N} is the normal distribution, M is the number of Gaussians of the GMM, c_{jm} is the weight coefficient of the m^{th} mixture of state j , and μ_{jm} and \mathcal{C}_{jm} are the mean and covariance matrix of the m^{th} Gaussian. The difficult part of this training phase is to find the parameters μ_{jm} , \mathcal{C}_{jm} and c_{jm} that best explain the distribution of the observation vectors in the training database. These parameters, as well as the HMM parameters A , B and π , are optimised using the Baum-Welch algorithm (Bahl et al., 1983; Baum et al., 1970).

Consequently, the HMM of one class is built by optimising the parameters A , B , π , μ_{jm} , \mathcal{C}_{jm} , c_{jm} that best explain the observation sequences contained in the manual database of the target class.

2.2.4 Summary

Figure 2.4 summarises the VSR functioning used to automatically classify the seismo-volcanic signals. This schematic diagram turns on three main processing phases: the training phase, the recognition phase and the feature extraction. The processing phases are represented on the left side of the diagram and the corresponding schematic explanation on the right side. The training phase is processed with a manual database (DB train) of several VT events for example. Each of them is transcript in a specific file that corresponds to a dictionary of available events. Furthermore, each of them is processed during the feature extraction phase. The seismic events are thus transformed in a sequence of feature vectors. This database of feature vectors is used to build the HMM for each class of events (M_{VT} , for example). Then, this has to be done for each class (M_{LP} , M_{Noise})

Once the models are trained for each class, it is possible to proceed to the recognition phase. The recognition phase can be done either with continuous records or with a database of known events to be tested (DB test). The first step of the recognition is the feature extraction leading to an observation sequence of feature vectors. The probability of this unknown observation to belong to the different trained classes is then evaluated and the HMM with which the maximum probability is obtained is the most probable class to which the unknown event belongs to. All the unknown events that have been recognised to belong to a certain class are gathered in a transcription file.

In this section, I have explained the theory of the VSR, assuming that the training database of events was already available. However, in most of the cases, the recognition has to be processed on a new target volcano or a new seismic station. So the database has to be preliminary by proceeding to the manual labelling of the signals (i.e. defining the class, and the beginning and end of a signal) corresponding to the target classes. The next section explains how to build a good database for the VSR to run properly and how the success rate of the VSR is evaluated.

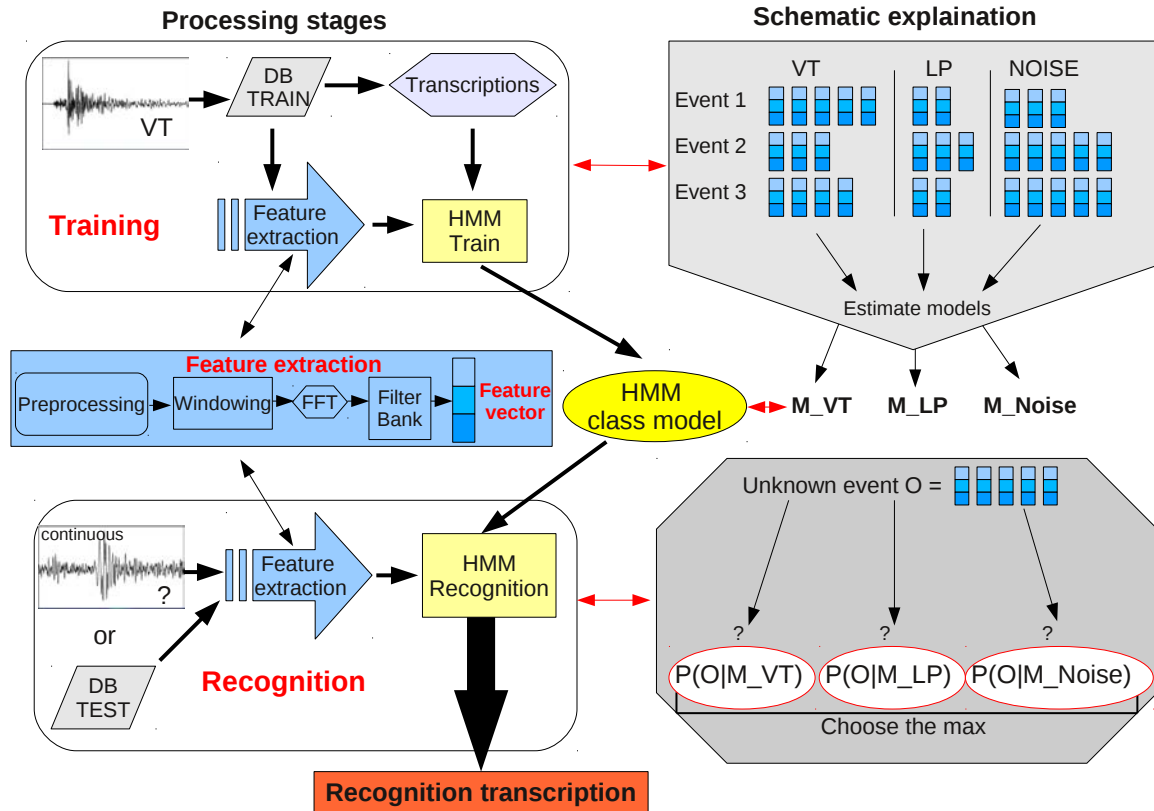


Figure 2.4: Schematic diagram of the VSR functioning. The outputs of the training phase are the HMM models for each class of events (M_{VT} , M_{LP} , M_{noise}), the outputs of the feature extraction are the feature vectors, used in both training and recognition phase. Finally the output of the recognition phase is a transcription file of the recognition processed either on continuous records or testing database. Double red arrows indicate the corresponding schematic explanation of the training and recognition phases.

2.3 Manual database

Building a good manual database of volcano-seismic events for each target volcano is essential to succeed automatic recognition. However, it is a tedious and delicate task which is composed of 3 steps:

- Definition of the target classes: determination of typical characteristics for each class of events and of which station to use.
- Manual segmentation and labelling of the seismic signals.
- Evaluation of the statistical performance of the VSR using the manual database.

In practice, I have adopted a recursive workflow to progressively improve the manual database and obtain a satisfying success recognition rate. In the following, I present the general guidelines I have followed and some of the tests I have performed.

2.3.1 Building the manual database

The VSR is based on a training phase so the construction of a manual database is of capital importance to succeed volcano-seismic event recognition. This task has to be carried out in the most rigorous and homogeneous manner as possible. The segmentation and the labelling of the signals will drive the quality of the manual database.

First of all, the different classes of seismic events have to be defined. Thus, a good knowledge of the target volcano is needed. It is required to define typical classes with homogeneous time and spectral characteristics, but without being too specific. On one hand, the least is the variability of events in one class, the better will be the recognition results of the VSR. However, if the characteristics of a recorded event are slightly different than the typical events of this specific class in the manual database, then it will not be recognised as belonging to this class. On the other hand, a great variability of examples for each class will lead to a more generalised recognition but it will also favor the confusion between the labelled classes. Moreover, it is recommended to include as many events as possible in one class (more than 100 events). Thus, for a more general recognition, it is recommended to define general classes with a good variability in time and spectral content and a sufficient number of events per class. For example, one has to decide whether to divide the class of LP events in several subclasses. At first, labelling and tests can be done with subclasses that can then be clustered in only one class if needed. For some classes like rockfalls, there is not a big variability in the spectral contents so the class definition is simple. It is also the case for lahars, but the difficulty will rather be to find 100 events for this class.

To ensure the homogeneity of the database, it has to be carried out by only one labeller. When processing the segmentation, the person who is in charge of labelling must be sure of the event label. The best way to do so is to define fixed characteristics for each class of signal, and to ask the question: why do I think it is this type of event ? If the answer fills in all the pre-defined characteristics, then it can be labelled. Otherwise, it is recommended to sort it in a "garbage" class which is not used for training. Moreover, the labeller needs to add a class of noise because the VSR is a classifier without event detector. Of course, segments of noise should not include other events.

The VSR segments seismic signals of one station, so the choice of the station for which the VSR will perform the automatic classification has to be thought carefully. On one hand, it is better to choose the closest station from the crater because it allows for detecting volcano-seismic events as close from the source as possible. The VSR is based on the time evolution of the spectral content of the signals so it is convenient to minimise the effect of the attenuation of the high frequency part of the signal by using a station close to the crater. However, close stations can record more saturated signals, producing fake high frequencies which are a source of error in the recognition. The closest stations from the crater were always chosen in this

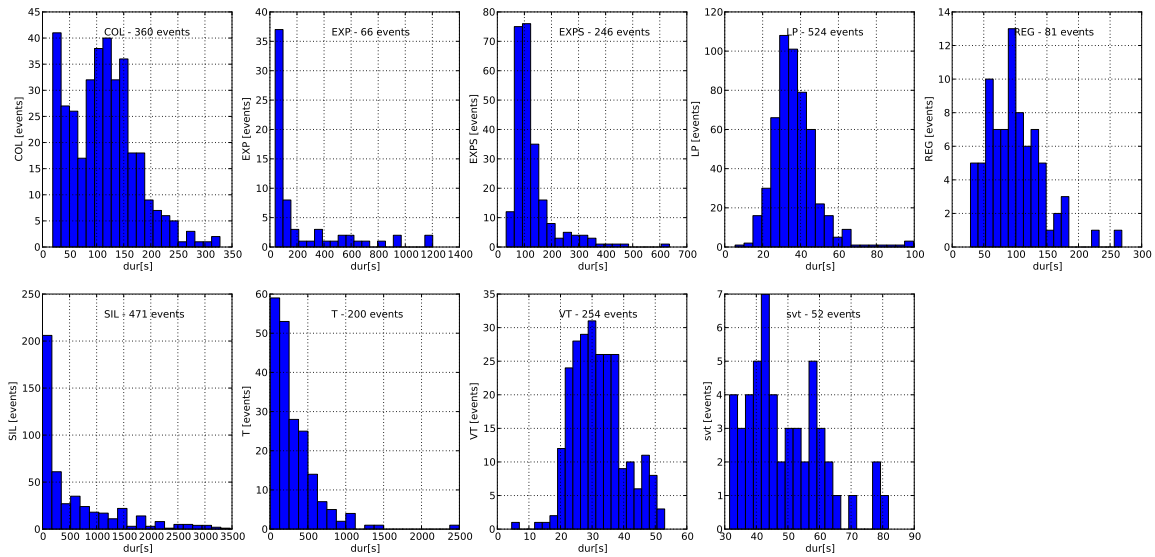


Figure 2.5: Histograms of event durations for each target class of the manual database: rockfalls (COL), explosions (EXP), saturated explosions (EXPS), long-period events (LP), tectonic earthquakes (REG), noise (SIL), tremor (T), volcano-tectonic events (VT), and saturated VT (svt).

thesis, and I decided to include a class of saturated events to limit wrong classifications.

Once the manual database is built, some statistical verifications must be carried out. It is recommended to check the variability of events in duration and the number of events for each class. If the variability or the number of events is not satisfying, more events have to be labelled. It is important to include all possible event durations. For example, when only long duration events have been segmented, there will be no chance to recognise small events in the continuous records, thus increasing the magnitude of completeness of the catalogue.

Figure 2.5 presents an example of statistics obtained with the Colima manual database. First of all, all classes except regional earthquakes (REG), explosions (EXP) and saturated VT (svt) contain more than 100 events. Saturated VT events are not common so I propose to ignore this class. Explosions are difficult to dissociate from LP events. As it is recommended not to classify the events on which the classifier hesitates, most of the EXP signals have been put in the garbage class, resulting in only 66 labelled explosions. Because explosions are not so frequent, it seems difficult to add more events in this class. Finally, regional events are not so common either so I had no other choice to keep on working with the 81 events.

For most of the classes of Figure 2.5, there is a clear dominant duration except for classes of REG and COL. Many different durations of tectonic earthquakes are recorded, depending on the distance of the station from hypocenters and on the magnitude. It is thus expected to have a great variability in duration for this class. The rockfalls (COL) however show a bimodal

distribution of the durations. Very small events have been classified as well as larger events. This can be a problem for the construction of Markov chains during the training phase because these two dominant durations are very different. However, I expect that it might not be a problem because the spectral content of this class of signals is quite homogeneous in time. The variability of the classes of noise (SIL) and explosions is rather poor. It is expected for the class of SIL that one long duration noise will be recognised in several pieces. The other classes seem to have a sufficient variability.

It is now necessary to proceed to recognition tests in order to verify the impact of the quality of the manual database on the recognition success. These tests will help to define the quality of the manual database and the success rate of the VSR.

2.3.2 Statistical evaluation

The recognition success must be statistically evaluated before proceeding to continuous signal recognition. This step enables to improve the manual database if needed and to know about the success rate of the recognition for the different classes of signals.

To do so, the manual database is split in different parts (usually two or three parts). One part of the database is used for the training phase, to build the Markov models for each class of events. The other part is used for the recognition phase.

Two tests can be carried out. The first one, called *closed test*, consists in recognising the same part of database that has been used to train the models. This test can be seen as *learning by heart* and repeating what the system learnt. It is a very useful test to determine the reliability of the manual database. If the database is well built, then the success of this test must be close to 100%. Otherwise, the database has to be completed or the events more accurately segmented. The second test, called *blind test*, consists in recognising another part of the manual database. This test is very close to a real-time situation and it permits to evaluate the success rate of the VSR, from which I will deduce the data uncertainty used later.

The results of these tests are presented in a so-called confusion matrix (Figures 2.6 and 2.7). The two entries of this table contain the classes of events used. Rows correspond to the number of true events in each class and columns to the events recognised by the VSR in the corresponding classes. The table thus gives the number of wrong classifications, called substitutions (S), of inserted events (I) and of the events that have not been recognised at all (deleted, Del). N being the total number of events in the recognition database, the mean success rate for each class is computed in three different ways:

- $\%c = \frac{N-S}{N}$ evaluates the success rate without inserted or deleted events,
- $\%acc = \frac{N-S-D}{N}$ evaluates the success rate including the events that have been deleted,

- $\%corr = \frac{N-S-D-I}{N}$ evaluates the success rate including the events that have been inserted and those that have been deleted.

The success rate which is the most representative of real continuous classification is the $\%corr$ as it includes the events that have been inserted or simply not recognised. The number of deleted events is generally close from reality because the events that have a too short duration to be classified are ignored. The number of inserted events is more tricky to interpret. Indeed, an event that has been inserted by the VSR is not necessary a mistake. Pieces of noise can contain volcano-seismic events that have not been noticed by the labeller because of a too small amplitude.

Closed and blind tests can be long and tedious processes if they are not well reasoned. Indeed, different configurations have to be tested to obtain the highest success rate. These configurations concern:

- the architecture of the HMM, such as the example displayed in Figure 2.2: number of states, types of transitions (left to right and/or right to left), same or different number of states for each classes.
- the parametrisation of the observation sequences (e.g. the feature vector extraction of Figure 2.3): duration of the observation windows and of the windows overlaps.
- the parametrisation of the feature vectors (e.g. the feature vector extraction of Figure 2.4): energy in different spectral bands and/or first derivative and/or second derivative of the energy. The more characteristics are considered in the feature vectors, the better will be the recognition results.
- number of considered Gaussians for the GMM. For very specific classes of events, few Gaussians are enough to ensure a good success rate whereas up to tens of Gaussians can be needed if classes of events are very heterogeneous.

Different configurations can lead to similar success rates. For the automatic classification of the continuous stream of seismic signal, I simply chosed one of the configurations that allows for the best success rates.

2.3.2.1 Closed test

For illustration, Figure 2.6 shows the confusion matrix obtained for one example of the numerous tests carried out with Volcán de Colima manual database. The success rate $\%c$ is comprised between 95% and 100% for all classes, except for the class of noise (SIL) for which only 86% of success is obtained. For this class, substitutions with COL, T, EXP and EXPS have occurred. I suspect that signals belonging to COL, EXP and EXPS classes might have been included in the SIL class. In particular, low amplitude tremors can easily be confused with noise. This inspection suggests that it is recommended to check the manual database of SIL, even if these

errors are probably not a problem for recognition in this case, because the number of events that have not been well recognised is small in comparison with the total number of SIL events, and the success rate of the other classes is excellent. When adding the inserted and deleted events (*%Corr* and *%acc*), the success rate of the closed test is lower, especially for the classes of SIL and EXP. Concerning SIL events, I introduced on purpose very short pieces of SIL to test if they could be recognised. However, they were too small to be recognised by the VSR, as we can see through the numerous deleted SIL events. It has no impact on the substitutions between events or the construction of HMM. Finally, I already noticed that the small number of EXP events should be a limitation for the recognition results.

```

WORD: %Corr=88.52, Acc=86.95 [H=902, D=93, S=24, I=16, N=1019]
----- Confusion Matrix -----

```

	COL	EXP	EXPS	LP	REG	SIL	T	VT	Del	[%c]	%Corr	%Acc
COL	176	0	0	0	0	0	0	2	5	[98.9]	96.17	95.08
EXP	0	19	1	0	0	0	0	0	7	[95.0]	70.37	70.37
EXPS	0	0	119	0	0	0	0	1	1	[99.2]	98.35	96.69
LP	0	0	0	245	0	0	0	0	9	[100.0]	96.46	95.67
REG	0	0	0	0	39	0	0	1	1	[97.5]	95.12	92.68
SIL	1	1	11	0	0	108	4	0	63	[86.4]	57.45	53.19
T	0	0	2	0	0	0	71	0	5	[97.3]	91.03	89.74
VT	0	0	0	0	0	0	0	125	2	[100.0]	98.43	98.43
Ins	2	0	2	2	1	8	1	0				

```

-----
class_mean: 87.92 86.48

```

Figure 2.6: Confusion matrix: closed test. Rows correspond to the number of true events in each class and columns present events recognized by the VSR in each class. Line denoted WORD shows the mean success rate all classes mixed together. H is the total number of events that have been well-classified, D the number of deleted events, S the number of substitutions, I the number of insertions and N the total number of events tested.

To conclude, this closed test reveals a good quality of the manual database, that could however be improved by adding more explosions and improving the SIL database. It is exactly what I did for the database of every volcanoes.

2.3.2.2 Blind test

For illustration, Figure 2.7 displays the confusion matrix of one of the blind tests achieved for Volcán de Colima manual database. The best recognition results are obtained for the classes of COL, EXPS, VT and LP with more than 85% success rate when taking into account the substitutions only, more than 80% success rate when counting the deletions (*%Corr*) and more than 75% success rate counting the deletions and insertions (*%Acc*). The highest success rate is thus obtained for the classes that I intend to use as precursors for eruption predictions, which is a very good news for the purpose of this thesis. The class of tremor has also a good success rates in term of *%c* and *%Corr* (more than 80%). However, because of the high number of insertions, the *%Acc* falls down to 50%. The VSR does not handle well long events and

consequently it is likely to be split in several pieces. As a consequence, if one long tremor or noise have to be recognised, it can be split in three parts for example, leading to the insertion of two events. Therefore, I recommend to have a look only at $\%c$ and $\%Acc$ for the classes of long duration events. This is also the reason why I will not consider tremors for the eruption predictions in Chapter 4 and 5. The class of explosions displays bad results because the number of events in the manual database is not sufficient enough to construct reliable HMM. Finally, classes of SIL and REG show rather bad recognition results with only about $75\%c$ and less than $70\%Corr/\%Acc$. It can be explained because of the high duration variability of REG.

WORD: $\%Corr=80.74$, $Acc=70.72$ [H=830, D=109, S=89, I=103, N=1028]

----- Confusion Matrix -----

	COL	EXP	EXPS	LP	REG	SIL	T	VT	Del	[%c]	%Corr	%Acc	
COL	165	0	0	0	0	0	0	2	8	[98.8]	94.29	89.71	
EXP	1	12	7	1	0	0	0	0	10	[57.1]	38.71	25.81	
EXPS	0	0	120	0	0	0	0	0	0	[100.0]	100.00	79.17	
LP	2	0	15	232	0	1	4	2	11	[90.6]	86.89	77.90	
REG	0	0	1	1	25	0	2	4	3	[75.8]	69.44	63.89	
SIL	1	3	16	2	0	92	5	0	73	[77.3]	47.92	41.15	
T	0	2	6	1	1	1	68	0	3	[86.1]	82.93	51.22	
VT	2	0	0	6	0	0	0	116	1	[93.5]	92.80	92.00	
Ins	8	4	25	24	2	13	26	1					
-----											class_mean:	76.62	65.11

Figure 2.7: Same as Figure 2.6 for a blind test.

The most important conclusions that have to be drawn from this test is the success rate for the classes of presumed precursors (VT and LP), which is very good. In addition, it is now possible to know the classes that can be confused. For example, LP can be mixed with explosions or tremors, as expected, and some VT can be mixed with LP or regional earthquakes. These confusions are quantified and will be of paramount importance to compute the uncertainties on the seismic data that will be used to carry out eruption predictions.

Of course, the results of the tests shown in this section can be improved by tuning the configuration parameters or by improving the manual database. The confusion matrix corresponding to the configuration that allowed to obtain the best success rates are displayed for each target volcano in Chapter 3.

To conclude, I wish to underline that even though closed and blind tests are very informative to improve the manual database and to quantify the success rate of the VSR, we should always keep an eye on continuous records for tuning the configuration that can improve the continuous recognition.

2.4 Recognition results

After having manually built a training database and processed recursive tests to determine which configurations give the highest success rate of the recognition, it is possible to use the VSR to carry out recognition on continuous seismic records of several years. This step allows for building years of catalogues of seismo-volcanic activity. As a further quality control, I also used the results of continuous recognition to visually check the results of random files and to improve the configuration and the manual database. Even if it is a tedious task, it allows for even better recognition results.

I chose on purpose four representative examples of the recognition results obtained at Volcán de Colima: one of them contains different types of events, the other one contains several VT events and the last one shows a bad or questionable recognition result.

Figure 2.8 is one example of the continuous recognition carried out with the VSR at Volcán de Colima. Four different types of events are successfully recognised: VT, LP, T and COL. Some mistakes can be noticed, such as the VT event at $t = 150$ s, which is actually the end of the previous COL event. This mistake can be easily understood when having a look at the spectral content of the end of this COL, which actually looks like the spectral content of a VT. The tremor which is recognised just after the latter VT is probably a mistake as well. The LP recognised at $t = 290$ s is questionable because most of its energy is below 5 Hz. Looking at the waveform, it seems to have an emergent onset. If I had to classify this event, I would put it in the garbage class. But the VSR is a machine only relies on the HMM built and thus this class was identified as the most probable, based on the manual database. For this kind of uncertain event, I would thus rather rely on the VSR that makes an objective decision. The last problem visible on Figure 2.8 is the COL event that has been divided into two COL instead of one.

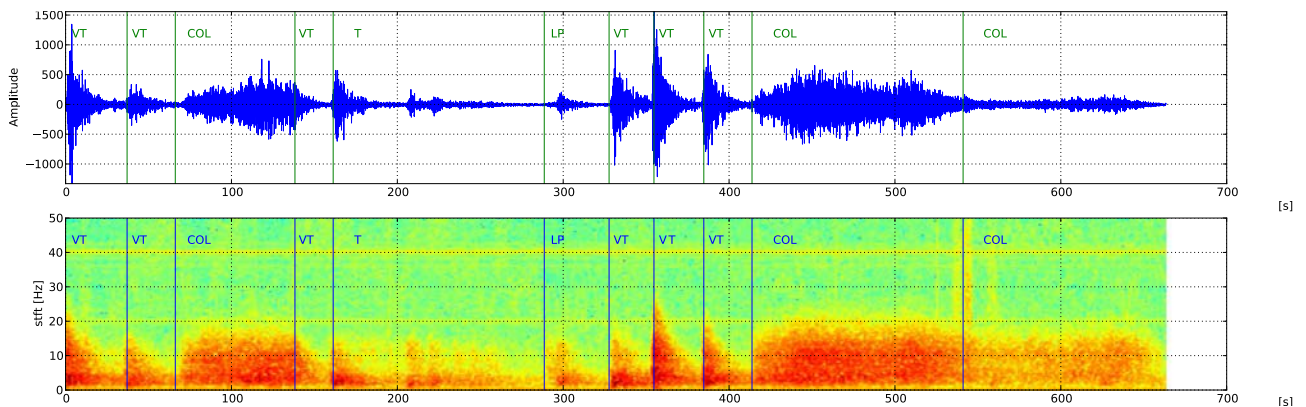


Figure 2.8: Example of a continuous seismic record that has been automatically segmented, with the corresponding spectrogram. Recognised events belong to the classes of COL, VT, LP and T.

As another example, Figure 2.9 presents successful results of classification of VT events.

The beginning of the classification of each event seems to start just at the moment where VT energy is detected. It thus seems to be quite accurate for picking the beginning of VT events. The uncertainty on the beginning and end of the segmentation was not quantified. The success in the recognition of this class of events can be explained by the very typical evolution of their spectral content.

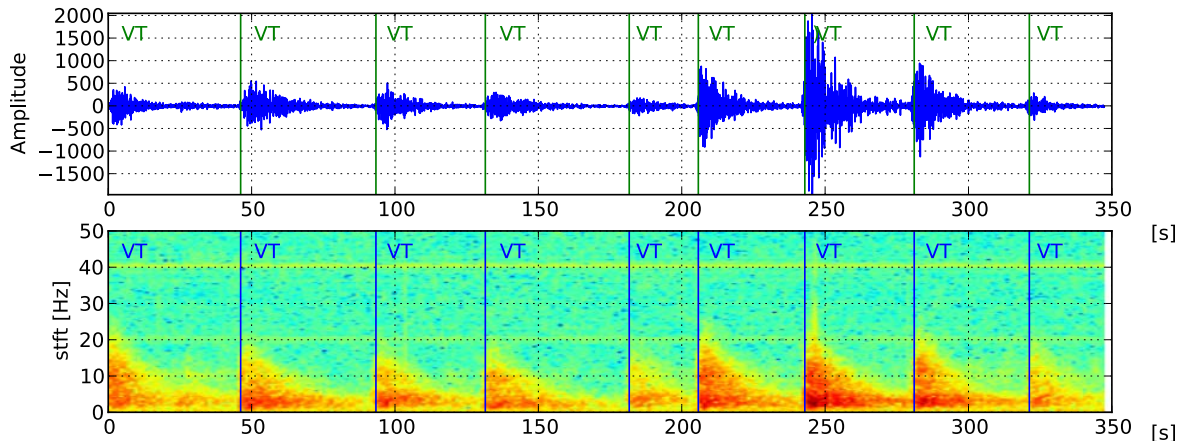


Figure 2.9: Example of a continuous seismic record that has been automatically segmented, with the corresponding spectrogram. Events belong to the class of VT.

On the contrary, Figure 2.10 illustrates classes that obtained the worse success rate at the blind test: T and SIL. A tremor with low energy seems to be difficult to dissociate from the noise. These mistakes will not be a problem in the following since these classes will not be analysed as precursors of volcanic eruptions.

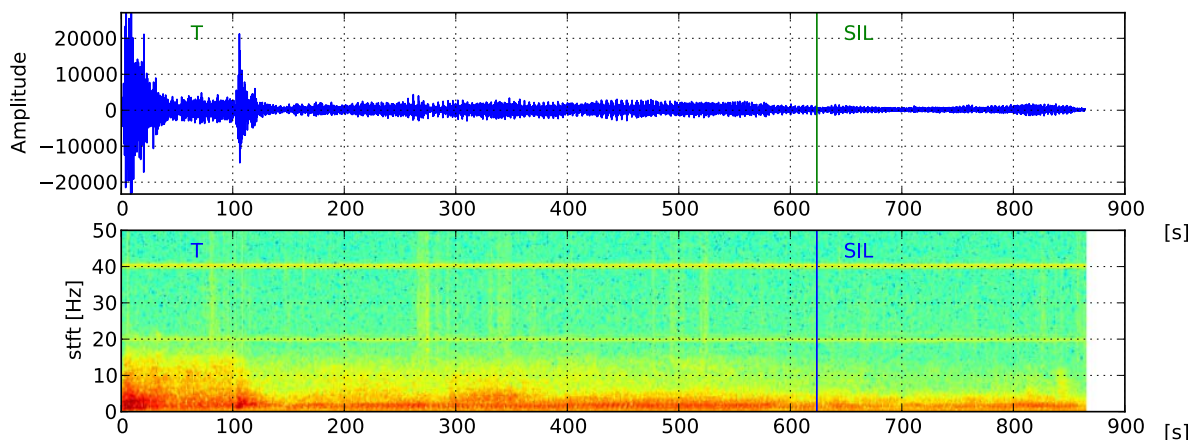


Figure 2.10: Example of a continuous seismic record that has been automatically segmented, with corresponding spectrogram. Recognised events correspond to the SIL and T classes.

This visual validation step is important to define which classes will be reliable for the analysis. For the example of Volcán de Colima database, the conclusion of all these tests is that the results of classification can be used with reliability for the classes of VT, LP, COL and

EXPS, while the class of tremor should be used with care.

Even if building the manual database and proceeding to the validity tests is a long and tedious task, it then allows for the rapid classification of continuous records. For example, the classification of 14 years of seismicity at Volcán de Colima has been done in less than one day.

Finally, I have to mention that this automatic classification tool has been implemented for near real-time monitoring at Volcán de Colima with the manual database constructed by Raúl Arámbula (Arámbula, 2011). Figure 2.11 is one example of the automatic classification results carried out every day in Colima. Each color represents a different class of event. Even if it is a useful tool for real-time monitoring, we can notice that some small events are systematically missed by the VSR (they remain blue on the seismogram). This is because small events have not been integrated in this database, consequently the magnitude of completeness of this catalogue is high. In my manual database I have made efforts for adding as many small events as possible to decrease this recognition threshold.

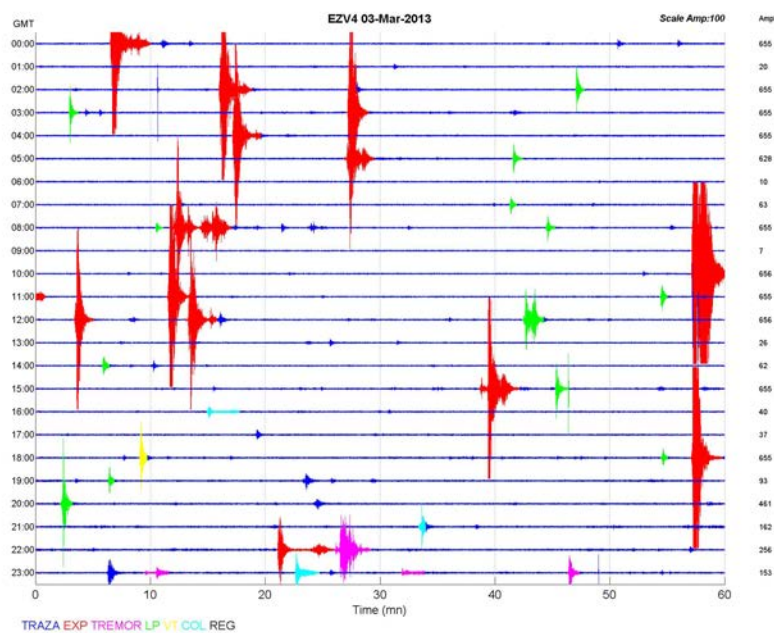


Figure 2.11: Near real-time automatic classification of seismo-volcanic signals through the implementation of the VSR in the earthworm system, in Colima. Figure provided by the RESCO (Red Sismologica Telemetrica del Estado de Colima).

In my treatment of the data, I have performed the analysis described in this section for each target volcano (see Chapter 3 for the associated results). In certain cases, the success rate of some classes were not sufficient enough to analyse them as precursors. In particular, the class of tremor is not analysed for any volcano because of its bad recognition results.

2.5 Conclusions on the VSR, advantages and limitations

The adaptation of the HMM recognition tool to seismic signals by Benítez et al. (2007), Cortés et al. (2009) and Cortés et al. (2014) is a major advance for volcano-seismology because it allows for detecting and classifying continuous flow of seismic records very rapidly. However, even though some advantages are obvious, there are some drawbacks that should be pointed out. These drawbacks arise because the application of a HMM recognition tool to volcano-seismic signal classification is in a very early stage.

The main advantages can be listed as follows:

- Rapid automatic classification of continuous records. For continuous recognition, a single training phase has to be done. Then, years of continuous records can be classified in few hours.
- All kind of classes can be included.
- The success rate of the VSR is very complete and informative.
- Easily integrable in monitoring systems thanks to the use of a high level language (Python).
- Output files are easily exploitable to build histograms of volcano-seismic activity.

However I may emphasise some limitations:

- Building the manual database is a long and tedious task.
- A good knowledge of the VSR system is required to define the configurations that gives the best success rates: no blackbox use is possible, unless the database is already built and tests already done.
- Long duration events are often split in several pieces.
- Recognition is possible at several seismic stations but one manual database must be built for each station.

Those limits lead to the following perspectives:

- Include more representative characteristics for the feature vectors, different from the spectral ones, as in Alvarez et al. (2009, 2012).
- Include a detector of events in the aim to better classify long and short duration events, but also to get rid of the noise class.
- Building a world database with all possible kind of events. If it is successful, then automatic classification of volcano-seismic signals could be possible for volcanoes in the phase of unrest and for which no manual database could be previously built.
- Multistation recognition could facilitate the classification of uncertain events. In the case of Merapi volcano for instance, two types of VT events are observed, as a function of

their depth. The only way to recognise them is to use two stations. In this case, it would be useful to carry out the automatic classification for two stations simultaneously.

Once the catalogues are created, it is possible to analyse years of seismic activity for different volcanoes. The next step is to identify precursory seismic patterns of eruptions.

Chapter 3

Seismic precursors of volcanic eruptions: three case studies

Contents

3.1	Introduction	70
3.2	Piton de la Fournaise (La Réunion island, France)	71
3.2.1	Volcanic activity and precursors	72
3.2.2	Precursory seismic patterns of effusive eruptions	77
3.3	Merapi volcano (Indonesia)	80
3.3.1	Precursors of the explosion of the 26 of October 2010	81
3.4	Volcán de Colima (Mexico)	85
3.4.1	Volcanic activity and precursors	87
3.4.2	Precursory patterns of vulcanian explosions	97
3.5	Summary and partial conclusions	100

3.1 Introduction

Various volcanic contexts are explored in this thesis, in order to analyse the potential of FFM for eruption forecasting and for its adaptation for real-time use. Indeed, different precursors are observed prior to eruptions in different volcanic context in terms of classes of events as well as different precursory durations. Furthermore, different volcanic contexts lead to different societal challenges. Until now, the variability of precursors and the objective quantification of the feasibility to success deterministic predictions in different volcanic contexts has never been explored.

The application of the FFM for eruption forecasting requires accelerating precursory patterns of seismic activity. In addition, the FFM theory is supposed to describe precursory damage of the surrounding rock prior to its failure (Voight, 1988). Consequently, VT activity is normally the relevant class of signal used for volcanic eruption forecasting using the FFM. However, LPs have also been observed to be a good precursor of explosions at Galeras in Colombia (Gil Cruz and Chouet, 1996), Tungurahua in Ecuador (Molina et al., 2004), Sakurajima in Japan (Maryanto et al., 2008), Ubinas in Peru (Traversa et al., 2011) or Colima in Mexico (Arámbula-Mendoza et al., 2011), for instance. Because LP activity is usually associated with violent and dangerous volcanic activity, it appears to be worth exploring its precursory patterns and potential use for deterministic eruption forecasting.

Results of deterministic eruption forecasting have only been published when predictions were successful and only by using VT events, following the FFM theory. The objectives of this Chapter are (1) to analyse the results of automatic classification of seismic signals for each target volcano and to compare the seismic activity to the reported volcanic activity, (2) to identify acceleration patterns for different classes of precursors for one shield volcano and two strato-volcanoes, (3) to quantify the number of precursor increases leading or not to eruptions, but also eruptions that are not preceded by seismic precursors; this point will help to have an idea of false alarms and forecast failure, (4) to show the interest of automatic classification.

These objectives will be fulfilled through the analysis of the seismic precursors of each studied volcano. The first case concerns the basaltic shield volcano Piton de la Fournaise (PdlF), which is a well-known edifice, and whose precursory activity is principally composed of VT events (Peltier et al., 2009). Then, I propose to move on towards andesitic strato-volcanoes. The 'hundred-year' eruption of Merapi volcano occurred in 2010 and displayed many types of volcano-seismic events. It is a perfect target to emphasise the interest of the automatic classification and of forecasting volcanic eruptions in a densely populated area. Complexity is then increased with the case of Volcán de Colima, for which Arámbula-Mendoza et al. (2011) reported that LP activity is a good precursor of vulcanian explosions, but seems more challenging for the use of FFM.

3.2 Piton de la Fournaise (La Réunion island, France)

Introduction

The Piton de la Fournaise (PdlF) volcano is a basaltic shield volcano situated on the French island of La Réunion in the western Indian Ocean (Figure 3.1). This volcano results from the activity of a hot spot (Duncan, 1990) and started erupting about 66 millions years ago with the Deccan Traps formation (Courtillot et al., 1986). The PdlF is one of the most active volcanoes in the world, with an average of one eruption every ten months. About 83 volcanic events occurred since 1985: 54 eruptions, two summit pit crater formations, 26 seismic crisis that were not followed by an eruption and one caldera collapse (Peltier, 2007). It is intensively monitored by 24 seismic stations (short period and broadband), a network of tens of permanent GPS and seven tiltmeters. It has been observed that every eruption or intrusion has been preceded by weeks of inflation of the edifice and by some hours to some weeks of increasing number of VT events. This well-known laboratory volcano is thus a perfect candidate to test the real-time forecasting method based on precursory seismic activity developed in this thesis.

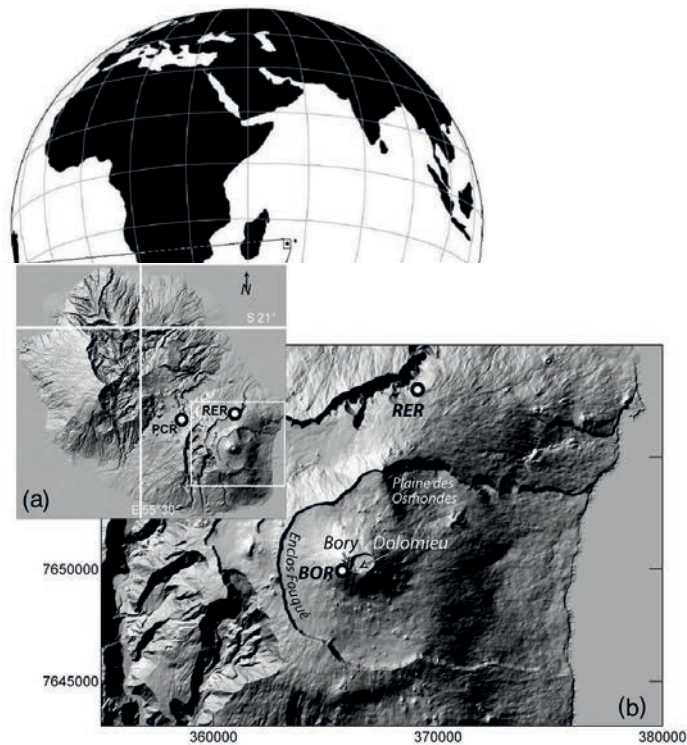


Figure 3.1: Geographic context of the Piton de la Fournaise volcano. (a) Located south-east of La Réunion island in the Indian Ocean. (b) Location of the eruption areas: Bory and Dolomieu crater and Enclos Fouqué caldera. BOR is the seismic station used in this study. Figure adapted from Roult et al. (2012) and Schmid et al. (2012).

Two periods of frequent eruptions have been contemporary observed, with volcanic activity that occurred mainly inside the caldeira of Enclos Fouqué, in 1972-1992 and 1998-2014. However, two eruptions outside the Enclos Fouqué in 1977 and 1986, both of them threatening populations. Roult et al. (2012) classified the volcanic events as a function of their location: eruptions that remain inside the summit craters (summit eruptions), eruptions that propagate laterally outside the crater (proximal eruptions) and eruptions that start outside the summit crater (distal eruptions). All eruptive cones and fissures are located in a 2 to 3 km radius around the summit of the volcano (Figure 3.1). Regarding the eruption locations, there is no major threat for the populations so the societal challenge of forecasting volcanic eruption in this context is limited. However, the active tourism in the area and the presence of infrastructures justifies the need to forecast eruptions.

PdlF eruptions are thought to be triggered by magma overpressure within a reservoir located below the Dolomieu crater approximately at the sea level (Nercessian et al., 1996; Peltier et al., 2005). However its geometry, its precise location and the connection with a deeper magma reservoir is still in debate. Lénat and Bachèlery (1990) argue for the presence of sills and dykes between 0.5 and 1.5 km under the Dolomieu crater. Grasso and Bachèlery (1995) suggest that magma bodies develop as a hierarchical network that takes the form of a multi-lens reservoir. Finally, it seems that eruptions are purely driven by volcano dynamics since there is no seismically active flank sliding and no tectonic activity.

In this study, I focus on the 2000-2010 eruptive period which is accurately reported and described in Roult et al. (2012). Contrary to other previous periods, these eruptive episodes display long-term geophysical precursors (Peltier et al., 2009). In the first section, I describe the precursors of the eruptions in parallel with the observed seismic activity that I automatically classified with the VSR. In the second section, I highlight the seismic precursory patterns and I quantify the number of seismic accelerations preceding eruptions and intrusions, as well as the number of eruptions that are not preceded by seismic acceleration.

3.2.1 Volcanic activity and precursors

The dense monitoring network of PdlF volcano allowed for studying the precursory potential of different geophysical observables. In the periods 1972-1992 and 1998-2000, Peltier et al. (2009) did not observe any significant precursory inflation of the volcano before eruptions. They observed less precursory VT activity (tens of events per day) than after the year 2000 (hundreds of events per day). Peltier et al. (2009), Roult et al. (2012) and Schmid et al. (2012) studied strong and significant seismic and deformation precursory activity after the year 2000 which might reflect some changes in the magma plumbing system in comparison with older eruptions. Using seismic noise correlation techniques, Brenguier et al. (2008) and Duputel et al. (2009) have highlighted the decrease of seismic velocity within the edifice few

weeks before the eruptions of July 1999 to December 2000, July 2006, April 2007 and January 2006 to June 2007. Seismic velocity decreases are thought to reflect edifice inflation because of increased magma pressure before eruptions. These studies suggest a magma transfer from a shallow magma storage towards the surface, starting with the damage of the magma storage area further leading to dyke propagation and eventually an eruption. The hypothetic major changes of the plumbing system before and after 2000 could be explained by changes in the geochemical composition of the magma (Peltier et al., 2009). Consequently, the presence of precursors of volcanic eruptions at PdIF seems to strongly depend on the geometry of the plumbing system.

Collombet et al. (2003), Grasso and Zialapin (2004) and Schmid et al. (2012) specifically highlight the precursory potential of seismic activity for forecasting volcanic eruptions between 1998 and 2006. These authors use pattern recognition techniques to forecast volcanic eruptions based on the precursory seismicity (Grasso and Zialapin, 2004) and on precursory seismic velocity variations, seismic rates and deformation together (Schmid et al., 2012). Schmid et al. (2012) analyse separately the prediction potential of each precursors and observe that the seismicity was the best precursor. The best forecast performance was however obtained using the three observables together. Since the precursory seismicity displays a mean power-law trend before eruptions (Collombet et al., 2003; Grasso and Zialapin, 2004; Schmid et al., 2012), it seems to be a good observable to forecast volcanic eruptions of the PdIF volcano using the FFM.

Catalogue of seismicity

I carried out the automatic classification of the PdIF seismicity between 2000 and 2007, with a performance reaching almost 90% of good recognition on average (Figure 3.2). The study is completed by the catalogue of the PdIF volcanic observatory (OVPF) for the period 2008-2010. The manual database has been built following the catalogue of the PdIF volcanic observatory considering the classes of events rockfalls (RF), VT and noise (SIL). Other classes such as LP or tectonic events have been ignored because they are rare in comparison with the number of VT and rockfalls. The seismic station chosen for the automatic classification is one of the closest station from the summit (BOR, vertical component, Figure 3.1). It is a short period seismometer L4C 1Hz Mark Products. This choice is justified based on the experience of the observers who manually pick the events on this seismic station because it displays the clearest waveforms.

Seismic events of small amplitude are not always recorded by the seismic station nor classified by the VSR. It follows that catalogues of seismicity are never complete, which can lead to a biased analysis. It is possible to correct the catalogue incompleteness by computing a threshold magnitude defined as the lowest magnitude above which all the earthquakes are

```

----- Overall Results -----
WORD: %Corr=87.38, Acc=78.97 [H=374, D=24, S=30, I=36, N=428]
----- Confusion Matrix -----
      RF  SIL  VTs  Del [ %c ]  %Corr  %Acc
RF  101  0   9   0 [91.8]  91.82  76.36
SIL  9   178  5   23 [92.7]  82.79  77.67
VT   7   0   95   1 [93.1]  92.23  84.47
Ins  17  11   8   -----
      class_mean:  88.95  79.50
-----

```

Figure 3.2: Confusion matrix of the blind test corresponding to the configuration used to process the automatic classification of volcano-seismic events, for the classes VT, rockfall (RF) and noise (SIL). Rows correspond to the number of true events in each class and columns present events recognised by the VSR in each class. The line denoted WORD shows the mean success rate all classes mixed together. H is the total number of events that have been well-classified, D the number of deleted events, S the number of substitutions, I the number of insertions and N the total number of events tested.

detected (Rydelek and Sacks, 1989). In the case of the PdIF catalogue, I computed the duration magnitude of each recognized event, following the PdIF observatory procedure, as $M_d = 2\log(T) + 0.0035D - 0.87$ (Lee and Lahr, 1975), where T is the duration of the signal in seconds and D is the epicentral distance in kilometers (which is neglected here because the station is close to the crater). I then estimate the magnitude of completeness M_c of the automatically classified catalogue is estimated by fitting the Gutenberg-Richter law to the observed frequency-magnitude distribution (Figure 3.3). The Gutenberg-Richter law is defined as $\log_{10}(N) = a - b(m - M_c)$ where N is the number of events with magnitude m , and a and b describe the earthquake productivity and the relative distribution of earthquakes size, respectively (Gutenberg and Richter, 1944). The magnitude of completeness M_c corresponds to the drop in the number of events as a function of magnitude, i.e. the magnitude for which the data departs from the linear trend of the Gutemberg-Richter law (Zuniga and Wyss, 1995). For the catalogue obtained through the automatic classification of VT events, the Gutenberg-Richter law has been adjusted with a routine provided by David Marsan (ISTerre, Université Savoie-Mont Blanc, Marsan and Daniel, 2007). I obtain a magnitude of completeness $M_c = 1.47 \pm 0.01$, which correspond to a minimum duration of completeness of 3.2 seconds. Consequently, the catalogue is truncated below this magnitude in the following, i.e. I remove all events that last less than 3.2 s.

The magnitude of completeness of the catalogue obtained with the VSR is higher than the magnitude of completeness calculated for the catalogue of the observatory ($M_c = 0.5$, which corresponds to a duration of 2 seconds). However, it seems difficult to compare the completeness of these catalogues because the beginning and end of a signal classified by the VSR always include a piece of noise, which is not the case for the catalogue of the observatory. A comparison of both catalogues is presented in Appendix A.

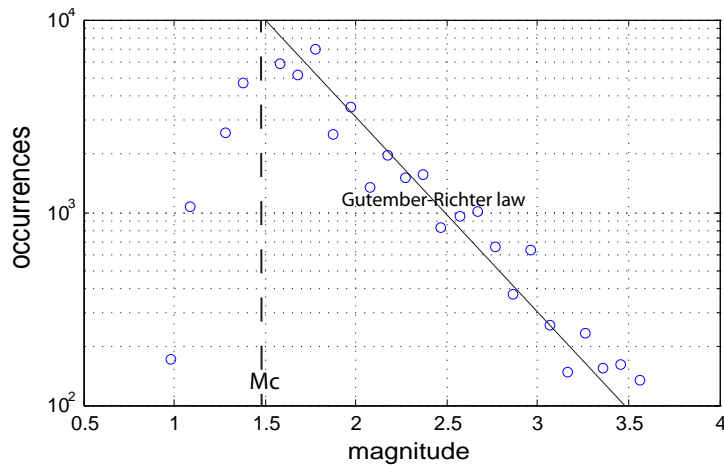


Figure 3.3: Number of VT occurrences as a function of their duration magnitude. The black line is the best fit of the Gutenberg-Richter law. M_c denotes the magnitude of completeness.

Seismic precursors

The seismic activity and eruptions from 2000 to 2010 are reported in Figure 3.4. In total, 30 eruptions, 2 collapses and 20 intrusions (18 of them occurred between 2008 and 2010) were reported in the period 2000-2010 by Roult et al. (2012). Following their eruption catalogue and definitions, eruptions that are separated by a few hours or days, are considered as one unique eruptive event.

According to the seismic activity automatically classified in this period Figure 3.4 and the study by Roult et al. (2012), 25 seismic crisis are not followed by an eruption. This activity might be the sign of magmatic intrusions. On the other hand, all eruptions are preceded by an increase of VT seismicity. It suggests that VT activity is a good precursor of magma intrusions at PdIF. In total, 25/55 intrusions (46%) did not reach the surface to form an eruption in this period. In terms of predictions based on seismicity, 46% of the precursory VT activity would have led to a false alarm. Most of these false alarms would have occurred in 2008 because about half of the intrusions occurred during this period.

Most of the time, the number of rockfalls is low, varying from 0 to tens of events per day. Their number usually increases during eruptions because of lava flows. Finally, it sometimes increases before eruptions and can be interpreted to reflect edifice instabilities, either due to the edifice deformation or simple gravity collapse. It would be interesting to compare deformation data and rockfall activity, but it is not the scope of this thesis.

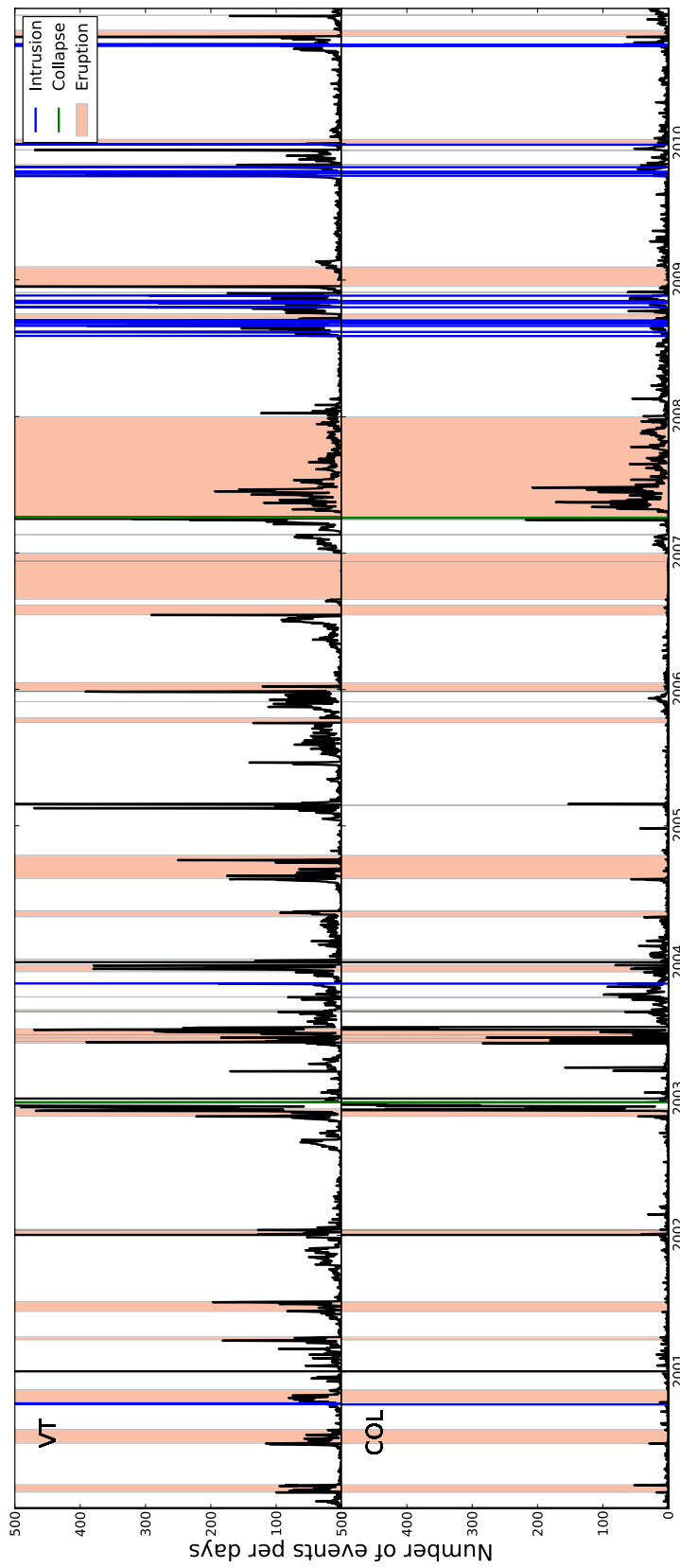


Figure 3.4: Catalogue of seismicity obtained by automatic classification of volcano-seismic events for the period 2000-2007 at PdIF volcano. Number of VT events per day is represented on the top panel and the number of rockfalls (COL) per day on the bottom panel. Eruption periods are embodied by red areas, intrusions by blue lines and major collapses by green lines.

The durations of the eruptions are variable, from hours to months, and they do not especially correlate with the duration or the intensity of the precursory seismicity. Eruptions are usually observed as lava fountains coming from fissures. In the period of study, we also observe the formation of a pit crater (small scale caldera) in 2002 and the collapse of the whole Dolomieu floor in 2007, both preceded by an intense rockfall and VT activity.

Once the precursory sequences have been identified and the number of increasing sequences not associated to eruptions is known, we can estimate 46% of the seismic increases would have led to a false alarm if prediction were only based on the detection of abnormal rate of seismicity, but we would never miss an eruption. The aim is now to identify patterns of increase of the precursory seismic activity leading to eruptions in order to determine if predictions can be carried out with the FFM.

3.2.2 Precursory seismic patterns of effusive eruptions

This section zooms on the precursory patterns of VT activity before eruptions in the aim to present the data that will be used to carry out eruption predictions with the FFM in Chapter 5. For readability the data are presented in a cumulative form and I describe them in a qualitative way. A more quantitative approach will be adopted in Chapter 5 when applying the FFM to non-cumulative data. Among the list of eruptions analysed, it is important to quantify the number of eruptions preceded by precursors, and among these events the number that are actually suitable precursors for the application of the FFM, i.e. those that have an accelerating power-law pattern with an asymptote that gives the time of eruption. However, identifying such power-law patterns is not straightforward in a first qualitative approach. Thus I will only identify accelerating pattern keeping in mind that cumulative accelerating patterns do not necessarily imply a power-law pattern for the corresponding non-cumulated data (see Chapter 4, Section 4.3.2.1).

Figure 3.5 presents precursory patterns of VT activity prior to 30 eruptions. For a better readability, they are arbitrarily classified in three different precursory durations: 10 h, 20 h and 30 h. Although most of the patterns are very different from one eruption to another, typical repetitive patterns can be highlighted. Most of the eruptions are preceded by few hours of VT swarm. Some of the patterns present a single acceleration of VT activity before the eruptions (e.g. 23 June 2000). Others present accelerations 5.5 to 7 days before the eruption (e.g. 21 September 2008, 27 November 2008, 5 November 2009). Finally, other patterns display increasing steps before the eruptions (e.g. 27 March 2001). Most of the observed precursory sequences display a mean accelerating trend. Finally, a seismic quiescence is usually observed between the accelerating patterns and the final VT swarm before eruptions (e.g. 14 December 2008).

In average, it seems that most of the observed precursory patterns are consistent with the

mean power-law of 10 to 15 days emphasised by Collombet et al. (2003) for PdIF eruptions from 1998 to 2001. This precursory pattern of VT reflects the volcano edifice damage close to failure, in response to magma intrusion (Grasso and Bachèlery, 1995). Grasso and Zialapin (2004) proposed a three-step interpretation for the average pattern of 10 to 15 days VT acceleration followed by a period of quiescence and finishing with a sharp increase of seismicity just before the eruption: (1) edifice damage (acceleration of seismicity), (2) onset of the magma flow (seismic quiescence), (3) damage of the open reservoir during fluid flow (sharp seismic increase). In the framework of eruption forecasts using the FFM, it is thus expected to forecast the onset of the magma flow (2) rather than the eruption at the surface itself.

A systematic application of the FFM to these precursory patterns is proposed in Chapter 5 and the results of predictions as well as the applicability of the FFM in this context will be discussed in Chapter 6.

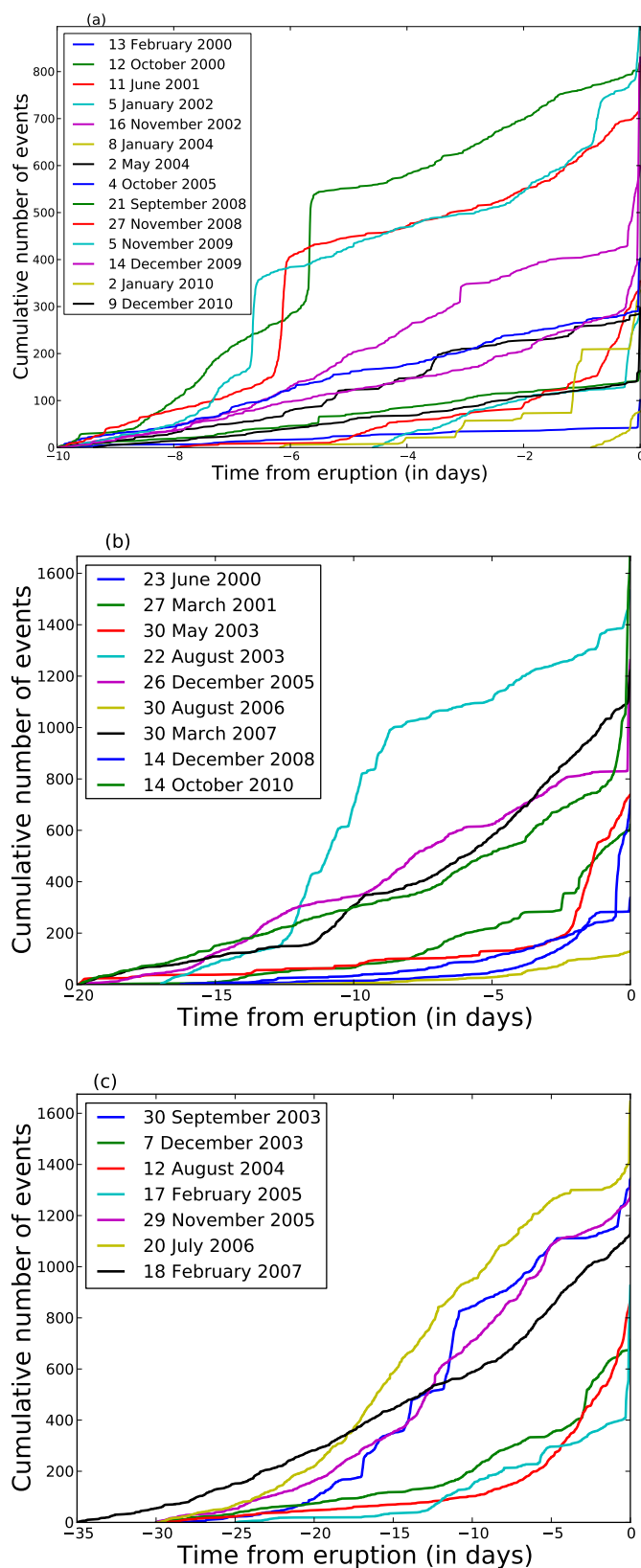


Figure 3.5: Precursory VT patterns of 30 eruptions of the PdlF between 2000 and 2010. For readability, VT events are represented with their cumulative values as a function of time and are sorted by duration before the eruptions: (a) less than 10 days, (b) 20 days and (c) 30 days

on seismic precursors. Their study reveals that the eruption could have been forecast 6 days in advance.

A monitoring network has for long been developed, consisting of tiltmeters and Electronics Distance Measurement (EDM) for deformation measurements, of four short period permanent seismic stations (Mark Product L-4) and 5 broadband stations. Various types of seismo-volcanic earthquakes have been registered before the 2010 eruption, making it a good target volcano to demonstrate the interest of automatic classification of seismic signals both for operational use when hundreds of events occur per day in periods of crisis, but also to extract accurate typical precursory patterns of seismic precursors. It is also a good target to see if the classification of volcano-seismic signals can improve eruption forecasting.

3.3.1 Precursors of the explosion of the 26 of October 2010

Most of Merapi eruptions were preceded by an increase of seismic activity, except in 1986 and 1994. Seismicity is thus a good precursor of eruptions for this volcano.

Surono et al. (2012) and Budi-Santoso et al. (2013) revealed the presence of long-term precursors of the 2010 eruption, consisting of an inflation of the edifice since November 2009 and four seismic swarms in 2009 and 2010. September 2010 was marked by a ground inflation, an increasing number of earthquakes and of their energy, increasing fumaroles temperature and abnormal amounts of H_2S and CO_2 . VT earthquakes hypocenters were localised in two separate clusters. The first one, between 2.5 km and 5 km, was active mainly before the 17 October and interpreted as a rapid magma ascent, damaging the surrounding rock. The second one was localised between 0 and 1.5 km below the summit and interpreted as the damage of the 2006 plug (Budi-Santoso et al., 2013). The eruption started with an explosion on the 26 October 2010. It was preceded by the acceleration of the deformation, of the number of seismic events and of their energy. The acceleration of the energy of the seismic activity before the 2010 eruption was about 3 times those of previous eruptions. Then, a period of quiescence took place between the 26 and the 28 October and small explosive events occurred until the 1 November. This period was then followed by a rapid dome growth, accompanied with LP events and small explosions, to finish with a large explosion the 5 November. Lava dome growth stopped the 8 November.

The seismic activity of Merapi volcano is classified as VT events, multiphase or hybrid events (MP), LP events, guguran or rockfalls (RF), tremors (T) and regional tectonic events (REG). Volcano-tectonic events are classified into deep VTs (VTA) and shallow VTs (VTB). The difference of amplitude of the first arrival between the PUS and DEL stations (Figure 3.6) can be used to recognise these two sub-classes.

MP earthquakes are thought to be related to the formation of the lava dome (Hidayat et al., 2000; Ratdompurbo and Poupinet, 2000). Ratdompurbo and Poupinet (2000) reported that

slow dome growth is usually characterized by some MPs, LPs, rockfall seismicity, and VTs while more MPs occur during periods of rapid lava dome growth. The rate of MPs thus seems to be correlated with the growth rate of the lava dome.

I refer to Budi-Santoso et al. (2013) for an extensive description of the seismic activity related to the 2010 eruption.

Catalogue of seismicity

The training database required for the automatic classification is based on the manual classification of volcano-seismic signals described in Budi-Santoso et al. (2013). However, subclasses of VT have been joint into a unique class because they can only be discriminated using two seismic stations, which is not possible to carry out with the VSR. The station used for the automatic classification is PUS which is the closest short period station from the summit (Figure 3.6). The results of the blind test carried out by training 66% of the manual database and recognising the other 33% are presented in Figure 3.7.

WORD: %Corr=83.80, Acc=75.35 [H=238, D=17, S=29, I=24, N=284]

----- Confusion Matrix -----											
	COL	LP	MP	REG	SIL	VT	Del	[%c]	%Corr	%Acc	
COL	45	0	9	2	0	0	6	[80.4]	72.58	64.52	
LP	0	14	2	0	0	2	0	[77.8]	77.78	77.78	
MP	1	0	64	2	0	2	4	[92.8]	87.67	79.45	
REG	0	0	1	11	0	0	0	[91.7]	91.67	25.00	
SIL	0	0	2	1	57	0	6	[95.0]	86.36	78.79	
VT	0	0	5	0	0	47	1	[90.4]	88.68	88.68	
Ins	5	0	6	8	5	0					
									class_mean:	84.12	69.04

Figure 3.7: Confusion matrix of the blind test of the automatic classification of volcano-seismic events at Merapi volcano, for the classes VT, LP, rockfall (COL), hybrid (MP), regional tectonic earthquakes (REG) and noise (SIL). Same legend as Figure 3.2.

The magnitude of completeness of this automatically classified catalogue of seismicity is computed following the method explained in Section 3.2. I obtain a magnitude of completeness $M_c = 2.67 \pm 0.17$ for the catalogue of VT and a magnitude $M_c = 2.3 \pm 0.06$ for the catalogue of MP.

Seismic precursors

Figure 3.8 displays the histogram of seismicity for the classes of interest (VT, LP, rockfall/COL, MP). The number of events per day are represented as a function of time before the 5 November 2010 eruption. There are two clear accelerations of the number of VT events before the first volcanic event of the 26 October. This acceleration starts more than one month before the explosion and the clear accelerating part begins about 6 days before this eruptive event. Very few LP are recognised during this period even though a clear increase from 0 to 5 events can

be noticed some days before the explosion. The number of rockfalls remain high and constant with about 100 events per day during a month followed by an acceleration 6 days before the explosion. Hundreds of MP occurred per day during about one month and a sharp increase started the 12 October, reaching about 600 events per day to then remain fairly constant until the explosion.

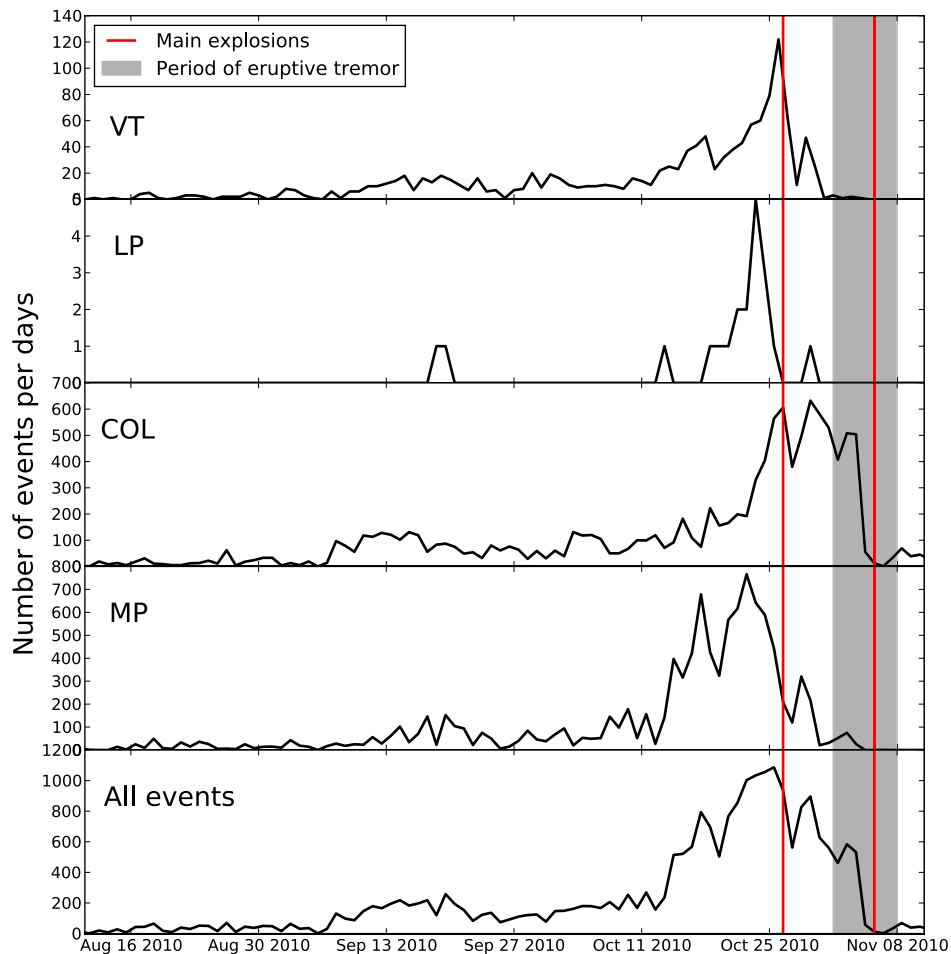


Figure 3.8: Catalogue of seismicity obtained by automatic classification of volcano-seismic events for the 2010 eruption. From the top to the bottom: number of seismic events per day as a function of time for the classes of VT, LP, rockfalls (COL), MP, and all events together, respectively. The red lines represent the main explosions and the grey area the period of eruptive tremor.

No observation of dome growth has been reported before the 26 October explosion, but a significant number of MP events were noticed. Ratdomopurbo (1991) and others associate MP activity to lava dome growth, thus we can suspect that this type of shallow seismicity is linked with the emplacement of a magma body as a plug in the magma conduit, favouring a pressure increase leading to the explosion.

The long acceleration in the number of VT before the explosion is a very important information concerning the damage of the edifice and the occurrence of an imminent failure. This observation would not have been possible by taking into account all the classes of events together (Figure 3.8) as the acceleration of VT events is hidden by the activity of other types of events, and mainly by the dominant classes MP and rockfalls. The classification of seismo-volcanic signals is thus of major importance for an accurate observation of precursory seismic patterns at Merapi volcano. We will investigate in Chapter 5 if this classification of volcano-seismic signals improves the results of eruption predictions carried out with the FFM.

3.4 Volcán de Colima (Mexico)

Introduction

Volcán de Colima is an andesitic strato-volcano of 3860 meters height, located in the western part of the Mexican Volcanic Belt resulting from the subduction of the Coco Plate under the North American Plate (Figure 3.9). It is the most active volcano of Mexico and displays a wide spectrum of eruption styles including small phreatic explosions, major block-lava effusions and large explosive events (Gonzalez et al., 2002). Some villages are settled on the flank of the edifice such as La Yerbabuena, which is the closest one (8.2 km from the crater). About 5,000 people live at less than 15 km from the active vent and the major town of Colima (250,000 inhabitants) is located at 30 km from the crater. Although a great part of this population does not live in high risk areas, a non-negligible number of persons are directly exposed to risks of pyroclastic flows, explosions, ash falls, lahars and lava flows. The effort in developing deterministic real-time eruption forecast in this context is thus justified by important societal challenges.

Luhr and Carmichael (1980) proposed that eruptive cycles at Volcán de Colima renew every 100 years, characterised by dome growth and intermittent explosive activity, culminating in a Plinian eruption. Based on geochemical studies, Luhr (2002) identified the previous two cycles ending in 1818 and 1913 by Plinian eruptions, where ash columns were sent up to 10 km height producing pyroclastic flows, reaching distances as far as 15 km away. They hypothesised that Volcán de Colima is now touching the end of the actual cycle that might finish with a Plinian eruption, such as the two preceding eruptive cycles.

The recent typical activity of Volcán de Colima is composed of growths of the lava dome, followed by periods of vulcanian explosions usually preceded by seismic precursors (Arámbula-Mendoza et al., 2011; Varley et al., 2010b). Major vulcanian explosions are sometimes associated with pyroclastic flows going down to several kilometers away from the crater. In this study, I consider vulcanian style explosive events of moderate to major size, i.e. that have been reported by the civil authorities and the University of Colima. Their plumes can be sent hundred meters to several kilometers above the summit. Moreover, ballistic bombs can be sent as far as 5 km from the crater. The type of effusive activity depends on the dome extrusion rate. When extrusion rate is slow, it is followed by blocky lava flows pouring on the flank of the volcano up to 4 km away from the crater. These effusive phases can last up to years. The remaining domes are in general blasted by vulcanian explosion periods. When extrusion rates are high, the effusive phase can be very short (maximum one day) and usually terminate with a vulcanian explosion.

The RESCO (Red Sismologica Telemetrica del Estado de Colima) operates the seismic monitoring network of Volcán de Colima. It is composed of four short period stations and two

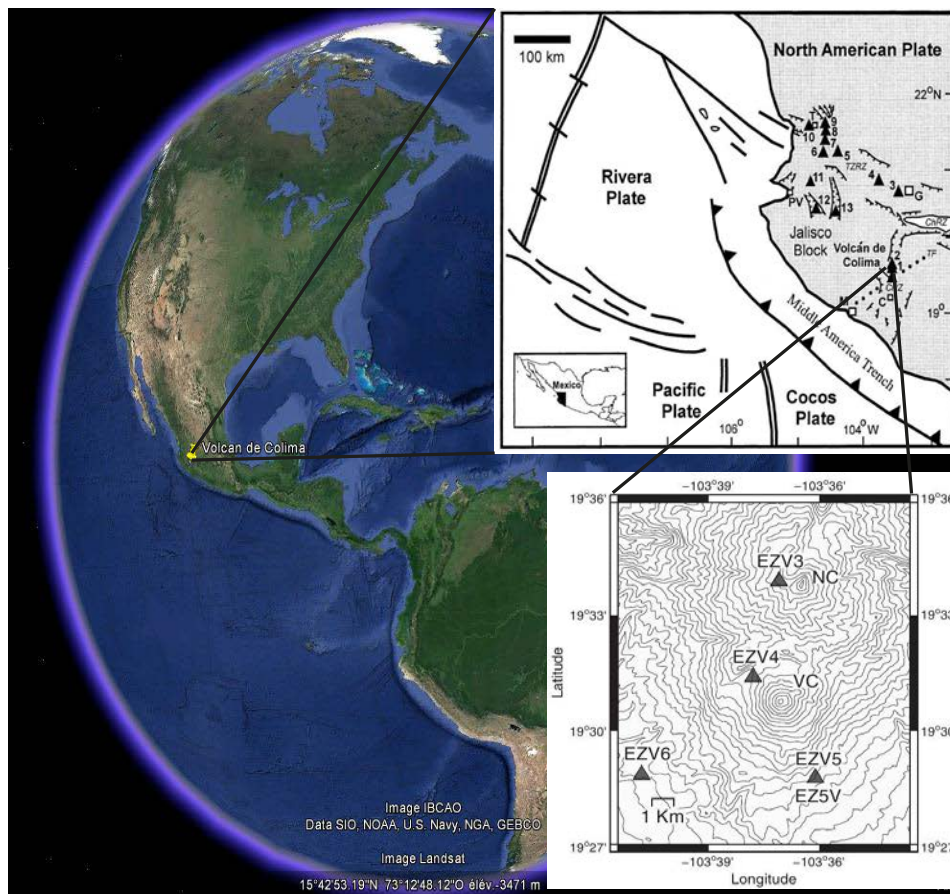


Figure 3.9: Geographic situation of Volcán de Colima, Mexico (adapted from Zobin et al. (2002) and Arámbula-Mendoza et al. (2011)). Upper right: tectonic context. Lower right: Seismic network. Triangles represent the permanent short period seismic stations. VC denotes the Volcán de Colima edifice.

broadband stations (Figure 3.9). In this study, I analyse the seismic record of the closest short period station (EZV4, 1.8 km from the crater), between 1998 and 2011.

Seismic stations at Volcán de Colima record a great diversity of seismic signals. First of all, it is common to observe regional tectonic earthquakes. Small to big explosion signals are also recorded, as well as rockfalls. Tremors sometimes appear but the major activity is represented by LP events and VT events, depending on the volcanic phase.

In this section, I describe the volcanic activity and its associated precursors for the most active periods of Volcán de Colima from 1998 to 2011. In particular, I focus on the different types of seismic activity automatically classified and associated with the different eruption styles described above. Finally, I analyse the precursory patterns of seismicity prior to vulcanian explosions.

3.4.1 Volcanic activity and precursors

The contemporary eruptive cycle of Volcán de Colima began in February 1991, preceded by an increase of VT and LP events. This activity preceded the extrusion of a lava dome. The dome finally collapsed and small explosions were then observed. The effusive activity was associated with rockfalls and ended by September 1991. A new period of activity then started at the beginning of July 1994 with an increase of VT events followed by LP swarms by the end of July. This precursory seismic activity led to a major vulcanian explosion the 21 July. The activity then ceased until the beginning of the period of study in July 1998. Unfortunately, seismic records from 1991 to 1997 were not available to complete this study, and continuous records are running only since 1998.

Catalogue of seismicity

Colima volcano is the target that has been used in Chapter 2 to explain the automatic classification processing. All details concerning the manual database are thus explained in Chapter 2. The magnitude of completeness of the catalogue was calculated at $M_c = 2$, following the method explained for the last two target volcanoes (Section 3.2 and 3.3). All seismic rates are thus truncated below this magnitude of completeness, except for LP events because their number were then too limited, especially for short duration precursory patterns preceding vulcanian eruptions.

An average success rate of 80% is obtained for the automatic classification. The corresponding confusion matrix is displayed in Chapter 4, Section 4.3.2.1 (Figure 4.1).

Precursors

In the following, I present the precursory seismic activity at Volcán de Colima on a year by year basis. Of course, this splitting is arbitrary and does not reflect exactly the periods of activity of the volcano.

1998 eruptive activity (Figure 3.10). This year was marked by a vulcanian explosion the 6 July and a lava dome extrusion the 20 November, followed by a lava flow. These major eruptive events were both preceded by months of anomalous seismicity. Seismic and volcanic activity are summarised as follows:

- March, May, June-July: VT swarms. This seismicity probably reflects magma movements in depth (Zobin et al., 2002).
- 6 July: vulcanian explosion preceded by some days of VT and LP activity. This precursory activity probably reflects magma movements making its pathway through the conduit, further leading to the explosion.

- July-October: seismic activity characterised by some LP and VT swarms.
- End of October: the LP activity sharply began, followed by an increase of VT events.
- November 1998: acceleration of the VTs prior to the dome extrusion, while the energy of LP remained at a high constant level. The number of rockfall events also accelerates. This seismic activity might reflect a great amount of magma making its pathway in the conduit.
- 19 November: observers noticed a fumarolic plume but no clear observations were possible because of cloudy weather (Navarro-Ochoa et al., 2002). Ongoing seismic activity. I interpret this observation as the enlarging of the conduit.
- 20 November: fresh lava observed in the crater in the morning. At the end of the day, the seismicity dropped to a lower level.
- 21 November: in the morning, the crater was filled by a lava dome. A rapid dome growth consequently occurred in 24 h ($4.4 \text{ m}^3/\text{s}$, Zobin et al., 2002). The dome started to pour out the crater by the morning of the 21 November (Navarro-Ochoa et al., 2002), which was associated with an increase in the number of rockfalls.
- end of 1998: lava flow continues to advance, marked by a high level of the rockfalls rate.

For this period, two swarms of VT events were not followed by an eruption and are interpreted as magma movements in depth. The other major seismic events were precursors of a vulcanian explosion and of a dome extrusion.

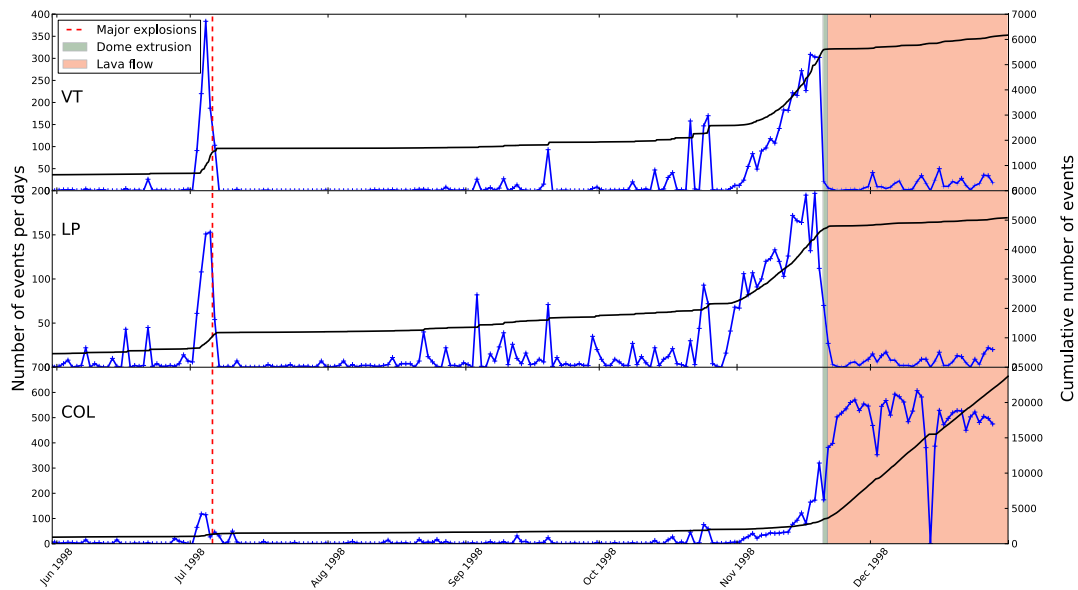


Figure 3.10: Rate of events (blue line) and cumulative number of events (black line) as a function of time for the year 1998 at Volcán de Colima. The red vertical dashed line represents the vulcanian explosion, the green area the period of dome extrusion and red area the period of lava flow, with the dome pouring out of the crater. Top: VT events. Middle: LP events. Bottom: Rockfalls.

1999 eruptive activity (Figure 3.11). This year is mainly characterised by a vulcanian explosion period, destructing the dome formed at the end of 1998. This vulcanian activity is composed of 4 major explosions.

- January: the November 1998 lava flow continues, accompanied with numerous rockfalls. A mean acceleration trend of LP activity is observed until the end of the month. A sharp increase of VT activity is also noticed at the end of the month. This phase can be interpreted as a new injection of magma.
- beginning of February 1999: end of the lava flow that began the 20 November 1998. This phase is accompanied with a decrease of all kind of seismicity, which still remained at high level.
- 10 February: major vulcanian explosion. The shockwave of this explosion broke windows and was felt and heard in the city of Colima. It was reported as the biggest explosion in the last 80 years. No clear precursors are observed, even though the level of seismicity was still at a high level since the end of the lava flow.
- end of January to April: exponential decrease of the rate of LP events.
- 10 May: a large explosion was felt and heard in Colima. It was preceded by some VT and LP events but with a rate only slightly above the mean level of tens of LP and rockfalls per days.

- June: degassing and small explosions continued.
- 17 July: major vulcanian explosion. This explosion was preceded by two days of LP increase.
- 21 July: major vulcanian explosion. This explosion was preceded by exhalations but no abnormalous seismic activity that remained at a low level since the explosion of the 17 July. These exhalations may be the sign of an open conduit, probably explaining why there were no seismic precursors.

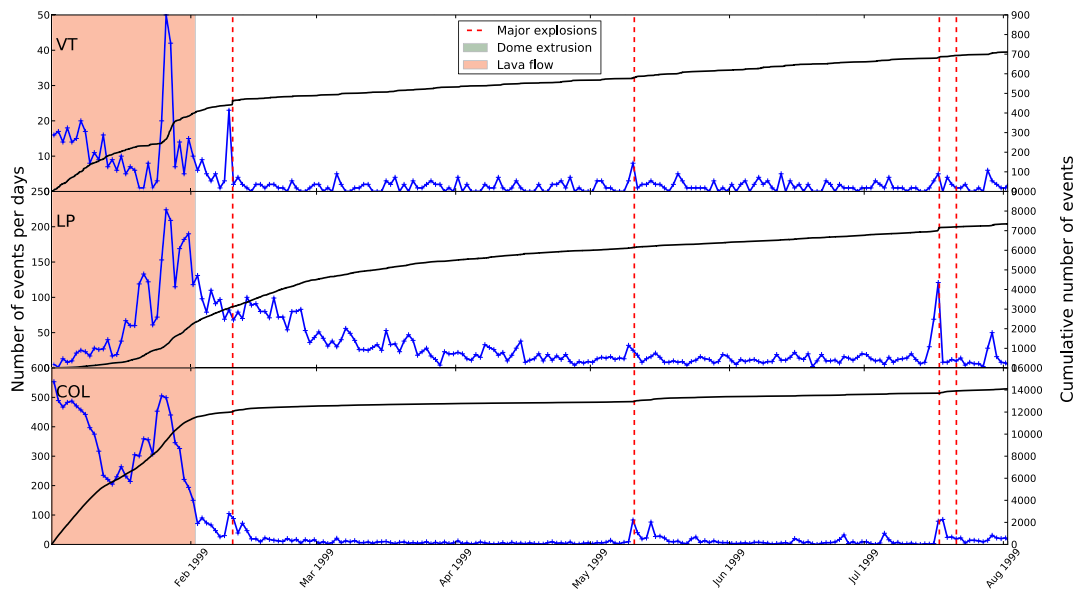


Figure 3.11: Rate of events (blue line) and cumulative number of events (black line) as a function of time for the year 1999 at Volcán de Colima. Red vertical dashed lines represent vulcanian explosions and red area the period of lava flow, i.e. the dome is pouring out of the crater. Top: VT events. Middle: LP events. Bottom: Rockfalls.

In conclusion, 1999 was characterised by a high seismicity that were not necessarily associated with visual volcanic activity. Only one explosion was preceded by an abnormalous increase of LP events. The volcanic activity then remained low until the year 2001, consisting of few microearthquakes and sporadic exhalations.

2001 eruptive activity (Figure 3.12). The volcanic activity of this year is characterised by one vulcanian explosion and a new effusive period that involved a slow dome growth until the end of 2001. The associated seismicity is described as follows:

- 22 February: major vulcanian explosion. This explosion was preceded by 2 days of LP increase.
- 10 May: a new dome appeared aseismically. The extrusion continued until February 2002

when a new lava flow began. The mean extrusion rate is low, probably explaining why there were no associated seismicity.

- 1-30 October: significant increase of LP activity. No visual observations possible during this episode.
- 31 October: a lava spine was observed, that probably grew during the LP crisis that occurred in the period 1-30 October.

As a conclusion, LP activity was a good precursor of the 2001 vulcanian explosion, while no seismicity were recorded during the slow extrusion of the lava dome, except during the probable extrusion of the spine, where the extrusion rate were possibly higher than previously, explaining the increase in LP activity.

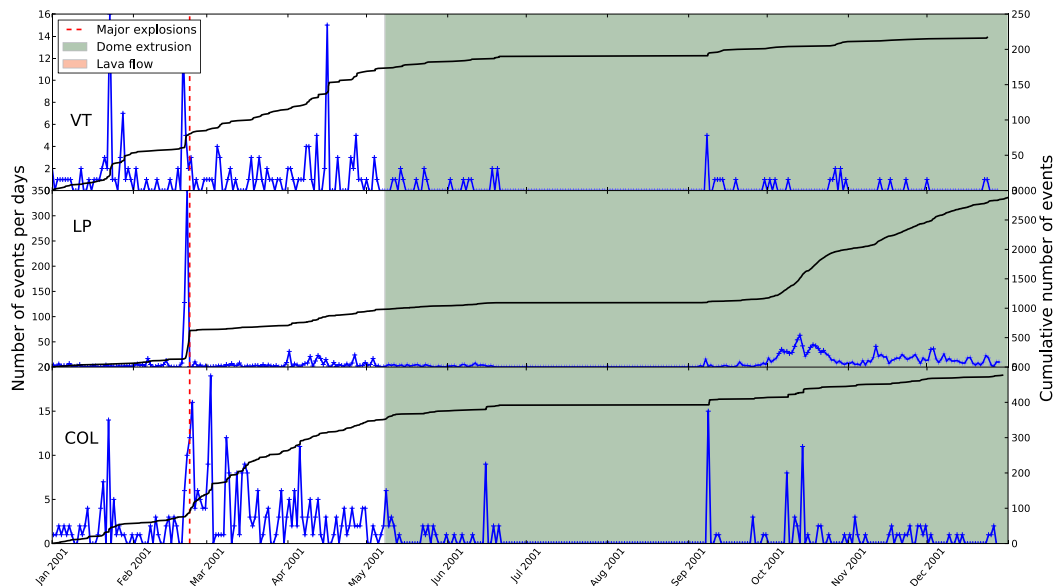


Figure 3.12: Rate of events (blue line) and cumulative number of events (black line) as a function of time for the year 2001 at Volcán de Colima. The red vertical dashed line represents the vulcanian explosion and the green area the period of dome extrusion. Top: VT events. Middle: LP events. Bottom: Rockfalls.

2002 eruptive activity (Figure 3.13). This year is mainly marked by lava flow activity, as well as landslides, lava avalanches and small explosions. The evacuation of hundred of persons occurred in May 2002, because of abnormal changes of geophysical and geochemical precursors. The seismic activity is mainly composed of rockfalls associated with the lava flow activity, but some episodes of VT and LP events were also observed, probably related with injection of magma from depth and degassing.

- End of January: increase of LP activity interpreted as a new magma injection or at least an increase in the rate of lava dome growth.

- 4 February: dome collapse and landslides. This episode is marked as the beginning of the lava flow because lava dome is pouring out the crater. Subsequent rockfall activity then begins to sharply increase, while LP activity decreases.
- March to mid-May: sharp increase of LP activity, then remaining at a constant level while VT events start to accelerate. This peak of VT activity is then followed by a peak of LP activity to finally terminate with a last peak of VT activity while LP events decrease.
- 18 May: scientists reported an increase of the edifice deformation, changes in the chemistry of spring water near the volcano, heightened temperatures recorded on infrared imagery and a change in the composition of ejected rocks. The seismic activity that occurred during March-May might be linked with these changes of geophysical record. A new injection of magma can be hypothesised. This anomalous activity of all kinds of geophysical and geochemical precursors led to the evacuation of hundreds of persons.
- December: slight increase of LP and VT activity.

For the year 2002, the seismicity was of high intensity and all types of signals were recorded. Clear anomalous variations in the number of seismic events were associated with minor volcanic events.

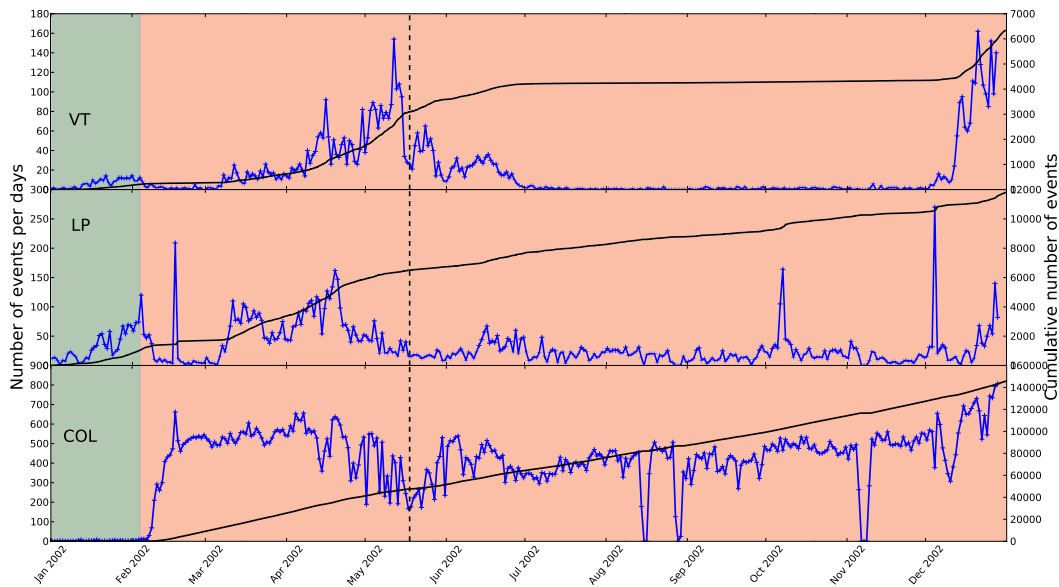


Figure 3.13: Rate of events (blue line) and cumulative number of events (black line) as a function of time for the year 2002 at Volcán de Colima. The red vertical dashed line represents the vulcanian explosion and the green area the period of dome extrusion. The black vertical dashed line represents the recording of anomalous variations of geophysical and geochemical precursors. Top: VT events. Middle: LP events. Bottom: Rockfalls.

2003 eruptive activity (Figure 3.14). For this year, the volcanic activity is marked by the end of the 2002 lava flow and a new period of vulcanian explosions.

- January: significant increase in LP and VT events, probably a sign of new magma injection.
- February: decrease of all kind of seismic events, probably an indication that the effusive period is touching the end.
- Beginning of March: end of 2001 lava flow.
- 17 July: 2 consecutive major vulcanian explosions. The first one was preceded by 24 h of slight LP and VT increase.
- 2 August: major vulcanian explosion. No seismic data available.
- 28 August: major vulcanian explosion. No seismic data available.
- 15 November: major vulcanian explosion preceded by an increase of LP rate.

The two major vulcanian explosions of 2003 that have been monitored were preceded by an increase of LP activity.

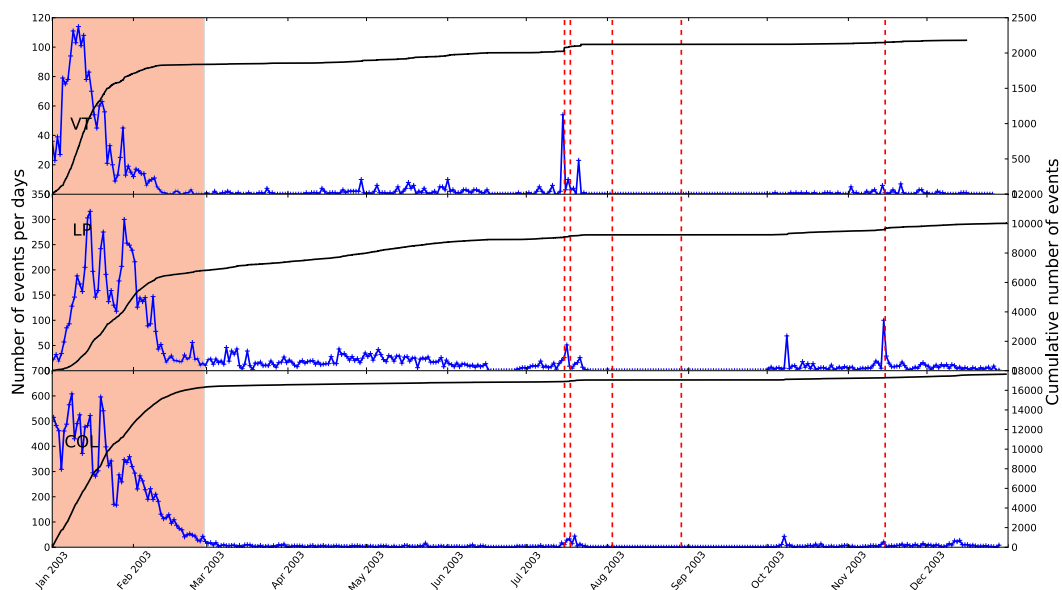


Figure 3.14: Rate of events (blue line) and cumulative number of events (black line) as a function of time for the year 2003 at Volcán de Colima. The red vertical dashed lines represent vulcanian explosions and the red area the period of lava flow. Top: VT events. Middle: LP events. Bottom: Rockfalls.

The 2004 eruptive activity (Figure 3.15). 2004 marks the end of the vulcanian explosion period and the beginning of a new effusive period. The seismicity remained at a low rate with no significant variations until the new extrusion period in October.

- 12 June 2004: major vulcanian explosion. No significant change in the seismic activity. This explosion marks the end of the period of vulcanian explosions that started in 2003.
- 26-28 September: LP activity increases. Probably the sign of magma rising up or of lava dome extrusion.
- 28 September: intensive fumarolic activity and observation of a new lava extrusion, at a mean growth rate of 6 to 8 m³/s (Varley et al., 2010b). Intense LP activity.
- 30 September: lava flow correlated with a high rockfall activity, that was preceded by a peak of LP rate. There is thus a probable increase of the rate of lava extrusion just before the lava poured out the crater.
- First half of October: a peak of VT events is followed by an anomalous peak in the LP activity. Zobin et al. (2008) also reported a peak in the lava dome extrusion rate at this time. The observed peak of seismic activity is thus correlated with a peak of dome extrusion rate, probably reflecting a new injection of magma.
- Beginning of December: end of lava flow.

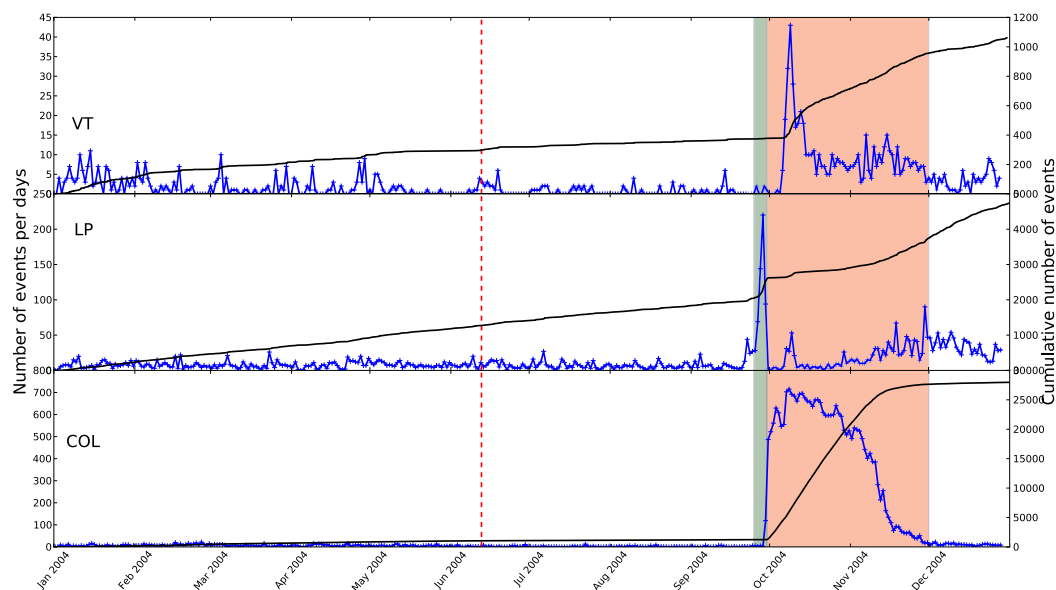


Figure 3.15: Rate of events (blue line) and cumulative number of events (black line) as a function of time for the year 2004 at Volcán de Colima. The red vertical dashed line represents the vulcanian explosion, the green area the period of dome extrusion and the red area the period of lava flow, with the dome pouring out of the crater. Top: VT events. Middle: LP events. Bottom: Rockfalls.

There are two major observations that can be emphasised after the analysis of the volcanic and seismic activity in 2004. The first point is that a major vulcanian explosion was not preceded by an increase of LP nor VT events. Thus, precursors of explosions are not systematic. Second,

an analysis of the extrusion rate by Zobin et al. (2008) confirms the hypothesis that LP activity is probably linked with the rate of lava extrusion.

The 2005 eruptive activity (Figure 3.16). This year is marked by an exceptional vulcanian activity that lasted from February to September. It is reported as the highest production rate of magma since 1998 (Varley et al., 2010a). This vulcanian period is characterised by an alternation between low magnitude vulcanian explosions and larger ones. Here I only focus on moderate and large explosions that have been reported by Arámbula-Mendoza et al. (2011) and Varley et al. (2010a) (Table 3.1). The explosivity culminated in May and June, and most of explosions were associated with lava dome growth. For the other ones, there is no clear evidence of lava dome but it is very likely that they were also associated with ascending magma. The major explosions of the serie produced pyroclastic flows that threatened the population. Forecasting these vulcanian eruptions would have been of great help for decision makers.

Date	Size of the vulcanian explosion	Duration of the precursory LP swarm	Other informations
17 February	moderate vulcanian explosion	10 h	
21 February	moderate vulcanian explosion	7 h	
10 March	major vulcanian explosion	7 h	
13 March	major vulcanian explosion	9 h	
24 March	moderate vulcanian explosion	13 h	
26 March	moderate vulcanian explosion	11 h	
12 April	moderate vulcanian explosion	4 h	
20 April	moderate vulcanian explosion	9 h	
22 April	moderate vulcanian explosion	15 h	
29 April	moderate vulcanian explosion	24 h	
1 May	moderate vulcanian explosion	14 h	
3 May	moderate vulcanian explosion	2 h	
4 May	moderate vulcanian explosion	11 h	
5 May	moderate vulcanian explosion	15 h	
8 May	major vulcanian explosion	21 h	
16 May	major vulcanian explosion	26 h	
24 May	major vulcanian explosion	28 h	lava dome observed
25 May	moderate vulcanian explosion	24 h	
30 May	major vulcanian explosion	48 h	
2 June	major vulcanian explosion	29 h	lava dome observed
5 June	major vulcanian explosion	24 h	lava dome observed
7 June	major vulcanian explosion	12 h	
10 June	major vulcanian explosion	22 h	lava dome observed
13 June	moderate vulcanian explosion	34 h	lava dome observed
5 July	major vulcanian explosion	64 h	
7 July	moderate vulcanian explosion	7 h	
27 July	major vulcanian explosion	56 h	
16 September	major vulcanian explosion	72 h	
27 September	major vulcanian explosion	48 h	

Table 3.1: List of the 29 vulcanian explosions that occurred in 2005 at Volcán de Colima.

In 2005, every significant peak of LP activity is associated with a vulcanian explosion, and every explosion is preceded by an increase of LP events. For Volcán de Colima, LP activity is usually correlated with magma extrusion. There are two possible interpretations for the precursory LP activity of vulcanian explosions: (1) they are all associated with magma extrusion even if lava dome could not be observed before every explosion. In this case, LP activity is associated with magma extrusion, and is not a precursor of the explosion itself; (2) LP activity is not necessarily associated with magma injections, but it might reflect the pressurisation of the magma conduit, further leading to an explosion. In this case, LP activity is directly linked with the occurrence of an explosion. Arámbula-Mendoza et al. (2011), Varley et al. (2010b,a) and Lavallée et al. (2008) hypothesise that LP activity during 2005 might reflect magma fracturing at the conduit wall. For the moment, it is not clear which one of these two hypothesis should be favoured.

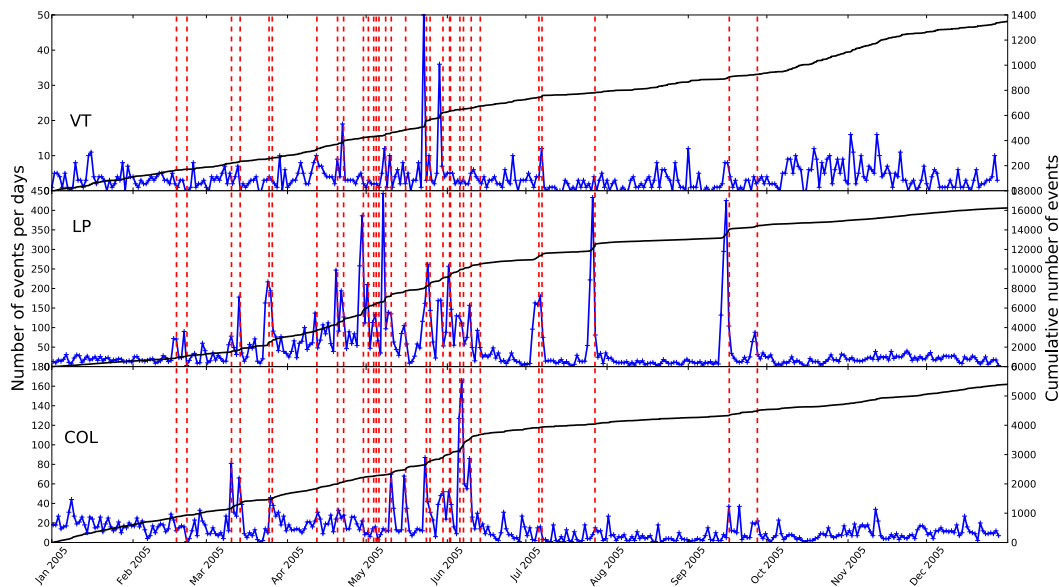


Figure 3.16: Rate of events (blue line) and cumulative number of events (black line) as a function of time for the year 2005 at Volcán de Colima. The red vertical dashed lines represent vulcanian explosions. Top: VT events. Middle: LP events. Bottom: Rockfalls.

Figures of the seismic activity for the period 2006-2012 are displayed in Appendix B. This period of activity is of less interest for this study, since there were no significant variations of the seismicity, and the volcanic activity only consisted of small explosions, exhalations and slow extrusion of domes.

During the years 2006-2007, only small explosions or exhalations took place and a new effusive period began in February 2007 with an extrusion rate of $0.0045 \text{ m}^3/\text{s}$ (BGVN, 2008a), slightly decreasing in the following months and then reaching $0.05 \text{ m}^3/\text{s}$ by the end of the year 2008. This effusive period was accompanied by small explosions/exhalations at a rate of 5 to

10 events per day. The dome almost filled the crater during fall 2009, probably explaining the periodic evolution of rockfalls during this period. The seismic activity remained at a low fluctuating rate of LPs, VTs and rockfalls during the period 2007-2009. The dome started to pour out the crater at the beginning of February 2010, correlated with the increase of rockfall activity. The end of the lava flow occurred in February 2011, but a lava dome still remained in the crater. The volcanic and seismic activity remained low until January 2013, where three moderate vulcanian explosions occurred, further followed by an episode of slow lava extrusion.

Following this review of the 1998-2012 activity, it seems that LP events always accompanied rapid dome extrusions ($>5 \text{ m}^3/\text{s}$), during the periods 1998-1999 and 2004. However, it is not the case for slow dome growth ($<1 \text{ m}^3/\text{s}$), such as in the 2001-2003, 2007-2011 and 2013-2014 activity. Lavallée et al. (2011) proceed to laboratory deformation experiments of Colima lava sample in the period 1998-2010, leading to the conclusion that magmas deform in a brittle manner and produce acoustic emissions, above a certain critical stress. Moreover, Varley et al. (2010b) and Arámbula-Mendoza et al. (2011) observed the same LP families during each LP swarm preceding vulcanian explosions, suggesting a common and repetitive source. These examples support the hypothesis of magma fracturing as being the source of most of LP events at Volcán de Colima. The question arising now concerns the precursory link of LP events with vulcanian explosions: are they directly linked with the occurrence of explosions or are they only linked with magma extrusion, eventually leading to an explosion?

Finally, even if most of the volcanic events at Volcán de Colima are preceded by seismic precursors, some of them have also been identified to occur without precursory seismic activity. Only five anomalous seismic activity were not followed by observable volcanic events during the 14 years of activity: two in 1998, one in 1999, one in 2006 and one in 2009. The various precursory signs of volcanic activity and the various types of volcanic events makes Volcán de Colima an interesting but challenging target to test the deterministic forecasting method developed in this thesis.

3.4.2 Precursory patterns of vulcanian explosions

This section zooms on the precursory patterns of LP activity before vulcanian explosions at Volcán de Colima in the aim to present the data that will be used in Chapter 5 to carry out eruption predictions with the FFM. As already explained for the presentation of the precursory VT patterns at PdIF (Section 3.2.2 of this Chapter), the data are presented in a cumulative form for readability and I describe them in a qualitative way. Among the list of vulcanian explosions analysed, it is important to quantify the number of explosions preceded by precursors, and among these events the number that are actually suitable precursors for the application of the FFM, i.e. those that have an accelerating power-law pattern with an asymptote that gives the time of eruption. Even though similar studies should be carried out on other volcanoes for the

results to be statistically relevant, this analysis on Volcán de Colima is a first clue to have an idea about the potential of prediction of the FFM on precursory LP activity.

For readability, precursory patterns are divided in three arbitrary categories: single accelerations (Figure 3.17a), multiple accelerations or long duration patterns (Figure 3.17b), and other patterns like linear increase of the cumulative number of events or no clear significant variation of the seismicity (Figure 3.17c). Figure 3.17 also displays precursory patterns with a deceleration of the activity some hours before the explosion. Among the 38 explosions studied during 14 years of activity, 2 of them occurred during seismic station breakdowns. From the 36 remaining explosions, 3 of them are not preceded by precursors, 24 precursory activities present an acceleration pattern (Figure 3.17a-b) and the other ones show a linear increase of the precursory seismicity (Figure 3.17c).

Among the 24 identified accelerations, some of them present multiple acceleration patterns (Figure 3.17b). These type of precursors will be challenging to use with the single acceleration model represented by the FFM. To sum up, 17 single accelerations and 7 multiple accelerations are available to evaluate the prediction potential of the FFM on LP events prior to vulcanian explosions.

Although the duration of the precursory LP activity varies from 4 h to almost 2 days, most of the durations remain in a range 4 to 20 h. This duration might be a limiting point in case of emergency since only few hours would be available to evacuate population.

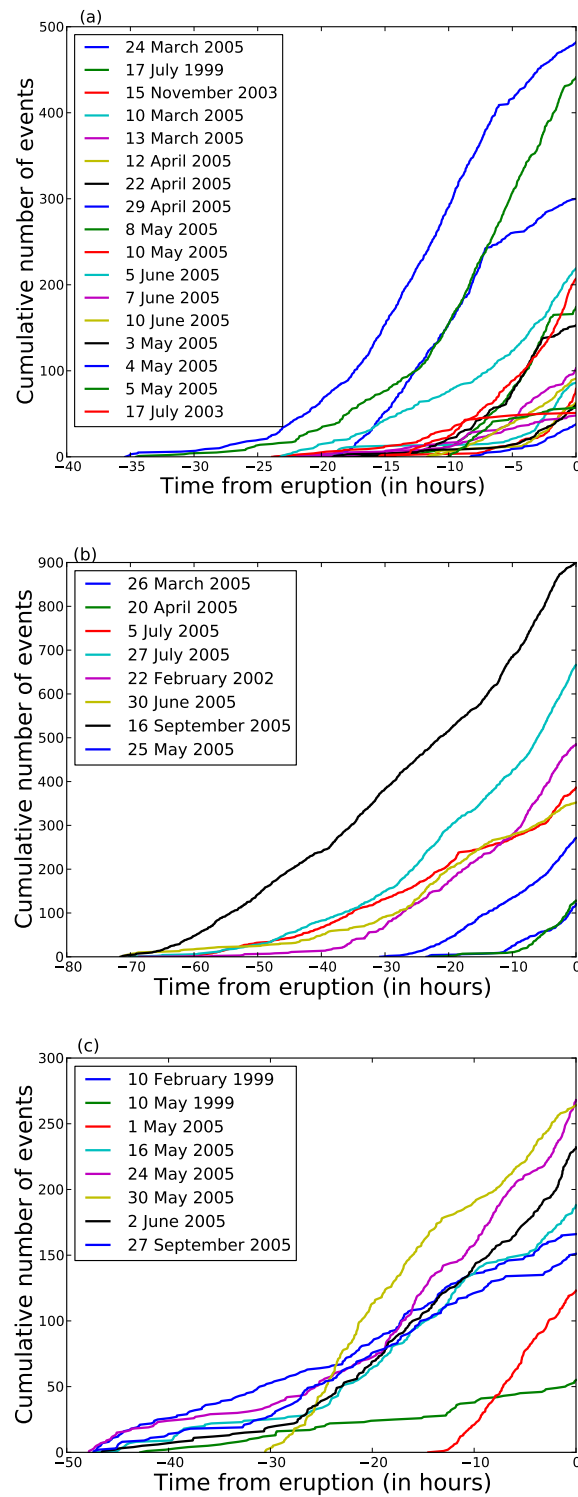


Figure 3.17: Precursory patterns of LP activity prior to the vulcanian explosions at Volcán de Colima, represented as the cumulative number of events as a function of time before the explosion (a) Single acceleration patterns. (b) Multiple acceleration patterns. (c) Other patterns.

3.5 Summary and partial conclusions

The precursory periods of volcano-seismic activity for different volcanic contexts can be summarised as follows:

- **Piton de la Fournaise.** The number of VT events systematically increase before eruptions, with typical durations of 3 to 30 days. Every eruption is preceded by precursory VT activity, and about more than half of the precursory periods present a mean acceleration trend, while the other ones accelerate by steps or just linearly increase. The observation of a final VT swarm just before the eruption is systematic. Finally, 25/55 seismic crisis do not lead to an eruption.
- **Merapi.** Hybrids and rockfalls are the dominant precursory classes of the 2010 eruption. They both sharply increase several weeks before the 26 October explosion. Although the class of VT is not dominant, it shows a clear acceleration starting some weeks before the explosion. This eruption was the first with a VEI=4 which occurred since 100 years. Radomopurbo and Poupinet (2000) and Voight et al. (2000) noticed that all other eruptive activities (VEI=2) were also preceded by VT and MP events, except two of them that are interpreted as gravitational collapses of the summit dome.
- **Volcán de Colima.** LP activity is a quasi-systematic precursor of dome extrusions and vulcanian explosions. Only 3/36 explosions were not preceded by LP events and 24/36 of them were preceded by an acceleration of LP events. VT activity is observed after the long repose time interval and sometimes during lava flow episodes. Accelerating patterns of LP events present single and multiple accelerations, sometimes followed by a deceleration. Duration of the precursory patterns are typically of 4 to 20 h. Probable reasons for the lack of precursors could be an open system or a phreato-magmatic explosion.

In average, most of the considered eruptions are preceded by seismic precursors at Merapi, Colima and PdlF volcanoes. The time scales of the precursory VT activity are very similar from one volcano to another. The time scale of precursory LP activity is shorter than the one of VT activity, suggesting different physical mechanisms.

At Colima and PdlF, more than half of the precursory activities present acceleration patterns that can be used to carry out eruption forecasting based on the FFM. It will be more difficult to draw conclusions on the precursors of the 2010 Merapi eruption as the studied eruption occurs in average once every century. However, it would be worth analysing the other eruptive periods of Merapi volcano which is a perspective of this thesis.

Finally, this analysis would not have been possible without the automatic classification of volcano-seismic signals that allowed for the classification of 22 years of seismic activity in total. Furthermore, the automatic classification of seismic signal allowed for the accurate description of the VT acceleration for the 2010 eruption at Merapi volcano, which would have been hidden

by the other dominant classes otherwise.

We will now see how to carry out eruption prediction by applying the FFM to these precursory sequences.

Chapter 4

Methodology for real-time eruption prediction using the FFM

Contents

4.1	Introduction	104
4.2	Modeling the evolution of seismicity prior to failure: the FFM	106
4.2.1	The FFM theory	106
4.2.2	Physical interpretations of the FFM	107
4.2.2.1	Physical interpretation of VT acceleration patterns	108
4.2.2.2	Physical interpretation of LP acceleration patterns	112
4.2.3	Critical analysis of the FFM	114
4.2.3.1	The inverse linear regression method	114
4.2.3.2	FFM with variable α	116
4.2.4	The FFM for real-time predictions	117
4.3	Bayesian inversion of seismic rates prior eruptions	119
4.3.1	Formulation	119
4.3.1.1	General Bayesian inversion	119
4.3.1.2	Least-square criterion	123
4.3.2	Data information	124
4.3.2.1	Computation of seismic event rates uncertainty	125
4.3.2.2	Cumulative vs non-cumulative data	126
4.3.2.3	Choice of tuning parameters	127
4.3.2.4	Impact of the structure of the data uncertainty on the model parameters estimation	129
4.4	Partial conclusions on the methodology	134

4.1 Introduction

The material Failure Forecast Method (FFM) makes use of an empirical power law for describing the precursory behaviour of geophysical precursors prior to landslides, rock failure and eruptions. It is the only deterministic forecasting method of volcanic eruptions. Since then, and because there exists no other method for deterministic forecasts, it has been widely used for eruption predictions in hindsight (using the whole precursory sequence until the eruption). Even if Voight and Cornelius (1991) started to question whether FFM forecasts are possible in real time, very few studies continued to tackle this point.

In a first part, I present the FFM power law and the parameters it involves. A review of the physical mechanisms proposed to explain the power-law behaviour of seismicity is carried out. I go through the physical explanation of VT accelerations proposed by different authors to give an idea of what physical parameters can influence the time of eruption prediction. In Chapter 3, precursory accelerations of LP events have also been presented. Therefore, I will discuss the applicability of the FFM to LP events and the possible physical interpretations of their precursory behaviour. Then, I propose to make an exhaustive review of the FFM applications both for hindsight and for real-time forecasting, to point out the limitations of its application until now. This review of the classical applications of the FFM strongly suggests that it is not possible to use these methods to carry out relevant real-time forecasting. Based on this reflexion, I will pose the problem of the real-time adaptation of the FFM. One of the main points to be tackled is to define criteria to decide whether the predictions are reliable or not. The first criterion is the uncertainty of the prediction made with the FFM at a given observation time. More precisely, I will look at the evolution of these uncertainties with time, and my criterion will be that the uncertainty must decrease with time, i.e. the prediction must become more certain as we get more data. Moreover, it is assumed that the estimated parameters of the FFM would stabilise if a sustained physical process takes place in the volcano. The second criterion is thus that predictions must stabilise with time. They are then likely to converge towards the true time of eruption. Consequently, we are seeking for a method that gives stable predictions along time, in addition to reliable associated uncertainties.

In a second part, I explain the inversion method chosen to adjust the FFM theory to the data, based on the requirements and limitations previously described. We here face a classical inversion problem, i.e. from the data available we want to evaluate the model parameters that allows for adjusting as well as possible the FFM law to the data. Most of studies define this optimisation problem in a least-square sense without evaluating the uncertainty of the *prior* data and solve it with local methods. Local methods are efficient to solve the inverse problem, however they do not allow to compute reliable *posterior* parameter uncertainties for non-linear problems, such as that of FFM. I thus solve the inverse problem with a global method, using the Bayesian approach. After presenting the concept of Bayesian inversion, I present how the

prior uncertainties of the data are computed. I show that an accurate evaluation of the prior data uncertainty is necessary for an optimal evaluation of the parameters and of their posterior associated uncertainties. Finally, the theoretical uncertainties implied in the FFM is the last ingredient of the Bayesian inversion that will be discussed in this chapter.

This methodological chapter is based on the published article (Appendix D): A. Boué, P. Lesage, G. Cortés, B. Valette and G. Reyes-Dávila. Real-time eruption forecasting using the material Failure Forecast Method with a Bayesian approach (2015). *Journal of Geophysical Research*. doi: 10.1002/2014JB011637.

4.2 Modeling the evolution of seismicity prior to failure: the FFM

4.2.1 The FFM theory

The FFM has first been used by Fukuzuno (1985) for landslides predictions. Voight (1988) then proposed a general material failure law to describe the behaviour of materials in terminal stage of damage in condition of constant stress loading and temperature. It is a simple relationship between the acceleration and the rate of change of some recorded data Ω , which can be either seismicity, the square root of the seismic energy release or the strain, who are supposed to vary proportionally to each other (Figure 4.1, left, Voight, 1988):

$$\ddot{\Omega}(t) = A\dot{\Omega}(t)^\alpha, \quad (4.1)$$

where A and α are empirical constants.

By integrating the equation (4.1), it is possible to describe the evolution of the observable $\dot{\Omega}$ as a function of time:

$$\dot{\Omega}(t) = \left(A(1 - \alpha)(t - t_0) + \dot{\Omega}_0^{1-\alpha} \right)^{\frac{1}{1-\alpha}}, \quad (4.2)$$

where t_0 is the beginning of the ongoing process and $\dot{\Omega}_0$ is the rate of observable at time t_0 . Example of precursory acceleration of deformation prior to a landslide at Mt Toc (Voight, 1989) is presented in Figure 4.1 (right), where the asymptote of the power law is identified at time $t_f - t = 0$. The position of the asymptote of function $\dot{\Omega}(t)$ is then:

$$t_f = -\frac{\dot{\Omega}_0^{1-\alpha}}{A(1 - \alpha)} + t_0. \quad (4.3)$$

The time t_f is interpreted as the failure time.

Combining expressions (4.2) and (4.3) leads to a more convenient formulation:

$$\dot{\Omega}(t) = k \left(1 - \frac{t}{t_f} \right)^{-p} \quad (4.4)$$

where $p = 1/(\alpha - 1)$ and $k = \dot{\Omega}_0$. Note that expression (4.4) is of the same form as the Inverse Omori Law, which is another empirical expression used to describe earthquake foreshock sequences (Utsu et al., 1995). This expression is consistent with damage mechanics models used to explain earthquake foreshock sequences (Main, 2000; Turcotte et al., 2003). This supports the hypothesis that the empirical FFM actually describes the volcano edifice damage before the opening of the magma conduit, which can lead or not to an eruption.

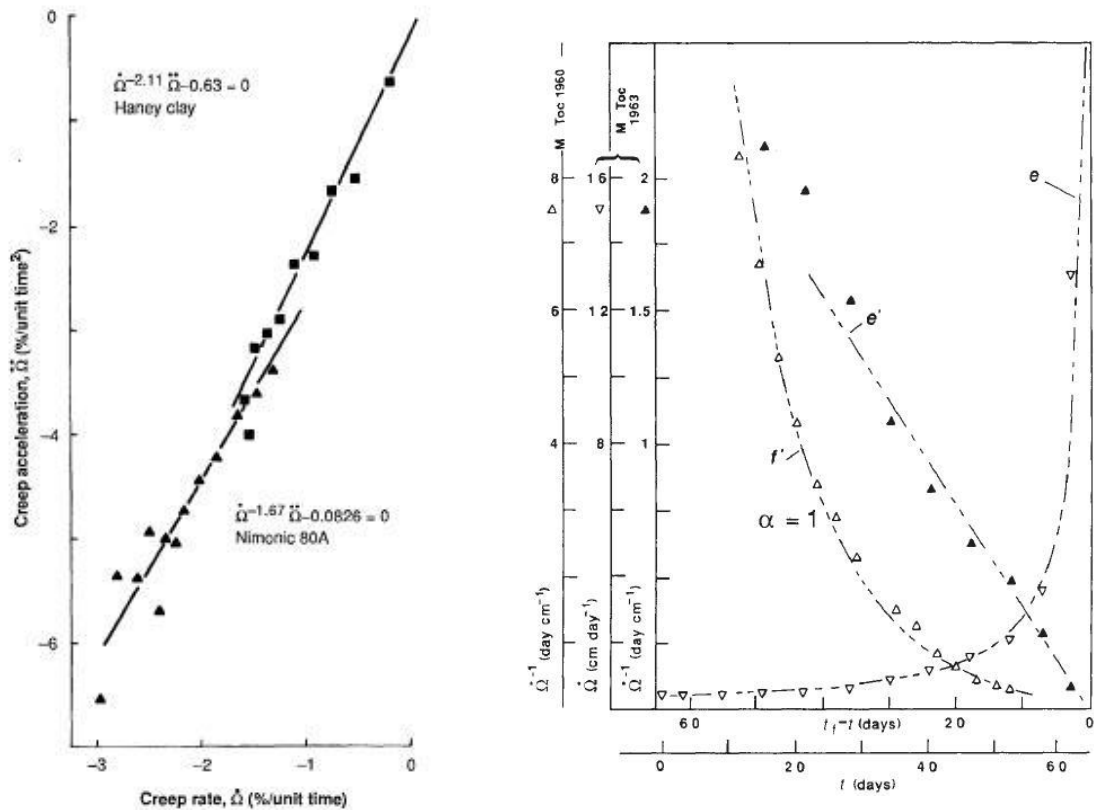


Figure 4.1: Left: Relationship between creep acceleration $\ddot{\Omega}$ and creep velocity $\dot{\Omega}$ before failure of an alloy in tension and a soil in compression (from Voight, 1988). Right: Displacement rate as a function of time before a landslide in Mt Toc (curve e) and its inverse value (curve e'). Curve f represents the displacement well described by an exponential trend, that did not precede any landslide (from Voight, 1989).

In this thesis, the observable Ω is the precursory seismicity. As already described in Chapter 1, VT seismicity is associated to rock fracturing. Consequently, rock mechanics concepts can physically justify the application of the FFM to VT seismicity, by helping to understand the processes leading to the acceleration of VT events in volcanic context. However, accelerations of LP events are also observed before vulcanian explosions, as described in Chapter 3. Therefore, the precursory behaviour of this class of events will also be discussed in the next section.

4.2.2 Physical interpretations of the FFM

Increases of VT and LP seismicity usually display accelerating patterns prior to eruptions, as observed in Chapter 3. It seems important to determine in which extent certain classes of events are reliable for the application of the FFM. In particular, this section considers the relevance of using classes of VT and LP. I will discuss the possible physical links between precursory

observables and eruptions in different cases, based on the literature. This non-exhaustive review also allows for understanding the physical meaning of the empirical parameters of the FFM, and the reasons for its classical applications discussed in Section 4.2.2.

4.2.2.1 Physical interpretation of VT acceleration patterns

When subjected to constant stress, rocks deform and eventually fail after a time delay that depends on the applied stress. The time-dependent brittle deformation of rocks is called creep or static fatigue. Brittle creep experiments have been used to investigate the response of a rock sample to time-dependent brittle deformation (Heap and Faulkner, 2008). Figure 4.2 exhibits the deformation as a function of time produced by these experiments. When the axial strain is plotted against time, the resulting curve has an apparent trimodal behaviour. This curve is commonly known as a creep curve and has been observed by many authors (e.g. Lockner, 1993; Baud and Meredith, 1997; Main, 2000). The three stages of the curve are conventionally been described as (1) primary or decelerating creep corresponding to the elastic response of the rock submitted to a constant stress, (2) secondary or steady state creep and (3) tertiary or accelerating creep. This three-stage creep is interpreted as the result of the damage of a rock that is weakening as a function of time. In the framework of the FFM for eruption forecasting, the tertiary creep is of particular interest. Indeed, this part of the creep curve can result in the macroscopic failure of the sample by propagation of a shear fault.

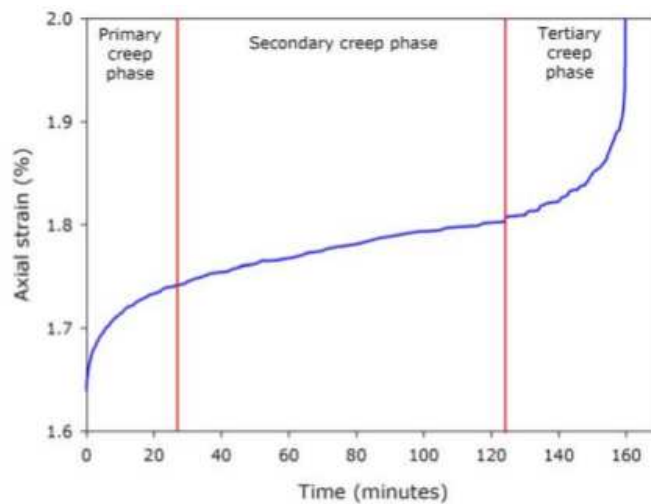


Figure 4.2: Classic trimodal creep curve for brittle material under constant differential stress (from Heap and Faulkner, 2008). The curve shows the three stages of brittle creep: (1) primary or decelerating, (2) secondary or steady state and (3) tertiary or accelerating creep.

The deformation of a sample is associated with fracturing. A failure is generally accompanied with the emission of an elastic wave generated by the rapid release of energy within the

material. In rock deformation experiments, this elastic wave can be recorded by acoustic sensors at the surface of the sample. It is then reported as acoustic emissions. The measurements of deformation and of acoustic emissions to analyse their evolution as a function of time are important in the study of rock deformation. Indeed, it has been observed that acoustic emissions mirror the relationship of the classic creep curve during brittle creep experiments (Wu and Thomsen, 1975; Ohnaka, 1983; Baud and Meredith, 1997). As a consequence, observing the evolution of acoustic emissions allows us to follow the progressive damage of the rock as a function of time. Acoustic emissions have been largely monitored during brittle creep experiments of rocks (Wu and Thomsen, 1975; Lockner and Byerlee, 1975; Ohnaka, 1983; Yanagidani et al., 1985; Hirata et al., 1987; Nishizawa and Noro, 1990; Baud and Meredith, 1997).

The first phase of the creep curve corresponds to the elastic behaviour of the rock, i.e. it deforms linearly with the applied stress and can go back to its initial form if the stressing is interrupted. This phase involves no cracking and no change in the molecular bounds. After some time of applied stress, the rock can deform in a plastic manner, and deformation then becomes irreversible. This second creep stage starts when dislocations occurs at the atomic scale (= lattice defects), eventually resulting in crack nucleations. Dislocation glides involve no volume change nor friction. Dislocation motion is favoured by temperature increase. These dislocations leads to the so-called stage of *strength hardening* where more stress is then needed to deform the rock. This results in the spreading of micro-cracking over the whole sample. The transition between dislocations and micro-cracks is still mainly qualitatively understood. The classical theory of damage mechanics actually states for a unique phase to explain part 1 and 2 of the creep curve (Reches and Lockner, 1994). Cruden (1973) suggests that there is a critical density of micro-cracks in the rock sample at which the cracks can start to intersect. These intersections then grow at an accelerating rate which ultimately leads in sample failure (stage 3 of the creep curve) due to the localisation of the deformation onto a single plane.

Even if time-dependent brittle deformation in rocks is a poorly understood phenomenon, studies by Anderson and Grew (1977), Atkinson (1984), Atkinson and Meredith (1987) and Costin (1987) propose that the stress corrosion is the main physical mechanism leading to rock damage. These studies allow for the quantification of the mechanisms that I have qualitatively described above. Stress corrosion cracking is the conjoint action of stress and of a corrosive environment leading to the formation of a crack, which would not have developed by the action of stress or environment alone. In volcanic contexts, these conditions can be due to the presence of corrosive geothermal fluids, for instance. This corrosive environment weakens the strained bonds at crack tips and thus eases crack propagation (Atkinson and Meredith, 1987). The trimodal behaviour of the typical creep curve is then explained by a widely-used and accepted theory of stress corrosion defined by Charles (1958):

$$\dot{x}(t) = V_0 \frac{K}{K_0}^{p'} , \quad (4.5)$$

where x is the crack length at time t , $\dot{x}(t)$ is the velocity of crack growth, V_0 is the initial crack growth velocity, $K = Y\sigma x^{1/2}$ is the stress intensity factor (also called the Griffith's criterion for unstable crack growth) that measures the degree of concentration of stress σ at a crack tip of length x (with Y a dimensionless constant), K_0 is the initial stress intensity at time t_0 and the exponent p' is the stress corrosion index which quantifies the chemically assisted process of crack growth. This exponent depends on the type of the rock (Atkinson and Meredith, 1987). After manipulation of equation (4.5) and assuming a constant applied stress, Main (1999) deduces the following model

$$\dot{x}(t) = V_0 \left(1 - \frac{t}{t_f}\right)^n, \quad (4.6)$$

for $n = p'/(p' - 2) < 1$. Expression (4.6) turns to be of the same form as expression (4.4), that was derived directly from the empirical FFM. If we assimilate that crack growth velocity \dot{x} to the observable $\dot{\Omega}$ it may generate, then the empirical exponent p of the FFM seems to be related to the corrosion index p' and the empirical constant k to the initial velocity of crack propagation V_0 . To summarise, based on Charles' law, the FFM model describes the crack propagation as a function of time, depending on the stress at the crack tips, the temperature and the chemical components of the surrounding rock. Describing the deformation as a function of time with the FFM amounts to generalise Charles' law for a population of cracks, assuming that the parameters are averaged over the population. We thus expect the same analytical form to hold for crack length or strain, even though we do not expect the exponent of the law to be the same.

Stress corrosion cracking thus seems to be the most likely responsible mechanism for the time-dependent precursory cracking, displacements and accelerating seismic activity that commonly precede volcanic eruptions (Voight, 1988, 1989; Cornelius and Scott, 1993; McGuire and Kilburn, 1997; Kilburn and Voight, 1998; Main, 1999). However, these studies do not address the interactions between the population of cracks and the fracturing of the rock at different scales. In material physics experiments, cracks occur everywhere within the sample but are concentrated in a preferred plane (Lockner, 1993). In volcanic contexts, i.e. at larger scales than a rock sample, the cracks are thought to be distributed everywhere in a cylindrical region around the volcano's axis between the magma body and the surface (Figure 4.3, left). The idea proposed by Kilburn (2003) is that, at micro-scale, micro-cracks grow and coalesce to extend a crack at macro-scale. These macro-cracks further extend to interact between each other (Figure 4.4, left), until the magma conduit opens (Figure 4.3c). Kilburn (2003) expresses the probability to create a micro-crack nucleus through the stress corrosion mechanism. Multiscale fracturing is modelled by calculating the probability of a crack to be supplied by a certain amount of energy, which is then extended to a population of cracks of different scales. The model shows that the rate of the number of activated fault increases exponentially (which corre-

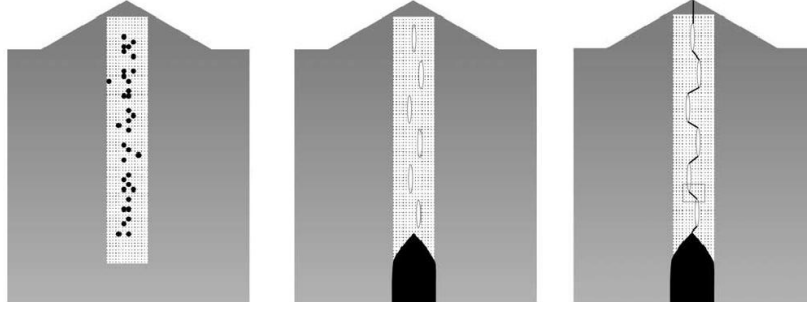


Figure 4.3: (left) The pre-eruptive seismicity is distributed everywhere between the magma body and the surface. This observation is interpreted by (middle) the reactivation and the extension of pre-existing fractures, further connecting (right) to form a magma pathway (from Kilburn, 2003).

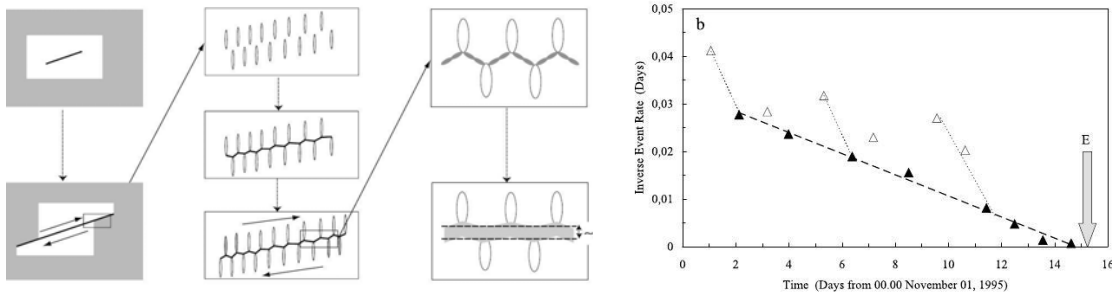


Figure 4.4: Left panel: Schematic explanation of multiscale fracturing. The fault extends by reactivating existing cracks around its tips (left, scale of a fault). At microscale (middle), tensile cracks open and coalesce and so on smaller scales (right). Right panel: Inverse of the precursory VT rates before the 1995 Soufriere Hills eruption. Different linear trends are observed: the secondary linear trends (empty triangles) are interpreted as the VT activity corresponding to the cracks coalescing around the tips of the major faults that also extend themselves and interact (main linear trend, filled triangle). Figure from Kilburn (2003).

sponds to $\alpha = 1$ in expression 4.2). Crack propagation is then modelled by the balance between the energy required to create new crack surfaces and the energy released by the surrounding rock as the crack grows. The resulting model for the terminal stage of damage resembles that of the linear form of the empirical FFM (expression 4.2) with $\alpha = 2$:

$$\dot{\Omega}(t)^{-1} = \dot{\Omega}_0^{-1} - A(t - t_0) \quad (4.7)$$

where in Kilburn's model the empirical constant A is actually the rate of energy released in extending the cracks. Inverse rates of precursory seismic events can thus be modelled with multiple linear trends corresponding to the extension of each major faults, whose interactions lead to the opening of the magma conduit (Figure 4.4, right). Therefore, the model of Kilburn

(2003) argues for the hypothesis that α can evolve from 1 to 2 as fracturing proceeds. Performing a dimension analysis of this model for the limiting cases of $\alpha = 1$ and $\alpha = 2$, it appears that α describes the degree of self-feeding behaviour of rock fracture around the margin of the fault. The constant A then depends on the rock properties and on the imposed stress conditions.

Of course, the stress history of rocks is generally more complex than a constant loading rate. In reality, a volcanic edifice is subject to repeated cycles of stress over time due to magma displacement from deep reservoirs to shallow depths and to the superimposed tectonic stresses. The influence of an applied differential stress on brittle creep has been studied by Baud and Meredith (1997). Intuitively, increasing the stress on a sample results in decreasing the time to failure. This is an important point in terms of volcanic eruption forecasting because small variations of stress can significantly change the time of prediction.

To summarise, using the FFM theory to forecast volcanic eruptions based on precursory VT activity seems appropriate because the power-law behaviour of VT seismicity is well understood. However, the hypothesis of constant loading underlying the FFM is probably too simplistic to analyse precursory seismicity in real volcanic contexts. Thus we can expect to encounter some difficulties in applying the FFM for real-time forecasting.

4.2.2.2 Physical interpretation of LP acceleration patterns

In Chapter 3, I have highlighted systematic patterns of acceleration and increase of LP activity before vulcanian explosions at Volcán de Colima. This kind of patterns were also observed at Galeras (Colombia, Gil Cruz and Chouet, 1996), Tungurahua (Ecuador, Molina et al., 2004), Ubinas (Peru, Traversa et al., 2011) or Sakurajima (Japan, Maryanto et al., 2008). It is thus tempting to apply the FFM in order to determine whether this precursory LP activity allows for forecasting vulcanian explosions. However, I should underline that the physical interpretation of these precursory LP patterns and their link with vulcanian explosions is a fully unexplored subject.

Among the proposed mechanisms for the generation of LP events reviewed in Chapter 1, the fracturing of ascending magma at the conduit wall is the only mechanism that depends directly on evolving magma dynamics. Therefore, it is the preferred mechanism for the control of accelerating LP behaviour. Moreover, fracturing of ascending magma is the most commonly accepted source mechanism of LP events at Volcán de Colima (Varley et al., 2010b,a; Arámbula-Mendoza et al., 2011; Lavallée et al., 2008, 2011). Thus, I propose to cross-check the literature on vulcanian explosions with the mechanisms of fracturing of ascending magma as a source of LP events. In the literature, the mechanism proposed as the source of LP events is either the brittle failure of magmas at the conduit wall or the stick slip of a solid plug. In the following I link these two mechanisms with proposed mechanisms for magma fragmentation.

Brittle failure of magmas Goto (1999) and Neuberg et al. (2006) propose that magma fracturing can be the source of LP events. Moreover, Papale (1999) propose that the fracturing of magma at the conduit wall is one of the mechanism that could trigger the fragmentation phase leading to an explosion. Thus, magma fracturing makes the link between LP activity and the occurrence of a vulcanian explosion.

Gonnermann and Manga (2012), Melnik et al. (2005) and Papale (1999) analyse the parameters controlling ascent rates and viscosity evolution for different depths. They show that an increasing gas and crystal content increases the viscosity and the ascent rate of the magma in an exponential manner, forcing the magma to accelerate (Papale, 1999). As a consequence, the conditions leading to accelerating magma fracturing are very likely to be fulfilled and can explain the behaviour of LP seismicity prior to vulcanian explosions.

Another trigger mechanism of vulcanian explosions, linked with magma fracturing and thus with LP activity, has been proposed by Holland et al. (2011). According to these authors, the interconnections of magma cracks at different places of the conduit wall can trigger a rapid decompression when reaching the surface, triggering the vulcanian explosion. This mechanism can be seen as a multi-scale fracturing leading to a major fracture at the conduit wall reaching the surface. This hypothesis is also supported by Denlinger and Hoblitt (1999) who propose a model of polymer extrusion to explain the generation of LP events through the stick-slip of the magma at the conduit wall. Forecasting vulcanian explosions based on LP precursory behaviour might thus be justified based on these models.

Stick-slip of a plug Stick-slip motion of the dome (Iverson et al., 2006) is one source mechanism of LP events that could explain their accelerating behaviour (Dmitrieva et al., 2013). A similar mechanism applied to a single fault is used by Dmitrieva et al. (2013) to explain the behaviour of LP events merging to gliding tremors at Redoubt volcano. Their results clearly show an increase of the LP rates. LP signals are then so close to each other that they merge into a tremor.

The decompression mechanism proposed by Holland et al. (2011) can also explain the link between the stick-slip of a plug and a vulcanian explosion, as already explained for brittle failure of magma. Indeed, when the interconnected fractures reach the surface, they can lead to a rapid decompression of the pressurised conduit, leading to a vulcanian explosion.

Following this discussion, the application of the FFM to LP events is thus justified, even if no theoretical model quantitatively demonstrates the link between the acceleration of LP events and the empirical FFM power-law, such as those of Kilburn (2003, 2012) to explain the acceleration of VT events. Consequently, I will empirically apply the FFM to LP precursors of vulcanian explosions in order to determine whether LP acceleration allows for predicting vulcanian explosions.

4.2.3 Critical analysis of the FFM

This section aims at performing an exhaustive review of the FFM for eruption predictions. The objective is to emphasise which methods should be applied for real-time perspectives.

4.2.3.1 The inverse linear regression method

The most popular way to use the FFM for eruption forecasting has from far been the so-called *inverse method*. Most studies use this method for its simplicity. Indeed, by setting the exponent $\alpha = 2$ in expression 4.2, the FFM becomes hyperbolic and its inverse is then linear (equation (4.7)). Consequently, it is easy to adjust this theory to the inverse of the observable $\dot{\Omega}$ using a linear regression. The intersection of this linear function with the abscissa then corresponds to the time of eruption. In addition, this method is supported by the models presented in Section 4.2.2, which suggest that α is supposed to be equal to 2 in the terminal stage of damage. However, experimental evidences contradict this theory. Here, I propose to briefly review the studies that use the inverse method for eruption predictions in order to point out the drawbacks of the inverse method for real-time forecasting.

Indeed, forecasts in hindsight sometimes display very poor correlation coefficients when fitting the FFM with $\alpha = 2$ to the data (e.g. Carniel et al., 2006; Ortiz et al., 2003). Another drawback arises from the amount of data available to adjust the model. In the literature, predictions in hindsight are often carried out with the linear method with less than six data points (e.g. Murray and Ramirez Ruiz, 2002; Lavallée et al., 2008). In these cases, the FFM is useful to describe the data trend but the model is poorly constrained, thus real-time analysis would not be difficult.

Voight and Cornelius (1991) and Cornelius and Voight (1994) started to question whether forecasts would be possible some times before the eruption, using incomplete sequences of acceleration. For a real-time application of the FFM, they propose to update the forecasts at given time intervals, using the FFM with $\alpha = 2$. They represent the prediction times t_f as a function of the observation time t_{obs} advancing towards the eruption. Their predictions converge towards the true time of eruption some times before the eruption, since the more data are being accumulated, the better constrained are the forecasts. An even more interesting result arises from Budi-Santoso et al. (2013) who perform a similar analysis where, in addition to converging, the predicted time of eruption stabilises close to the true eruption date several days before the eruption onset. In this study, it has been verified that α was close to 2.

Because very few cases of real-time forecasting using the FFM with the linear method have been published, and because, as already pointed out in Chapter 1, α does not always equal 2, I question the efficiency of the linear method if the precursory accelerating sequence displays a value of α different from 2. In order to test the sensitivity of the predictions to this assumption,

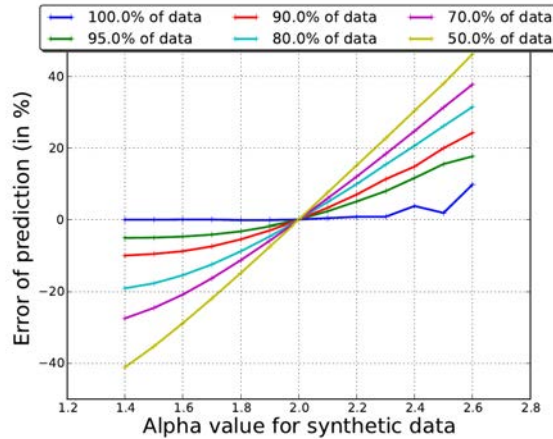


Figure 4.5: Error of prediction obtained using the linear FFM method as a function of the α value used to build synthetic precursory data. The different line colors represent the amount of data used to make the eruption predictions.

I constructed several synthetic sequences using expression (4.2) with the same theoretical time of eruption t_e but with different α values ranging from 1.4 to 2.6. For each of these different synthetic data with different α values, I applied the linear method, assuming $\alpha = 2$, to retrieve the theoretical eruption time in a real-time perspective, i.e. for each observation time t_{obs} before the eruption, as proposed by Voight and Cornelius (1991) and Cornelius and Voight (1994). Figure 4.5 represents the relative error of prediction $(t_f - t_e)/t_e$ as a function of the α value used to build the synthetic data and of the amount of data used to forecast the theoretical eruption. For synthetic data built with $\alpha = 2$, the time of eruption is always perfectly retrieved, even when few data are used. For all datasets, the linear method also gives perfect predictions using the whole acceleration (100% of the data). However, for datasets built with $\alpha \neq 2$, the error significantly increases when incomplete data are available for the forecasts. The less data are available, the greater is the error on the predicted eruption date. Obviously, the further from 2 is the α value used to build the synthetic data, the larger is the error on the prediction date.

To summarise, the inverse method will always give the good prediction if it is carried out in hindsight (with 100% of the data), but it will give wrong predictions if working in real time with precursory sequences that are best described by $\alpha \neq 2$. Of course, it will be successful in real time if the precursory data are well described by $\alpha = 2$, but this is an information that is impossible to verify in real time. Voight and Cornelius (1991) carried out both linear and non-linear adjustments of the FFM with variable α on the same datasets. These authors show that, even in the cases where the linear method is satisfying, the non-linear use of FFM leads to more accurate predictions, with a better adjustment. Consequently, I recommend to avoid using the FFM with the linear method for carrying out real-time eruption predictions. Instead, the exponent α should be optimised.

4.2.3.2 FFM with variable α

Other applications of the FFM were achieved by adjusting the two parameters A and α in expression (4.2), to then calculate the resulting time of prediction using expression (4.3). Even though different ways of finding these parameters are proposed by Cornelius and Voight (1995), the most direct and relevant method is to process a non-linear regression.

Cornelius and Voight (1994) compare prediction results obtained with the linear method and with variable α values. For hindsight predictions, it is clear that the time of prediction is closer from the true eruption date using the FFM with variable α than with the linear method. However, all real-time trials were performed with the linear method. The predictions then converge very late towards the true time of eruption. Hindsight forecasts were also carried out with variable α values by Cornelius and Voight (1995). In this study, it is clear that the linear method would have led to less accurate forecasts than with the non-linear method because α is very different from 2.

More recently, Smith et al. (2007) analysed the α values of VT precursory sequences for different eruptions at Mt St Helens. In this case, the authors clearly show that the mean α value is almost never equal to 2, and that the uncertainty on the α value is usually very large. Most of their real-time predictions converge towards the true time of eruption, but the predictions are very unstable as a function of time, leading to the conclusion that it might have been difficult to choose which time of eruption was the most probable one, in a real-time point of view. In the aim to compare the different methods for real-time forecasting, Smith and Kilburn (2010) propose to confront the linear and the variable- α method on Mt Pinatubo eruption in 1991. In this case, their conclusion is that the linear inverse method gives more accurate predictions with narrower uncertainties. Moreover, the stability of the predictions as a function of time with the linear inverse method is by far better than using the variable- α method. This is simply explained by the fact that, in this case, the α value is actually very close from 2. So, in these conditions, it is not surprising that the inverse method leads to better results because the exponent α is fixed to its true value.

Another point that is well emphasised in Cornelius and Voight (1994) is when the signal to noise ratio of the precursory trend is low. This problem simply arises because of the different sources of uncertainty of the data used for the adjustment of the FFM. When working with RSAM or even SSAM, different types of signals associated to different source mechanisms are mixed together, which is probably one source of uncertainty. Consequently, a classification of the seismic events could allow a better signal-to-noise ratio. Instead, these authors propose to choose the data points that follow the best desired trend. Although it might be a solution, it is clearly not applicable in real-time.

In general, the uncertainty of the time of prediction is not evaluated. In the rare cases where the uncertainty is calculated, it is roughly approximated from the residuals of the fitting

procedure. This point was recently addressed by Bell et al. (2011) who pointed out that the fitting procedure used to adjust the FFM (based on the L_2 or L_1 norms) has a great impact on the accuracy of the prediction and on its associated uncertainty. They conclude that the discrepancy between the results obtained with different optimisation methods mainly comes from the structure of the data uncertainty assumed (Gaussian vs. Poissonian). I develop this point in more details in the next section.

Finally, some accelerating patterns showed in the latter studies display multiple-acceleration phases interspersed with decelerations, making it difficult to adjust the FFM model that describes only single accelerations. Consequently, this empirical law may be well adapted for laboratory experiments of rock fractures, where the loading conditions are controlled, but it suffers from intrinsic limitations when the considered physical processes are more complicated and not well understood.

To conclude this review, I now summarise the limitations to the application of the FFM that have been put in relief.

- First, regarding the variability of the α values, it is clear that α is not always equal to 2, either for VT or LP precursors. It is consequently necessary to use FFM with variable α , and to optimise the value of the exponent α (or p in the form I will consider, expression 4.4).
- Second, it is difficult to forecast eruptions with real data because of the fluctuations and uncertainties in data calculations. This leads to the instability of the predictions as a function of time. This points out the need for a careful consideration of the data uncertainties in the fitting procedure.
- A third question concerns the optimal fitting procedure that should be used to adjust the FFM model to the data (Bell et al., 2013).
- Finally, Cornelius and Voight (1995) objectively mention the difficulty of deciding whether a prediction is more relevant than another when thinking in a real-time situation. It is thus of paramount importance to determine reliability criteria for the adaptation of the FFM for real-time forecasting.

In the next part, I discuss the requirements needed to use the FFM in the most well-reasoned way for real-time applications. Based on this discussion, I propose some solutions to overcome the limitations listed above and apply the FFM to succeed real-time predictions.

4.2.4 The FFM for real-time predictions

In order to adapt the FFM and evaluate its real-time potential, I propose to adjust the model each time new data are collected, as already proposed by Voight and Cornelius (1991) and Cornelius and Voight (1994).

First of all, we have to choose the most adapted solution of the differential equation (4.1) to proceed real-time eruption predictions. The most important parameter is clearly the time of eruption t_f . Because we need a simple, accurate and reliable way of evaluating the uncertainty of the prediction t_f made at each observation time t_{obs} , it seems natural to work with expression (4.4), which explicitly involves the parameter t_f , rather than with expression 4.2, which requires first to evaluate the best parameters A and α and their associated uncertainties, to then being able to calculate the time of prediction t_f using expression (4.3). From now, I will work only with the model (4.4), which involves the parameters k , p and t_f . I recall that in this case, $p = 1/(\alpha - 1)$.

The choice of the initial time t_0 is not a problem when working with synthetic or laboratory data because the beginning of the creep is known. But when working with real seismo-volcanic data, the beginning of the time window where we start adjusting the model to the data is important since it potentially leads to different prediction results (Smith and Kilburn, 2010). Indeed, the power law defined by expression (4.4) consists in a first part with low and almost constant slope, and in a second part characterised by a strong increase of the slope (acceleration). In order to well constrain the model, the fitting window must include both parts of the power-law. Thus, the origin time t_0 must be set accordingly.

Besides, when adjusting the power law to the data, a trade-off appears between the three parameters. This means that the estimation of the exponent p in expression (4.4) is strongly coupled with the estimation of k and so it is for the time of prediction t_f . Actually, this trade-off might explain the large variability of the α values reported in the literature, since this parameter is generally estimated while fixing the other ones in expression (4.2) (e.g. the starting date t_0 , and hence the initial rate $\dot{\Omega}_0=k$).

We aim at computing reliable uncertainties of the parameters k , p and t_f and at analysing their evolution as a function of the observation time t_{obs} while it advances towards the eruption time t_e . However, it might be difficult to determine if one prediction is better than another when working in real time. The latter point has never been addressed although it appears essential to define criteria to decide whether a prediction is reliable or not. In particular, we assume that the estimated parameters of the model will stabilise if a sustained physical process takes place in the volcano. We also expect that, while the time of eruption is approaching, the uncertainty of the parameters will decrease. Consequently, I define two criteria to evaluate the quality of the prediction:

1. decreasing parameter uncertainties as we advance towards the eruption,
2. temporal stability of the estimated parameter t_f .

Finally, because the FFM is tested for real-time applications, we face a less constrained problem than when considering the adjustment of the whole acceleration in hindsight. Here, it is important to point out the need for including the acceleration part in the adjusted data in

order to well constrain the model. Thus we do not expect to make reliable predictions only with the first constant part of the power-law. This point can be limiting for real-time forecasting when only short precursory sequences are available. Another limitation of the method that can already be emphasised is the stability criterion. Indeed, as already seen in Section 4.2.2.1, changes in loading or temperature conditions might greatly influence the time of the asymptote of the law (i.e. the time of prediction t_f). As a consequence, if those variabilities occur before an eruption, I expect the acceleration pattern of the data to change significantly, which will result in a poor-quality prediction. I must recall that the FFM is a single power-law model. As a consequence, other patterns of acceleration before an eruption might lead to a very limited applicability of the real-time forecasting method proposed in this work.

Following the requirements and limitations evoked here above, and in the aim to use the most relevant method as possible, we must choose the most adapted way of adjusting the FFM model to the data both to obtain the most precise and stable predictions as a function of time and to compute reliable uncertainties of the predicted eruption time. The next part discusses why a Bayesian approach seems the most suitable for this purpose. It also demonstrates why the classical least-square approach used in the literature is not adapted.

4.3 Bayesian inversion of seismic rates prior eruptions

4.3.1 Formulation

4.3.1.1 General Bayesian inversion

An inverse problem aims at finding some physical parameters of interest from the recorded data that result from the corresponding physical process. This definition is very general and thus used in many scientific fields that collect data to understand the environment of interest by inferring physical properties. In order to infer parameters from recorded measurements, we implicitly assume a link between each other. In geophysics, this link is a physical theory relating the observed data vector \mathbf{d}_{obs} to the vector of model parameters \mathbf{m} . In our case, the theory is the empirical law represented by the FFM, the data \mathbf{d}_{obs} are the seismic signals recorded on the volcanoes and the model parameters are the parameters of the FFM (expression 4.4):

$$\mathbf{m} = \begin{pmatrix} k \\ p \\ t_f \end{pmatrix}. \quad (4.8)$$

The relation between the data and the parameters is called the *forward problem* and can be formalised as follows:

$$\mathbf{d}_{\text{obs}} = g(\mathbf{m}) \quad (4.9)$$

with g representing the considered theory, in our case the FFM function (expression 4.4). Given the parameters k , p and t_f , the forward problem (4.9) enables to compute synthetic seismic data. For the moment, I deliberately keep the general notation d_{obs} for referring to these data. I will detail later which form they should exactly take (cumulative vs non-cumulative counts of events).

Reciprocally, solving the inverse problem consists in deducing the parameters k , p and t_f from the recorded seismic data. In particular, we are interested in estimating the time of eruption t_f , and in evaluating the uncertainty of this estimation. There are different ways of solving an inverse problem, depending on the degree of linearity of the problem, on the number of parameters involved, and on whether we wish an accurate evaluation of the parameter uncertainties or a rapid evaluation of the best model parameters. It is thus important to correctly understand the requirements of the problem we want to solve.

One of our reliability criterion for real-time predictions is the uncertainty of the eruption prediction t_f . Thus it is of paramount importance to calculate it as precisely as possible. Unfortunately, the FFM law (4.4) is non-linear with respect to the parameters k , p and t_f , which makes the estimation of parameter uncertainties difficult by using local optimisation methods based on the least-square criterion, because it is difficult to define an appropriate data covariance matrix. However, and fortunately, the FFM model is composed of only three parameters, which enables us to envisage the use of a global optimisation method at a reasonable computation cost. In our case, the most suitable technique for solving our inverse problem is therefore the Bayesian approach. Indeed, it is the most general and complete way of solving an inverse problem since it performs an exhaustive exploration of the whole parameter space, thus fully accounting for the non-linearity of the problem. Moreover, it enables an accurate estimation of the posterior uncertainties of the estimated parameters.

As inputs, the Bayesian method requires a good knowledge of the data and of their associated uncertainties. Fortunately, this is an information that is well known in our case, thanks to the confusion matrices of the automatic recognition tool used to classify seismo-volcanic events. Based on this knowledge, we can easily follow the Bayesian approach proposed by Tarantola and Valette (1982b), which I will now present in a very general way. Contrary to most of optimisation methods that consider the inverse problem as the minimisation of some misfit function between observed and synthetic data, the Bayesian approach aims at combining the information we have on the data (measurements), on the model parameters (*a priori* knowledge) and on the relation between both (physical theory). The combination of this *a priori* information, represented under the form of *prior* probability density functions (*prior pdfs*), leads to a *posterior pdf* that represents a new state of information on the model parameters (Tarantola and Valette, 1982a).

For the seek of generality, let \mathbb{D} be the data space, \mathbb{M} the model space and g a function of \mathbb{M} in \mathbb{D} such that $\mathbf{d} = g(\mathbf{m})$. The vector \mathbf{d} represents the observations (i.e. the rate of seismic

events $\dot{\Omega}(t_{obs})$ available at a given time of observation t_{obs} , \mathbf{m} gathers the model parameters k , p and t_f we want to determine and g is the law that describes the data (equation 4.4) for a given model. We write $\mathbf{x} = (\mathbf{d}, \mathbf{m})$ a vector of the space $\mathbb{X} = \mathbb{D} \times \mathbb{M}$, i.e. a combination of a data set and of a set of model parameters. The aim is now to estimate the probability of realisation of a given set $\mathbf{x} = (\mathbf{d}, \mathbf{m})$, or more precisely the conditional probability that the parameters take a given value \mathbf{m} , knowing the recorded data \mathbf{d}_{obs} .

To do so, we need to evaluate two *pdf* for \mathbf{x} . The first one represents the *a priori* information on \mathbf{x} , formalised by the prior *pdf* $\rho_{prior}(\mathbf{x})$, and computed as

$$\rho_{prior}(\mathbf{x}) = \rho_{prior}(\mathbf{m})\rho_{obs}(\mathbf{d}) \quad (4.10)$$

where $\rho_{prior}(\mathbf{m})$ is the prior *pdf* of the model containing the *a priori* knowledge we have on the parameters t_f , p and k , and $\rho_{obs}(\mathbf{d})$ is the prior *pdf* of the data that I will compute using the recorded counts of events and the confusion matrices of the VSR (See Section 4.3.2). The second *pdf* depending on \mathbf{x} is the theoretical *pdf* $\Theta(\mathbf{x})$ expressing the relation between \mathbf{d} and \mathbf{m} :

$$\Theta(\mathbf{x}) = \theta(\mathbf{d}|\mathbf{m})\mu(\mathbf{x}) \quad (4.11)$$

where $\theta(\mathbf{d}|\mathbf{m})$ is the conditional *pdf* of \mathbf{d} knowing \mathbf{m} , i.e. it is the probabilistic expression of the forward problem (4.4), and $\mu(\mathbf{x}) = \mu_m(\mathbf{m})\mu_d(\mathbf{d})$ is the density measure of null information. In practice, the *pdfs* μ_d and μ_m are defined as uniform on the data space \mathbb{D} and on the model space \mathbb{M} , respectively.

Following Tarantola and Valette (1982b), the posterior *pdf* of \mathbf{x} is then:

$$\begin{aligned} \rho_{post}(\mathbf{x}) &= \frac{\Theta(\mathbf{x})\rho_{prior}(\mathbf{x})}{\mu(\mathbf{x})}, \\ &= \frac{\rho_{prior}(\mathbf{m})\rho_{obs}(\mathbf{d})\theta(\mathbf{d}|\mathbf{m})}{\mu_d(\mathbf{d})}. \end{aligned} \quad (4.12)$$

Since the *pdf* $\mu_d(\mathbf{d})$ is uniform, this relation can be reduced to simple proportionality and the marginal law on \mathbf{m} is obtained by integration of $\rho_{post}(\mathbf{x})$ over \mathbb{D} :

$$\begin{aligned} \rho_{post}(\mathbf{m}) &= \int_{\mathbb{D}} \rho_{post}(\mathbf{x}) d\mathbf{d} \\ \rho_{post}(\mathbf{m}) &\propto \rho_{prior}(\mathbf{m}) \int_{\mathbb{D}} \rho_{obs}(\mathbf{d})\theta(\mathbf{d}|\mathbf{m}) d\mathbf{d} \end{aligned} \quad (4.13)$$

Equation (4.13) is the most general form of solving the inverse problem with a Bayesian approach. To apply it in the frame of the FFM, we now need to evaluate the prior *pdf* of the parameters $\rho_{prior}(\mathbf{m})$, the prior *pdf* of the data $\rho_{obs}(\mathbf{d})$ and the prior *pdf* of the theory $\theta(\mathbf{d}|\mathbf{m})$.

Concerning the latter one, I should specify that I do not consider uncertainties related to the theory in this work, so the theoretical *pdf* reduces to a Dirac delta function,

$$\theta(\mathbf{m}|\mathbf{d}) = \delta(\mathbf{d} - g(\mathbf{m})). \quad (4.14)$$

Concerning the prior *pdf* of the data, its calculation will be detailed in Section 4.3.2. In the following, I focus on the prior *pdf* of the model parameters.

The model space \mathbb{M} is generated by the three dimensions corresponding to the real numbers k , p and t_f . For defining the prior *pdf* $\rho_{prior}(\mathbf{m})$, we assign uniform prior densities for $k \in [0, n]$, for $t_f \geq t_{obs}$, and for $p \in [0.4, 4]$ based on the relation $p = 1/(\alpha - 1)$ and on the values of α reported in the literature. The choice of a uniform prior is motivated by the lack of *a priori* knowledge on the model. Consequently we rely only on the data information. Another possibility could have been to use the posterior *pdf* obtained at t_{obs-1} as the prior *pdf* at t_{obs} , in a data assimilation approach. I have tested this alternative but it appears that using a previous posterior *pdf*, which is generally poorly constrained due to the consideration of a partial dataset at early observation times, can bias further predictions. At a given time t_{obs} , the most relevant information is the newest acquired data and it is probably not consistent to consider older prior information.

Following the Bayesian approach with these uniform prior *pdfs* and neglecting the error on the theory, the posterior *pdf* of the model parameters is given by (Tarantola and Valette (1982b), eq. 6.9):

$$\rho_{post}(\mathbf{m}) \propto \rho_{prior}(\mathbf{m}) \rho_{obs}(\dot{\Omega}(\mathbf{t})). \quad (4.15)$$

For an application in real time, we aim at computing this posterior *pdf* for each time of observation advancing toward the time of eruption. For simplicity, and because the posterior *pdf* will be computed as a function of time, I choose to represent only the marginal *pdf* of t_f and p instead of the joint probabilities. The marginal *pdf* can be computed as:

$$\rho_{post}(t_f) = \int_p \int_k \rho_{post}(\mathbf{m}) dp dk \quad (4.16)$$

and

$$\rho_{post}(p) = \int_{t_f} \int_k \rho_{post}(\mathbf{m}) dt_f dk. \quad (4.17)$$

Both in the aim to objectively quantify the spread of the marginal *pdf* of t_f and to provide a tool for decision-makers, I propose to compute the Shannon index (Shannon, 1948) of the posterior *pdf* at each time of observation:

$$I(t_{obs}) = - \int_{t_f} \rho_{post}(t_f) \times \log(\rho_{post}(t_f)) dt_f \quad (4.18)$$

The lowest the Shannon index $I(t_{obs})$ is, the most relevant is the *pdf* of t_f at the corresponding time of observation.

In a *real-time perspective* eruption forecast, the maximum likelihood (i.e. the maximum of the posterior *pdf* of t_f) should stabilise with time if there is one single acceleration of the rate of seismic precursors. Stabilisation occurs during an accelerating trend because (a) it is consistent with the assumption of equation (4.4) as the *best-fit model* and (b) more data is accrued. Moreover, the prediction should be more precise when approaching the time of eruption as the model becomes more and more constrained. This should be indicated by the narrowing of the *pdf* around its maximum. Such narrowing of the posterior *pdf* has already been shown for synthetic data by Bell et al. (2013), for a theoretical relation of the form of equation (4.4). In this study, I propose to quantify the narrowing using the Shannon index, that should decrease with the observation time. The spread of the posterior *pdfs* can be also evaluated by the 95% and 99% confidence levels, which I will indicate on the figures presenting the prediction results.

The last ingredient of equation (4.13) that I did not detail yet is the computation of the prior *pdf* of the data, $\rho_{obs}(\mathbf{d})$. In the next section, I first present the well-known least-square criterion, which is generally used in the literature for solving the inverse problem, and which amounts to consider Gaussian distributions for the prior data *pdf*. But we will see that the least-square criterion has limitations because of the Gaussian hypothesis on the structure of the data uncertainty. Consequently, in a second time, I will consider a more general approach by computing the prior data *pdf* directly from the statistical performance tests of the automatic classification tool.

4.3.1.2 Least-square criterion

Optimisation methods based on the least-square criterion are very popular for solving inverse problems. Basically, they aim at minimising the difference between the observed data \mathbf{d}_{obs} and synthetic data computed with the available theory, $\mathbf{d}_{cal} = g(\mathbf{m})$. Solving the inverse problem then amounts to minimise the following misfit function

$$S(\mathbf{m}) = \frac{1}{2} |\mathcal{C}_d^{-1}(\mathbf{d}_{obs} - g(\mathbf{m}))|_D^2 \quad (4.19)$$

where $|\cdot|_D$ denotes the norm of the data space \mathbb{D} and \mathcal{C}_d is the data covariance matrix containing the data variances (i.e. uncertainties) and, eventually, their covariances (i.e. correlations). In expression (4.19), it should be underlined that introducing the data uncertainties under the form of a covariance matrix implicitly assumes that the prior data *pdf* is a Gaussian distribution:

$$\rho_{obs}(\mathbf{d}) \propto e^{-\frac{1}{2}(\mathbf{d} - \mathbf{d}_{obs})^t \mathcal{C}_D^{-1}(\mathbf{d} - \mathbf{d}_{obs})}. \quad (4.20)$$

According to Tarantola and Valette (1982a), if the theory g is a linear function, then the posterior *pdf* of the model parameters is also a Gaussian. More exactly, it can be expressed as

$$\rho_{post}(\mathbf{m}) \propto e^{-S(\mathbf{m})}, \quad (4.21)$$

which shows that minimising the misfit function (4.19) is strictly equivalent to finding the maximum likelihood of equation (4.21).

Optimisation methods based on the least-square criterion are thus intimately related to Gaussian statistics. Even in the case of non-linear forward problems, least-square methods somehow assume that the data follow a Gaussian distribution. But in non-linear cases, the posterior *pdf* of model parameters has no reason for being Gaussian (Tarantola and Valette, 1982b). The estimation of the posterior parameter uncertainties might then be biased.

Because seismic occurrences are rather described by a Poisson process, Greenhough and Main (2008), Bell et al. (2011) and Bell et al. (2013) started to question whether the Gaussian hypothesis underlying the use of the least-square method can be a source of bias in the determination of the time of prediction. They actually show that this hypothesis influences the uncertainty and the accuracy of the estimated model parameters in comparison with a Poisson distribution assumption. Even though a Poisson distribution for the data uncertainties seems to be a more justified assumption than the Gaussian distribution because we deal with counts of seismic events, it still remains a strong hypothesis.

The error structure of the data thus impacts the posterior model parameters uncertainty. This point can be limiting concerning the uncertainty criterion we will use for real-time prediction. To avoid making any hypothesis on the data uncertainty and succeed robust and reliable predictions, I propose a method for the objective computation of the seismic event rates uncertainties based on the confusion matrices of VSR used for automatic classification.

4.3.2 Data information

The precise and well-designed analysis of the data is one of the most important tasks in order to succeed accurate forecasts based on precursory seismic activity. Two main points have to be considered: the manner of counting the seismic events and the rigorous evaluation of their uncertainty. The workflow of my data processing is thus composed of (1) an automatic classification of continuous seismic signals (Chapters 2 and 3), (2) the count of events gathered into binned temporal windows (non-cumulative data), and (3) the computation of a prior probability distribution for each binned window. In this section I will also compare the posterior *pdf* I obtain with the Bayesian formulation with the results obtained with the classical least-square approach. To emphasise the interest of my new application of the FFM for real-time forecasting.

4.3.2.1 Computation of seismic event rates uncertainty

As seen in Chapter 2, the success rate of the recognition is estimated using the manually-labelled database by evaluating the number of substitutions between classes and the number of deletions (events that are not recognised). The statistics on the recognition are usually represented through a confusion matrix (Table 4.1), which gives the number of events that have been successfully recognised in each class. The confusion matrix gives the rate of recognition success for each class (*%tot*) and the conditional probability $P(i|j)$ for an event to belong to a given class i knowing that it has been identified by the VSR as an event of class j :

$$P(i|j) = \frac{M_{ij}}{\sum_i M_{ij}} \quad (4.22)$$

where M_{ij} is the corresponding element of the confusion matrix M and $\sum_i M_{ij}$ is the total number of events identified as belonging to class j by the VSR. This conditional probability quantifies the uncertainty on the counts of seismic events.

$i \backslash j$	COL	EXP	EXPS	LP	REG	SIL	T	VT	Del	% tot
COL	152	1	1	0	0	0	0	3	19	86.36
EXP	0	19	4	1	0	0	0	0	3	70.37
EXPS	0	5	122	0	0	0	0	0	1	95.31
LP	0	1	19	224	2	0	1	1	5	83.90
REG	0	0	0	0	30	0	2	3	1	83.33
SIL	0	6	7	0	0	48	0	0	15	63.16
T	0	1	3	1	4	0	48	1	5	76.19
VT	0	0	1	5	2	0	0	113	4	90.40
									mean %	81.13

Table 4.1: Confusion matrix obtained from the VSR. Rows correspond to the number of true events in each class i and columns present events recognised by the VSR as belonging to class j . The column denoted *%tot* represent the percentage of events well recognised by the VSR, including the deleted events (Del).

Given the identification by the VSR of a total of n events in a time window Δt , the probability $P_i(m)$ that there are m events actually belonging to class i ($m \leq n$) can be evaluated based on the conditional probabilities $P(i|j)$ as:

$$P_i(m) = \sum_{\substack{|\mathbf{k}|=m \\ k_j \leq n_j}} \prod_{j=1}^c \binom{n_j}{k_j} P(i|j)^{k_j} (1 - P(i|j))^{n_j - k_j} \quad (4.23)$$

where c is the number of event classes ($c = 8$ in the example of Table 4.1), n_j is the number of events identified by the VSR in class j , $|\mathbf{k}|$ stands for $\sum_{j=1}^c k_j$, and $\binom{n_j}{k_j}$ denotes binomial coefficients. To obtain expression (4.23), we must evaluate all the possibilities for having exactly

m events belonging to class i . Each of the m events may have been identified by the VSR as belonging to one of the c possible classes. This leads to consider all the decompositions of m as sums of c numbers k_j with $k_j \leq n_j$ for $j = 1, \dots, c$, which justifies the first sum in expression (4.23). The probability of each of these occurrences must then be evaluated. Given a class j , for which the VSR has identified n_j events over the time window, the probability that exactly k_j of those events belong to class i is $\binom{n_j}{k_j} P(i|j)^{k_j} (1 - P(i|j))^{n_j - k_j}$ where $\binom{n_j}{k_j}$ is the number of k_j -combinations among n_j elements, and where $P(i|j)$ (respectively $1 - P(i|j)$) is the probability that an event identified by the VSR as belonging to class j belongs in fact (respectively does not belong) to class i . Since the choice of the events within each class may be done independently, the product of these factors must be done as in formula (4.23). This calculation is repeated for each time window centred around the time of observation $[t_{obs} - \Delta t/2, t_{obs} + \Delta t/2]$ where Δt is a window width which has to be defined will be discussed in the Section 4.3.2.3.

Finally, I transform by linear interpolation this discrete probability $P_i(m)$ into a continuous prior *pdf*, $\rho_{obs}(\mathbf{d})$, over the range $[0, n]$, where n is the total number of events around the given observational time. Beyond the value of n , the probability $\rho_{obs}(\mathbf{d})$ is set to zero.

Once the prior probability of the data $\rho_{obs}(\mathbf{d})$ are determined for each t_{obs} and each Δt , we use the Bayesian approach that yields the posterior *pdf* of the model parameters.

4.3.2.2 Cumulative vs non-cumulative data

It is now time to define which form to consider for the data \mathbf{d} . The FFM can be applied using either cumulative or non-cumulative values of the data. When cumulating data, each new data depends on the previous ones, leading to correlations between data associated to consecutive time windows. If these correlations are neglected, it will perturb the result of the inversion, yielding potentially spurious trends (Greenhough et al., 2009). This point has also been addressed by Hardebeck et al. (2008) in the framework of Accelerating Moment Release (AMR) who showed that an apparent AMR can be identified in synthetic data that actually does not contain any AMR. However, no binning is required for computing cumulative data, which is a practical advantage in comparison with using non-cumulative data (Bell et al., 2013). Furthermore, it is possible to adjust the mean trend of multiple acceleration patterns using cumulative data, that are by definition monotonically increasing, which is more difficult with non-cumulative data. This is a delicate point because one may adjust a theory that actually does not describe the data, which might lead to unreliable and biased results. Consequently, the choice of the type of data faces a competing balance between theoretical and practical advantages. In this study, I prefer theoretical advantages and choose to use non-cumulative data, i.e. the rate of events at a given time as observable. In other words, I must evaluate the instantaneous derivative $\dot{\Omega}$ for every given time interval, which involves some tuning parameters.

4.3.2.3 Choice of tuning parameters

This section discusses the choice of some tuning parameters, namely the window width Δt , the update frequency of predictions and the initial time t_0 , which need to be defined for using the FFM in a real-time perspective.

The evaluation of $\dot{\Omega}$ at a certain t_{obs} requires a numerical approximation of the time derivative of the number of events Ω . Different values of Δt lead to different approximations of $\dot{\Omega}(t_{obs})$: A too small window Δt can hide a precursory pattern if the signal is dominated by noise fluctuations. On the other hand, a too large window may smooth too much the acceleration pattern. I thus explore a range of reasonable values for Δt excluding too small values, which do not allow for visual detection of the acceleration sequences to be detected, as well as large values that produce too strong smoothing. Figure 4.6 presents the prior *pdf* of the rates of LP events, as a function of the observation time t_{obs} , calculated with four window widths Δt , prior to the major vulcanian explosion of the 5 June 2005 at Volcán de Colima. In this case, the precursory pattern appears to be clearer for $\Delta t = 1.5$ h and $\Delta t = 2$ h. This observation can be carried out in real time by plotting the data in parallel for different Δt at every new time of observation, as displayed in Figure 4.6. In practice, and if necessary, the prediction results can be computed in parallel for different Δt until the time of eruption (as explained in the following for the choice of t_0). The most stable and accurate results can be selected as our prediction of the time of eruption.

Another point concerns the frequency at which the data have to be updated. In periods of volcanic crisis, hundreds of events can occur everyday, so new data streams can be updated very often. To evaluate the stability criterion in real time, when precursory seismic activity is short, we need to update forecasts as frequently as possible. For the case of Volcán de Colima, the time scale of the precursory LP activity is about one day (Arámbula-Mendoza et al., 2011). Thus, I will update the calculation of $\dot{\Omega}(t)$ each thirty minutes to make a new forecast. This pragmatic choice introduces correlations in the data because the increments will overlap on the cases where $\Delta t > 1$ h. The resulting prediction uncertainties will thus be slightly perturbed but the proper quantification of this bias is difficult to evaluate due to the non-linearity of the problem.

In the aim to estimate the effect of overlapping windows on the posterior *pdf* of the model parameters, I propose to test the method of prediction on the precursory sequence of VT events before the 23 June 2000 eruption at PdlF volcano, for two different ways of computing the rates of events (Figure 4.7): (A) with a window width $\Delta t = 10$ h and no overlap between consecutive windows, and (B) with a window width $\Delta t = 14$ h and a 4 h overlap. These two ways of computing the data ensure the same number of points for the inversion thus the model is equally constrained in both cases. In Figure 4.7, we can observe that the spread of the marginal posterior *pdfs* $\rho_{post}(t_f)$ and $\rho_{post}(p)$ is larger with non-overlapping data than with

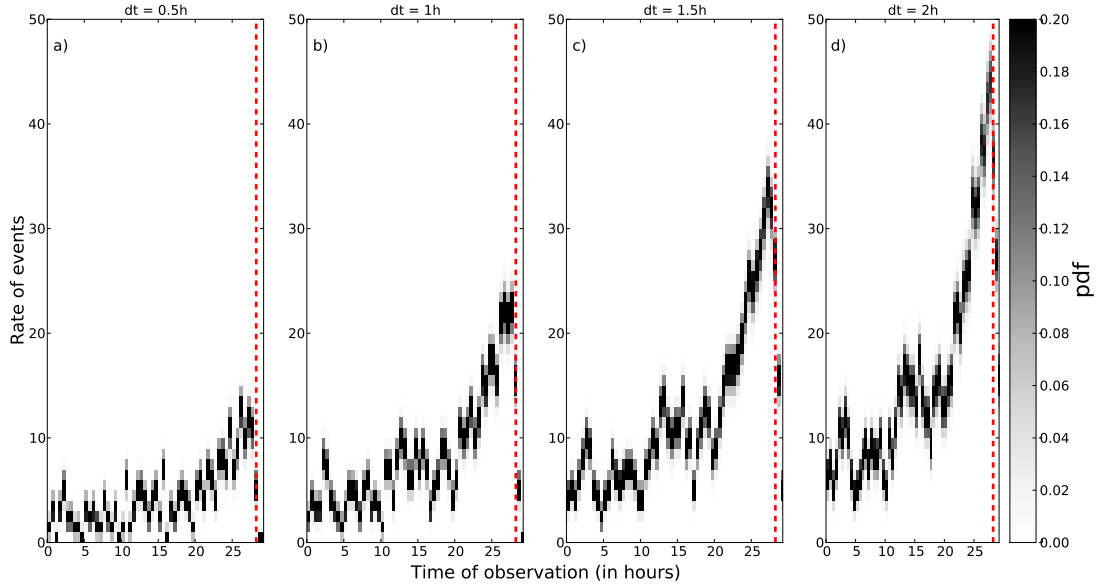


Figure 4.6: Prior *pdf* of the rates of LP events as a function of time for the vulcanian explosion of the 5 June 2005 at Volcán de Colima, computed for different time windows Δt : a) $\Delta t = 0.5$ h, b) $\Delta t = 1$ h, c) $\Delta t = 1.5$ h, d) $\Delta t = 2$ h. The red dashed line represents the time of explosion.

overlapping ones. Consequently, overlapping data leads to underestimate the uncertainties of the model parameters, and hence to overestimate the reliability of the predictions. Even if overlapping data have practical advantages when precursory sequences are short, we will have to keep this result in mind, when interpreting the prediction results in Chapter 5.

For an application in real time, the observer needs to set the beginning time t_0 of the power law to adjust, once the beginning of seismic acceleration is noticed. There is no absolute way for choosing an adequate value for t_0 . Here, I propose a practical way to do so. Figure 4.8 shows the results of prediction displayed in parallel for different tested values of t_0 . The prediction results are similar when a long-enough time serie is available to constrain the model parameters. Except for the furthest $t_0 = -32$ h, all the predictions stabilise around the true time of explosion, but with different uncertainties and stability duration. As expected, the prediction results obtained with t_0 values that are closer to the beginning of the acceleration phase ($t_0 = -24$ h in particular) display larger uncertainties and stabilise during a shorter time than using other t_0 values. Based on the stability and accuracy criteria, the observer could have chosen $t_0 = -28$ h, -29 h or -30 h. Figure 4.8 thus emphasises that it is possible to choose t_0 in real-time in an objective way, even if this choice is made *a posteriori*, after the trial of several t_0 values. It also shows that the choice of t_0 is only critical when the chosen value is either very close or very far from the acceleration onset.

The choice of the appropriate window width Δt can be carried out the same way as for the

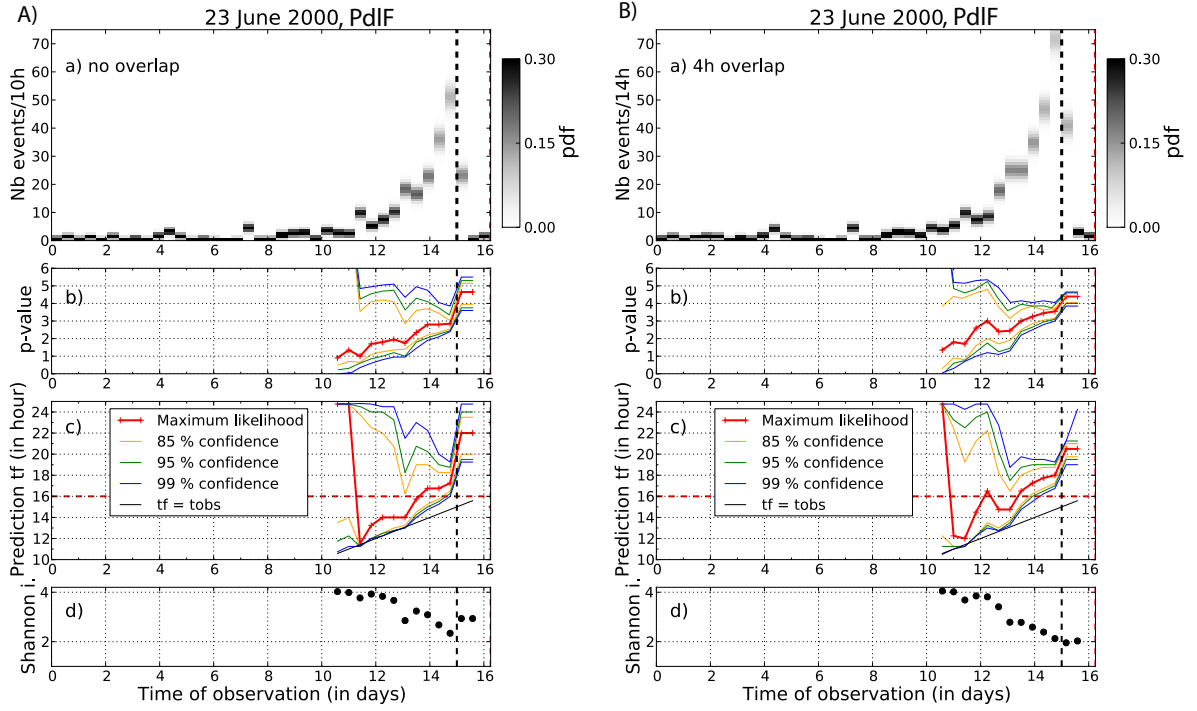


Figure 4.7: (A) Rates of events are calculated with a window width $\Delta t = 10$ h and no overlap between consecutive windows. (B) Rates of events are calculated with a window width $\Delta t = 14$ h and an overlap of 4 h between consecutive windows. a) Prior *pdfs* of the data for the 23 June 2000 eruption at PdlF volcano, as a function of the observation time t_{obs} . The true time of eruption is $t_e = 16$ days (red dashed line). The black dashed line indicates the time of deceleration. b) Posterior marginal *pdfs* of p as a function of the observation time t_{obs} . The red line is the maximum likelihood of the *pdf* and the yellow, green, and blue lines indicate the 85%, 95% and 99% intervals of confidence, respectively. c) Posterior marginal *pdfs* of the prediction t_f as a function of the observation time t_{obs} . The red line is the maximum likelihood of the *pdf* and the yellow, green, and blue lines indicate the 85%, 95% and 99% intervals of confidence, respectively. The black line corresponds to $t_f = t_{obs}$. d) Shannon's index of the marginal *pdfs* of t_f as a function of the observation time.

choice of t_0 .

4.3.2.4 Impact of the structure of the data uncertainty on the model parameters estimation

In the review carried out in Section 4.2.3, I have shown that the assumption of setting the exponent $p = 1$ (or $\alpha = 2$) is not always relevant because the estimated values of p can significantly vary from one sequence to another. Up to now, there are few published studies on eruption forecasts in a real-time perspective using the FFM with a non-fixed exponent (p or α) and addressing the question of uncertainties. For instance, Smith and Kilburn (2010)

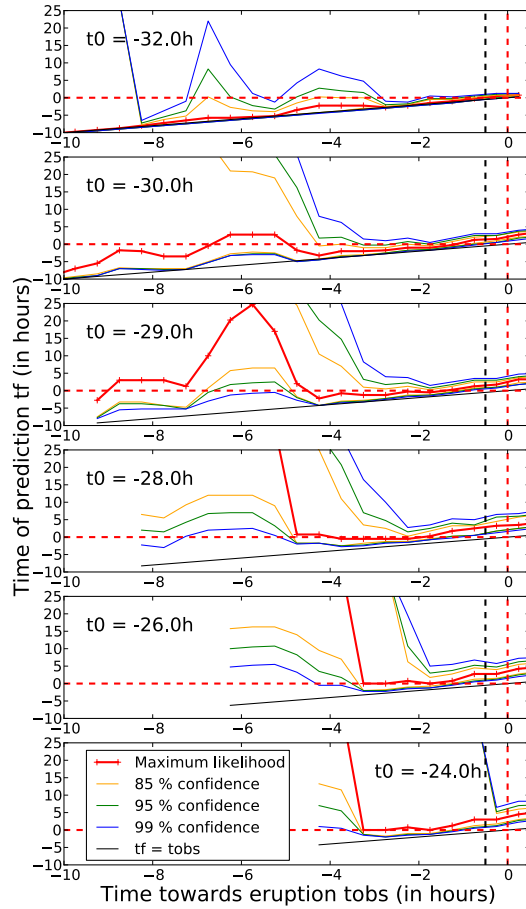


Figure 4.8: Results of prediction t_f as a function of time for the 5 June 2005 explosion at Volcán de Colima. Each panel represents the results obtained for different starting time t_0 . The red line is the maximum likelihood of the pdf and the yellow, green, and blue lines indicate the 85%, 95% and 99% intervals of confidence, respectively. The explosion occurs at $t_{obs} = 0$ (dashed red line) and the abscissa corresponds to the number of hours remaining before the explosion occurs.

and Smith et al. (2007) carry out data fitting in a least square sense, which implies an implicit assumption of a Gaussian distribution of the data. However, they do not quantify the data uncertainties, and consequently their error in the forecast times are probably not reliable. Moreover, the forecast times do not stabilise as a function of the observation time. Besides, Bell et al. (2013) assume that the precursory seismic sequence is distributed according to a non-stationary Poisson process (Ogata, 1983), whose intensity follows equation (4.4). Then, they determine a maximum likelihood estimation of the parameters. They compare their method with a classical least square approach on several synthetic datasets. They obtain more accurate results than with least squares fitting if the exponent is set to its true value. However they get large errors when the exponent must be estimated. On real data, and considering the exponent as an unknown parameter, they obtain stable forecast times in the last part of the sequence

for only a few study cases.

Figure 4.9 shows the prior *pdfs* of the data for the Volcán de Colima explosion of 5 June 2005 at three different observation times. Gaussian and Poisson distributions are adjusted to these *pdfs*. In this case, it appears that the error structure of the data is much better described by a Gaussian distribution than by a Poisson one. *A posteriori*, this suggests that a weighted least squares procedure could also be used to perform the inversion but the determination *a priori* of appropriate values for the data standard deviation is far from trivial. Moreover, these examples of Volcán de Colima are relatively simple because one type of event predominates the seismic activity (namely the LP events). In more complex cases characterised by a larger diversity of seismic classes, we expect that the *pdfs* of the data would have different patterns and would not be correctly described by a Gaussian distribution. The Bayesian approach can anyway be applied as it does not require any hypothesis on the data information. On the other hand, in cases where the error distribution cannot be correctly determined because of unavailable uncertainties on the observable, a Gaussian law could be assumed but a standard deviation on the data should be estimated.

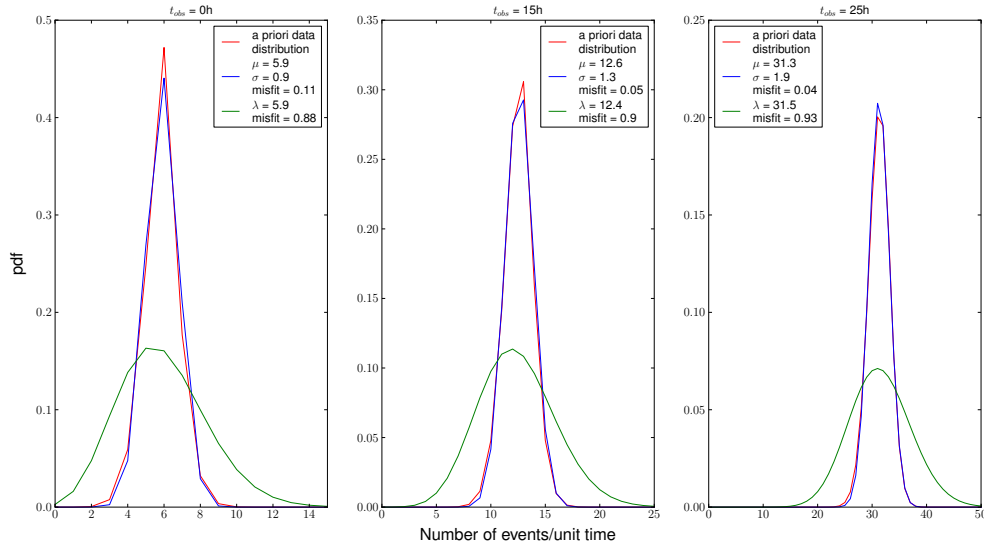


Figure 4.9: Prior *pdfs* of the data (red curve) for three different times of observation t_{obs} , for the example of 5 June, and their best fits using a Gaussian distribution of mean μ and standard deviation σ (blue curve) and a Poisson distribution of intensity λ (green curve). The quantities μ , σ and λ are expressed in number of events per unit time. Distributions are adjusted using the L1-norm.

To illustrate the influence of the type of data information on the evaluation of the parameters t_f and p of the FFM, I present their posterior marginal probabilities in Figure 4.10. This figure displays, for the example of the 5 June event at Volcán de Colima, the marginal *pdf* of p and

t_f which is obtained by integrating $\rho_{post}(k, p, t_f)$ over k . Results are shown for five different t_{obs} and for the following methods:

1. the Bayesian method of this study (first row),
2. the Bayesian method with a Gaussian assumption on the data information, with two different standard deviations: $\sigma = 1$ event per unit time (second row) and $\sigma = 3$ events per unit time (third row),
3. the maximum likelihood estimate of the parameters with the method used in Bell et al. (2013) (non-stationary Poisson process, red dot in each panel).

In Figure 4.10, we first notice that the uncertainty is not reliable in the case of the Gaussian assumption when the value of σ is underestimated ($\sigma = 1$ event per unit time), as the 99 % confidence contour almost never contains the time of explosion. On the other hand, a large σ value leads to large uncertainties on the estimated parameters because the uncertainty on the data might be overestimated. However for $t_{obs} = 26$ h, the value of $\sigma = 3$ events per unit time seems to be well adapted since the corresponding uncertainties obtained are comparable to that of our method. The method used in this study yields to reasonable uncertainties on the parameters, with the time of eruption always inside the confidence contours. Furthermore, the maximum of the posterior distributions are stable around the time of eruption as a function of the observation time, which is not always the case for the other methods tested. The maximum likelihood estimates of the predictions made with the other methods are similar for observation times greater than $t_{obs} = 24$ h and gives the same values as in this study for $t_{obs} = 25$ h and $t_{obs} = 26$ h. This suggests that the hypothesis made on the structure of the data has less impact on the results when enough data are available to constrain the model. The way of defining the prior data pdf is thus very important to obtain stable results with reliable uncertainties. Consequently, the method proposed in this study provides the most reliable calculations of uncertainties (keeping in mind that we slightly underestimate the uncertainties by overlapping time windows) and the most stable estimation of the eruption time as a function of observation time, at least for the specific examples studied here.

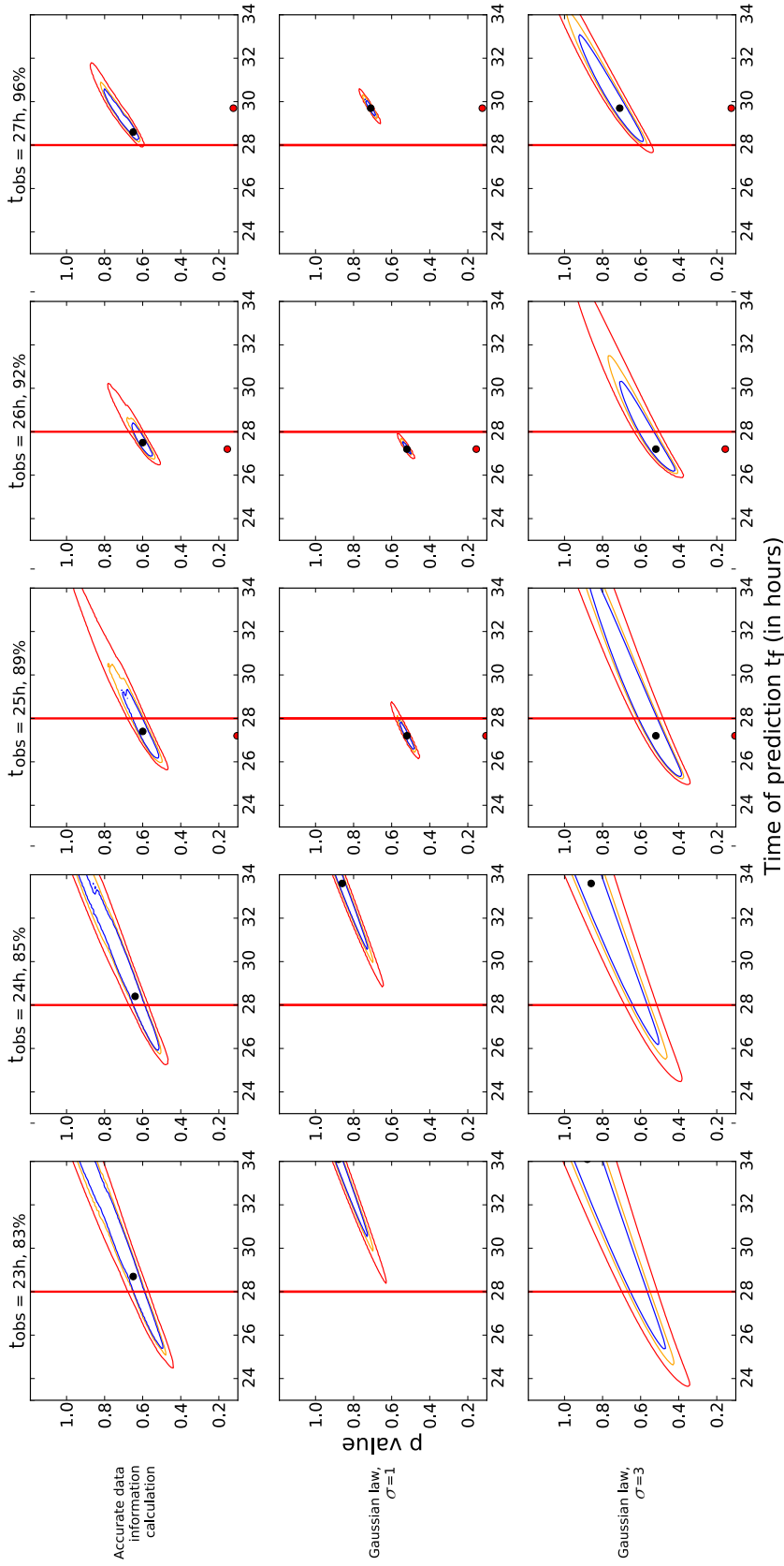


Figure 4.10: Joint $pdfs$ of p and t_f for the 5 June 2005 event at Volcán de Colima. Each row corresponds to a different hypothesis on the data error structure. Each column presents the joint $pdfs$ obtained for a particular time of observation t_{obs} . The corresponding fraction of the accelerating sequence is indicated in percent. The red line represents the true time of explosion, the black dot corresponds to the maximum likelihood of each pdf and the red dot to the maximum likelihood obtained with the non-stationary Poisson process hypothesis. Blue, orange and red curves corresponds to 80%, 90% and 99% levels of confidence, respectively.

4.4 Partial conclusions on the methodology

In this Chapter we have presented a new method of volcanic eruption forecasting based on the FFM model adapted real-time applications. The Bayesian approach used here provides an objective, robust and flexible way of solving the inverse problem and to estimate the model parameters and their uncertainties from the prior *pdf* of the data. The form of the FFM model I chose (equation 4.4) allows us a direct estimation of the time of eruption t_f and of its associated posterior *pdf*. These estimations are repeated along the observation time. Thus the reliability of the forecast can be evaluated along with two criteria: the stability of t_f as a function of time and the evolution of the uncertainty of its estimation.

The success and utility of the method of eruption forecasting based on precursory seismic activity rely on the following obvious conditions. First, seismic events must occur and this activity must present an acceleration behaviour. The reasons why some eruptions are not preceded by earthquakes are not well understood and requires more research. Second, the duration of the seismic unrest and the level of activity must be sufficient for the method to be carried out and, when an eruption is forecast, the delay for civil protection to act must be long enough.

Some main drawbacks can be underlined. The data increments are overlapped for the numerical approximation of $\dot{\Omega}$ leading to a correlation in the data and thus an underestimation of the prediction uncertainty. This bias is very difficult to quantify because of the non-linearity of the problem. It might however be minor in comparison with the theoretical uncertainties arising from the FFM model. For instance, it could be possible to evaluate this uncertainty for each $\dot{\Omega}(t)$ with the hypothesis that earthquakes occurrence in each interval follows a Poisson process (Ogata, 1983). For the moment, the uncertainty on the theory is neglected but this point should be further investigated. However, the FFM theory is empirical, so a major improvement would rather be to propose a physical model to explain VT and LP precursory patterns.

The method developed in this Chapter is now applied on precursory sequences of vulcanian explosions and effusive activity at Volcán de Colima and Merapi volcano.

Chapter 5

Real-time applications of the FFM

Contents

5.1	Introduction	135
5.2	Real-time predictions	137
5.2.1	Testing the forecasting method on textbook cases	137
5.2.1.1	Application on VT precursors: Piton de la Fournaise and Merapi volcanoes	137
5.2.1.2	Application on LP precursors: Volcán de Colima	142
5.2.2	Complex cases for real-time applications	143
5.2.2.1	Acceleration-deceleration patterns	144
5.2.2.2	Multiple acceleration patterns	147
5.2.2.3	Too short precursory sequences	150
5.2.3	Comparison with results of the literature	153
5.3	Systematic application and statistical performance	156
5.3.1	Global applicability of the method	156
5.3.2	Accuracy of the method when applicable	162
5.3.2.1	Accuracy of real-time forecasts	162
5.3.2.2	Accuracy of hindsightforecasts	164
5.4	Partial conclusions on the application of the FFM for real-time forecasting	166

5.1 Introduction

The FFM has for long been used for forecasting particular isolated eruptions and mainly for analysis in hindsight. Systematic applications of this method in the aim to evaluate its statistical performance has never been carried out, either in hindsight or in real time. In this Chapter,

I show successful results obtained with the method developed in this thesis, but I also show the power of objectively analysing a huge amount of precursory sequences of eruptions thank to the automatic classification of seismo-volcanic signals. By doing so, it is possible to estimate the global applicability of the method, as well as its overall accuracy when it is applicable. In the following, I apply the method of real-time eruption forecasting developed in this thesis on all the precursory seismic sequences presented in Chapter 3. In total, 65 sequences are analysed on three different volcanoes. Consequently, the statistical meaning of the results presented in this Chapter aims to be significant.

The new method of real-time forecasting designed for real-time applications will first be tested on textbook cases. I define as "textbook cases" precursory sequences presenting a simple and long acceleration pattern, that allows for successful results of real-time prediction. The aim is to evaluate the potential of the method on simple examples. The method is tested on VT precursory activity, which is supposed to be the most relevant observable for the use of FFM. Then, the method is applied on LP precursory patterns of vulcanian explosions. I show that results of predictions can be impressive when simple cases are chosen and when successful results are isolated. However, when a systematic and objective analysis is carried out, we face more complicated precursory patterns, that are not necessary well described by the FFM. In some cases, real time predictions are nevertheless successfully carried out, opening the discussion concerning the precursory physical mechanisms and their link with the eruption. In other cases they lead to poorly constrained results that would not be useful for real-time applications. I finish this Chapter with a quantification of the success rate of the FFM for real-time applications, that will open the discussion on the true utility of the FFM for real-time forecasting.

For the operational application of the forecasting tool, we have to set the conditions for which it can be used, i.e. in which cases the reliability criteria defined in Chapter 4 are expected to be encountered. On successful examples, I quantify the amount of data from which it would be possible to obtain well-constrained predictions. Based on this information, it is possible to evaluate the time at which an alarm could be triggered before the eruption.

A scientific article based on this Chapter is in preparation:

Boué A., Lesage P., Cortés G., Valette B., Spica Z., Reyes-Dávila G., Arámbula-Mendoza R. and Budi-Santoso A.. *Performance of the 'Material Failure Forecast Method' in real-time situation: a Bayesian approach applied on effusive and explosive eruptions* (2015, in prep.). *Journal of Volcanology and Geothermal Research*.

5.2 Real-time predictions

In this section, I analyse the results of real-time predictions carried out on exhaustive precursory sequences of eruptions at the three volcanoes presented in Chapter 3. Different precursory patterns of seismicity are encountered thanks to the important number of sequences treated with the automatic classification tool. I first show the results of prediction obtained with simple precursory acceleration patterns of seismicity ("textbook cases"). However, the majority of the precursory patterns analysed in this study display more complicated patterns. For these cases, the interpretation of the prediction results are more difficult or real-time predictions using a single power-law model are simply not possible.

5.2.1 Testing the forecasting method on textbook cases

I first present the results of predictions carried out with VT precursors at PdlF and Merapi volcanoes. I then move on with LP sequences at Volcán de Colima.

5.2.1.1 Application on VT precursors: Piton de la Fournaise and Merapi volcanoes

Piton de la Fournaise

At PdlF volcano, three seismic patterns can be identified as textbook cases: the 30 May 2003, the 23 June 2000 and the 12 August 2004 eruptions.

30 May 2003. The eruption of the 30 May 2003 at PdlF was preceded by two days of increasing VT rates (Figure 5.1a). The acceleration pattern is clear with $\Delta t = 2$ h. The precursory VT pattern is an acceleration followed by 8 h of seismic quiescence to finish with a last peak of seismicity just before the eruption. According to the optimal starting time t_0 determined following the methodology explained in Chapter 4, the time of eruption is $t_e = 2.5$ days. The p -value estimate for this case oscillates around 2 (Figure 5.1b). The first precise prediction occurs at $t_{obs} = 1.58$ days, with a 99% confidence interval ranging from $t_f = 1.8$ days to $t_f = 4$ days (Figure 5.1c). Then, the maximum likelihood of the predictions remain close to $t_f = 2.35$ days with a confidence interval getting narrower until the time of deceleration at $t_{obs} = 2.20$ days, as indicated by the Shannon index (Figure 5.1d). For this case, the stability lasts 16 h (corresponding to 16 data points). An accurate and precise prediction in real time based on the criteria defined in Chapter 4 (stability of the predictions and decreasing Shannon index) could have been made at $t_{obs} = 1.6$ days, i.e. more than half a day before the eruption, with the a 99% confidence interval between $t_f = 2$ days and $t_f = 2.5$ days.

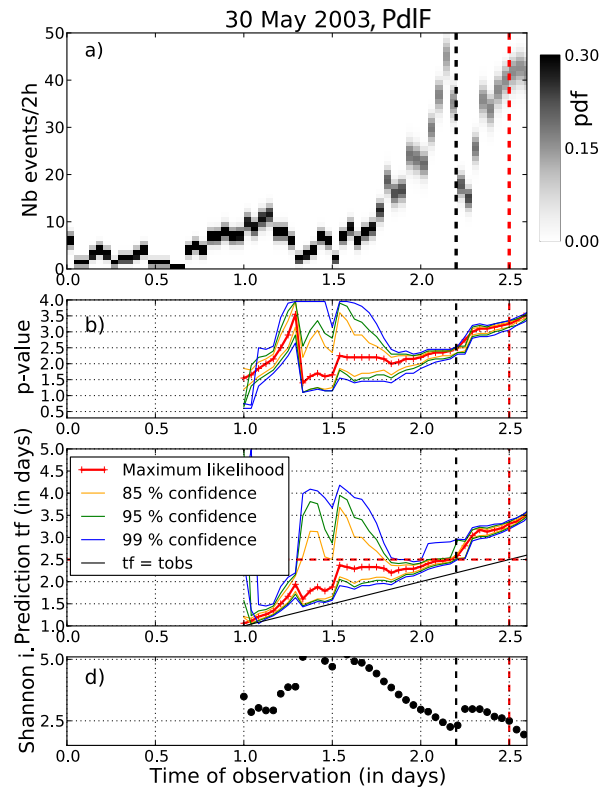


Figure 5.1: a) Prior *pdfs* of the data for the 30 May 2003 eruption at PdIF, as a function of the observation time t_{obs} . The true time of eruption is $t_e = 2.5$ days (red dashed line). The black dashed line indicates the time of deceleration. b) Posterior marginal *pdfs* of p . The red line is the maximum likelihood of the *pdfs* and the yellow, green, and blue lines indicate the 85%, 95% and 99% intervals of confidence, respectively. c) Posterior marginal *pdfs* of the prediction t_f . The red line is the maximum likelihood of the *pdf* and the yellow, green, and blue lines indicate the 85%, 95% and 99% intervals of confidence, respectively. The black line corresponds to $t_f = t_{obs}$. d) Shannon's index of the marginal *pdfs* of t_f .

23 June 2000. The eruption of the 23 June 2000 was preceded by about 16 days of increasing VT rate (Figure 5.2a). In this case, the acceleration pattern is clear with $\Delta t \geq 12$ h. The precursory pattern is composed of an acceleration followed by 1.5 days of quiescence before the eruption ($t_e = 16$ days). Again, p -value estimates are close from 2 as shown in Figure 5.2b. Maximum likelihood estimates of the prediction times are unstable until $t_{obs} = 11$ days and then stabilise during 1.5 days around $t_f = 14$ days (Figure 5.2c), with a decreasing Shannon index (Figure 5.2d) but with large uncertainties. The predictions then stabilize around $t_f = 15$ days in the interval $t_{obs} \in [12 - 13.5]$ days, with the 99% of confidence interval getting narrower. At $t_{obs} = 13.5$ days, 99% intervals show that an eruption can be expected between $t_f = 14$ days and $t_f = 16.5$ days, with a maximum likelihood at $t_f = 15$ days. Based on the real-time criteria, an eruption could thus have been successfully forecast 2.5 days before the eruption. After this time, there is a deceleration of the seismicity lasting one day and then followed by a

last acceleration, which explains why the predictions are not stable anymore until the time of eruption.

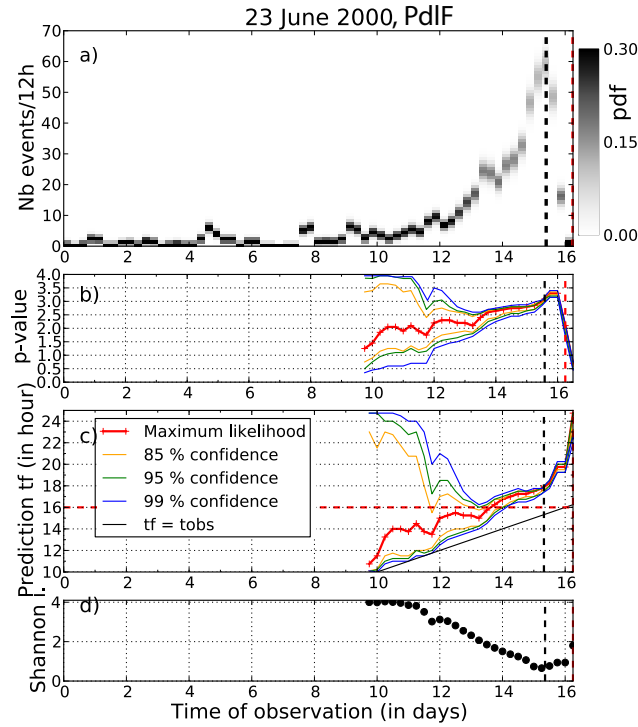


Figure 5.2: a) Prior *pdfs* of the data for the 23 June 2000 eruption at PdIF, as a function of the observation time t_{obs} . The true time of eruption is $t_e = 16$ days (red dashed line). The black dashed line indicates the time of deceleration. Panels b), c) and d) same as Figure 5.1(b-d).

12 August 2004. The eruptive event that occurred on the 12 August 2004 was preceded by a sequence of about ten days of acceleration (Figure 5.3a), with the eruption occurring at $t_e = 18$ days. The acceleration pattern becomes clear with a window width of $\Delta t = 12 h$. The predictions are unstable until $t_{obs} = 13$ days and stabilise at $t_f \simeq 18$ days during 1.5 days (until $t_{obs} = 14.5$ days), with a 99% confidence interval between $t_f = 17$ days and $t_f = 20$ days (Figure 5.3c). After that, t_f becomes unstable during the deceleration part. So, in this case we could have made a precise prediction 3.5 days before the eruption between $t_f = 17$ days and $t_f = 20$ days with 99% of confidence, and with a greater probability that it occurs at $t_f = 18$ days. Note that the *p*-value estimate of the sequence is around $p = 2.5$ (Figure 5.3b).

Partial conclusions These particular textbook cases at PdIF volcano clearly shows a good potential of the method developed in this thesis for real-time applications of the FFM for several reasons. First, the stability and accuracy criteria are helpful indicator of an incoming eruption

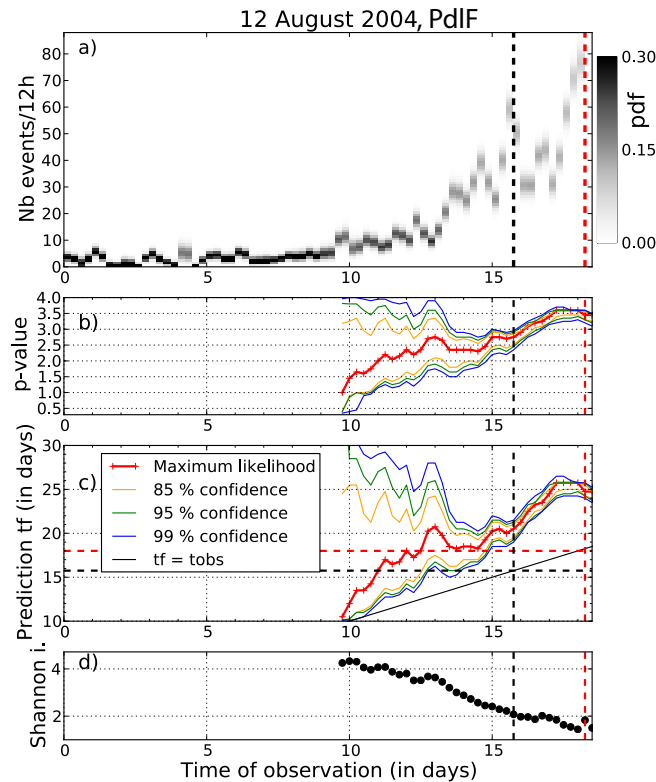


Figure 5.3: a) Prior *pdfs* of the data for the 12 August 2004 eruption at PdIF, as a function of the observation time t_{obs} . The true time of eruption is $t_e = 18$ days (red dashed line). The black dashed line indicates the time of deceleration. Panels b), c) and d) same as Figure 5.1(b-d).

as they allows for giving the true time of eruption. Second, the 99% confidence interval is smaller than the time interval remaining until the eruption. Third, from the time a prediction is delivered, several days are available for potential crisis management.

For the three cases presented here, there seem to be systematic two-phases accelerations, which limits the applicability of our method on the first part of the acceleration. However, even with this limit, it is possible to carry out successful real time predictions.

Merapi, 26 October 2010

The hundred-year eruption of Merapi volcano which occurred in 2010 was preceded by an acceleration of VT events of about 50 days, with a time of eruption $t_e = 51$ days (Figure 5.4a). Within this acceleration, we can observe 5 days of stronger VT activity between $t_{obs} = 36$ days and $t_{obs} = 41$ days. The predictions displayed in Figure 5.4c are unstable until $t_{obs} = 45$ days. After this time, the maximum likelihood of t_f stabilises around $t_f = 55$ days until $t_{obs} = 48.5$ days and the Shannon index decreases only between $t_{obs} = 46.5$ days and $t_{obs} = 48.5$ days (Figure 5.4d). The 99% confidence intervals are found between $t_f = 52$ days and $t_f = 59$ days.

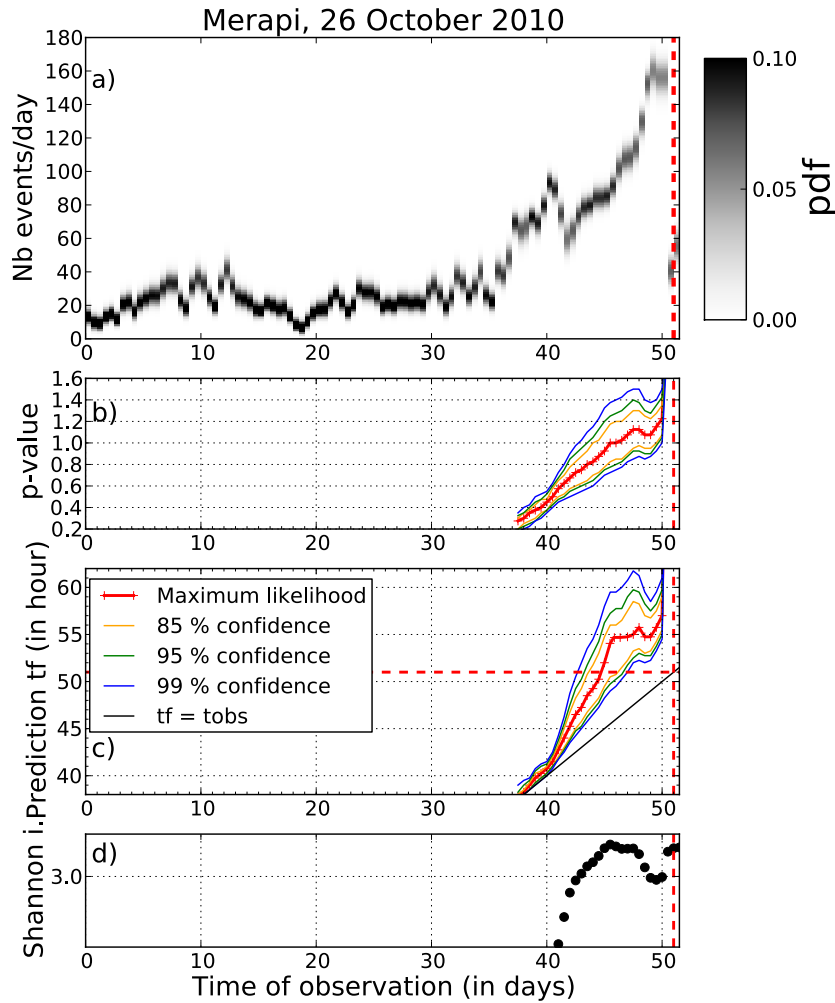


Figure 5.4: a) Prior *pdfs* of the data for the 26 October 2010 eruption at Merapi, as a function of the observation time t_{obs} . The true time of eruption is $t_e = 18$ days (red dashed line). The black dashed line indicates the time of deceleration. Panels b), c) and d) same as Figure 5.1(b-d).

Thus, in a real-time situation, a prediction could have been made three days before the eruption ($t_{obs} = 48$ days), between $t_f = 52$ days and $t_f = 59$ days, with a greater probability that it occurred at $t_f = 55$ days. In this case, the prediction is one day later than the true eruption time. It might be possible that the prediction time was delayed by the 5-day long burst of the seismicity that interspersed the acceleration. This example typically shows the necessity of looking at the data at the same time as predictions are made in real-time. Finally, we can notice that the p -value is close to 1 (Figure 5.4b).

5.2.1.2 Application on LP precursors: Volcán de Colima

At Volcán de Colima, the precursory acceleration of LP rates before the 5 June 2005 and the 10 May 2005 can be considered as textbook cases for the application of FFM.

5 June 2005. The explosion of the 5 June 2005 was preceded by a sequence of accelerating LP rates of about twenty hours (Figure 5.5a) with a time of eruption at $t_e = 28$ h. A deceleration of the activity is observed 0.5 h before the explosion. Window sizes $\Delta t = 1.5$ h and $\Delta t = 2$ h are both suitable for evaluating the LP event rates. Figure 5.5c represents the prediction t_f as a function of the observation time t_{obs} . The accelerating sequence of LP events starts at $t_{obs} \simeq 21$ h and the first prediction that seems (*a posteriori*) satisfying when compared with the true eruption time is obtained at $t_{obs} = 23$ h, i.e. 5 h before the explosion, but its uncertainty is large (its 99% confidence interval ranges from $t_f = 26$ h to $t_f = 60$ h). The estimated value of t_f remains quite stable until $t_{obs} = 26$ h while its precision is getting better, as indicated by the Shannon index (Figure 5.5d). Moreover, the lower bound of the 99% confidence intervals of t_f is equal to the time of observation t_{obs} while the upper bound remains at an almost constant value in a range $t_f \in [30, 34]$ h from $t_{obs} = 26$ h until the eruption time. Therefore, a prediction could have been made 5 hours before the eruption, in an interval between $t_f = t_{obs}$ and $t_f = 34$ h, at a confidence level of 99%, with a maximum likelihood around $t_f = 28$ h which is very close to the real time of eruption. The maximum likelihood of the p -value varies with time and is close but not equal to 1 in the last part of the acceleration (Figure 5.5b).

10 May 2005. Before the major vulcanian explosion of the 10 May, an acceleration of the LP seismicity occurred during about 30 hours (Figure 5.6a, $t_e = 37$ h). A window width $\Delta t = 2$ h produces the most stable and precise t_f distributions. As for the 5 June event, a 0.5-hour-long deceleration occurred before the explosion. Maximum likelihood estimates of the prediction times are unstable until $t_{obs} = 26.5$ h and then stabilise around $t_f = 29$ h during 3 h, i.e. during the first part of the acceleration (Figure 5.6c), with a decreasing Shannon index (Figure 5.6d). The upper 95% of confidence is quite stable around $t_f = 32$ h. Thus an explosion could have been expected between the observation time and $t_{obs} = 32$ h. However, this sequence is followed by a slight deceleration over 3 h and then by a second acceleration. For times of observation in the interval $[29, 32]$ h, i.e. in the short deceleration part, the prediction time t_f is very close to t_{obs} . Even though the Shannon index is relatively low in this interval, the prediction is not reliable due to the unstability of t_f with respect to the time of observation. Reliable accurate predictions are obtained since $t_{obs} = 32.5$ h, i.e. 4.5 hours before the explosion, and give an estimation of $t_f \simeq 38$ h. In this case however, there is probably a bias in the estimations because the fitting interval includes the 3 h long deceleration phase. For the observation times in the interval $[32.5, 36]$ h the maximum likelihood of t_f remains stable between $t_f = 37$ h and $t_f = 38$ h and the pdf of t_f gets more precise until the time of

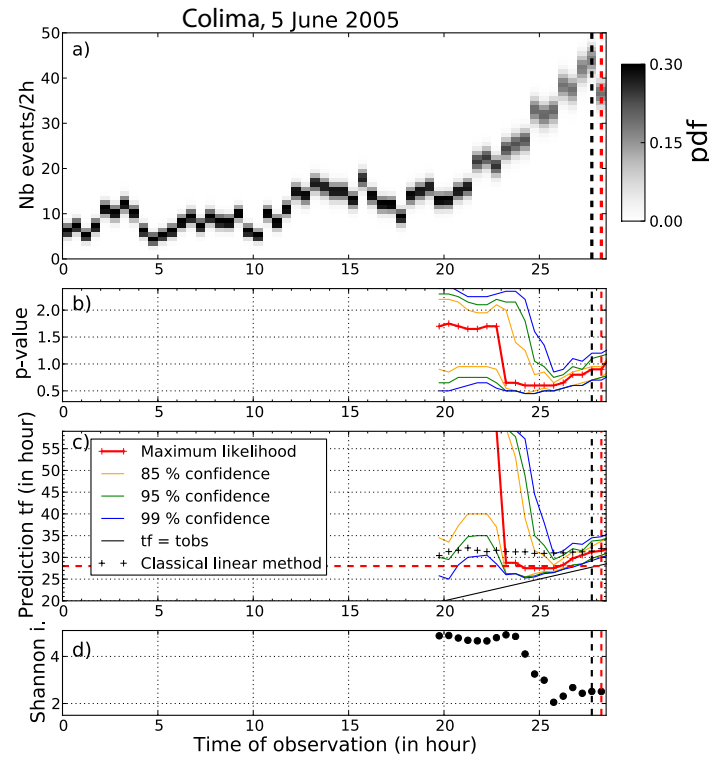


Figure 5.5: a) Prior *pdfs* of the data for the 5 June 2005 explosion at Volcán de Colima, as a function of the observation time t_{obs} . The true time of eruption is $t_e = 28h$ (red dashed line). The black dashed line indicates the time of deceleration. b) Posterior *pdfs* of p . The red line is the maximum likelihood of the *pdf* and the yellow, green, and blue lines indicate the 85%, 95% and 99% intervals of confidence, respectively. c) Posterior marginal *pdfs* of the prediction t_f . Black crosses represent the prediction t_f obtained for $p = 1$ and k being the maximum likelihood of the prior *pdf* of Ω_0 . The red line is the maximum likelihood of the *pdf* and the yellow, green, and blue lines indicate the 85%, 95% and 99% intervals of confidence, respectively. The black line corresponds to $t_f = t_{obs}$. d) Shannon's index of the marginal *pdfs* of t_f .

deceleration. Thus, an explosion could be expected to occur at a time between $t_f = 36.5$ h and $t_f = 39$ h with 95% of confidence, with a maximum likelihood of t_f ranging between 37 h and 38 h, at a time of observation about 4 h before the explosion.

5.2.2 Complex cases for real-time applications

In the literature, the results of predictions obtained with the FFM are generally shown for simple textbook cases, i.e. using simple acceleration patterns. However, these simple precursory patterns are not the most common ones. For a comprehensive overview, it is important to present the different patterns we can encounter in volcano-seismic sequences. This section shows results of real-time predictions carried out with complicated patterns of precursory seismicity at

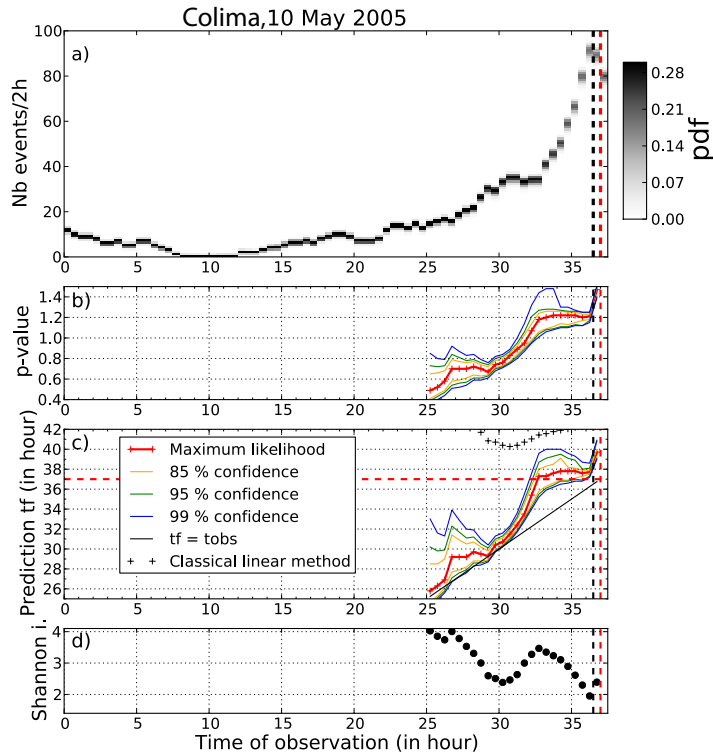


Figure 5.6: a) Prior $pdfs$ of the data for the 10 May 2005 at Volcán de Colima, as a function of the observation time t_{obs} . The true time of eruption is $t_e = 37h$ (red dashed line). The black dashed line indicates the time of deceleration. Panels b), c) and d) same as Figure 5.5b-d.

Colima and PdIF volcanoes. Some successful results open the question concerning the physical processes going on before eruptions while others demonstrate the limitations of the FFM for real-time forecasting.

5.2.2.1 Acceleration-deceleration patterns

At PdIF volcano, it is common to observe a seismic quiescence between the end of the precursory acceleration and the eruption, as displayed in Figure 5.7 (left) for the 2 May 2004. This pattern is also observed at Colima volcano, as for example before the 29 April 2005 explosion (Figure 5.7, right) or before the 7 June and 8 May 2005 explosions (Figure 5.8). I do not present all cases presenting such an acceleration-deceleration pattern, other cases are displayed in Appendix C. I applied the method of prediction to these cases to determine whether accelerations at PdIF allows for predicting the eruption or the failure of the edifice.

2 May 2004, PdIF. The 2 May 2004 eruption at PdIF volcano was preceded by about three days of VT acceleration followed by three days of deceleration of the seismicity (Figure 5.7a, left). The prediction results never stabilise probably because the duration of the acceleration

is too short. However, predictions oscillate about $t_f = 6$ days at $t_{obs} = 5.5$ days, with the 99% confidence intervals between $t_f = t_{obs}$ and $t_f = 10$ days. Thus, the predicted time does not correspond to the time of eruption $t_e = 10.5$ days. Similar conclusions are drawn for the examples displayed in Appendix C. So, these cases lead to wrong eruption predictions.

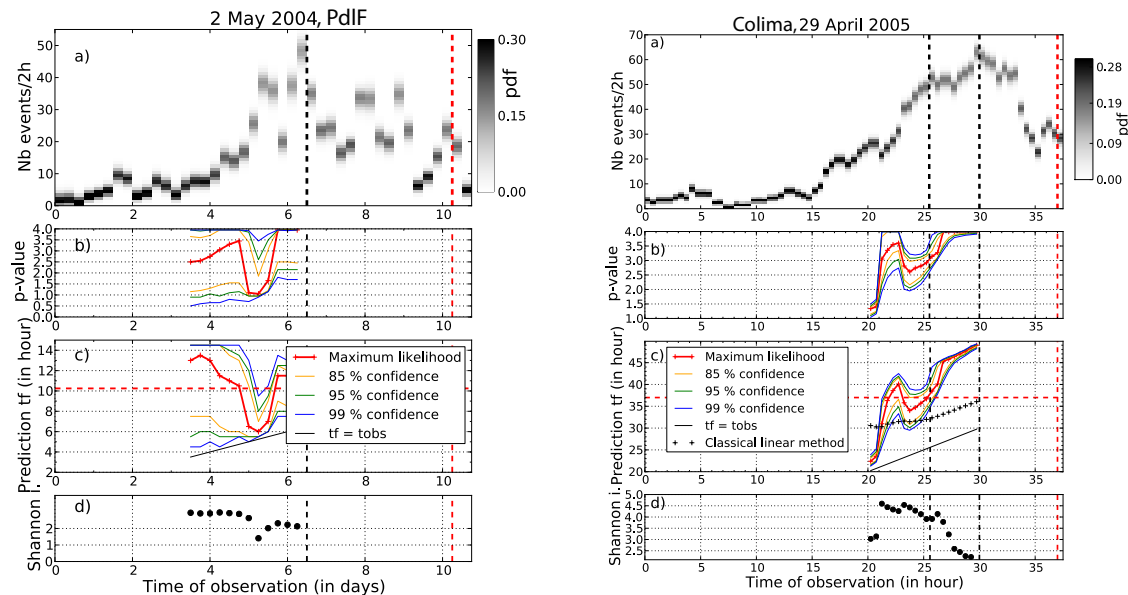


Figure 5.7: Left panel: a) Prior *pdfs* of the data for the 2 May 2004 eruption at PdlF volcano, as a function of the observation time t_{obs} . The true time of eruption is $t_e = 10.25$ days (red dashed line). The black dashed line indicates the time of deceleration. Panels b), c) and d) same as Figure 5.1b-d. Right panel: a) Prior *pdfs* of the data for the 29 April 2005 explosion at Colima volcano, as a function of the observation time t_{obs} . The true time of eruption is $t_e = 37h$ (red dashed line). The black dashed line indicates the time of deceleration. Panels b), c) and d) same as Figure 5.5b-d.

Some of the precursory LP activities of vulcanian explosions at Colima volcano also present acceleration patterns followed by seismic quiescence, as displayed in Figure 5.7 (right) and Figures 5.8. These cases can be interesting since such a behaviour of LP rates prior to vulcanian explosion is still unexplained.

29 April 2005, Colima. The explosive event that occurred on the 29 April 2005 was preceded by a sequence of about 15 hours of LP acceleration, followed by more than ten hours of deceleration (Figure 5.7a, right), with the eruption occurring at $t_e = 37$ h. A window width $\Delta t = 2$ h produces the most stable and precise t_f distributions. The predictions are unstable until $t_{obs} = 21$ h and then oscillate in the range $t_f \in [35, 40]$ h during 5 h (until $t_{obs} = 26$ h), with the 99% confidence intervals ranging from $t_f = 32$ h to $t_f = 40$ h (Figure 5.7c, right). After that, the prediction t_f becomes unstable during the deceleration part. So, in this case we could have made a prediction between $t_f = 32$ h and $t_f = 40$ h with 99% of confidence

and a greater probability that it occurred in the range [35, 40] h, at a time of observation 11 h before the explosion. Note that the maximum likelihood estimate of the p -value is very different from 1 and is not constant (Figure 5.7b, right). This example consequently shows successful real-time prediction, even with ten hours of quiescence preceding the explosion.

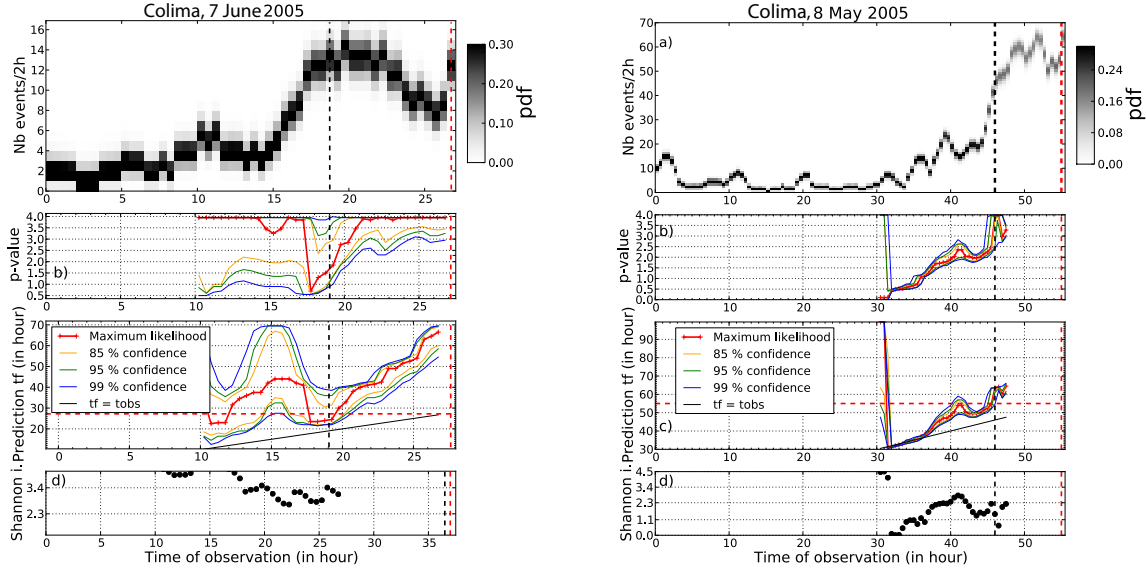


Figure 5.8: Left panel: Left panel: a) Prior $pdfs$ of the data for the 7 June 2005 explosion at Colima volcano, as a function of the observation time t_{obs} . The true time of eruption is $t_e = 29$ h (red dashed line). The black dashed line indicates the time of deceleration. Panels b), c) and d) same as Figure 5.1b-d. Right panel: a) Prior $pdfs$ of the data for the 8 May 2005 explosion at Colima volcano, as a function of the observation time t_{obs} . The true time of eruption is $t_e = 55$ h (red dashed line). The black dashed line indicates the time of deceleration. Panels b), c) and d) same as Figure 5.1b-d.

7 June 2005, Colima. A major explosion occurred the 7 June 2005, preceded by about thirty hours of precursory LP activity (Figure 5.8a, left). The precursory pattern is composed of a five-hour increase of LP activity followed by 8h of deceleration until the explosion at $t_e = 29$ h. The predictions stabilise at $t_f \simeq 24$ h during two hours, between $t_{obs} = 17.5$ h and $t_{obs} = 19$ h (Figure 5.8c, left), with a slightly decreasing Shannon index (Figure 5.8d, left). The uncertainty remains large with a 99% confidence interval between $t_f = 23$ h and $t_f = 39$ h. After that, the predictions become unstable because of the deceleration of LP seismicity. Thus, even if the reliability criteria of the predictions are fulfilled in this case, the large uncertainties of the predictions would have led to a limited applicability of the method in real time. However, an *a posteriori* analysis of the predictions shows that it is possible to forecast the time of explosion even when a long quiescence precedes the explosion.

8 May 2005, Colima. A last example of acceleration-deceleration precursory pattern of LP is illustrated by the LP sequence that occurred before the explosion of the 8 May 2005 at Volcán de Colima (Figure 5.8a, right). This explosion was preceded by 25 h of LP activity, composed of a 15 h acceleration of LPs followed by about 10 h of deceleration until the explosion ($t_e = 55$ h). The maximum likelihood of the predictions stabilises during three hours around $t_f = 50$ h at $t_{obs} = 42$ h, with 99% confidence intervals between $t_f = 48$ h and $t_f = 52$ h. Moreover, the Shannon index decreases during the period of stabilisation. Thus a prediction made at $t_{obs} = 45$ h (i.e. 10 h before the explosion) would have been expected between $t_f = 48$ h and $t_f = 52$ h, with a greater probability that it occurs at $t_f = 50$ h. The true time of prediction falls 3 h after the 99% confidence interval. Real-time predictions would have fail to give the true time of prediction in this case. However, the error of prediction is small in comparison with the time remaining before the explosion and we can still wonder what is the link between the precursory LP acceleration and the explosion, knowing that there is a delay of ten hours between them.

To summarise, in the case of PdIF volcano it seems clear that the FFM applied on VT activity allows for forecasting a failure of the edifice before the eruption, but not the eruption itself. However, in the case of Volcán de Colima the FFM applied on precursory patterns of LP actually forecast the explosion time. This point will be further discussed in Chapter 6.

5.2.2.2 Multiple acceleration patterns

The textbook cases presented in Section 5.2.1 also present two-acceleration patterns just before the time of eruption. In these cases, the second part of the acceleration was short in comparison with the first part that displayed a much longer pattern. As a consequence, predictions could be carried out using the first acceleration. In addition, the seismic quiescence between the accelerating pattern and the eruption was short. Even though the predictions were successful in these cases, I question whether the time of prediction was supposed to forecast the failure of the conduit or the eruption itself. Other cases such as the precursory seismic sequence of the 5 January 2002 at PdIF (Figure 5.9) present a multiple acceleration pattern of VT activity, with a delay of several days between the end of the multiple acceleration and the eruption (other examples of this kind of pattern are presented in Appendix C). Moreover, the eruption is usually preceded by some hours of intense seismic activity, which is interpreted as a dyke propagation towards the surface (Taisne et al., 2011).

This kind of pattern is also observed at Volcán de Colima for the precursory LP activity of vulcanian explosions but there is no physical interpretation to explain this pattern. Results of eruption predictions in this case are presented for the 27 July 2005 explosion and other cases in Appendix C.

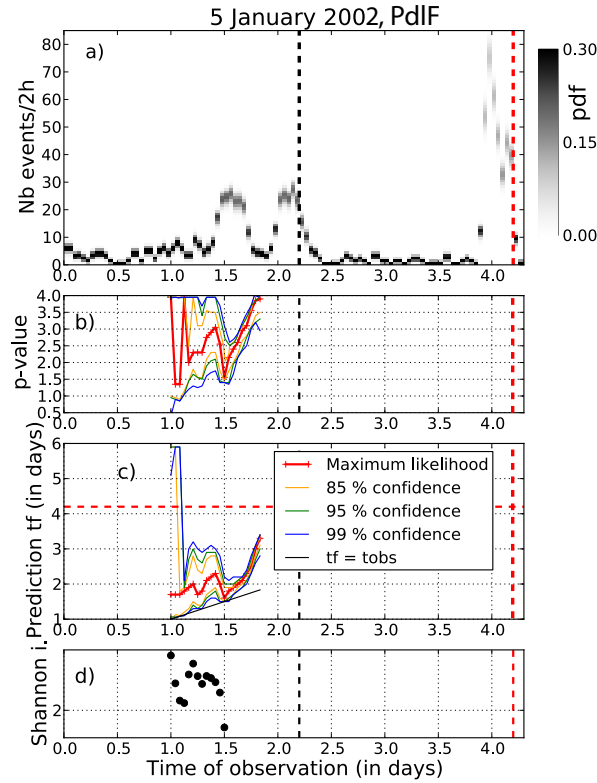


Figure 5.9: a) Prior *pdfs* of the data for the 5 January 2002 eruption at PdIF volcano, as a function of the observation time t_{obs} . The true time of eruption is $t_e = 4.3$ days (red dashed line). The black dashed line indicates the time of deceleration. Panels b), c) and d) same as Figure 5.1b-d.

5 January 2002, PdIF. The 5 January 2002 eruption is preceded by 6 h of VT swarm (Figure 5.9a). This sharp increase does not present an acceleration pattern of the seismicity and is too short to test the forecasting method developed in this thesis. However, a two-acceleration pattern is observed two days before the eruption. Predictions were carried out with the first acceleration. They do not clearly stabilise in time because of the few available data points, leading to a badly constrained model. An *a posteriori* analysis of the predictions is useful to notice that the time of maximum likelihood of t_f oscillates around $t_f = 2$ days, which corresponds to the second peak of seismicity. This result is also obtained for other cases presented in Appendix C. For these cases, the eruption predictions obtained are unsuccessful to predict the true time of eruption. However, whether the failure of the edifice is well-predicted is an open question.

It is difficult to use these patterns for real time predictions for several reasons. First, the FFM is based on a single power-law pattern that does not describe multiple accelerations. Second, the physical meaning of these patterns is poorly understood so the signification of applying the FFM is not clear. Third, if this multiple pattern is effectively related to the

failure of the edifice, it might not necessary lead to an eruption, thus leading to false alarms in terms of predictions. Furthermore, if it actually leads to an eruption, the delay between the predicted failure and the magma reaching the surface is observed to vary from one eruption to another.

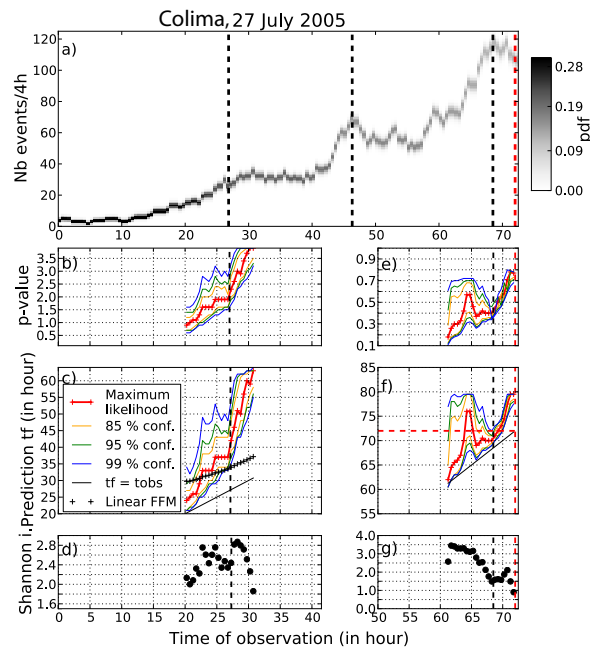


Figure 5.10: a) Prior $pdfs$ of the data for the 27 July 2005 explosion at Colima volcano, as a function of the observation time t_{obs} . The true time of eruption is $t_e = 72h$ (red dashed line). The black dashed line indicates the times of deceleration. Panels b), c) and d) same as Figure 5.5b-d. Panels e), f), g) same as b), c), d) for a beginning of the fitting window at $t_0 = 50 h$.

27 July 2005, Colima. The explosion that occurred the 27 July was preceded by a sequence including three phases of acceleration during more than 70 h in total ($t_e = 72 h$, Figure 5.10a). The first acceleration phase lasted about 30 h and ended at $t_{obs} = 28 h$. It was followed by about 10 h of constant LP activity until $t_{obs} = 40 h$. Then, another short phase of acceleration and deceleration took place until $t_{obs} = 60 h$. This complicated pattern ended with a sharp increase of the seismicity during 10 hours, followed by a constant activity of 4 h before the explosion. During the first phase of the acceleration, until $t_{obs} = 30 h$, relatively stable maximum likelihood of t_f are obtained in the range [33, 37] h during 4 h, with upper 99% of confidence stabilising around $t_f = 49 h$ (Figure 5.10c). Figure 5.10(b) shows that p -values stabilise close to 2. Although the posterior pdf of t_f is very spread (Figure 5.10d), an eruption could have been expected until $t_f = 50 h$. During the phases of deceleration and fluctuation of the seismicity, the FFM theory is no more valid and thus the results are meaningless. For t_{obs} in the interval [40, 45] h, i.e. when the second phase of acceleration is included, it is difficult to fit a simple power law to the whole complex sequence. A trial was done by setting the origin time t_0 at

the beginning of the second phase (i.e. taking $t_0 = 35$ h) and by adjusting the power law to this sub-sequence only. However, the model is then poorly constrained because the data set is too small. The third accelerating phase is longer than the second one and predictions can be performed by setting the beginning of the fitting window to $t_0 = 50$ h. Even if the acceleration phase is short, the maximum likelihood of t_f stabilises around $t_f = 70$ h for t_{obs} ranging from 65.5 to 68 h (Figure 5.10f), with a decreasing Shannon index (Figure 5.10g). The method is thus successful but the stabilisation criterion would have been difficult to use in real-time because of the short duration of the acceleration phase. Note that the p -values are far from the value of $p = 1$ (Figure 5.10e). In addition, the time lag between the prediction made with the first acceleration part and the true time of eruption is about 35 hours, close to the duration of the phases of decrease and fluctuations of seismicity, which appears to have delayed the onset of the eruption. We may speculate that this delay is related to changes in the physical conditions within the magmatic conduit.

5.2.2.3 Too short precursory sequences

Of course, the FFM requires that precursory sequences contain a sufficient number of data points. Too short precursory sequences are problematic in two respects. First, if few data points are available to adjust the theory to the data, then the model and thus the prediction will be poorly constrained. Second, the assessment of the stability criterion requires a minimal number of predictions. Consequently, short precursory sequences are an obviously strong limitation for the real-time prediction method.

30 September 2003, PdIF. One example of short precursory sequence and its associated predictions is displayed in Figure 5.11 for the 30 September 2003 eruption at PdIF volcano. In this case the pattern increases only during one day and because the increase is clearer with $\Delta t = 12$ h, it can be observed with only two data points. It results that the posterior *pdf* of the predictions display large uncertainties and that the maximum likelihood stabilises during only 1.5 days, i.e. 3 data points. In this case, the result of predictions is successful in hindsight but its applicability for real-time eruption forecasting is very limited.

13 March 2005, Colima. Short precursory patterns are also observed before vulcanian explosions at Volcán de Colima. Figure 5.12a shows the precursory LP pattern of the vulcanian explosion of the 13 March 2005 ($t_e = 24$ h). The precursory LP sequence lasts about 3 h in this case. The uncertainty of the predictions becomes acceptable only about 1 h before the eruption with $t_f = t_e$, leaving no time for strategic decisions in the case of volcanic crisis. In hindsight, the results are successful because the maximum likelihood stabilises around the time of explosion and the uncertainty becomes smaller (i.e. decreasing Shannon index in Figure 5.12d), but the method is not successful in real time.

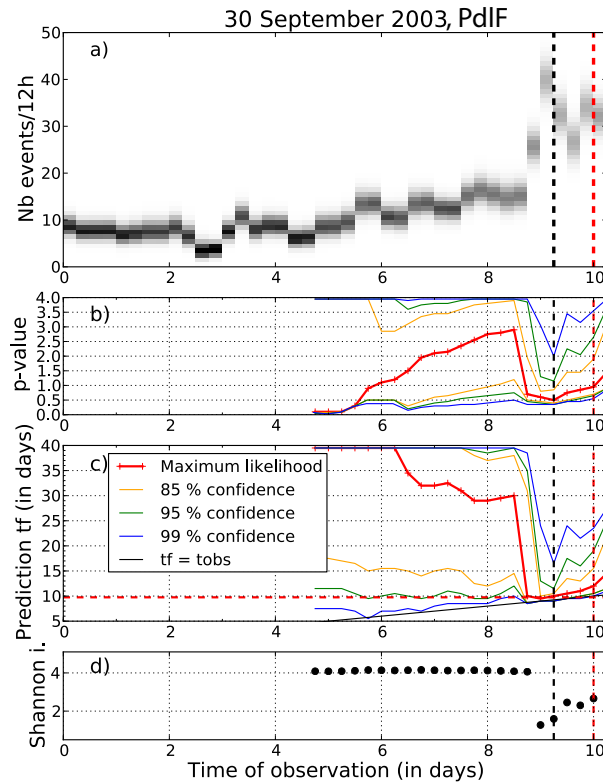


Figure 5.11: a) Prior *pdfs* of the data for the 30 September 2003 eruption at PdIF volcano, as a function of the observation time t_{obs} . The true time of eruption is $t_e = 10$ days (red dashed line). The black dashed line indicates the time of deceleration. Panels b), c) and d) same as Figure 5.1b-d.

These examples of short duration increase of the precursory seismicity at Volcán de Colima and PdIF volcano confirms that real-time eruption predictions using the FFM can be successful only when the acceleration part of the precursory sequence is long enough to constrain the model and ensure stability of the predictions as a function of time. This fact is quite obvious but it is always worth to remind it. This is the reason why forecasting eruptions is so difficult on volcanoes displaying very few precursors before eruptions. More examples of these patterns are presented in Appendix C.

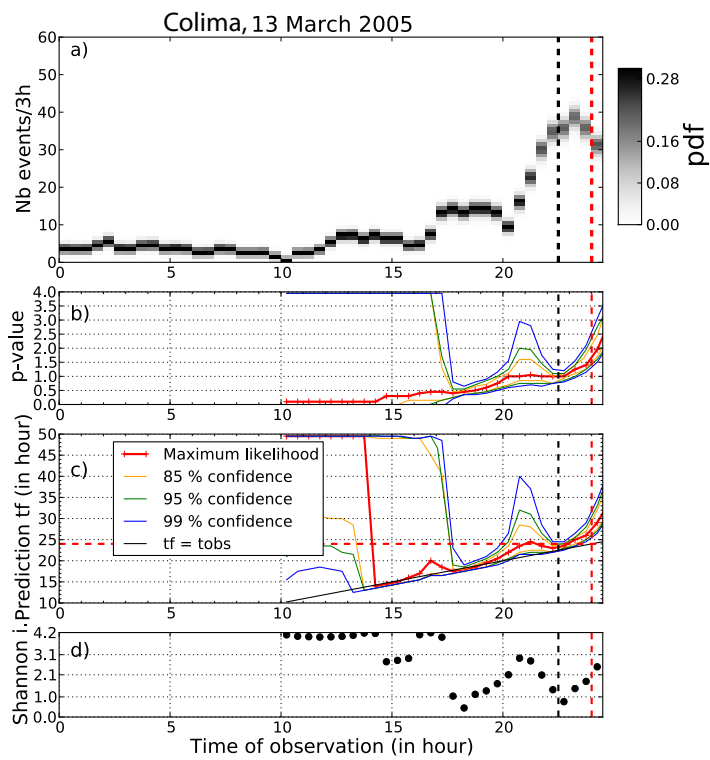


Figure 5.12: a) Prior *pdfs* of the data for the 13 March 2005 explosion at Colima volcano, as a function of the observation time t_{obs} . The true time of eruption is $t_e = 24$ h (red dashed line). The black dashed line indicates the time of deceleration. Panels b), c) and d) same as Figure 5.1b-d.

5.2.3 Comparison with results of the literature

The results of predictions obtained with the method proposed in this paper are now compared with predictions made with the classical FFM theory where the value of the exponent is set at $p = 1$ (or $\alpha = 2$) and the value $\dot{\Omega}_0$ is set at the maximum likelihood of the prior *pdf* of the data at $t_0 = 0$. These results are displayed as black crosses in Figures 5.5c, 5.7c (right), 5.6c and 5.10c, for Volcán de Colima. For the examples of 29 April, 10 May and 27 July, the predictions made with the classical method always give less accurate forecasts than the method proposed in this thesis. Moreover, these predictions never stabilise with the classical method and no reliable uncertainty can be evaluated on the time of prediction t_f as the uncertainty on the data is not taken into account. It would thus be impossible to obtain reliable and accurate real-time predictions with this method. The predictions made with the classical method on the 5 June are very stable around the time of prediction $t_f = 32$ h during the whole period of analysis. This is probably due to the fact that the value of $p = 1$ is a good estimation of the true p -value in this case. However, the time lag of 4 h between the forecast and the true time of the eruption is explained by an estimated p -value slightly smaller than one. As a consequence, I expect the patterns that are well described by $p = 1$ to display stable results of prediction earlier with the classical linear method than with the method developed in this thesis. This is simply explained because there is one degree of liberty less for the linear method, as the exponent is set to $p = 1$. On the other hand, assuming that $p = 1$ when it is not the case leads to biased and unstable results.

Our results can also be compared with those of Arámbula-Mendoza et al. (2011) who performed predictions in hindsight on the sequence of vulcanian explosions that occurred in 2005 in Volcán de Colima. They apply the classical FFM and they use the Root Mean Square of the energy of the continuous seismic signal filtered in the range [1, 3] Hz (SSEM) with the whole sequence of acceleration as fitting window. In their study, no prediction could be obtained for the 5 June 2005 eruption while good results are obtained in the present work. For the 10 May 2005 event, their prediction is 5 h later than the time of eruption, while our approach provides an excellent forecast ($t_f = t_e = 37h$), 4 h before the explosion, with a 95% confidence interval comprised between $t_f = 36.5$ h and $t_f = 39$ h. Their prediction for the 27 July 2005 is 14 h later than the explosion whereas our maximum likelihood of t_f is 3 h earlier the explosion and the 99% confidence interval encompasses the true eruption date. Finally, the prediction made by these authors for the 29 April event is 11 h later than the explosion while our forecasts oscillate between 2h before and 3h after the explosion. To summarise, I obtain closer predictions than the ones carried out by Arámbula-Mendoza et al. (2011) in 14 cases while they obtain better predictions in 5 cases. The other ten prediction results are similar in both studies, even if one have to keep in mind that the comparison is not totally straightforward because they do not calculate the uncertainty on their predictions.

Finally, It is also possible to compare the results of real-time predictions obtained for the

2010 eruption of Merapi volcano with Budi-Santoso et al. (2013). In their study, they also consider the SSEM, like Arámbula-Mendoza et al. (2011). They carry out real-time predictions using the FFM with the classical linear method without calculating the uncertainty on the predictions. They obtained stable predictions around the true time of eruption ($t_f = t_e$) between $t_{obs} = 21$ October and $t_{obs} = 26$ October (5 days of stability) while our predictions stabilise during 3.5 days around a prediction delayed of one day from the true eruption time. The stability of their predictions is obtained one day earlier than in this study.

In order to better compare my results with those obtained by Budi-Santoso et al. (2013), I propose to carry out real-time predictions by setting the exponent $p = 1$ in the Bayesian inversion. Prediction results are displayed in Figure 5.13. Even in this case, Budi-Santoso et al. (2013) predict a time of eruption closer from the true time of eruption than this study. Moreover, this study gives a beginning of stabilisation 5.5 days before the eruption (during 3.5 days with p variable and 4.5 days with $p = 1$) while in their study the stabilisation begins 6 days before the eruption and remains stable until the time of eruption. This suggests that the energy of the events instead of their number may lead to a better shaped power law pattern because the last events before the eruption are generally more energetic, thus enhancing the acceleration of energy rates. More researches are still needed to determine whether one observable is more reliable than another for the application of FFM.

Finally, we can notice that the main difference between the results obtained with a variable p -value (Figure 5.4) and those obtained with $p = 1$ (Figure 5.13) is the uncertainty of the predictions that are smaller when setting the exponent to 1. The maximum likelihood of the pdf of t_f is closer from the true time of eruption when setting $p = 1$, however the 99% confidence intervals does not contain the true time of eruption and its lower limit is one day later than with a variable p . We can suspect that the posterior uncertainty of t_f is more realistic when using the FFM with p variable than with $p = 1$. Therefore, $p = 1$ does not seem to be the most adapted p -value in this case. To conclude, setting the exponent $p = 1$ leads to more stable predictions but leads to slightly bias results of prediction.

Partial conclusions on the case to case study

This case to case study emphasises the complexity of pre-eruptive patterns in both basaltic and andesitic volcanic contexts, at least for the studied volcanoes. Predictions using the FFM are sometimes difficult to carry out and their interpretation in real-time would be complicated. For VT precursors, simple cases are not the majority and it seems that successful predictions occurred because the delay between the predicted failure and the eruption was short. In other cases, eruption predictions would have been wrong. LP precursory patterns, however, enable to predict the true eruption time, even with complicated patterns. Finally, the method of prediction proposed here outperforms the published studies, except in the case of the 2010

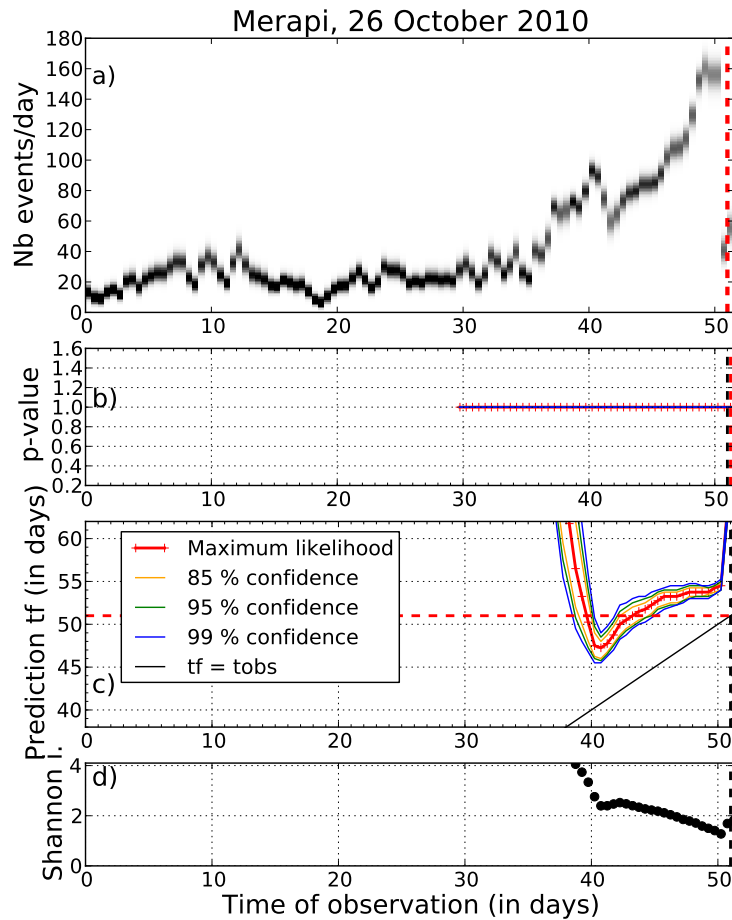


Figure 5.13: a) Prior *pdfs* of the data for the 26 October 2010 eruption at Merapi volcano, as a function of the observation time t_{obs} , with $p = 1$. The true time of eruption is $t_e = 18$ days (red dashed line). The black dashed line indicates the time of deceleration. Panels b), c) and d) same as Figure 5.1b-d.

eruption at Merapi volcano. However, the comparison of the published studies with the results obtained in this thesis are difficult since the uncertainties are not evaluated in Arámbula-Mendoza et al. (2011) and Budi-Santoso et al. (2013).

In the next Section, I quantify the success rate of the prediction method for both real-time and hindsight applications.

5.3 Systematic application and statistical performance

This section presents a general overview of the results of prediction. I report all the prediction results obtained both in real-time and in hindsight in the aim to evaluate the prediction potential of the FFM. The first section shows the amount of cases for which the FFM is applicable, i.e. for which the reliability criteria are encountered in real time or for which patterns are suitable for an hindsight forecast (increase or acceleration of seismicity). In a second section, I focus on the applicable cases to estimate the real-time and hindsight performance of the method in terms of prediction accuracy.

5.3.1 Global applicability of the method

The performance of a forecasting tool has to be analysed in a general point of view, i.e. by quantifying the number of cases for which the method can be applied. In particular, I am interested in quantifying the number of precursory sequences for which the FFM could be applied in *a posteriori* and for which the reliability criteria defined in Chapter 4 are encountered in real time. Because the FFM can only be applied on suitable precursory sequences (i.e. presenting a power law pattern), I also quantify the number of cases for which real-time predictions could have been carried out among the accelerating sequences only.

Table 5.1 present the results of predictions carried out on every eruption reported at PdlF volcano from 2000 to 2010. Table 5.2 and Table 5.3 present the results of predictions for Volcán de Colima and Merapi volcanoes. These tables report the characteristics of the non-cumulative precursory patterns encountered:, i.e. the type and duration of the precursory sequence $\hat{\Omega}(t)$. The types of the patterns are defined as follows: 'single' for single acceleration, 'multiple' for multiple acceleration, 'increase' for patterns with no clear acceleration, 'constant' for abnormalous constant seismicity and 'short swarm' for a burst of seismicity. In addition, I reported the delay between the end of the pattern used for eruption forecasting and the eruption (time lag pattern-eruption). I have considered that there was no sense of carrying out predictions in hindsight in cases for which the precursory seismicity is constant or for which a short swarm were observed. For the 5 cases denoted in red in the Tables, precursory sequences seems to be suitable for the use of FFM, but the posterior maximum likelihood of the exponent p equates the upper bound of the tested values. It was also the case when this bound was extended so I considered that the corresponding α value tends to 1 and thus, that these patterns tend to an exponential trend rather than a power-law trend, which does not enable any prediction (no asymptote).

The applicability of the method for real-time predictions is reported as follows: the consecutive number of stable predictions is reported in Table 5.1, 5.2 and 5.3 (Stab.), as well as the cases of decreasing Shannon index (Shannon: Yes/No). If both criteria are fulfilled then I consider that the method could be applied in real-time.

Date	Pattern	Duration of precursors (in days)	Time lag pattern-eruption (in days)	Hindsight prediction t_f (lower/ML/upper) (in days)	Estimated p-value (lower/ML/upper)	Figure number	Δt	Real-time criteria Stab./Shannon
13/02/2000*	Multiple	2	1.26	-1.53/-1.43 /-1.33	1.4/2.5/3	Fig. C.6	3h	0 / No
23/06/2000**	Single	8	1	-2/-1/+0.5	1.75/2.1/2.5	Fig. 5.2	12h	12 / Yes
12/10/2000	Short swarm	-	-	-	-	-	-	0 / No
27/03/2001**	Single	14	0.5	-0.25/+0.5/+3	1/1.2/1.8	Fig. C.2	12h	3/Yes
11/06/2001*	Single	7	0	-1/0/+2.5	0.8/1.5/3	Fig. C.1	24h	0 / No
05/01/2002*	Multiple	4	2	-2.5/-2.6/-2	1.9/1.5/3	Fig. 5.9	2h	0 / No
16/11/2002**	Multiple	10.75	2.75	-5.75/0/+3.25	1.5/3.9/4	Fig. C.13	12h	8 / Yes
30/05/2003**	Single	2.4	0.2	-0.25/0/+0.1	2.25/2.4/2.45	Fig. 5.1	2h	16 / Yes
22/08/2003	Constant+swarm	-	-	-	-	-	-	0 / No
30/09/2003**	Single	10	1	-0.75/0/+7	0.4/0.5/2	Fig. 5.11	12h	3 / Yes
07/12/2003	Constant+swarm	-	-	-	-	-	-	0 / No
08/01/2004	Increasing steps	-	-	-	-	-	-	0 / No
02/05/2004*	Multiple	10.5	4	-5/-4.5/-0.5	0.9/1/3.5	Fig. 5.7	12h	0 / No
12/08/2004**	Single	18	2.5	-1/+0.5/+2.5	1.9/2.4/3.3	Fig. 5.3	12h	6 / Yes
17/02/2005	Constant+swarm	-	-	-	-	-	-	0 / No
04/10/2005	Short swarm	-	-	-	-	-	-	0 / No
29/11/2005	Constant+swarm	-	-	-	-	-	-	0 / No
26/12/2005**	Multiple	15	4	-6/-4/+5	1.5/2.2/3.7	Fig. C.7	24h	3 / Yes
20/07/2006**	Multiple	27	12.5	-15.5/-12.5/-12	0.7/0.9/1	Fig. C.8	12h	5 / Yes
30/08/2006*	Multiple	16	2.5	-3.5/-2.5/+6.5	0.5/0.9/3.8	Fig. C.3	24h	0 / No
18/02/2007**	Multiple	35	2	-3/-2/+1.5	0.5/0.6/0.75	Fig. C.14	24h	4 / Yes
30/03/2007	Increases	-	-	-	-	-	-	0 / No
21/09/2008*	Multiple	7	6	-6/-5.7/-5	0.5/0.6/0.75	-	12h	0 / No
27/11/2008**	Multiple	6	1	-1.75/-0.75/+7	0.5/0.6/3.5	Fig. C.16	12h	3 / Yes
14/12/2008**	Multiple	15	1.5	-1.5/0/+9	0.6/1/2.4	Fig. C.15	24h	3 / Yes
5/11/2009*	Multiple	3	0.75	-0.75/-0.5/0	0.4/0.6/0.8	-	12h	0 / No
14/12/2009	Short swarm	-	-	-	-	-	-	0 / No
2/01/2010	Short swarm	-	-	-	-	-	-	0 / No
14/10/2010**	Multiple	1.75	0.25	-0.3/-0.25/+0.1	1.5/1.6/2.5	Fig. C.9	2h	5 / Yes
09/12/2010**	Multiple	35	5	-9/+3/+40	0.55/1/2	Fig. C.17	24h	6 / Yes

Table 5.1: Results of eruption predictions carried out on PdIF volcano, from 2000 to 2010. The columns correspond to: the date of each eruption; the type of the pattern; the precursory duration used to apply the FFM; the delay between the end of the pattern used to carry out eruption forecasting and the eruption (quiescence); the results of the prediction t_f in terms of maximum likelihood (ML) and lower and upper bounds of the 99% confidence interval; the p-value of the sequence with its 99% confidence interval; the Figures numbers; the size of the window width Δt ; the reliability criteria fulfilled or not. The predictions are reported as error of prediction, i.e. $t_f - t_e$ (in days). Patterns with a p-value estimate close to 4 are underlined in red.

For PdIF volcano, predictions in hindsight could be carried out for 19/30 eruptions (63%). The limiting pattern for the application of the FFM in this case is the short swarm sequences. Only 12/30 precursory sequences (40%) could have been used for real-time forecasting. Among the sequences that could be used for predictions in hindsight, 12/19 could be used in real-time (63%). Consequently, 63% of the precursory sequences display suitable power law patterns at PdIF and among these patterns only 63% could have been informative to forecast the eruption in real time. Note that $p = 1$ ($\alpha = 2$) is comprised in the 99% confidence interval for 9/19 of these suitable precursory patterns (47%). Thus, precursory sequences that are best described by $\alpha = 2$ are not the majority.

A systematic application of the FFM was also carried out on precursory sequences of vulcanian explosions at Volcán de Colima, from 1999 to 2012. Table 5.2 and Table 5.3 present the results of eruption forecasting as well as the precursory patterns encountered. Among the 35 explosions analysed there were no data for 2 of them and 16 of them displayed precursory patterns that were suitable for the application of predictions in hindsight (16/33 or 48%). Real-time predictions could be performed for 9/33 cases in total (28%) and in 9/16 cases for which the precursory sequence is suitable for hindsight applications (56%). For Volcán de Colima, the main limitations for the application of the FFM are the short duration of the precursory sequences, and the multiple acceleration patterns. Indeed, these patterns usually display several short accelerations of LP seismicity before eruptions. Finally, only 6/16 sequences are best described by $p = 1$ (38% of the suitable sequences).

Only one eruption is analysed for Merapi volcano. In this case, real-time forecasting could have been informative. The p -value that well-describes the precursory sequence is close to one.

When analysing all the eruptions for which data were available, 39/64 were preceded by an accelerating sequence of precursors that were suitable for the application of the FFM in hindsight (61%) and among these ones, 22/39 could have been used for real-time applications (56%). Finally, $p = 1$ was found to be comprised in the 99% confidence intervals for 16/39 precursory sequences (41%).

The statistical performance of the method is similar from one volcano to another. It seems that the accelerating precursory sequences that are suitable for the application of the FFM represent a bit more than half of the eruptions. The seismicity is informative but, because the application of deterministic eruption forecasting requires long-enough-accelerating sequences, which are encountered for only half of the cases, the use of deterministic real-time forecasting is limited.

Besides, less than half of the studied precursory accelerations can be well described by $p = 1$ ($\alpha = 2$). According to the results and conclusions of Section 5.2, the application of the classical inverse linear method on the other patterns would thus have led to biased hindsight predictions and to wrong real-time forecasting.

To conclude, I wish to point out the main limitations of the FFM for eruption forecasting: (1) precursors are required, (2) precursors have to display accelerating pattern, (3) these patterns must be long enough to constrain the model.

Based on the sequences that are suitable for the application of FFM, I now propose to evaluate the accuracy of the forecasting method developed in this thesis, both for real-time hindsight applications.

Date	Type of pattern	Duration of precursors	Quiescence before eruption	Hindsight prediction t_f (in hours)	estimated p-value	Figure	Δt	Real-time application Stab./Shannon
10/02/1999	Constant	-	-	-	-	-	-	-
10/05/1999	Constant	-	-	-	-	-	-	-
17/07/1999*	Single	13h	0	+7/+10/+12	2.5/3.9/4	-	1h	0/No
22/02/2001*	Increase	40h	6h	-5/-2/+18	0.6/1.2/3.9	-	2h	0/No
17/07/2003	Constant	-	-	-	-	-	-	-
2/08/2003	No data	-	-	-	-	-	-	-
29/08/2003	No data	-	-	-	-	-	-	-
15/11/2003*	Single	8h	0	0/+1.5/+8	0.6/1.2/3.5	Fig. C.5	2h	0/Yes
10/03/2005*	Single	10h	4h	-2/-1/+1	1.9/2.7/3.5	-	2h	0/No
13/03/2005**	Single	24h	1.5h	-1.5/-1/0	0.8/1/1.2	Fig. 5.12	3h	6/Yes
24/03/2005*	Increase	24h	0	-5/-3.5/-2.5	2.5/3.85/4	-	3h	0/No
26/03/2005	Constant	-	-	-	-	-	-	0/No
12/04/2005*	Single	10h	3h	-3/0/+2	1.5/3.9/4	-	2h	0/Yes
20/04/2005**	Multiple	15h	0.5h	-5/-2/0	2/4/4	Fig. C.10	2h	7/Yes
22/04/2005**	Multiple	21h	1h	-8/-1.5/0	0.5/0.7/1.4	Fig. C.11	3h	8/Yes
29/04/2005**	Single	37h	12h	-2/0/+3	2.5/3/3.5	Fig. 5.7	2h	9/Yes
01/05/2005	Multiple	-	-	-	-	-	-	-
03/05/2005**	Multiple	11h	0	-2/0/+4	1.3/3.4/3.9	Fig. C.4	2h	5/Yes
04/05/2005	Constant	-	-	-	-	-	-	-
05/05/2005	Constant	-	-	-	-	-	-	-
08/05/2005**	Single	55h	10h	-7/-5/-4	1.7/2/2.1	Fig. 5.8	2h	5/Yes
10/05/2005**	Multiple	37h	0.5h	0/+0.5/+1.5	1.15/1.2/1.25	Fig. 5.6	2h	8/Yes
16/05/2005	Constant	20h	-	-	-	-	-	-
24/05/2005	Multiple	40h	-	-	-	-	-	-
25/05/2005	Multiple	30h	-	-	-	-	-	-
30/05/2005*	Multiple	70h	25h	-24/-21/-17	1.1/1.25/1.7	-	2h	4/Yes

Table 5.2: Results of eruption predictions carried out on Volcán de Colima volcano, from 1999 to 2012. Same organisation as Table 5.1.

Date	Type of pattern	Duration of precursors	Quiescence before eruption	Hindsight prediction	Estimated p-value	Figure	Δt	Real-time application Stab./Shannon
02/06/2005*	Increase	30h	0	0/0/+1	0.1/0.3/1	-	4h	0/No
05/06/2005**	Single	28h	0.5h	-1/0/+3	0.5/0.6/0.9	Fig. 5.5	2h	7/Yes
07/06/2005**	Single	26h	9h	-4/-3/+13	1/1.8/4	Fig. 5.8	2h	4/Yes
10/06/2005	Increase	10h	-	-	-	-	-	-
05/07/2005*	Multiple	50h	0.5h	-0.5/0/+1	0.4/0.6/0.8	Fig. C.12	3h	0/Yes
07/07/2005*	Multiple	27h	0h	0/0/+1	0.45/0.45/0.5	-	3h	0/No
27/07/2005**	Multiple	72h	4h	-3/-2/0	0.35/0.4/0.45	Fig. 5.10	4h	5/Yes
16/09/2005	Multiple	72h	-	-	-	-	-	-
27/09/2005	Constant	48h	-	-	-	-	-	-
26/10/2010 Merapi**	Multiple	51 days	0.5 days	+1/+4/+8	0.9/1.1/1.4	Fig. 5.4	24h	7/Yes

Table 5.3: Same as Table 5.2 for Volcán de Colima and Merapi (continued)

5.3.2 Accuracy of the method when applicable

In this section, I define as a *success* a prediction for which the true time of eruption is comprised in the 99% confidence interval of the posterior *pdf* of t_f ; as *missed* precursory sequences for which the reliability criteria are not encountered; and as *informative* predictions for which the 99% confidence interval is shorter than the remaining time before eruption.

5.3.2.1 Accuracy of real-time forecasts

Now that the global applicability of the FFM has been evaluated, it is important to estimate the accuracy of the forecasts. Two criteria are defined for the real time application of the method developed in this thesis: the stability of the predictions as a function of time and their uncertainty that are expected to get better as time advances (decreasing Shannon index). In an exploratory perspective, the stability criterion is defined only qualitatively: I define as *stable* at least N consecutive predictions that are *close* to the same value where *close* is qualitatively estimated. If this criterion is fulfilled and the Shannon index decreases, then the method is considered to be applicable for real-time perspective (Table 5.1, 5.3, 5.2) and the forecast is considered as reliable.

In Figure 5.14, I report the effective error of predictions $t_f - t_e$ as a function of the remaining time before eruption for PdIF and Merapi volcanoes, and for Volcán de Colima, each time the criteria are encountered. Three stability criteria are tested in real-time perspective: results of prediction are reported when Shannon index decreases and either 3, 4 or 5 points of stability are obtained.

In the case of PdIF and Merapi volcanoes with a 3-point stability criterion (Figure 5.14, left), 15/16 real-time predictions contain the true time of eruption. For 8/16 cases, the uncertainties are smaller than the remaining time before eruption. Thus, almost all real-time predictions would have been successful, but half of them are associated with large uncertainties. The success rate is the similar for a 4-point criterion where 9/16 forecasts can be carried out and the other eruptions are missed. With a 5-point criterion, half of the eruptions are predicted with all predictions being successful and only one of them display a large uncertainty. Consequently, a demanding stability criterion gives accurate and informative predictions but half of the eruptions are missed, while a less demanding stability criterion allows for forecasting all the eruptions but one of them is completely wrong and only half of them have an informative uncertainty. Finally, in any cases most of the real-time predictions could have been carried out at least two days before the eruption.

The same analysis can be carried out for the results of real-time predictions obtained for Volcán de Colima. The results obtained for the 30 May 2005 are not reported in the Figure since the prediction results are totally wrong ($t_f - t_e = -21$ h), but they are counted in the

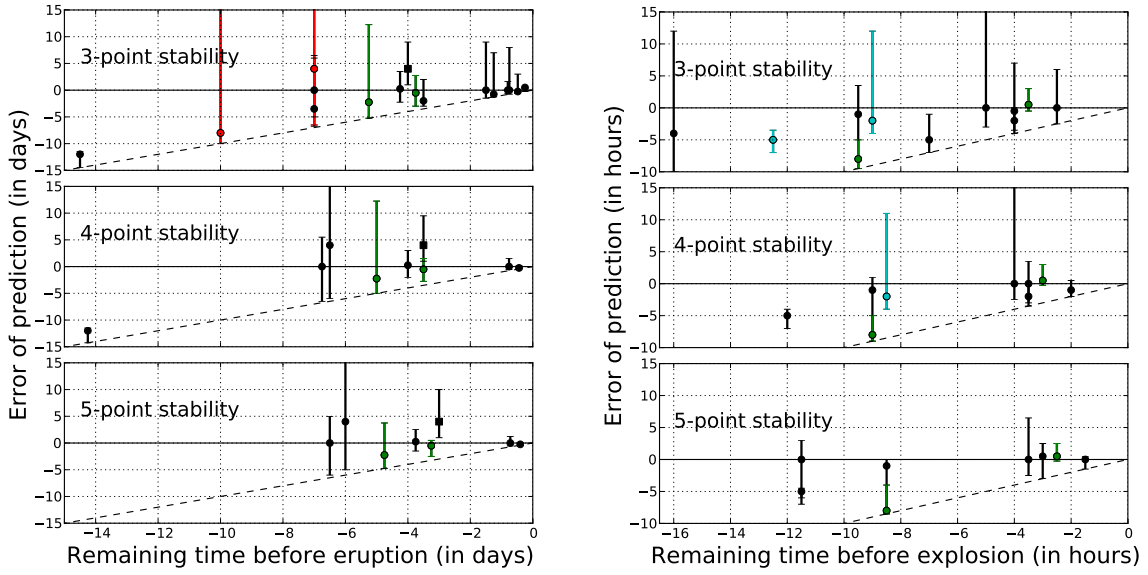


Figure 5.14: Results of real-time predictions showing the error of prediction $t_f - t_e$ as a function of the time remaining before the eruption. The results are reported for three different stability criteria, considering 3-point, 4-point or 5-point stability in the Figures of Section 5.1. Eruptions for which the criteria are fulfilled only one time are represented in black and eruptions for which stability is reached several times are denoted in color. Black dashed lines represent $t_{obs} = t_f$. Left panel: results obtained for PdIF eruptions (full dot) and Merapi eruption (full square). Right panel: results obtained for Volcán de Colima explosions.

statistics. For a 3-point stability criterion, 8/12 cases contain the true time of explosion but only 4 of them display an uncertainty that is smaller than the remaining time before explosion. If the number of required stability points is increased to 4, then 9/12 explosions are forecast with two of them giving a wrong prediction. However, 5/9 predictions have an uncertainty that is smaller than the remaining time before explosion. The success rate is the same with a 5-point stability criterion but one more explosion is missed. The conclusion is the same as for the PdIF and Merapi volcanoes: the more demanding is the stability criterion, the more accurate will be the predictions but the least eruptions are forecast. For Volcán de Colima, real-time predictions could have been carried out at least two hours before the explosions.

The method of deterministic real-time predictions proposed here is obviously dependent on the amount of data available for carrying out eruption forecasting at a given time. It might be interesting to determine from which amount of data it is possible to use the method. To do so, Figure 5.15 shows the relative error of predictions as a function of the proportion of precursory sequence available at the time were the stability and accuracy criteria are encountered, such as Figure 5.14. The real-time predictions carried out for all volcanoes are displayed in this figure. For a 3-point stability criteria, only 4/28 successful predictions are made with less than 60% of the precursory sequence while more than half of the successful predictions (15/28) are possible

with less than 80% of the sequence. The conclusions are the same for 4-point stability and 5-point criteria, where 10/19 and 10/16 successful predictions are possible with less than 80% of the sequence, respectively.

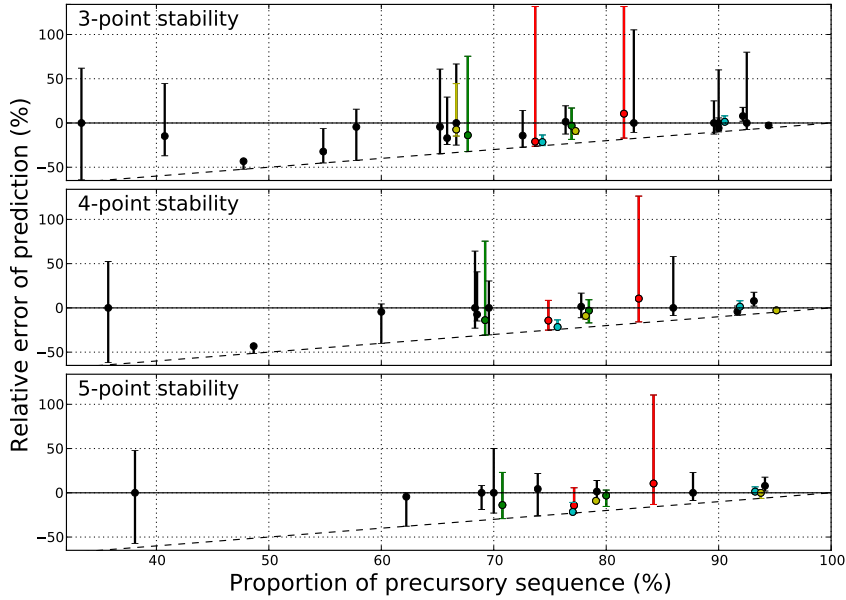


Figure 5.15: Results of real-time predictions showing the relative error of prediction $(t_f - t_e)/t_e$ as a function of the proportion of precursory sequence used to make the prediction, for all the eruptions studied. The results are reported for three different stability criteria, considering 3-point, 4-point or 5-point stability in the Figures of Section 5.1. Eruptions for which the criteria are fulfilled only one time are represented in black and eruptions for which stability is reached several times are denoted in color. Black dashed lines represent $t_{obs} = t_f$.

Among all the real-time predictions carried out with 61% of the accelerating sequences that are exploitable for real-time forecasting, 23/28 cases give successful predictions (82%) with a 3-point stability criterion, 15/19 with a 4-point stability criterion (79%) and 14/16 with a 5-point criterion (88%). Even though less eruptions are missed with a 3-point criterion, it is important to keep in mind that the more demanding is the criterion, the more informative will be the *pdf* of the predictions.

5.3.2.2 Accuracy of hindsightforecasts

Hindsight predictions are reported in Figure 5.16 for the 61% of the total precursory sequences that displayed acceleration sequences before the eruptions studied in this thesis. These predictions are carried out in hindsight with the whole accelerating sequence preceding each eruption. In this case, 35/40 tested examples gives the true time of eruption within the 99% confidence interval. Only 4/20 predictions are wrong for PdlF volcano and 3/20 for Volcán de Colima. The prediction carried out for the 2010 eruption of Merapi volcano is delayed of one day but

I still question whether it could have been successful by considering that the 5-days increase that interspersed the acceleration sequence had delayed the prediction made of this duration.

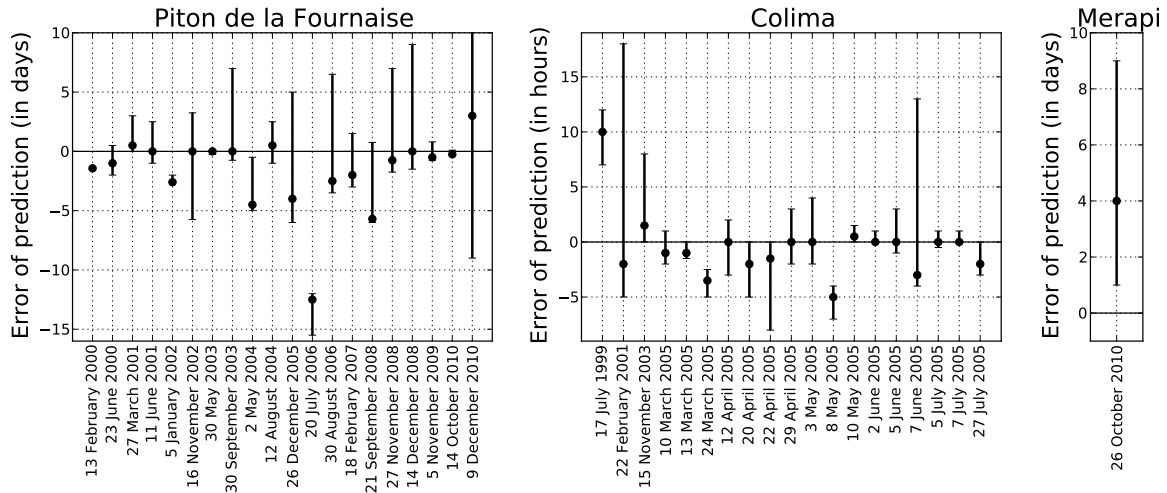


Figure 5.16: Results of predictions carried out in hindsight with the whole precursory sequence, for every studied eruptions. The error of prediction ($t_f - t_e$) is represented as a function of the case studied.

Summary In total, half of the cases lead to a successful prediction in hindsight (35/64, 55% of success) while 23/64 precursory sequences could lead to successful real-time forecasting (36% of success). These results lead to understand why most of the predictions using the FFM reported in the literature are carried out in hindsight rather than in real time.

Although the success rate of the method is low in real-time because of the requirements concerning the precursory patterns of seismicity before eruptions, very few wrong predictions are obtained when the reliability criteria are fulfilled (about 83% of success in average, depending on the stability criteria). Thus, the real-time forecasting tool developed in this thesis could never be applied alone, but can be very useful if used in parallel with other probabilistic forecasting method, such as pattern recognition for example. Moreover, this Chapter also demonstrates the necessity of using the method developed in this thesis by keeping an eye on the data for an optimal success rate. This suggests that this tool could probably not be fully automatised.

5.4 Partial conclusions on the application of the FFM for real-time forecasting

Some conclusions can be drawn concerning this Chapter that aimed to apply the real-time deterministic forecasting method developed in this thesis.

First of all, such a systematic analysis of the potential of FFM for eruption forecasting has never been carried out before. Even though the analysis is limited to 14 years of activity at Volcán de Colima, 10 years of activity at Piton de la Fournaise volcano and one eruption at Merapi volcano (64 eruptions in total), some preliminary conclusions can be drawn that starts to have a significant statistical meaning.

1. It is a necessity to dispose of precursory sequences that are well described by the FFM. Actually, only 61% of the precursory sequences analysed in this thesis were suitable. This low rate of suitable sequences is due to the complexity of the precursory patterns, reflecting the complexity of the precursory processes going on before the eruptions. Researches about the pre-eruptive physical mechanisms are still needed to improve deterministic eruption forecasting by providing more suitable models.
2. Some textbook cases displayed impressive real-time forecasting results, that could allow for successful predictions more than one day before the eruption and with small uncertainties. However, when we analyse these textbook cases among all the other cases, results are less impressive as they represent only 6/64 eruptions...This conclusion highlights the bad representativeness of the studied cases in the literature.
3. Half of the eruptions are successfully forecast in hindsight but only 36% in real-time. From this observation, we can conclude that successful in hindsight predictions are not representative of the performance of the method in real time.
4. On the other hand, 83% of the predictions carried out in real time that fulfil the criteria of stability and decreasing Shannon index lead to successful predictions. Thus, we can have a good confidence on the method when the reliability criteria are encountered.
5. Successful vulcanian explosion forecasts could be carried out using LP events, and sometimes with decelerating LP rates some hours before the explosion. This opens the question of the physical link between LP events and vulcanian explosions.
6. The best fit of the model to precursory acceleration sequences is obtained with a p -value that is different from one in most of the cases, i.e. $\alpha \neq 2$. Moreover, the Bayesian approach of the FFM developed in this thesis allows for better prediction results than the one obtained with the classical inverse linear method, when the best p -value is different from 1. This underlines the need for considering the p -value as a free parameter in the inversion.

7. This forecasting method outperforms the results found in the literature for Volcán de Colima. Concerning the 2010 eruption of Merapi volcano, a better stability and accuracy is obtained by Budi-Santoso et al. (2013) with the classical linear inverse method and the SSEM as observable. Although the comparison cannot be fully carried out because their study does not provide uncertainties, this suggests that energy may be considered as a relevant observable.

Chapter 6

Discussion and general conclusions

Contents

6.1 Discussion	170
6.1.1 Limitations of the real-time forecasting method	170
6.1.2 LP precursory patterns of vulcanian explosions	174
6.1.3 VT precursory patterns of eruptions	175
6.1.4 Applicability of the FFM in volcano observatories	175
6.2 Conclusions	177
6.3 Perspectives	178

6.1 Discussion

This thesis fully explored the potential of the FFM for real-time eruption predictions through a Bayesian approach, which is the most general and robust way of solving inverse problems. Thus, I consider that I took as much advantages of the FFM as possible through the method developed but also through the exhaustive analysis of different volcanic contexts, thanks to the automatic classification tool. The method led to a 83% success rate when the reliability criteria were met and could be applied successfully to 36% of all eruptions considered. Consequently, the method is reliable but cannot be applied in many cases and several limitations should be underlined. Starting from the limits of our understanding of the sources of precursory events, I discuss possible mechanisms for explaining the behaviour of LP events before vulcanian explosions, as well as the precursory patterns of VT events. Finally, I discuss the applicability of the method for volcano observatories.

6.1.1 Limitations of the real-time forecasting method

Choosing appropriate window width Δt and starting date t_0 . The choice of the window width Δt is delicate since the instantaneous derivative $\dot{\Omega}(t)$ has to be approached as precisely as possible. The starting date t_0 is also important to ensure as much data as possible to constrain the model. Since this choice is not straightforward, I proposed to carry out real-time forecasts in parallel at every observation time t_{obs} , and for different values of Δt . The optimal Δt and t_0 were identified as those returning the most stable predictions. Note that these trials are carried out in parallel at each time of observation. Therefore, the method requires a high computational cost, even though it is non-critical since the computing time is always much smaller than the data increment, leaving time to update predictions in case of volcanic crisis. For example, 9 results of real-time predictions have to be plotted in parallel if 3 different increments are tested with 3 different values of t_0 . For an operational use, there is a need of a user-friendly interface that would display all results in parallel, and there will always be a need for a human intervention to choose the optimal couple t_0 - Δt .

Estimation of the forecast update periods. As already discussed in Chapter 4, Section 4.4.2.1, the choice of the data type (cumulative or non-cumulative) is a trade off between theoretical and practical advantages. In this work, we chose theoretical advantages, leading to two main limits:

1. Working with non-cumulative data implies calculating the rates $\dot{\Omega}(t)$, which is in theory an instantaneous derivative. This calculation is approached using finite differences. The uncertainty arising from this method should therefore be reported.

2. Data frequency update is the second main methodological limitation. This period does not necessary match the size of the window width Δt . In some cases, such as for LP events, precursory patterns are expected to have a short duration. In these cases, it is desirable to update the predictions as often as possible to be able to evaluate the stability criteria before the eruption occurs. If the update period is smaller than the window width Δt , then successive data window overlaps and correlations are introduced in the data. Consequently, these overlaps create a bias in the posterior uncertainty of the time of prediction. The proper quantification of this bias is difficult due to the non-linear nature of the problem. However this limitation should be carefully considered.

In order to overcome both of these theoretical problems, one may work with cumulative data but then the correlation between consecutive *pdfs* would be a clear source of bias. More generally the problem is rather to evaluate the uncertainty on the FFM theory. This aspect has been set aside for the moment. The theoretical uncertainty on the computation of the instantaneous rate $\dot{\Omega}(t)$ for each interval could be evaluated by assuming that the number of earthquakes follow a Poisson process with a power law intensity.

A single power law theory. The main limitation of the method remains in the applicability of the single power law theory to multiple acceleration patterns, for both VT or LP precursory sequences. This limitation is thus intrinsic to the theory, which is too simple to describe most real-life data. So, instead of trying to apply an overly simplistic empirical theory on half of the suitable precursory sequences, we rather need to move forward and understand the physics underlying the different precursory patterns observed for the volcanoes considered in this thesis.

Efforts towards a finer understanding of the underlying processes would allow us to explain several features in the observed precursory sequences, for example the unexplained delay between the acceleration patterns at PdIF volcano and the time of eruption. No relationship between the extent of this delay and the style, duration or location of eruptions were observed. The use of FFM to forecast the eruptions of Volcán de Colima based on LP event rates has to be justified since the FFM was originally developed for damage processes linked to VT activity.

Choosing the observable The comparison of the prediction results obtained in this thesis using the rate of events as observable with the results reported in the literature for the Merapi volcano (Budi-Santoso et al., 2013) and Volcán de Colima (Arámbula-Mendoza et al., 2011) using the SSEM begs the question of which observable is the most adapted for deterministic eruption forecasting. Indeed, Budi-Santoso et al. (2013) obtained more accurate predictions than the present study while the results obtained by Arámbula-Mendoza et al. (2011) led to less accurate forecasts. The physics underlying the behaviour of these observables remain poorly known so they are mainly empirically used. Further investigations are required to determine

which observable is the most relevant for eruption forecasting. However, it is non-trivial to compute the prior probability of these other types of observables (e.g. energy or SSEM).

Classification of volcano-seismic signals In Chapter 1, I presented the source mechanisms of the seismo-volcanic events encountered at the target volcanoes and highlighted that some of these mechanisms are still being debated. This results in different classification conventions for the manual databases built in different observatories. In this study, I built my own manual databases according to the classification of each volcano observatory, and following the interpretation of the signals by Varley et al. (2010b); Arámbula-Mendoza et al. (2011); Lavalée et al. (2008); Ratdomopurbo and Poupinet (2000); Budi-Santoso et al. (2013); Chouet and Matoza (2013) and others.

More particularly, I question whether the VT, MP and LP signals result from rock failure, from magma failure or from stick-slip of the plug. The difference between these mechanisms is subtle and thus it is not always straightforward to classify the resulting signals in one class or another (VT vs. MP vs. LP). In my analysis, I could observe that some events are classified as VT in Colima although they seem to also have the characteristics of MP events at Merapi.

For example, Figure 6.1 shows a VT (according to me) that is classified as a VT by Colima observatory (event 1, upper left), one event that is classified as a VT by the automatic classification tool (event 2, upper right), one MP (according to me) classified as a MP event by Merapi observatory (event 3, lower left) and one LP (according to me) classified as a LP by Colima observatory (event 4, lower right). The spectral contents of event 1 and event 2 are very similar. This is why the VSR classified event 2 as a VT event. However, the waveform of event 2 is not as characteristic of VT events as event 1: Event 1 has a more impulsive onset than event 2. In addition, looking at the MP event at Merapi volcano (Figure 6.1, lower left), the spectral content is similar to the event 2 at Colima (Figure 6.1, upper right). Thus, using the training database of Colima, the VSR would have recognised MP events as VTs, and conversely VT events at Colima would have been identified as MP events using the manual database constructed for the Merapi volcano. This is consistent with our interpretation since MP events have been interpreted as related to dome extrusions and VT types events of the same kind as event 2 have been observed during the 1998 dome extrusion of Volcán de Colima. Moreover, both of the eruptions of Merapi 2010 and Colima 1998 have similar features.

Some of the source mechanisms proposed for LP events are also linked with dome extrusion activities. Consequently, the boundary between VT, MP/hybrid and LP events is not obvious. This is limiting because it leads to a subjective classification, i.e. different from one volcano observatory to another. As a consequence, it might be detrimental to an accurate description of precursory behaviours as well as to a fine understanding of pre-eruptive processes. Hence, the issue of classification is still an open question in volcanic seismology. This point is one of my perspectives.

At this point, the reader is reminded that these observations were carried out using one component of one station only. Observing multi-component data or data at other stations would help making the difference between these events or, on the contrary, to assess their similarity. This strongly underlines the need for a more exhaustive overview of the data, comprising several components, several stations, and other potential perturbations (e.g. propagation effects, Bean et al., 2013).

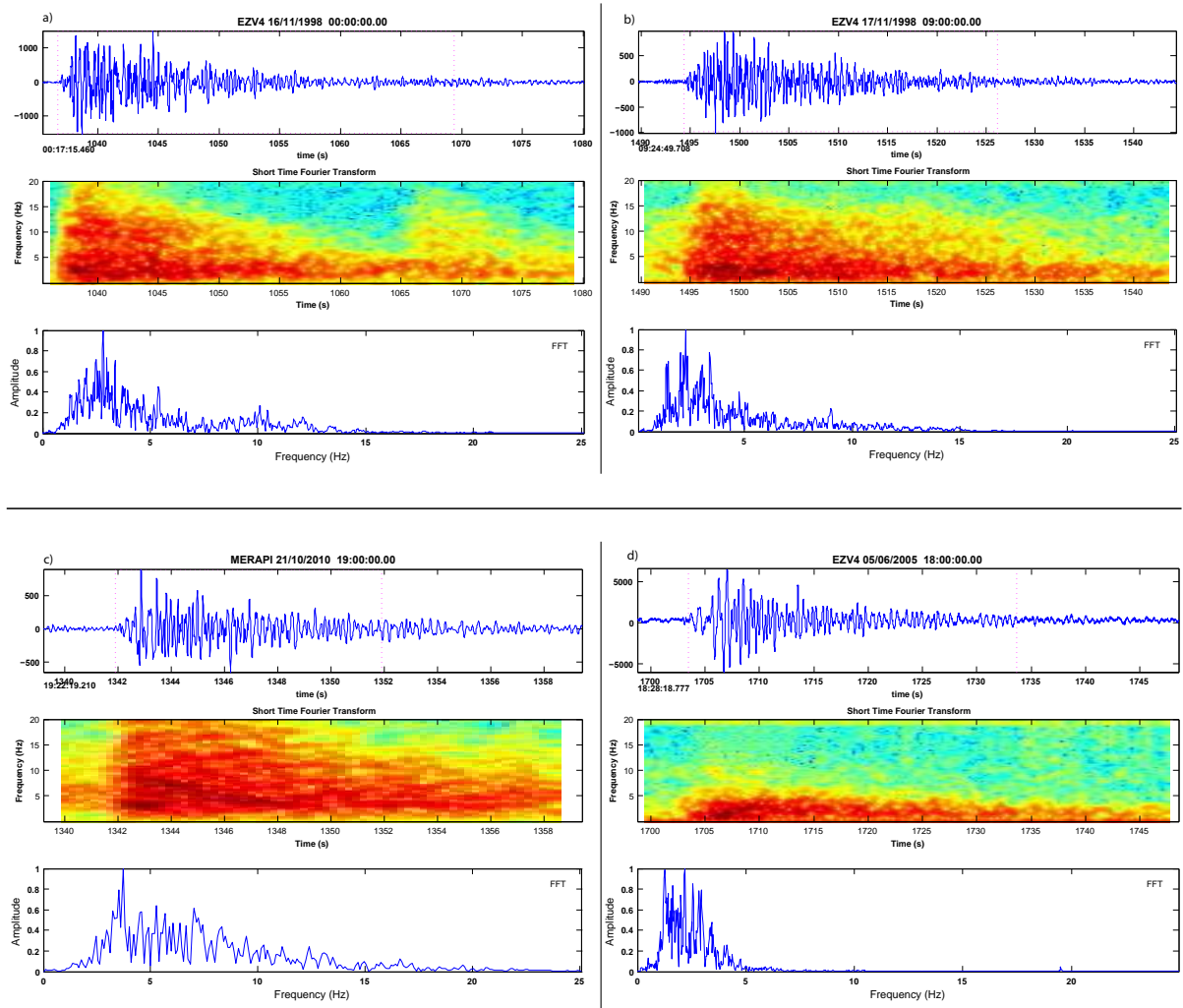


Figure 6.1: (a) Signal classified as a VT by Volcán de Colima observatory. (b) Signal classified as a VT at Volcán de Colima by the VSR. (c) Signal classified as a MP by Merapi volcano observatory. (d) Signal classified as a LP by Volcán de Colima observatory.

6.1.2 LP precursory patterns of vulcanian explosions

In the case of precursory VT activity, the acceleration pattern has been interpreted as being caused by damaging processes of the solid rock associated with intrusions and possible conduit widening (Voight, 1988; Kilburn, 2003, 2012). On the other hand, similar LP patterns are relatively common and have been interpreted, for instance prior to vulcanian explosion on volcanoes such as Galeras (Colombia, Gil Cruz and Chouet, 1996), Tungurahua (Ecuador, Molina et al., 2004), Sakurajima (Japan, Maryanto et al., 2008) or Ubinas (Peru, Traversa et al., 2011). More particularly, the power law gives also a good representation of the LP activity preceding several eruptions of Volcán de Colima, which is the basis of reliable eruption forecasting. From these observations, two questions arise: what are the source mechanisms of these LP events and what are the physical processes involved in the acceleration of this type of seismicity? Several source models of LP events, including oscillations of fluid-filled cavities, brittle fractures within magmas or slow ruptures have been proposed (Neuberg et al., 2006; Chouet and Matoza, 2013; Bean et al., 2013). In the end, the mechanisms behind such events most likely depends on the type and on the state of the volcano.

Geological observations (Tuffen et al., 2003; Tuffen and Dingwell, 2005), laboratory experiments (Tuffen et al., 2008; Lavallée et al., 2012) and models of magma conduits (Neuberg et al., 2006; Goto, 1999) suggest that, in the case of viscous magma intrusions, LP events can be generated by brittle fracturing of the ascending magma due to large strain rates close to the conduit walls. Moreover, the laboratory experiments of Lavallée et al. (2008, 2011) on magmas from Volcán de Colima, showed that complete sample failure can be forecast using the FFM on acoustic emissions. The shear bands that develop close to the conduit walls due to strain localization can produce reduction of the friction between the ascending magma and the solid rock (Hale and Muhlhaus, 2007). This decreasing friction could correspond to a mechanism of magma flow acceleration and to its associated seismicity. On the other hand, following the model of Holland et al. (2011), brittle fractures of magmas can generate a network of cracks that progressively become interconnected. An explosion would then be the result of these networks of fractures being filled by gas and reaching the surface and producing a rapid decompression. Although most of the processes described above are likely to be involved in the pre-eruptive phenomena, the exact scenario, describing the interactions between these processes and producing an acceleration of LP activity just before eruptions, still has to be modeled. A better understanding of these complex mechanisms would help interpreting the observations and justify the use of the FFM on LP activity for eruption forecasting. Finally, it could help understand the multiple acceleration patterns of LP activity, as well as the meaning of the deceleration observed before explosions and in particular the reason why the FFM can give good predictions in this case. At Volcán de Colima, LP activity is mainly observed during rapid dome extrusions. Moreover, it seems that most of the major explosions were associated with rapid dome growth (at least those that could have been observed). I question whether

multiple LP acceleration patterns could be linked with multiple episodes of rapid ascending magma.

6.1.3 VT precursory patterns of eruptions

The presence of single and multiple accelerating patterns at PdIF opens the question of the mechanisms behind such precursory seismicity. Despite the common occurrence of delays between the accelerating pattern and the swarm preceding the eruption, accelerations immediately followed by a seismic swarm were observed before the eruption, e.g. 23 June 2000, 11 June 2001, 30 May 2003, 12 August 2004, 14 December 2008, 14 October 2010. Taisne et al. (2011) localised the events associated with one of these seismic swarms (before the January 2010 eruption) and interpreted the upward migration of seismicity upward as an image of the dyke propagation during the hour preceding the eruption. The acceleration of VT seismicity is thought to be related to the damage of the surrounding rock (Kilburn, 2003, 2012; Main, 2000; Amitrano and Helmstetter, 2006) under the stress induced by magma pressure. When failure occurs, pressure may be released and could explain the seismic quiescence between the acceleration pattern and the last VT swarm (Carrier et al., 2015). This quiescence might reflect the moment where the material is unstable and close to its yield strength. An overpressure due to a replenishment of a magma chamber could trigger a chaotic behaviour wherein the dyke then propagates itself towards the surface. When looking at VT events, the prediction target of the FFM is thus more probably the failure of the edifice rather than the eruption itself. Thus, it is confirmed by the eruption predictions carried out with these complicated patterns. Successful predictions may thus be obtained when the replenishment of the magma chamber occurs just after the edifice failure, such as for the eruptions of 23 June 2000, 30 May 2003 and 12 August 2004. In the other cases, the eruptions are predicted too early and the lack of knowledge on the replenishment of the magma chamber, a precise prediction seems difficult to obtain.

6.1.4 Applicability of the FFM in volcano observatories

The method proposed in this thesis is thought for further integration in operational monitoring systems and for producing real-time forecasts of eruptions. However, because of the current limitations, it may not be sufficient in itself. When the reliability criteria are fulfilled, the success rate of the method makes an helpful tool in 36% crises. The forecasting tools developed in this thesis have to be integrated to a more global strategy of eruption forecasting, such as Bayesian event trees (Marzocchi. et al., 2008) or coupled with pattern recognition. For example, if the probability calculated with the Bayesian event trees or if an alarm is triggered thank to pattern recognition techniques, deterministic predictions could be carried out. Another alternative consists in integrating the prediction method developed in this thesis as a parameter of the Bayesian event trees, in order to increase the knowledge of the ongoing volcanic activity.

In addition, the method should be tested with other precursors, such as seismic events energies, deformations or gas emissions data. In each case, the prior *pdf* should be calculated carefully.

This thesis explored several ways of adapting the FFM for real-time forecasting, in near real-time situations. However, proper statistical evaluation of the success rate of the method will have to be carried out before full real-time testing. Indeed, this work was thus far merely exploratory. The success rates have been evaluated as objectively as possible, by taking into account all eruptions, even those that were not preceded by precursors, as well as seismic crises that were not followed by an eruption. However, success rates cannot be fully objective since the method has not been automatised. The full automation of our real-time forecasting method will be difficult, for the following:

- The detection of accelerations is straightforward but once the acceleration sequences have been detected, the increment Δt and the initial time t_0 should be tested in an automatic manner. This would require a significant computational cost.
- Both the detection of the stability criterion and decreasing Shannon index should be automatised. It would require setting thresholds, that should be calibrated on a large number of examples.

Although I am convinced that an operator should always keep an eye on the data, such a study would require a large amount of data to compute the success rate in a statistically relevant manner. Thus, in operational situations, volcanologists should still follow a precise protocol consisting of: 1) detecting the increases and decreases of activity, setting the initial time t_0 and eventually, in the case of complex sequences, modifying t_0 ; 2) evaluating the stability criteria and the uncertainty of the forecast times (the Shannon index can be useful for this purpose); and 3) informing decision makers in implementing alert levels, taking into account the results of the forecasting method together with all the available information.

One of the aims of this work is to circulate the method to any interested researcher or observatory. Thus, building a userfriendly interface would be necessary. However, the method of eruption forecasting developed in this thesis requires a good knowledge of the uncertainty of the data being used. We proposed a way of computing posterior probabilities of the data, based on the VSR provided by the University of Granada. This is the main limitation to circulate the forecasting method since I showed, in Chapter 2, that the use of the VSR requires a good expertise of the classification tool and an accurate manual database. An interesting alternative would be to share the manual databases, following the idea of the WOVODAT Programme (www.wovodat.org) and to give a parametrized VSR, with the optimal parameters already tuned and ready to use, at each volcano.

6.2 Conclusions

The objective of this thesis is to test and improve the use of the FFM and assess its potential for the real-time forecasting of volcanic eruptions. Such predictions may then help decision making procedures.

I have presented a new method for volcanic eruption forecasting derived from the FFM theory and adapted for real-time applications. The Bayesian approach provides an objective, robust and flexible way of solving the inverse problem as well as to estimate the model parameters and their respective uncertainties from the prior *pdf* calculated for the data. The formulation of the FFM theory we chose (equation 4.4) allows for a direct estimation of the time of eruption t_f through its posterior *pdf*. These estimations are repeated during the observation period. Thus the reliability of the forecast can be evaluated along with two criteria: the stability of t_f as a function of time and the uncertainty of its estimation.

The automatic classification tool of seismo-volcanic events allowed for real-time testing of the forecasting method on a number of volcanic records: Volcán de Colima (14 years), Piton de la Fournaise volcano (10 years) and one eruption at Merapi volcano (64 eruptions in total). The systematic analysis of the potential of the FFM for eruption forecasting in various volcanic contexts had never been carried out before. Thus, the conclusions drawn from this thesis begins to show a significant statistical meaning.

The FFM could be applied in hindsight for 62% of the precursory sequences. This relatively low proportion of suitable sequences is imputable to the complexity of the precursory patterns which reflects the complexity of the pre-eruptive processes. Nevertheless, 36% of sequences were compatible for real-time forecasting and 83% of those returned successful predictions. The method thus proved to be reliable when the criteria are met. More than a half of the successful real-time forecasts were achieved using less than 80% of the corresponding precursory sequences used, hence leaving some time for proper evacuation.

The reliability of eruption forecasting methods based on precursory seismic activity hinges upon the following conditions. First, seismic events must occur and this activity must feature an accelerating pattern. The reason why some eruptions are not preceded by earthquakes remains unclear and requires further research. Secondly, the duration of the seismic unrest and the level of activity must be sufficient for the method to be applied and, when an eruption is forecast, the remaining time must be long enough for an evacuation to take place.

Finally, the limited applicability of the method shows that the FFM should not be applied alone for real-time forecasting. Considerable efforts towards understanding the different patterns of precursory seismic activity is paramount to improving volcanic eruption forecasting.

6.3 Perspectives

This thesis clearly demonstrates the potential of the FFM for real-time eruption forecasting. However, the method would greatly benefit from the following improvements. First, the uncertainty of the theory for the inversion process should be assessed. This would likely lead to more realistic uncertainties, since the problem of overlapping windows and the approximation of $\dot{\Omega}(t)$ would be addressed. However, I expect the uncertainty of t_f to be much larger than that obtained in this thesis, and thus probably less informative (though perhaps more realistic). Secondly, the preliminary study of the Popocatepetl volcano should be pursued in order to complete the prediction results.

The adaptation of the method to signals other than counts of events will have to be investigated. Precursory acceleration patterns of deformation and of the energy of volcano-seismic signals have been reported prior to eruptions and the application of the FFM to these precursors could potentially be useful. However, finding a way of computing the uncertainty of the energy of seismic signals, appears to be non-trivial since the uncertainty on the energy of events may be greater than that of the counts.

This work would also benefit from the development of a user-friendly interface. It would allow for an easy circulation and use of the programs. Nonetheless, the end user would still be required to have a good understanding of the uncertainty of the data to use.

Finally, it would be interesting to test the method for eruptions preceded long quiescence period (e.g. centuries), such as before the eruptions of the Mount Pinatubo or Chaiten. It would allow for testing the efficiency of the real-time forecasting method developed in this thesis in a closed volcanic system, wherein a long period of seismic precursors is expected. However, this scenario is not widespread, and most dormant volcanoes are not monitored. In the case where the volcano is seismically monitored, the construction of the manual database of volcano-seismic events would not be possible because of the limited number of seismic events. When no or few seismicity have been contemporary monitored, our method could not be applied. This issue may be circumvented by building a universal manual database of volcano-seismic events that includes all the classes encountered around the world.

The longer term development of this work should focus on understanding the physical mechanisms leading to the observed precursory patterns. So far, the power-law patterns of precursory VTs is well explained (Kilburn, 2003, 2012). However, no physical models have thus far been proposed the behaviour of LPs before vulcanian eruptions. Understanding these precursory patterns would help better understand which types of precursory patterns will effectively lead to an explosion. Thus, it will help improving deterministic eruption forecasting as well as better understanding pre-explosive mechanism. The idea is to describe the time and space evolution of the magma stresses within a magmatic conduit bounded by stick-slip conditions at its margins (Denlinger and Hoblitt, 1999). It will allow for determining the location and rates of fracturing

processes using the thresholds above which brittle fracturing of magma is possible (Lavallée et al., 2008, 2011). The coupling of thermal and rheological models proposed by Papale (1999), Melnik et al. (2005) and Gonnermann and Manga (2012) could be used to describe the rates of gas release and the changes in magma rheology during crystallisation. Consequently, the aim becomes that of modelling the observed data (= posing the forward problem). Such a forward problem may be used to forecast volcanic eruptions with the Bayesian method presented in this thesis. This aspect will be at the heart of my research for the year to come.

Appendices

Appendix A

Comparison of the automatic classification with the OVPF catalogue

The availability of the catalogue of seismicity built at the observatory allows for the comparison of the rates of events manually classified by the observers of the ovpf with the automatic classification of the events carried out with the VSR used in this thesis. This preliminary comparison should be further investigated.

I chose on purpose a period where there are several eruptions as well as periods of seismic quiescence. Figure A.1 shows the rates of events for the period July-December 2003, for the recognition of VT and rockfall events. The trends of VT rates obtained with the VSR are similar to that obtained with the catalogue of the observatory. However, in periods of intense seismic activity, less events are recognised by the VSR. It could simply be explained by the fact that the VSR probably recognises several overlapped events as one single event. VT events recognised during the periods of eruptions actually probably correspond to the eruptive tremor, which has not been considered for the recognition.

Rockfall event rates display different patterns when looking at the ovpf and VSR catalogues. More rockfalls are recognised by the VSR. When having a look at the seismograms, it seems that many rockfalls are not classified by the observers. Therefore the VSR allows for classifying more events than the observers.

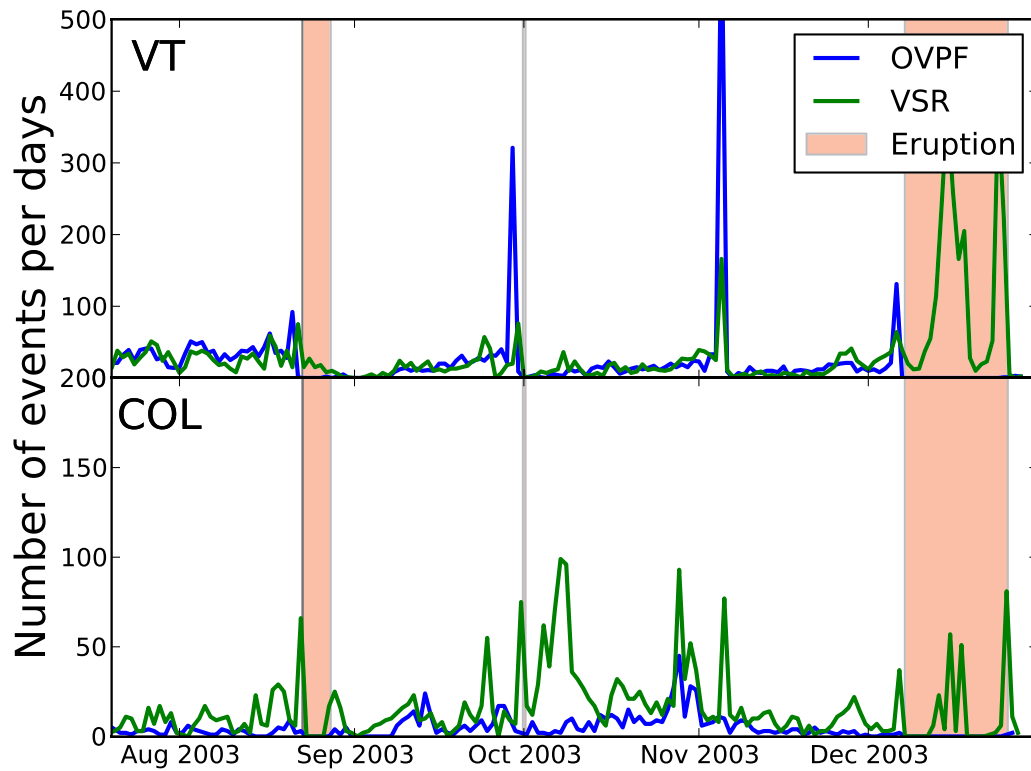


Figure A.1: Histogram of the VT and rockfall activity at Piton de la Fournaise volcano, for the period July-December 2003. The blue line represents the rates calculated with the catalogue of the PdIF observatory. The green line represents the rates calculated with the catalogue obtained with the VSR.

Appendix B

Catalogues of volcanic seismicity at Volcán de Colima

In Chapter 3, I presented the catalogue of seismicity for the years of interest, i.e. with significant volcanic activity. This appendix displays the other catalogues of seismicity obtained with the VSR.

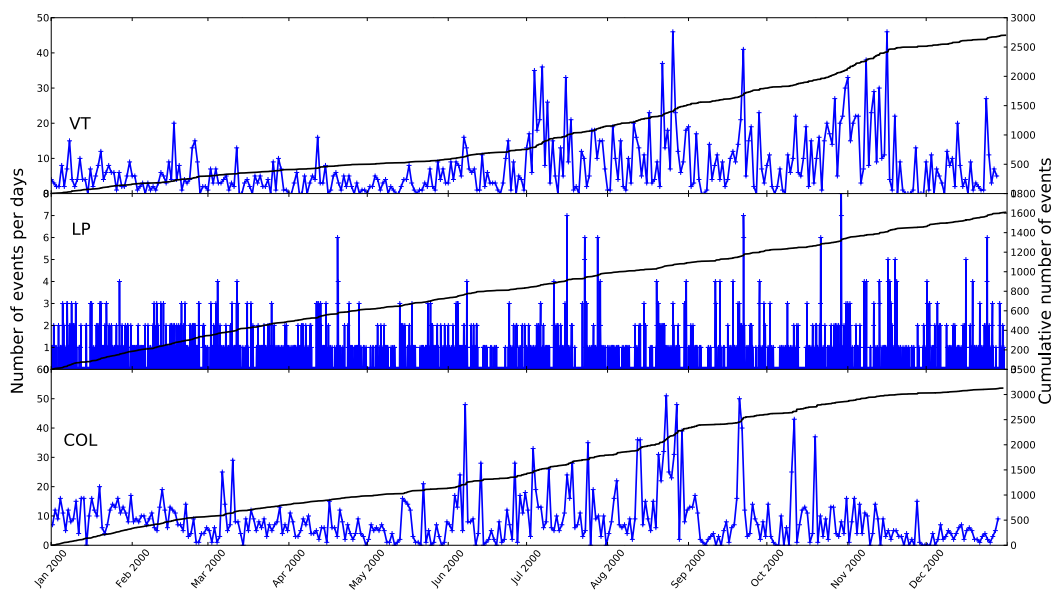


Figure B.1: Rate of events (blue line) and cumulative number of events (black line) as a function of time for the year 2000 at Volcán de Colima. Top: VT events. Middle: LP events. Bottom: Rockfalls.

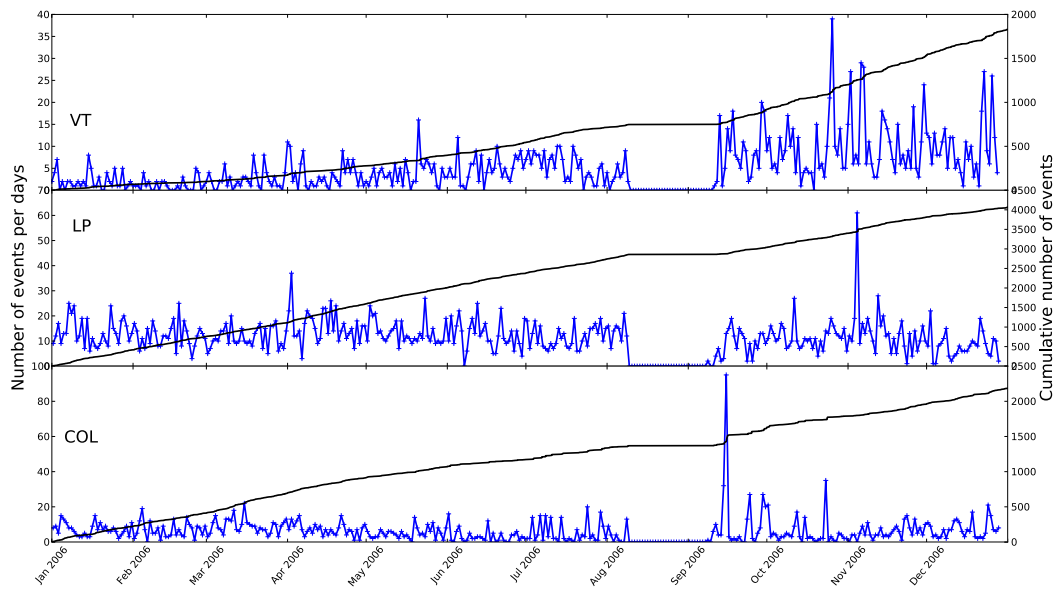


Figure B.2: Rate of events (blue line) and cumulative number of events (black line) as a function of time for the year 2006 at Volcán de Colima. Top: VT events. Middle: LP events. Bottom: Rockfalls.

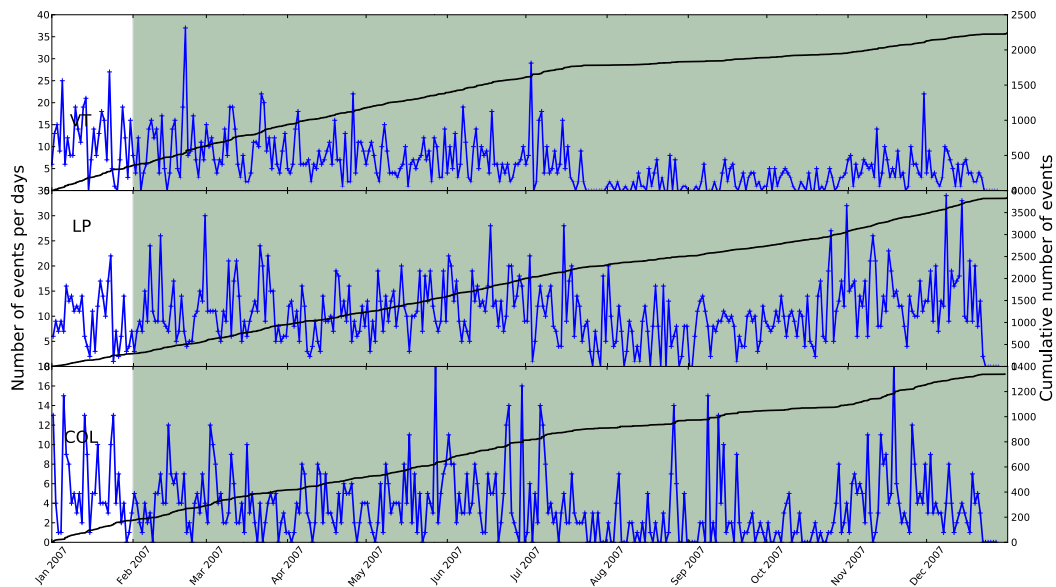


Figure B.3: Rate of events (blue line) and cumulative number of events (black line) as a function of time for the year 2007 at Volcán de Colima. Green areas represent the period of dome extrusion and red area the period of lava flow, i.e. the dome is pouring out of the crater. Top: VT events. Middle: LP events. Bottom: Rockfalls.

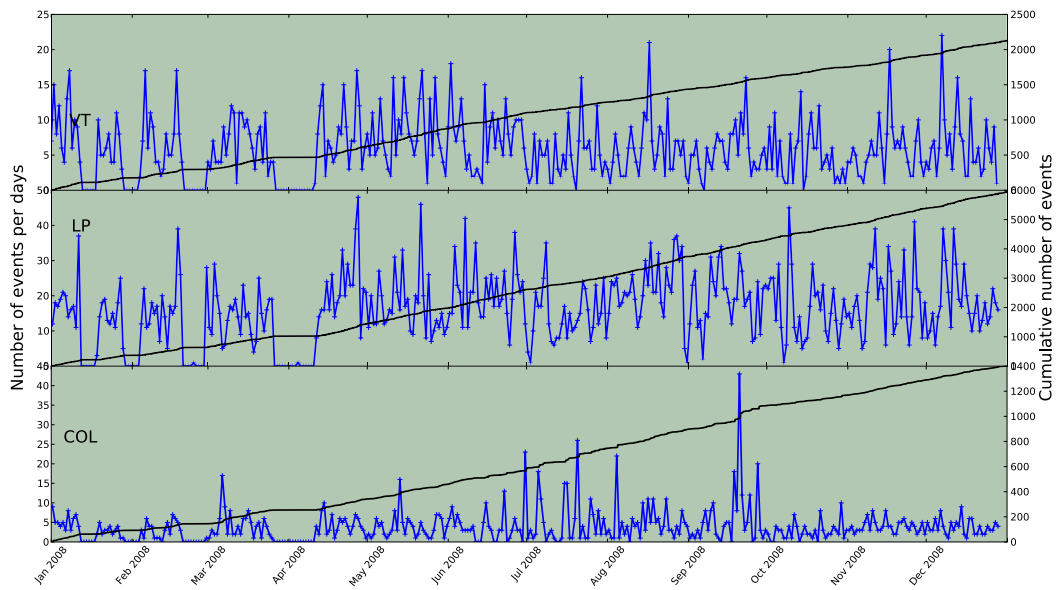


Figure B.4: Rate of events (blue line) and cumulative number of events (black line) as a function of time for the year 2008 at Volcán de Colima. Green areas represent the period of dome extrusion and red area the period of lava flow, i.e. the dome is pouring out of the crater. Top: VT events. Middle: LP events. Bottom: Rockfalls.

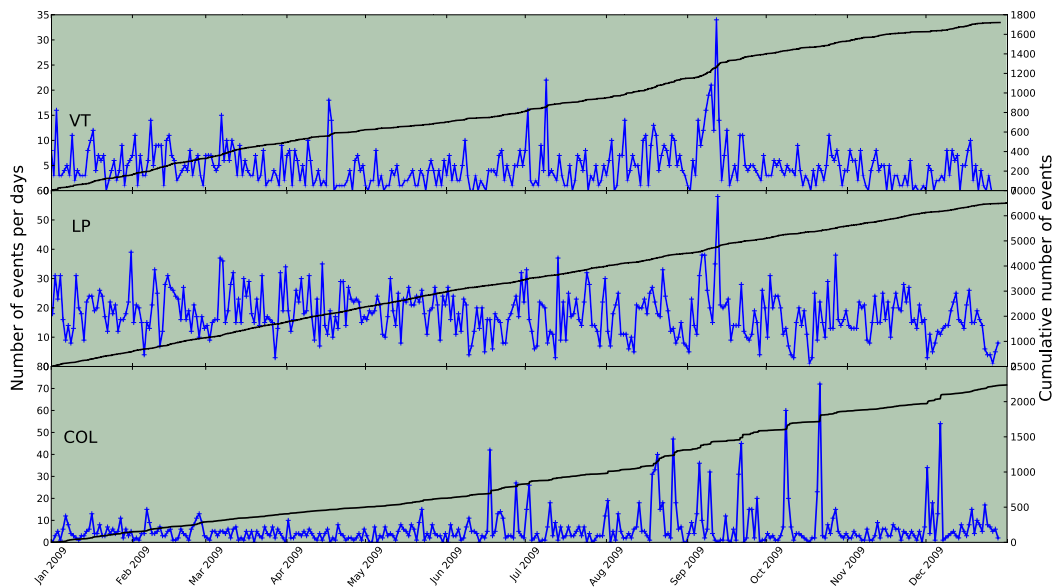


Figure B.5: Rate of events (blue line) and cumulative number of events (black line) as a function of time for the year 2009 at Volcán de Colima. Green areas represent the period of dome extrusion and red area the period of lava flow, i.e. the dome is pouring out of the crater. Top: VT events. Middle: LP events. Bottom: Rockfalls.

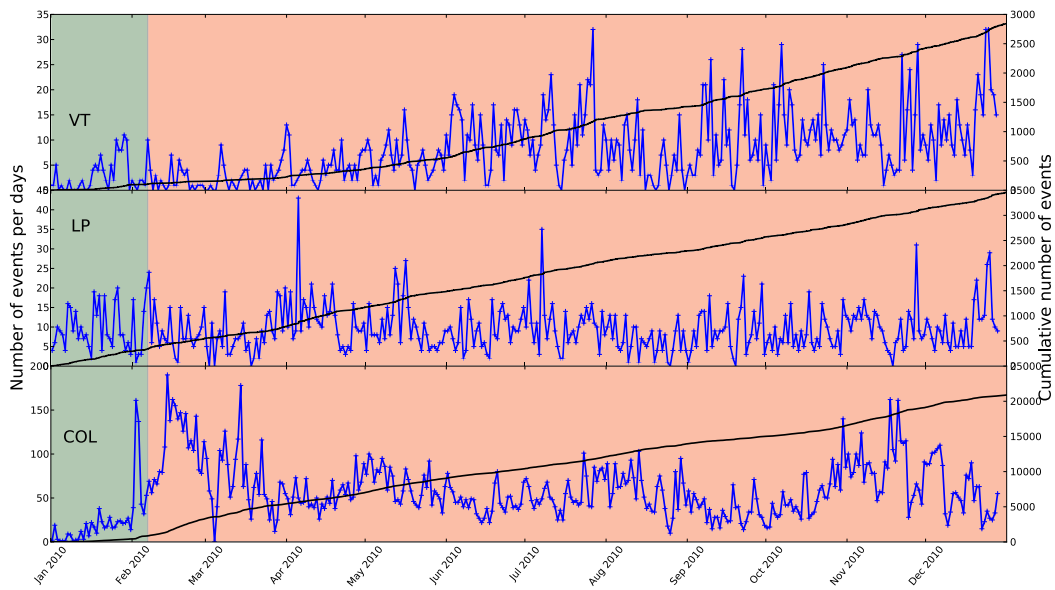


Figure B.6: Rate of events (blue line) and cumulative number of events (black line) as a function of time for the year 2010 at Volcán de Colima. Green areas represent the period of dome extrusion and red area the period of lava flow, i.e. the dome is pouring out of the crater. Top: VT events. Middle: LP events. Bottom: Rockfalls.

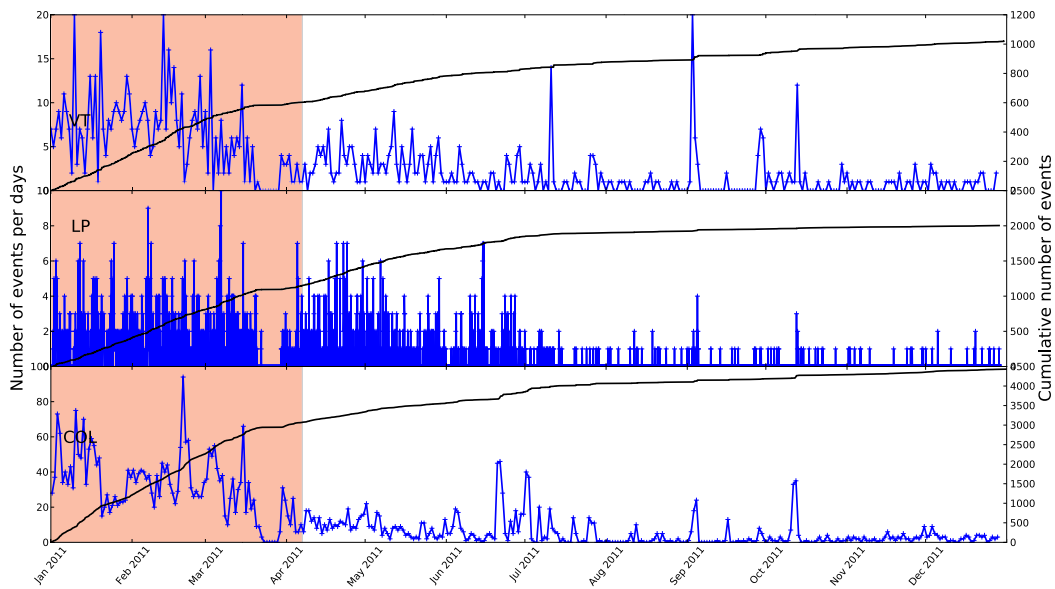


Figure B.7: Rate of events (blue line) and cumulative number of events (black line) as a function of time for the year 2011 at Volcán de Colima. Green areas represent the period of dome extrusion and red area the period of lava flow, i.e. the dome is pouring out of the crater. Top: VT events. Middle: LP events. Bottom: Rockfalls.

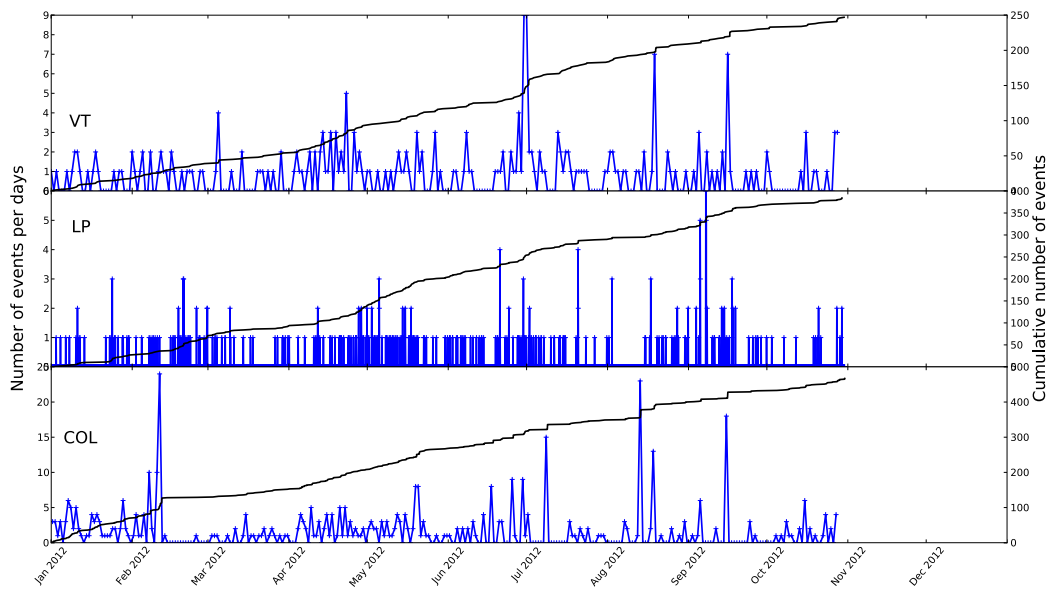


Figure B.8: Rate of events (blue line) and cumulative number of events (black line) as a function of time for the year 2012 at Volcán de Colima. Top: VT events. Middle: LP events. Bottom: Rockfalls.

Appendix C

Results of real-time predictions with complicated precursory patterns

Section 5.1 presented examples of real-time predictions carried out on textbook cases but also on more complicated precursory patterns. Some patterns are identified to be a limitation for the application of the deterministic real-time eruption prediction method developed in this thesis.

Among them, the most limited patterns are the short duration precursory patterns. One of the criteria of the prediction method is based on the stability of the prediction as a function of time, hence a short duration precursory sequence does not allow for the stabilisation of the predictions. Moreover, the model is less constrained when few data points are available to carry out prediction with the FFM, leading to large uncertainties.

Numerous multiple acceleration patterns have been identified at PdIF and Colima volcanoes, leading to complicated applications of the FFM. One have to question which acceleration is the most relevant for the application of the method. Even if it seems complicated to test every sequence, the predictions usually stabilise around the true eruption time with the first acceleration, but with large uncertainties. In other cases such as the 5 July 2005 explosion at Colima volcano (Figure C.12), multiple accelerations are too short to apply the method.

Finally, other patterns can be encountered. Most of them do not accelerate but the method was tested. They lead to predictions that stabilise around the true time of eruption, with large associated uncertainties.

All these patterns are presented in this appendix, with their associated results of real-time prediction.

C.1 Short duration precursory patterns

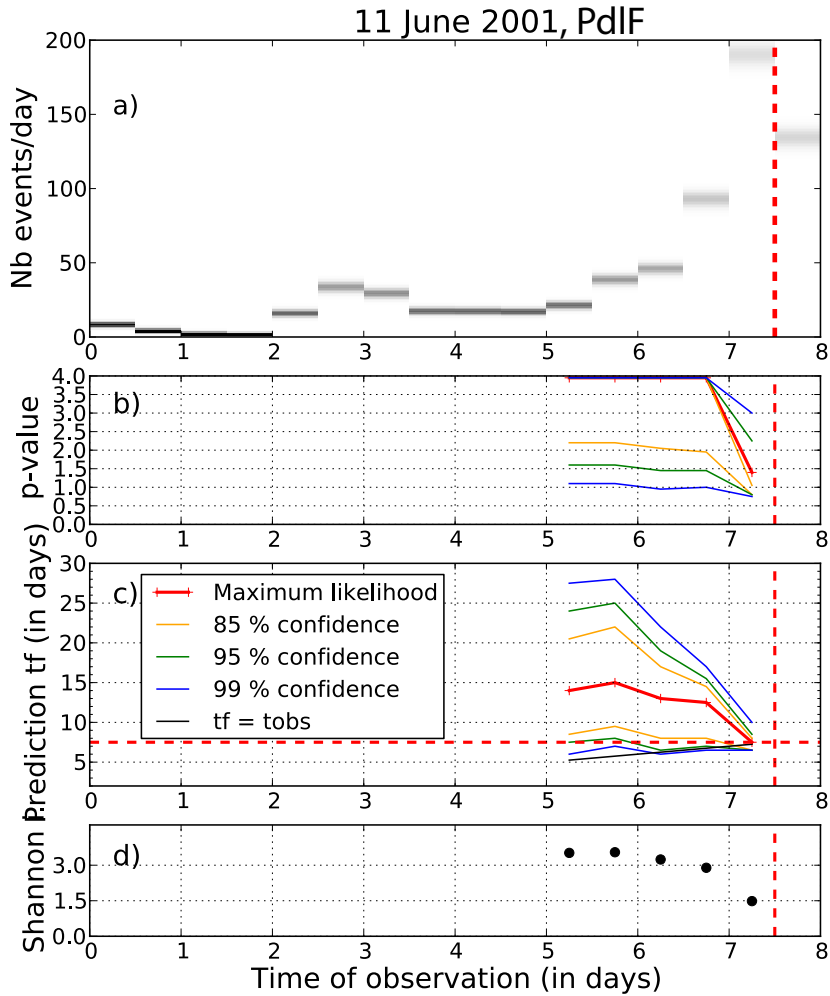


Figure C.1: a) Prior *pdfs* of the data for the 11 June 2001 eruption at PdIF volcano, as a function of the observation time t_{obs} . The true time of eruption is $t_e = 7.5$ days (red dashed line). The black dashed line indicates the time of deceleration. b) Posterior marginal *pdfs* of p . The red line is the maximum likelihood of the *pdf* and the yellow, green, and blue lines indicate the 85%, 95% and 99% intervals of confidence, respectively. c) Posterior marginal *pdfs* of the prediction t_f . The red line is the maximum likelihood of the *pdf* and the yellow, green, and blue lines indicate the 85%, 95% and 99% intervals of confidence, respectively. The black line corresponds to $t_f = t_{obs}$. d) Shannon's index of the marginal *pdfs* of t_f .

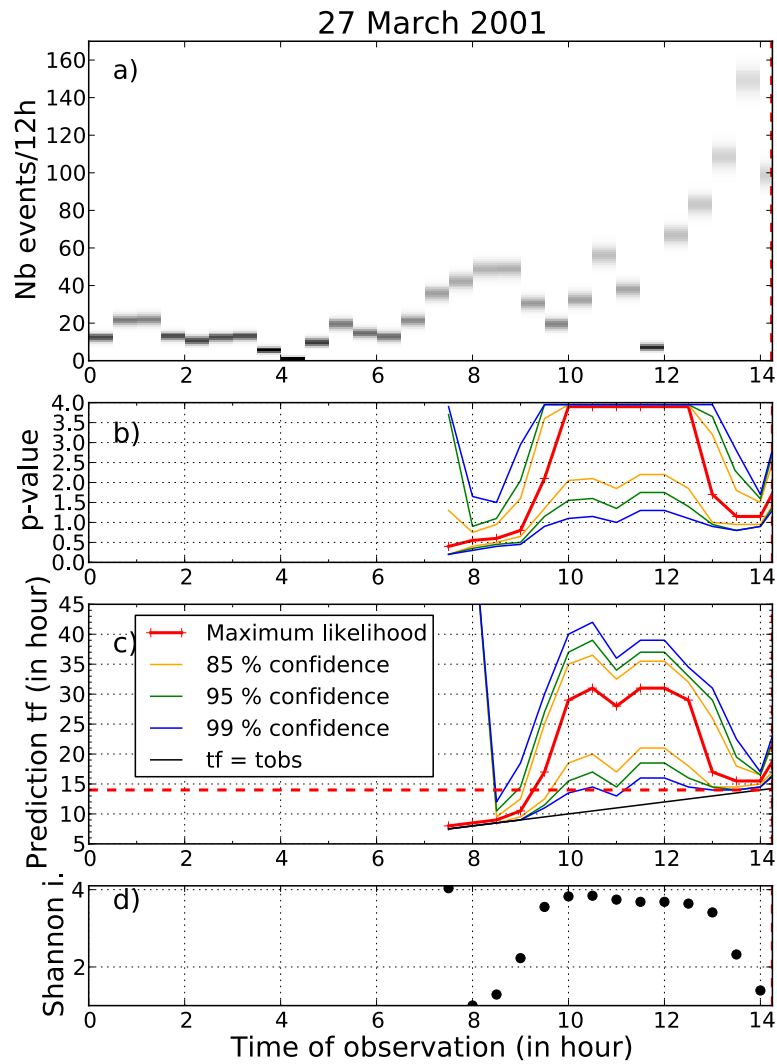


Figure C.2: a) Prior *pdfs* of the data for the 27 March 2001 eruption at PdIF volcano, as a function of the observation time t_{obs} . The true time of eruption is $t_e = 14$ days (red dashed line). The black dashed line indicates the time of deceleration. Panels b), c) and d) same as Figure C.1b-d.

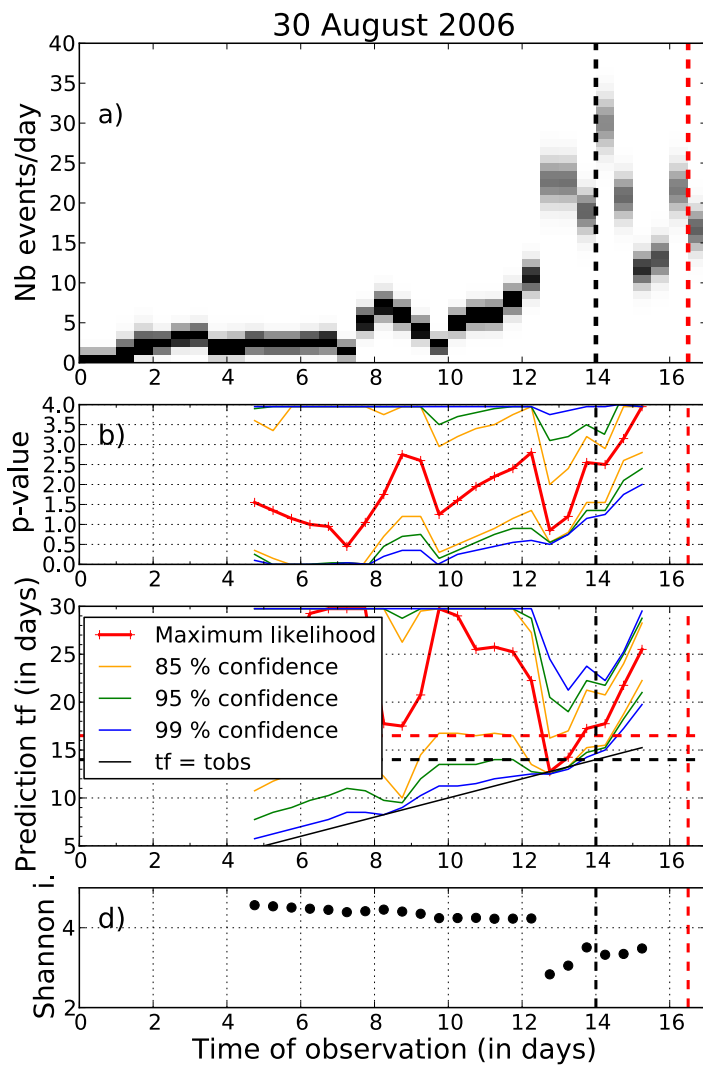


Figure C.3: a) Prior *pdfs* of the data for the 30 August 2006 eruption at PdIF volcano, as a function of the observation time t_{obs} . The true time of eruption is $t_e = 16.25$ days (red dashed line). The black dashed line indicates the time of deceleration. Panels b), c) and d) same as Figure C.1b-d.

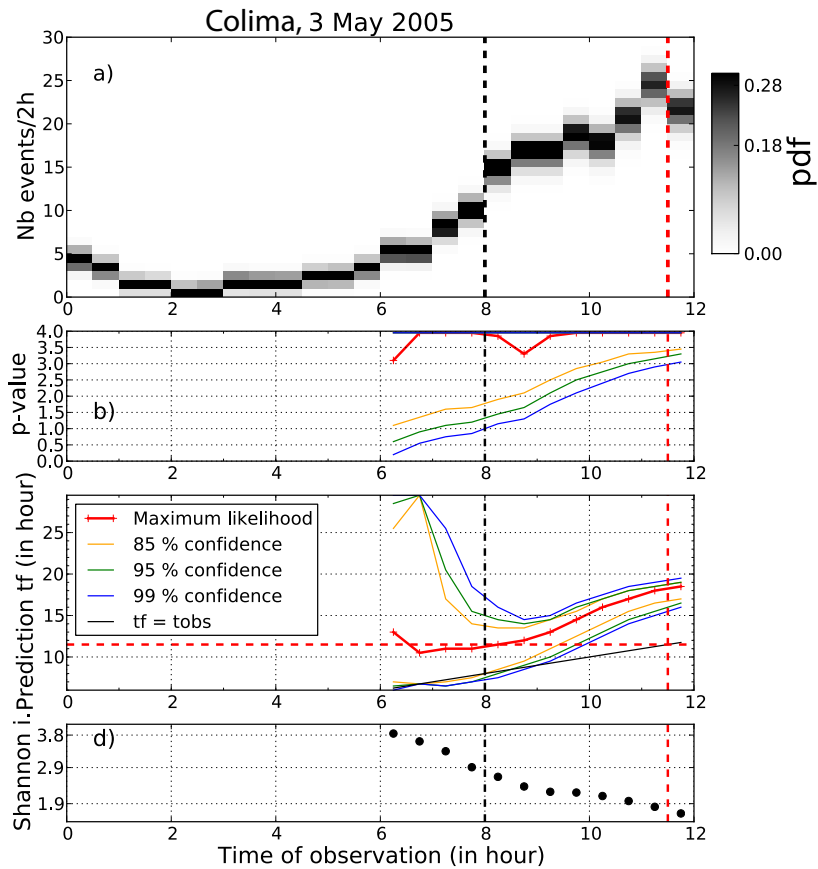


Figure C.4: a) Prior *pdfs* of the data for the 3 May 2005 explosion at Colima volcano, as a function of the observation time t_{obs} . The true time of eruption is $t_e = 11.5$ h (red dashed line). The black dashed line indicates the time of deceleration. Panels b), c) and d) same as Figure C.1b-d.

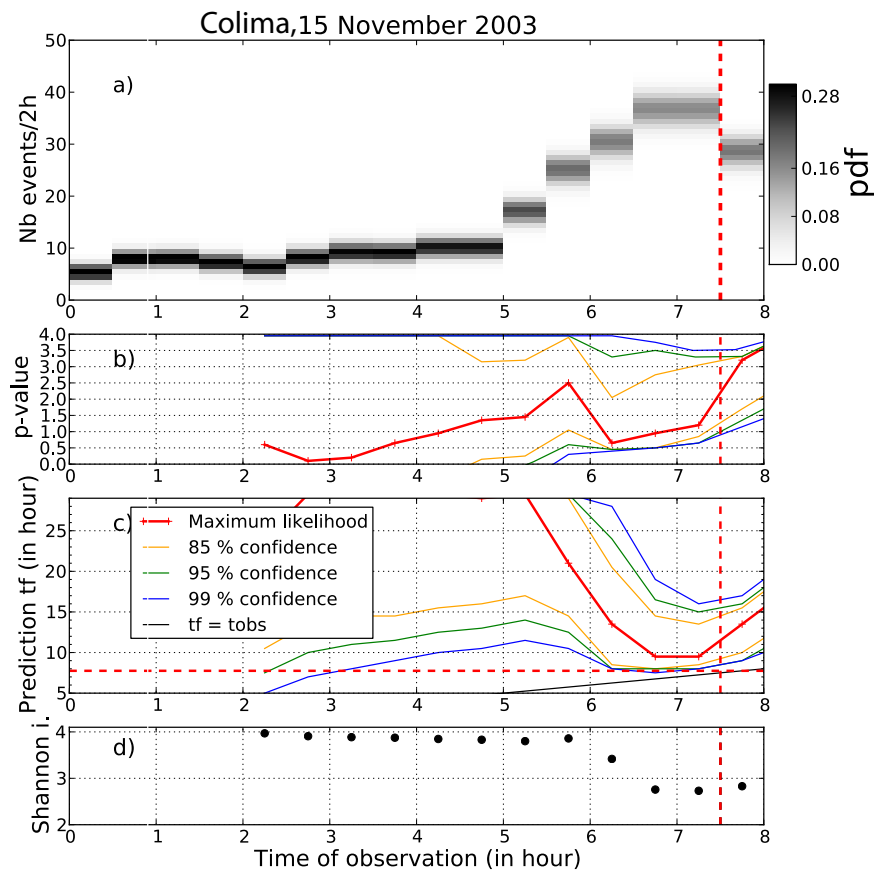


Figure C.5: a) Prior *pdfs* of the data for the 15 November 2003 explosion at Colima volcano, as a function of the observation time t_{obs} . The true time of eruption is $t_e = 7.5$ h (red dashed line). The black dashed line indicates the time of deceleration. Panels b), c) and d) same as Figure C.1b-d.

C.2 Multiple precursory patterns

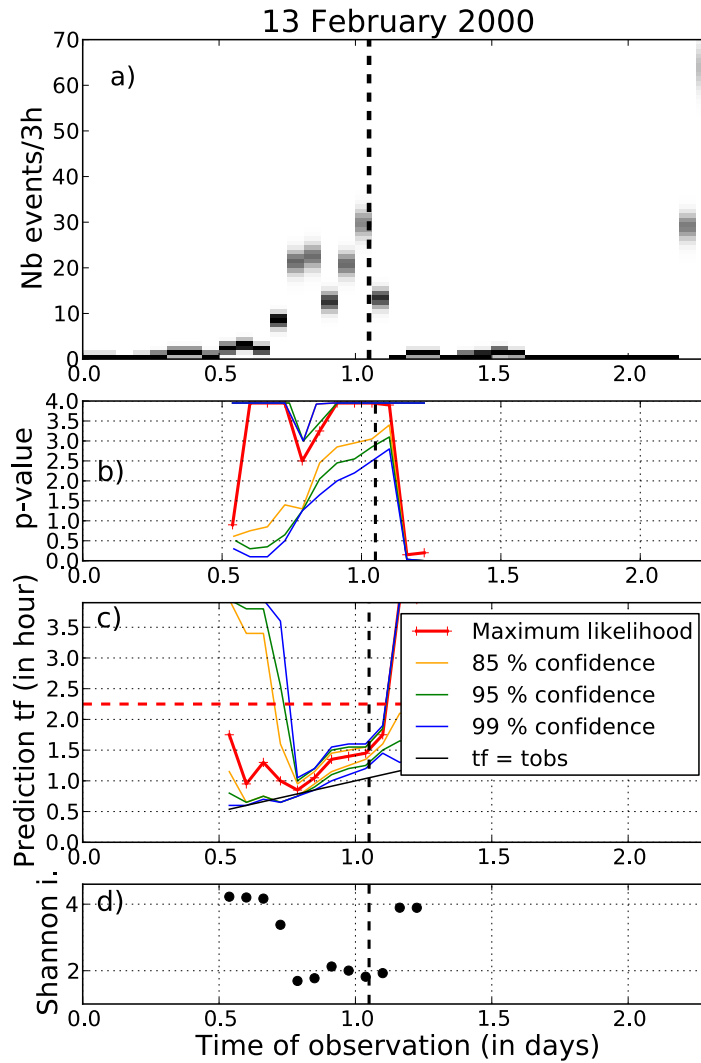


Figure C.6: a) Prior *pdfs* of the data for the 13 February 2000 eruption at PdIF volcano, as a function of the observation time t_{obs} . The true time of eruption is $t_e = 2.3$ days (red dashed line). The black dashed line indicates the time of deceleration. Panels b), c) and d) same as Figure C.1b-d.

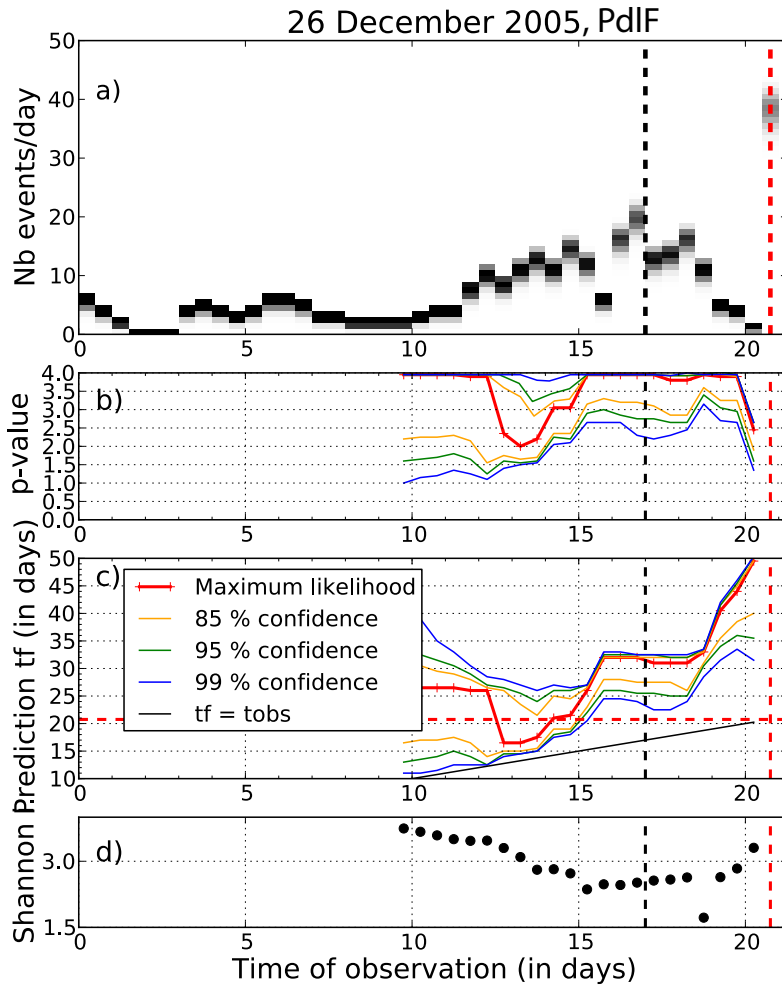


Figure C.7: a) Prior *pdfs* of the data for the 26 December 2005 eruption at PdIF volcano, as a function of the observation time t_{obs} . The true time of eruption is $t_e = 20.5$ days (red dashed line). The black dashed line indicates the time of deceleration. Panels b), c) and d) same as Figure C.1b-d.

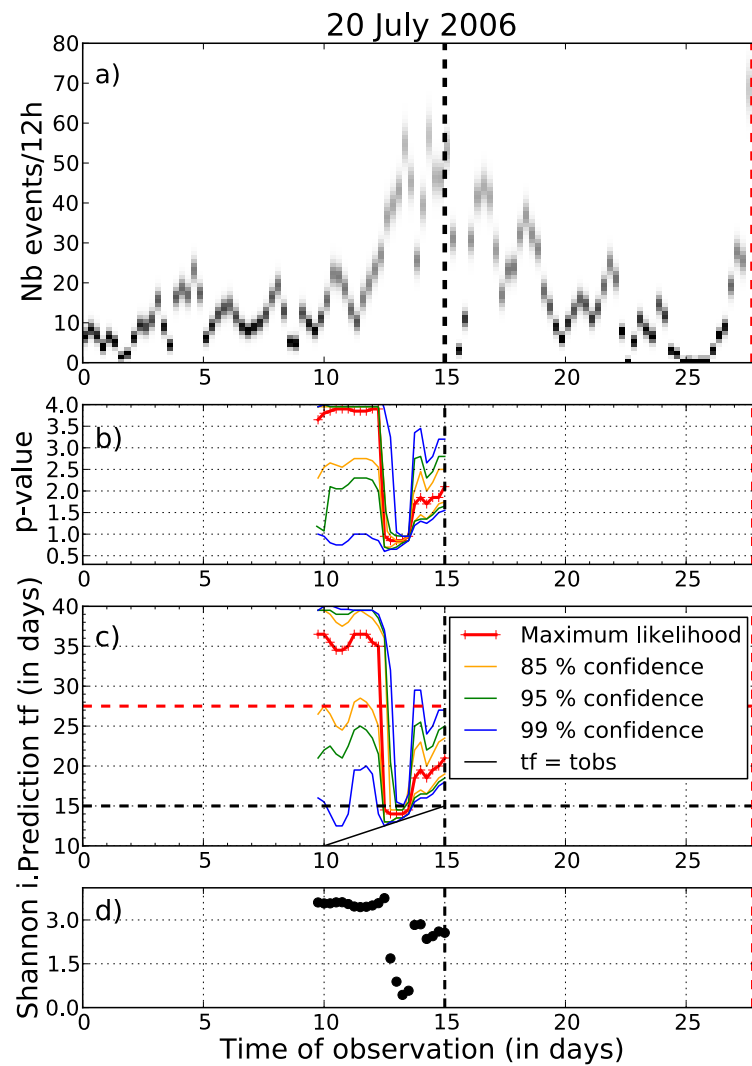


Figure C.8: a) Prior *pdfs* of the data for the 20 July 2006 eruption at PdlF volcano, as a function of the observation time t_{obs} . The true time of eruption is $t_e = 27$ days (red dashed line). The black dashed line indicates the time of deceleration. Panels b), c) and d) same as Figure C.1b-d.

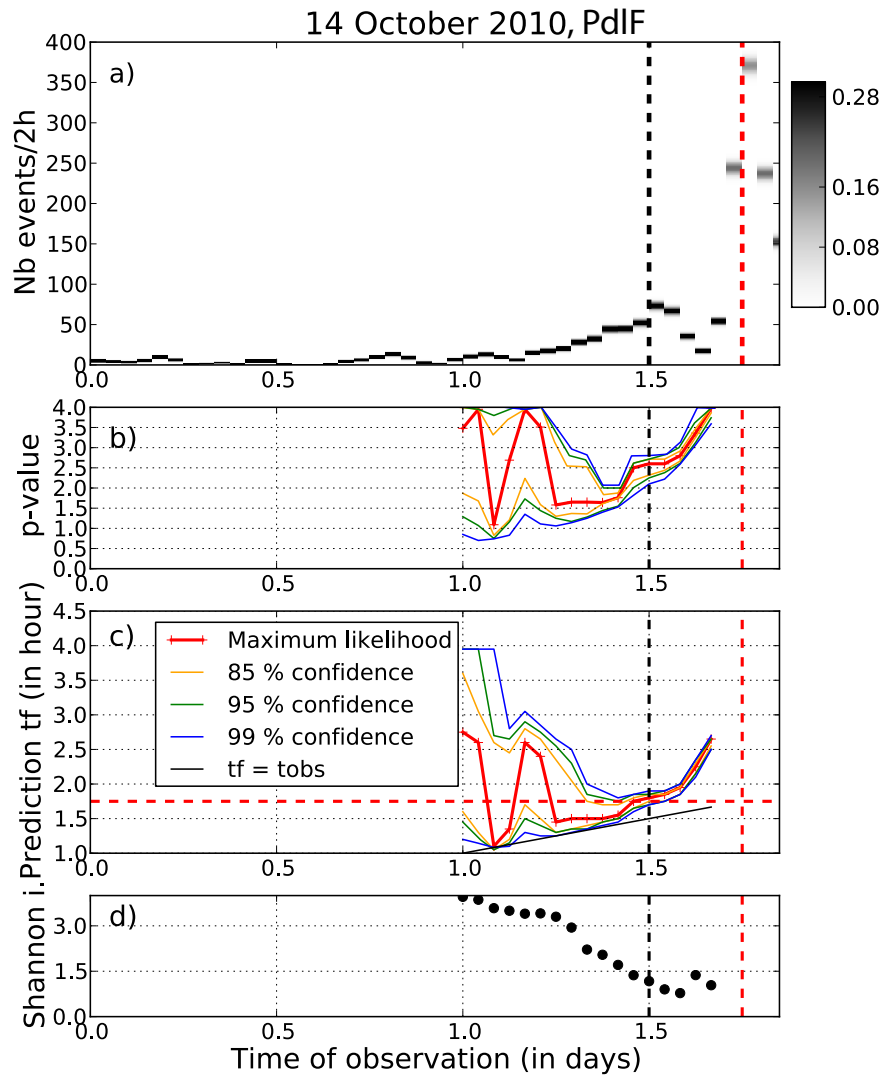


Figure C.9: a) Prior *pdfs* of the data for the 14 October 2010 eruption at PdIF volcano, as a function of the observation time t_{obs} . The true time of eruption is $t_e = 1.75$ days (red dashed line). The black dashed line indicates the time of deceleration. Panels b), c) and d) same as Figure C.1b-d.

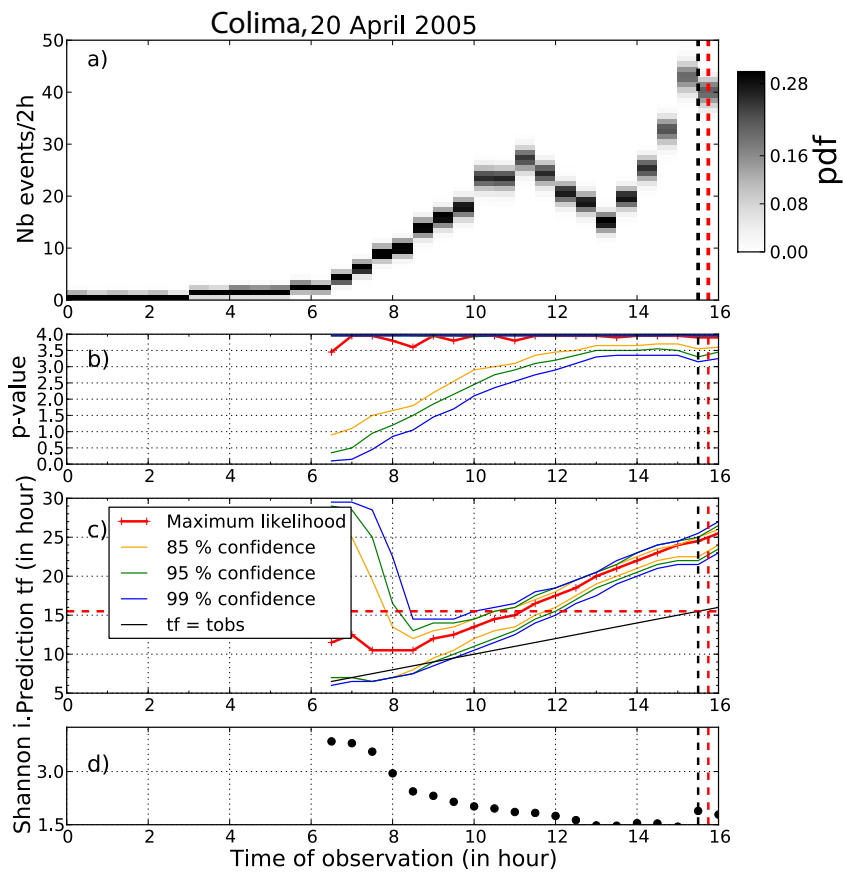


Figure C.10: a) Prior *pdfs* of the data for the 20 April 2005 explosion at Colima volcano, as a function of the observation time t_{obs} . The true time of eruption is $t_e = 15.5$ h (red dashed line). The black dashed line indicates the time of deceleration. Panels b), c) and d) same as Figure C.1b-d.

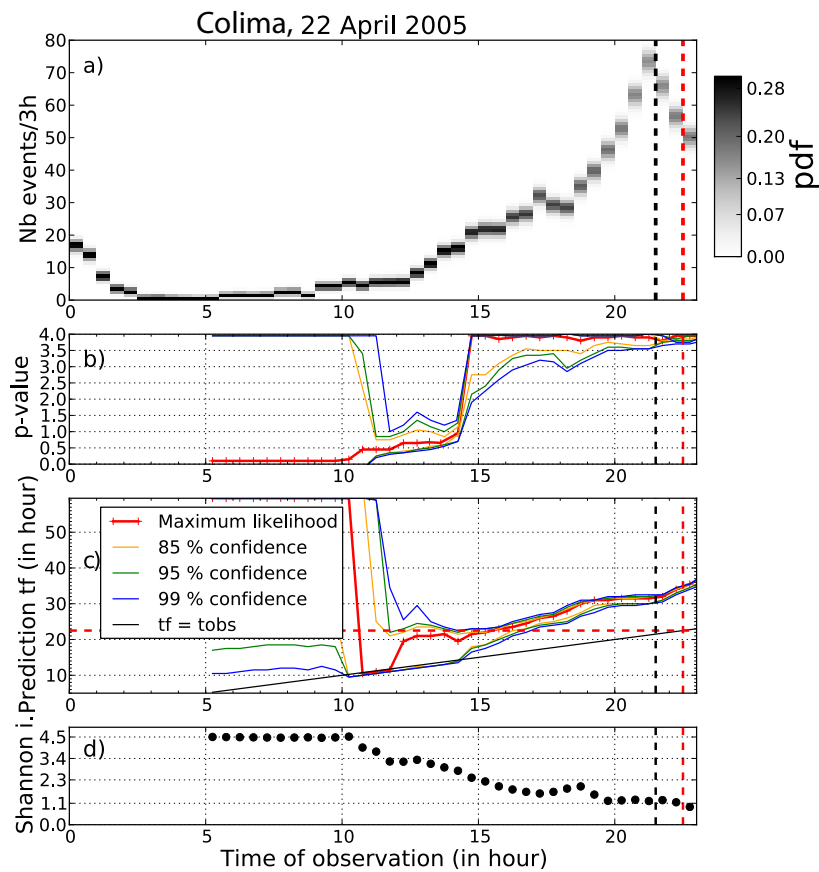


Figure C.11: a) Prior *pdfs* of the data for the 22 April 2005 explosion at Colima volcano, as a function of the observation time t_{obs} . The true time of eruption is $t_e = 22.5$ h (red dashed line). The black dashed line indicates the time of deceleration. Panels b), c) and d) same as Figure C.1b-d.

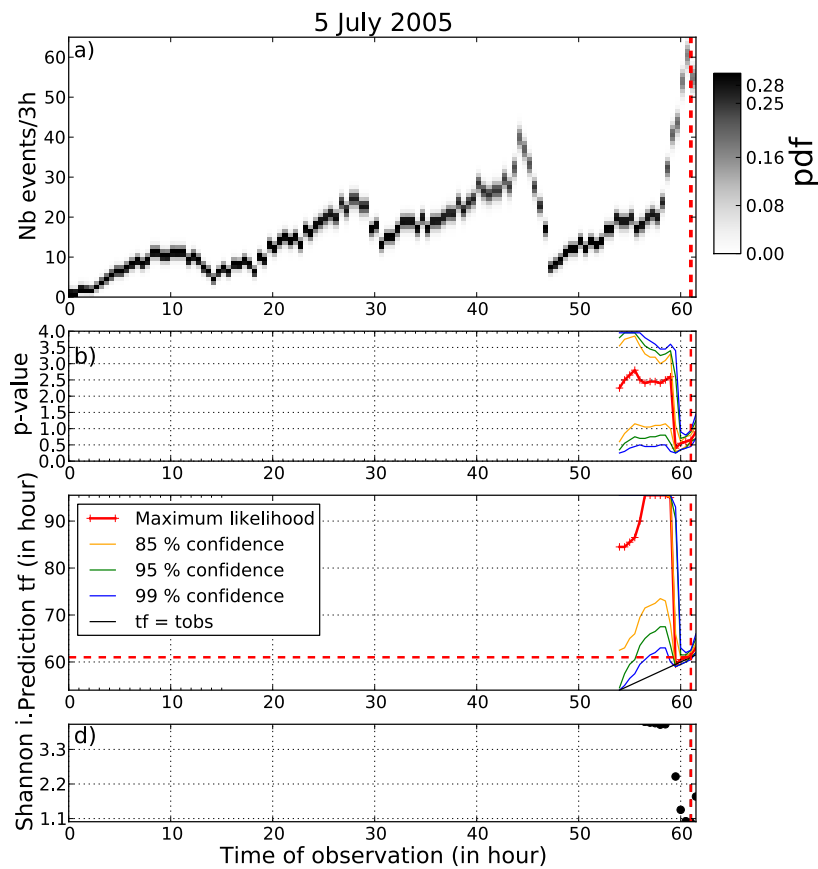


Figure C.12: a) Prior *pdfs* of the data for the 5 July 2005 explosion at Colima volcano, as a function of the observation time t_{obs} . The true time of eruption is $t_e = 62$ h (red dashed line). The black dashed line indicates the time of deceleration. Panels b), c) and d) same as Figure C.1b-d. The starting point is $t_0 = 50$ h.

C.3 Other patterns

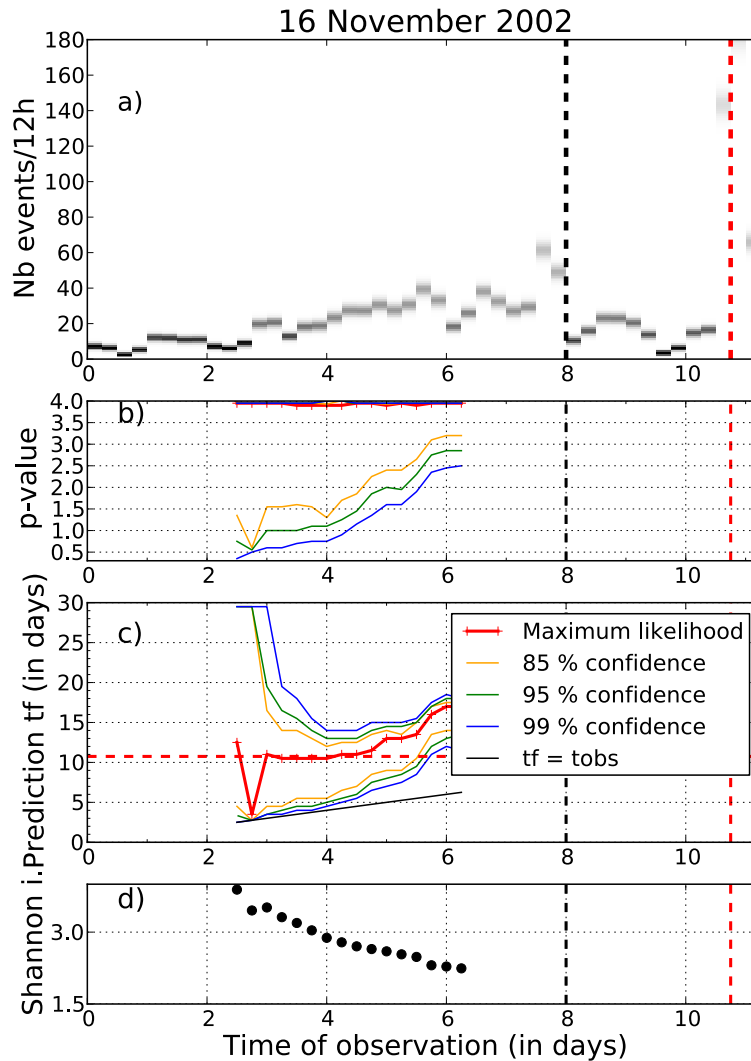


Figure C.13: a) Prior *pdfs* of the data for the 16 November 2002 eruption at PdIF volcano, as a function of the observation time t_{obs} . The true time of eruption is $t_e = 11.5$ days (red dashed line). The black dashed line indicates the time of deceleration. Panels b), c) and d) same as Figure C.1b-d.

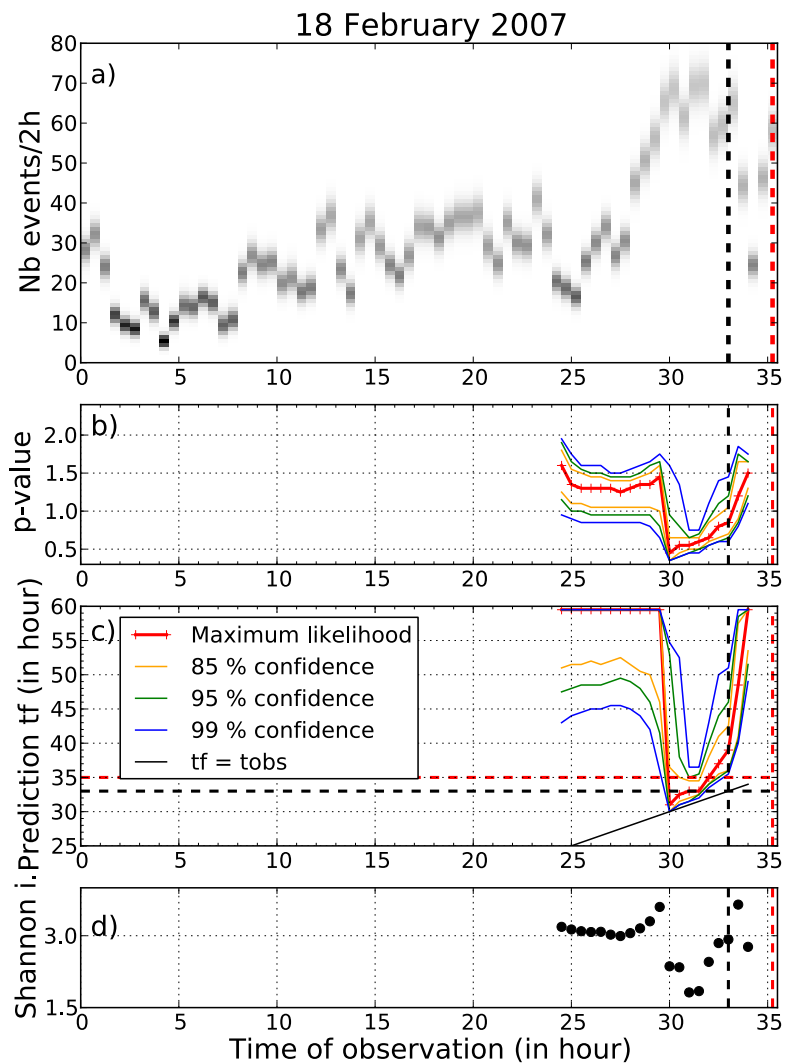


Figure C.14: a) Prior *pdfs* of the data for the 18 February 2007 eruption at PdIF volcano, as a function of the observation time t_{obs} . The true time of eruption is $t_e = 35$ days (red dashed line). The black dashed line indicates the time of deceleration. Panels b), c) and d) same as Figure C.1b-d.

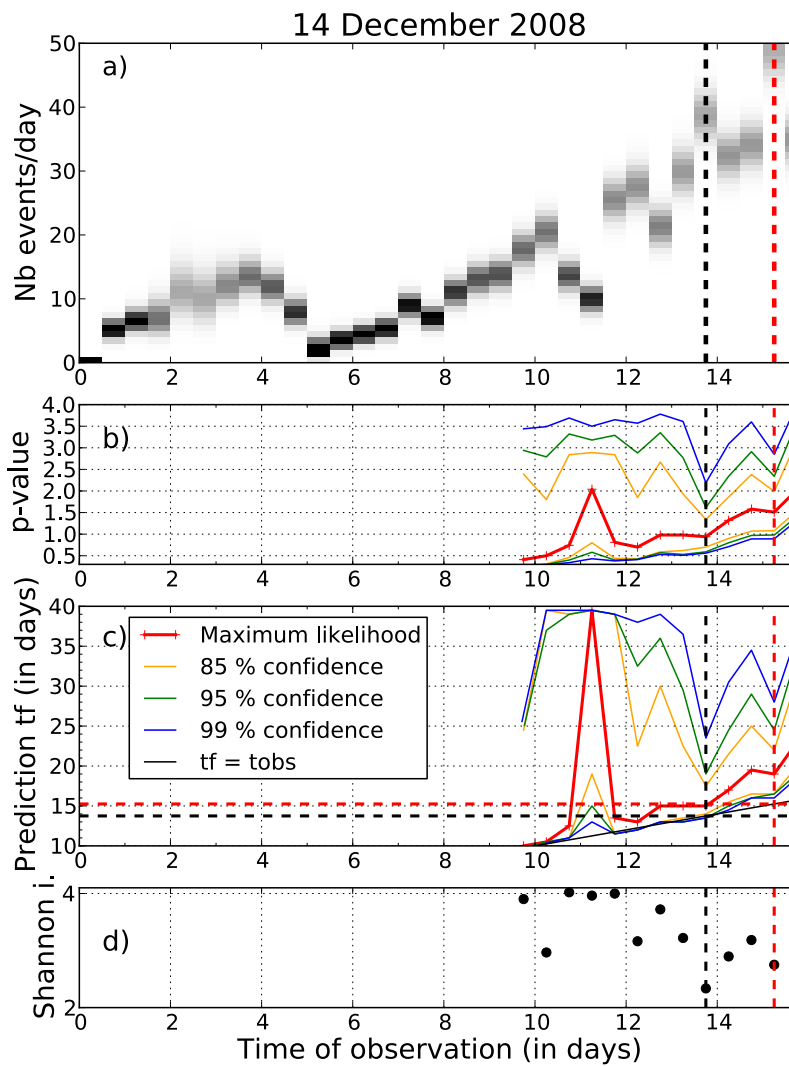


Figure C.15: a) Prior *pdfs* of the data for the 14 December 2008 eruption at PdIF volcano, as a function of the observation time t_{obs} . The true time of eruption is $t_e = 15.25$ days (red dashed line). The black dashed line indicates the time of deceleration. Panels b), c) and d) same as Figure C.1b-d.

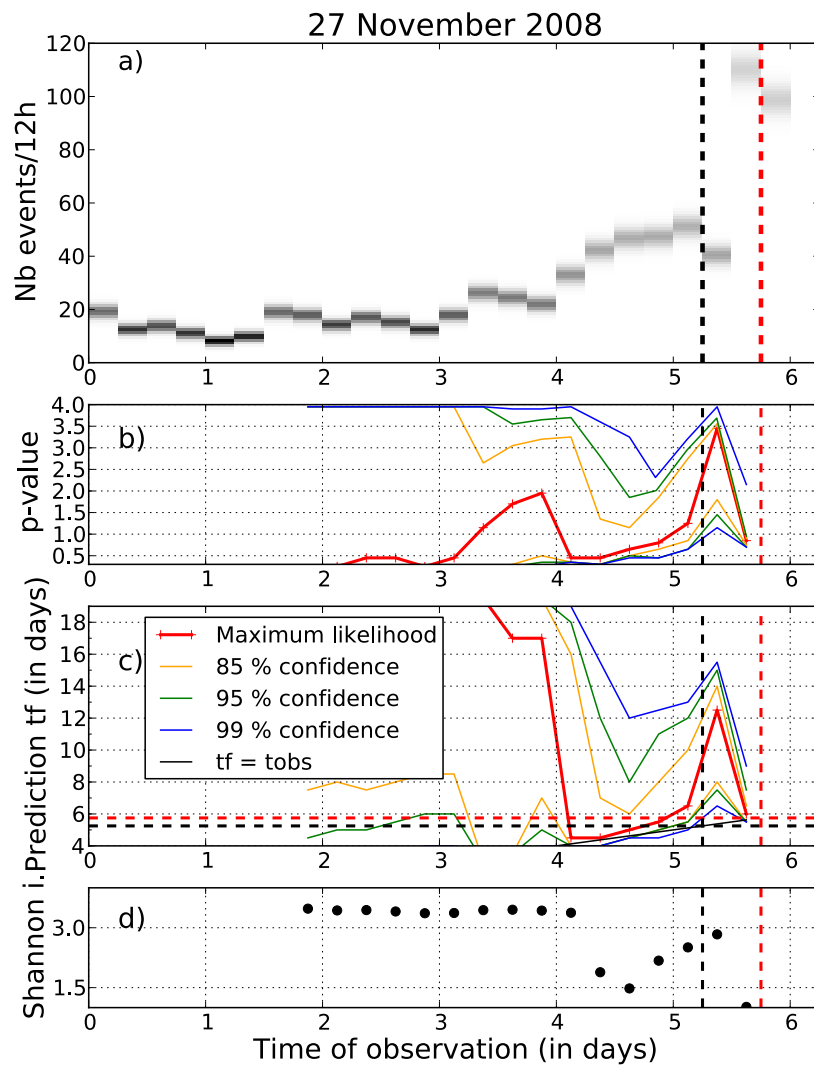


Figure C.16: a) Prior *pdfs* of the data for the 27 November 2008 eruption at PdIF volcano, as a function of the observation time t_{obs} . The true time of eruption is $t_e = 5.75$ days (red dashed line). The black dashed line indicates the time of deceleration. Panels b), c) and d) same as Figure C.1b-d.

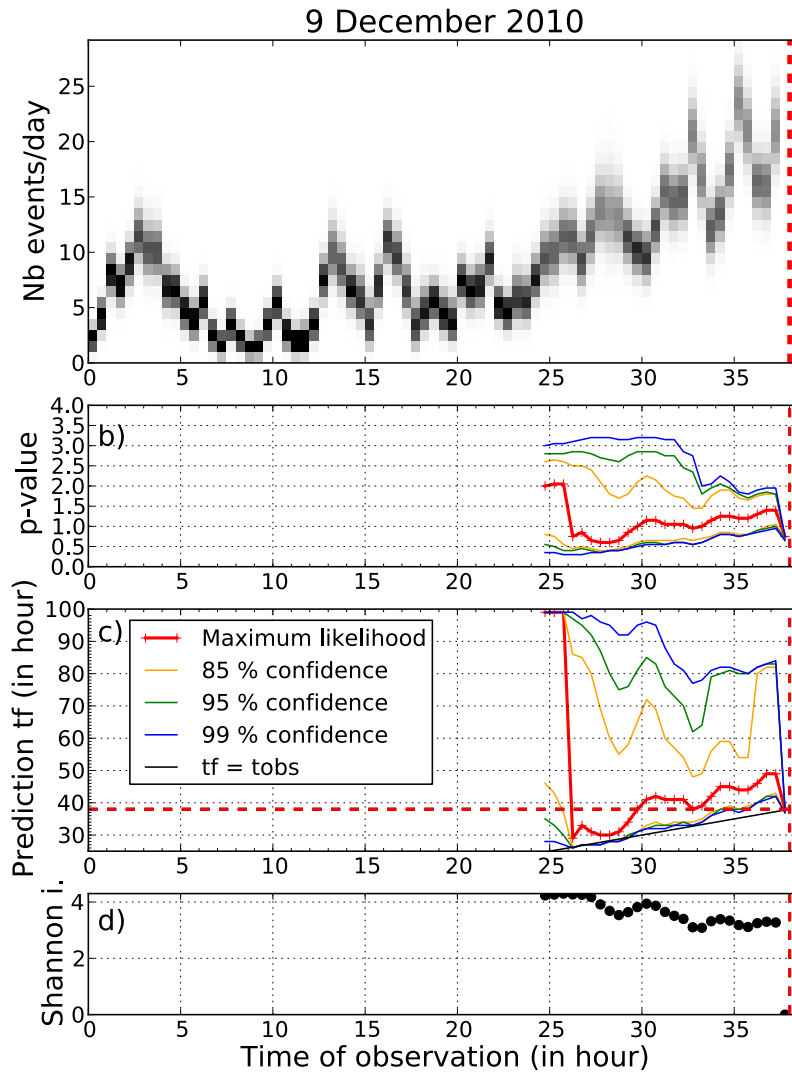


Figure C.17: a) Prior *pdfs* of the data for the 9 December 2010 eruption at PdIF volcano, as a function of the observation time t_{obs} . The true time of eruption is $t_e = 38$ days (red dashed line). The black dashed line indicates the time of deceleration. Panels b), c) and d) same as Figure C.1b-d.

Appendix D

Publication Boué *et al.* (2015),
Journal of Geophysical Research

SPI	Journal Code:				Article ID				Dispatch: 01.03.15	CE: MAEE
	J	G	R	B	5	1	0	4	6	No. of Pages: 19

RESEARCH ARTICLE

10.1002/2014JB011637

Key Points:

- Using the FFM with a Bayesian approach allows real-time eruption prediction
- Time stability of the predictions and their uncertainty are reliability criteria
- The pdf of the data are inferred from statistical performance of classification tool

Correspondence to:

A. Boué,
Anais.Boue@univ-savoie.fr

Citation:

Boué, A., P. Lesage, G. Cortés, B. Valette, and G. Reyes-Dávila (2015), Real-time eruption forecasting using the material Failure Forecast Method with a Bayesian approach, *J. Geophys. Res. Solid Earth*, 120, doi:10.1002/2014JB011637.

Received 26 SEP 2014

Accepted 13 FEB 2015

Accepted article online 17 FEB 2015

Real-time eruption forecasting using the material Failure Forecast Method with a Bayesian approach

A. Boué¹, P. Lesage¹, G. Cortés², B. Valette¹, and G. Reyes-Dávila³

¹ISTerre, CNRS, Université Savoie-Mont Blanc, IRD, Le Bourget du Lac, France, ²Centro Universitario de Estudios e Investigaciones en Vulcanología, Universidad de Colima Colima, Mexico, ³Departamento de Teoría de la Señal, Telemática y Comunicaciones, Escuela Técnica Superior de Ingeniería Informática, Universidad de Granada, Granada, Spain

Abstract Many attempts for deterministic forecasting of eruptions and landslides have been performed using the material Failure Forecast Method (FFM). This method consists in adjusting an empirical power law on precursory patterns of seismicity or deformation. Until now, most of the studies have presented hindsight forecasts based on complete time series of precursors and do not evaluate the ability of the method for carrying out real-time forecasting with partial precursory sequences. In this study, we present a rigorous approach of the FFM designed for real-time applications on volcano-seismic precursors. We use a Bayesian approach based on the FFM theory and an automatic classification of seismic events. The probability distributions of the data deduced from the performance of this classification are used as input. As output, it provides the probability of the forecast time at each observation time before the eruption. The spread of the a posteriori probability density function (*pdf*) of the prediction time and its stability with respect to the observation time are used as criteria to evaluate the reliability of the forecast. We test the method on precursory accelerations of long-period seismicity prior to vulcanian explosions at Volcán de Colima (Mexico). For explosions preceded by a single phase of seismic acceleration, we obtain accurate and reliable forecasts using approximately 80% of the whole precursory sequence. It is, however, more difficult to apply the method to multiple acceleration patterns.

1. Introduction

The development of strategies for eruption forecasting is one of the most important issues in volcanology. For example, probabilistic approaches have been investigated for short- and long-term eruption forecasts, i.e., respectively shorter and larger than interruptive time [Marzocchi and Bebbington, 2012]. These methods are usually based on the historical activity of a particular volcano, such as the cyclicity pattern of interruptive times [Connor et al., 2003] or on pattern recognition techniques to determine reliable eruption precursors for eruption alarm periods [Schmid et al., 2012]. In the aim to determine eruption dates instead of wide alarm periods, efforts toward deterministic forecasting of eruption and landslides have been developed since more than 30 years. Fukuzuno [1985] started to use an empirical power law to model the patterns of surface displacements prior to slope failure. Later on, Voight [1988] proposed a general materials failure law to characterize patterns of deformation and acoustic emissions prior to rock failure. This law has been widely used until now to describe precursory phenomena of landslides, rock failure, or volcanic eruptions or to process hindsight deterministic predictions. However, its potential for real-time volcanic eruption forecasts has been evaluated in very few studies [Voight and Cornelius, 1991; Bell et al., 2011, 2013].

Many eruptions are preceded by an increase in volcano-seismic activity, deformation of the edifice, or gas emission. These signals are used as precursors of incoming eruptions as they are often linked to the magma movement at depth. In many cases, the precursory seismic activity shows patterns of acceleration that can be used as a robust precursor of volcanic eruptions [McNutt, 1996]. The underlying physical process is meant to be related to the failure of the surrounding rock caused by magma rising up from depth [Voight, 1988]. Volcano-tectonic earthquakes (volcano-tectonic (VT)) are directly related to this mechanism, but other types of volcano-seismic events are also commonly observed. The precursory sequences can also be composed of tremors related to magma degassing or of long-period events (LP) associated with magma fracturation [Lavallée et al., 2008; Neuberg et al., 2006] or with resonances in fluid-filled cavities [Chouet and Matoza, 2013]. The precursory seismicity can be quantified by its energy, by the number of recorded events per

unit time, or by the mean level of the seismic signal. Many observations showed that the acceleration in the number, energy, or level of seismic signals or acoustic emissions prior to eruptions, landslides, or rock failure can be described by an empirical power law relating the rate of change of a given precursor $\dot{\Omega}$ (e.g., deformation and seismicity) to its acceleration $\ddot{\Omega}$ [Fukuzuno, 1985; Voight, 1988, 1989] as

$$\ddot{\Omega} = A\dot{\Omega}^\alpha, \quad (1)$$

where the coefficients α and A are empirical constants that determine how the rate $\dot{\Omega}$ changes with time. When it exists, the vertical asymptote of function $\dot{\Omega}(t)$ (i.e., the time when the observable rate $\dot{\Omega}$ is virtually infinite) is commonly interpreted as the opening of a crack that is, for volcanoes, the opening of the magma conduit toward the surface, leading to an eruption. Adjusting such a power law to the observed seismic observations allows us to extrapolate the time position of the asymptote, corresponding to the time of rupture t_f , which is considered as the forecast of the eruption time. This method of prediction of rock failure, extended to landslides and eruptions, is called the material Failure Forecast Method (FFM) [Voight, 1988].

Cornelius and Scott [1993] linked the FFM with the accumulation of damage (i.e., increase and connections of cracks) in the surrounding rock submitted to the stresses caused by magma rising. More recently, other damaging models have been proposed to explain accelerating seismicity or deformation prior to rock failures [Main, 1999], eruptions [Kilburn, 2003], or landslides [Helmstetter et al., 2004]. All these models are associated with a power law of the same form as equation (1) with an exponent α supposed to be equal to 2 for the terminal stage of the damaging process. More precisely, Kilburn [2003, 2012] demonstrate that α can evolve from 1 to 2 as fracturing proceeds.

Most of the studies about volcanic eruption forecasting use the FFM to describe the whole sequence of acceleration and to carry out hindsight forecasting of the date of eruption [see Ortiz et al., 2003; Voight, 1988; Cornelius and Voight, 1995; Kilburn and Voight, 1998; Chastin and Main, 2003; Arámbula-Mendoza et al., 2011; De La Cruz-Reyna and Reyes-Davila, 2001]. The common application of the FFM consists in setting the exponent $\alpha = 2$ which corresponds to a hyperbolic law. This is the easiest manner of using the FFM because in this case, the inverse of $\dot{\Omega}$ decreases linearly with time and fitting the data can be achieved by simple linear regression. Although this method gave good results for a posteriori analysis of laboratory failure experiments, landslides, and eruptions [Cornelius and Voight, 1994; Murray and Ramirez Ruiz, 2002; Carniel et al., 2006; Budi-Santoso et al., 2013], the correlation coefficients obtained for the linear regression are low in most of the studies. This suggests that the value $\alpha = 2$ is not always adequate for explaining the observed data.

Experimental evidences show that the exponent α may take other values than 2. For instance, Cornelius and Scott [1993] found α values between 1.47 and 2.12 for laboratory experiments of rock damaging. Voight [1989] deduced values of $1.74 < \alpha < 2.01$ from experiments on metals, $1.9 < \alpha < 2.1$ for experimentally deformed soils, and $2.0 < \alpha < 2.2$ for landslides. Cornelius and Scott [1993] and Voight and Cornelius [1991] found most values in the range [1.0, 2.0], with typical values near 1.5 for precursory phenomena at Mount St. Helens (USA) from 1980 to 1986. Finally, Smith and Kilburn [2010] found that α takes values of up to 3.30 for the 1991 Mount Pinatubo eruption (Philippines).

Consequently, the assumption of setting $\alpha = 2$ appears to be too simplistic and poorly reliable. Furthermore, its physical basis is not well established and does not take the natural variability of α values into account. Even though some successful hindsight eruption forecasts were carried out using the FFM with variable α values [Cornelius and Scott, 1993; Cornelius and Voight, 1994; Smith and Kilburn, 2010], the number of published examples is still too limited to conclude about the best way of using FFM for eruption forecasting.

In addition, the common application of the FFM suffers from some other issues:

1. On volcanoes, the seismic observables used as precursors usually mixed together numerous types of seismic events that are associated with different physical mechanisms at the source: brittle rupture (VT), resonance of fluid-filled cavities and/or brittle rupture of magma (LP), degassing (tremors), collapses, regional earthquakes, or noise. For instance, when the observable is the mean level of the seismic signal, described by Real-time Seismic Amplitude/Energy Measurement (RSAM/RSEM) [Endo and Murray, 1991; De La Cruz-Reyna and Reyes-Davila, 2001], it can include rockfalls, tectonic earthquakes, or other signals that are not related to damage processes within the volcano [Ortiz et al., 2003; De La Cruz-Reyna and Reyes-Davila, 2001]. Therefore, in order to clearly identify acceleration sequences associated with single

physical process described by a power law and thus to be able to carry out precise predictions, it is of paramount importance to process the different classes of events separately. In this perspective, the Spectral Seismic Amplitude/Energy Measurement (SSAM/SSEM) [Stephens et al. [1994]] can be used as observable. It is obtained by calculating the level of the signal in various spectral bands which can correspond to different types of events. The use of SSAM/SSEM [Tarraga et al., 2006; Cornelius and Scott, 1993], or similar function [Budi-Santoso et al., 2013] instead of RSAM/RSEM provides more suitable accelerating sequences and better results of eruption prediction using the FFM. However, different classes of signals are still mixed if they have energy in the same frequency ranges (tremors and LP or regional earthquakes and VT for example). In this study, we rather use an automatic recognition tool to separate the classes of events.

2. The FFM can be applied using either cumulative or noncumulative values of the data. When cumulating data, each new data depends on the previous ones, leading to data correlation. If these correlations are neglected, it will perturb the result of inversion, yielding potentially spurious trends [Greenhough et al., 2009]. This point has also been addressed by Hardebeck et al. [2008] in the framework of Accelerating Moment Release (AMR) who showed that apparent AMR can be identified in synthetic data that actually do not contain any AMR. However, no binning is required which is a practical advantage in comparison with using noncumulative data [Bell et al., 2013]. Furthermore, it is possible to adjust the mean trend of multiple acceleration patterns using cumulative data that are monotonically increasing, which is more difficult with noncumulative data. This is a delicate point because one may adjust a theory that actually does not describe the data which might lead to unreliable and biased results. Consequently, the choice of the type of data faces a competing balance between theoretical and practical advantages. In this study, we use the rate of events at a given time as observable. In other words we must evaluate the instantaneous derivative $\dot{\Omega}$ for every given time interval even though it is not a precise concept, which must be practically approached.
3. Although the uncertainty on the predicted time of eruption would be a highly valuable information for decision makers during crises, the errors on the eruption forecast are not calculated in most of the studies or they are roughly approximated. The first step in calculating these errors reliably is to estimate the uncertainty on the observable. This has been addressed by Bell et al. [2011, 2013] who assumed that earthquake occurrences follow a Poisson distribution [Marsan and Nalbant, 2005; Greenhough and Main, 2008]. In this study, we use the output of the automatic recognition system to compute the a priori probability density function (*pdf*) of the event rates. Thus, we do not make any assumptions concerning the uncertainty structure of the data, and we use all the prior information for the inversion process, which is an improvement in comparison with earlier studies.
4. Real-time predictions address a less constrained inverse problem than hindsight forecasts because they deal with partial data sets that end at the time at which the prediction is done. Voight and Cornelius [1991] and Cornelius and Voight [1994] question whether forecasts would be possible before the eruption, using incomplete sequences of acceleration. For a real-time application of the FFM, they propose to update the forecasts at given time intervals and they find that the predictions tend to converge toward the eruption date some time before the eruption, using the FFM with $\alpha = 2$. More recently, Smith and Kilburn [2010], Bell et al. [2013], and Budi-Santoso et al. [2013] applied similar approaches. They represented the prediction times t_f as a function of the observation time t_{obs} advancing toward the eruption. In Budi-Santoso et al. [2013] who used the FFM with $\alpha = 2$, it is clear that the predicted time of eruption stabilizes close to the eruption date several days before the eruption onset. However, this is not so clear in Smith and Kilburn [2010] and Bell et al. [2013] who used FFM with variable α . Assuming that α is fixed does introduce a bias, unless α is actually equal to 2, whereas considering it as variable reduces the bias while it greatly increases the formal uncertainty in failure time prediction. In any case, confidence criteria regarding the predictions are required to evaluate whether a prediction is reliable or not. In this study, we do not set $\alpha = 2$ and we define reliability criteria of the predictions.

The objectives of the present study are, first, to find the most robust and accurate way of using the FFM on volcano-seismic data and, second, to propose criteria to estimate the reliability of the predictions made in real time and evaluate the real-time potential of FFM for eruption forecasting.

In the first part of this paper, we present the material Failure Forecast Method and we discuss how the method can be implemented in real time during crisis when new data are recorded continuously by the monitoring network. In the following, we will call *eruption forecast in a real-time perspective* the

corresponding procedure. To test the capability of FFM for real-time perspective, we will consider sequences that are selected in hindsight. Statistical evaluation of the success rate of the predictions is not carried out in this paper. It would be one step farther for the development of a real-time method. In a second part, we propose an approach to evaluate accurately uncertainties in the rate of seismic events. We process automatic detection and classification of seismic events which provides both the quick counting of the events during crises for the class of interest and the information for calculating data uncertainties. In a third part, we present the Bayesian formulation used to adjust the FFM theory to the rate of seismic events. This method allows for working only with a priori probabilities on the data and on the model parameters and provides the a posteriori pdf of the time of prediction as output. It is consequently the most objective inverse method that can be used to solve this problem. In particular, we do not make any hypothesis on the structure of the data uncertainties. Finally, we present some applications of our approach, in a *real-time perspective*, to precursory seismic activity observed in 2005 before several vulcanian explosions of Volcán de Colima (Mexico).

2. Forecasting Approach in a Real-Time Perspective

In this study, we apply the FFM with the observable $\dot{\Omega}$ associated with the precursory LP seismicity prior to vulcanian explosions. We choose to use noncumulative or incremental values of data ($\dot{\Omega}$) to adjust the forecast model. Cumulative data (Ω) are sometimes preferred because it avoids binning and it naturally smoothes the curves. However, it presents some drawbacks as discussed in section 1.

Differential equation (1) must be integrated to express the LP rates $\dot{\Omega}$ as a function of time. In the case where $\alpha > 1$ and $A > 0$, the solution of equation (1) describes a power law increase of the data $\dot{\Omega}$ as a function of time t :

$$\dot{\Omega}(t) = [A(1 - \alpha)(t - t_0) + \dot{\Omega}_0^{1-\alpha}]^{\frac{1}{1-\alpha}}, \quad (2)$$

where t_0 is the beginning of the fitting window and $\dot{\Omega}_0$ is the data at time t_0 . The position of the asymptote of function $\dot{\Omega}(t)$ is as follows:

$$t_f = -\frac{\dot{\Omega}_0^{1-\alpha}}{A(1-\alpha)} + t_0. \quad (3)$$

The failure time t_f is interpreted as the prediction of the eruption time.

Combining expressions (2) and (3) leads to a more convenient formulation:

$$\dot{\Omega}(t) = k \left(1 - \frac{t}{t_f}\right)^{-p}, \quad (4)$$

where $p = \frac{1}{\alpha-1}$ and k is a constant of the dimension of $\dot{\Omega}_0$. The advantage of equation (4) in comparison with other formulations is that t_f is directly involved in the data adjustment and thus directly yields the pdf of t_f . This theory of eruption forecast is consequently composed of three parameters: k , p , and t_f .

The choice of the initial time t_0 is important especially when working with real data from volcanoes. A power law as defined in equation (4) consists in a part with low and almost constant slope and another one characterized by a strong increase of the slope. In order to well constrain the model, the fitting window must include both parts of the power law. Thus, the origin time t_0 must be set accordingly. In practice, we will explain how it can be set in real-time perspective by analyzing prediction results in parallel for different t_0 .

Besides, when adjusting the data to the power law, a trade-off appears between the three parameters. In particular, the estimation of the exponent α in equation (1), or p in equation (4), is strongly coupled with that of k . Therefore, part of the variability of the values of α reported in the literature may originate from the fitting procedure used.

We aim at computing reliable a posteriori pdfs of the parameters k , p , and t_f and at analyzing their evolution as a function of the time of observation t_{obs} while it advances toward the time of eruption t_e . We assume that the estimated parameters of the theory would stabilize if a sustained physical process takes place in the volcano. We also expect that while the time of eruption is approaching, the a posteriori pdf on the parameters would become narrower and thus that the corresponding uncertainties would decrease.

We consequently define two criteria to evaluate the quality of the prediction: (1) the uncertainty on the predicted time t_r that can be derived from the corresponding pdf and (2) the temporal stability of parameter t_r . The first step includes the definition of the most suitable observable for a given eruptive crisis, the data processing, and the reliable estimation of the uncertainties on observations. These topics are presented in the next section. The whole methodology is tested through the practical examples of Volcán de Colima.

3. Seismic Data of Volcán de Colima

3.1. Precursory Sequences of 2005 Vulcanian Explosions at Volcán de Colima

Volcán de Colima is an andesitic stratovolcano of 3860 m height above sea level, located in the western part of the Mexican Volcanic Belt. It is the most active volcano of Mexico and displays a wide spectrum of eruption styles including small phreatic explosions, major block-lava effusions, and large explosive events [Gonzalez et al., 2002]. Recent typical activity is composed of the growth of lava dome, followed by periods of vulcanian explosions usually preceded by seismic precursors. Major vulcanian explosions are sometimes associated with pyroclastic flows going down to several kilometers away from the crater. Some villages are settled on the flank of the crater such as La Yerbabuena, which is the closest one (8.2 km from the crater). About 5000 people live at less than 15 km from the active vent, and the major town of Colima is located at 30 km from the crater. The effort in developing deterministic real-time eruption forecast in this context is thus justified by important societal challenges. The seismic records analyzed in this paper were recorded by the closest short period station EZV4, located 1.8 km from the crater.

The 2005 explosive activity is composed of 30 major and moderate vulcanian explosions usually preceded by rapid dome growth. All of them are preceded by an increase of the number of LP events, and most of them display accelerating behaviors. The LP activity is mixed mainly with rockfalls and some tremors and regional tectonic earthquakes. The duration of the precursory activity is variable, from few hours to several days. We chose to test our method on four representative examples of precursory activity already studied by Varley et al. [2010a, 2010b] and Arámbula-Mendoza et al. [2011]. Two of them present a single accelerating sequence of seismicity prior to an explosion with a duration of about 20 h (29 April and 5 June 2005) followed by 10 h and 0.5 h of deceleration before the explosion, respectively. The two other ones display complex sequences with multiple acceleration phases during more than 1 day preceding the major vulcanian explosions of 10 May and 27 July 2005. The latter are of course more challenging to tackle with the simple FFM theory. These examples are used to evaluate the potential and the limits of the real-time prediction method with real data.

3.2. Seismic Data Processing

The precise and well-designed analysis of data is one of the most important tasks in order to succeed accurate forecasts based on precursory seismic activity. Two main points have to be considered: the manner of counting the seismic events and the rigorous evaluation of their uncertainty. The workflow of the data processing is thus composed of (1) an automatic classification of continuous seismic signals, (2) the count of events gathered into binned temporal windows (noncumulative data), and (3) the computation of a priori probability distribution for each binned window.

First of all, different classes of seismic signals related to different source mechanisms are recorded by the seismographs. The major activity during the period of 2005 is composed of LP events, whose physical mechanism is supposed to be related to the fracturation of magma at the conduit wall [Varley et al., 2010a; Lavallée et al., 2008, 2011]. Volcano-tectonic (VT) activity, related to the fracturation of the surrounding rock, and tremor (T) activity, associated with degassing processes, are rare in 2005. Many rockfalls (or collapses, COL) are also observed. Some regional tectonic events (REG) are usually detected and are sometimes very energetic in comparison with volcano-seismic activity. Small to major explosions (EXP) are also recorded.

The seismic signals presented above have to be classified. This task must be achieved very rapidly, even when hundreds of events are recorded per day, in order to make near-real-time forecasting. For this purpose, we use an automatic recognition system based on Hidden Markov models Young et al. [2006] designed for speech recognition. It has also been used in other areas such as sign language. It was adapted for the Volcano-Seismic Recognition system (VSR) Cortés et al. [2014] and is very efficient to proceed rapid classification. Similar to speech signals, continuous seismic records are considered as time sequences with varying spectral contents. A data stream is converted into a temporal sequence of overlapped frames which are parametrized to describe the temporal evolution of the spectral. A training database of events must

Table 1. Confusion Matrix Obtained From the Volcano-Seismic Recognition System^a

<i>i</i>	<i>j</i>								Del	% Tot
	COL	EXP	EXPS	LP	REG	SIL	T	VT		
COL	152	1	1	0	0	0	0	3	19	86.36
EXP	0	19	4	1	0	0	0	0	3	70.37
EXPS	0	5	122	0	0	0	0	0	1	95.31
LP	0	1	19	224	2	0	1	1	5	83.90
REG	0	0	0	0	30	0	2	3	1	83.33
SIL	0	6	7	0	0	48	0	0	15	63.16
T	0	1	3	1	4	0	48	1	5	76.19
VT	0	0	1	5	2	0	0	113	4	90.40
									mean %	81.13

^a Rows correspond to the number of true events in each class *i*, and columns present events recognized by the Volcano-Seismic Recognition system in each class *j*. The column denoted % tot represents the percentage of events well recognized by the VSR, including the deleted events (Del).

be manually classified to build one Markov model for each class of volcano-seismic signals. Once these Markov models are built during the training phase, the system can rapidly process years of recordings to automatically classify a continuous flow of data. Consistent catalogues can be easily obtained for each type of events.

For Volcán de Colima, we used the classes presented above (LP, VT, COL, REG, T, and EXP) plus a class of saturated explosions (EXPS) and another one for the seismic noise (SIL, for silence).

The success rate of the recognition is calculated using the manually labeled database by evaluating the number of substitutions between classes and the number of deletions (events that are not recognized). The statistics on the recognition are usually represented through a so-called confusion matrix (Table 1), which gives the number of events that have been successfully recognized in each class, as well as the number of substitutions and deletions. It gives a way to calculate the rate of recognition success for each class (%tot) and the conditional probability $P(i|j)$ for an event to belong to a given class *i* knowing that it has been identified by the VSR as an event of class *j*:

$$P(i|j) = \frac{M_{ij}}{\sum_i M_{ij}}, \quad (5)$$

where M_{ij} is the corresponding element of the confusion matrix M and $\sum_i M_{ij}$ is the total number of events identified as belonging to class *j* by the VSR. This conditional probability quantifies the uncertainty on the counts of seismic events.

Given the identification by the VSR of *n* total events in a time window, the probability $P_i(m)$ that there are *m* events actually belonging to class *i* ($m \leq n$) can be evaluated based on the conditional probability $P(i|j)$ as

$$P_i(m) = \sum_{\substack{|\mathbf{k}|=m \\ k_j \leq n_j}} \prod_{j=1}^c \binom{n_j}{k_j} P(i|j)^{k_j} (1 - P(i|j))^{n_j - k_j}, \quad (6)$$

where *c* is the number of event classes ($c = 8$ in our example), n_j is the number of events identified by the VSR in class *j* over the time window, $|\mathbf{k}|$ stands for $\sum_{j=1}^c k_j$, and $\binom{n_j}{k_j}$ denotes binomial coefficients. To obtain formula (6), all the possibilities to have exactly *m* events belonging to class *i* must be evaluated. Each of the *m* events may have been identified by the VSR as belonging to one of the *c* possible classes. This leads to consider all the decompositions of *m* as sums of *c* numbers k_j with $k_j \leq n_j$ for $j = 1, \dots, c$ which justifies the first sum in formula (6). The probability of each of these occurrences must be then evaluated. Given a class *j*, for which the VSR has identified n_j events over the time window, the probability that exactly k_j of those events belong to class *i* is $\binom{n_j}{k_j} P(i|j)^{k_j} (1 - P(i|j))^{n_j - k_j}$ where $\binom{n_j}{k_j}$ is the number of k_j combinations among n_j elements, and where $P(i|j)$ (respectively $1 - P(i|j)$) is the probability that an event identified by

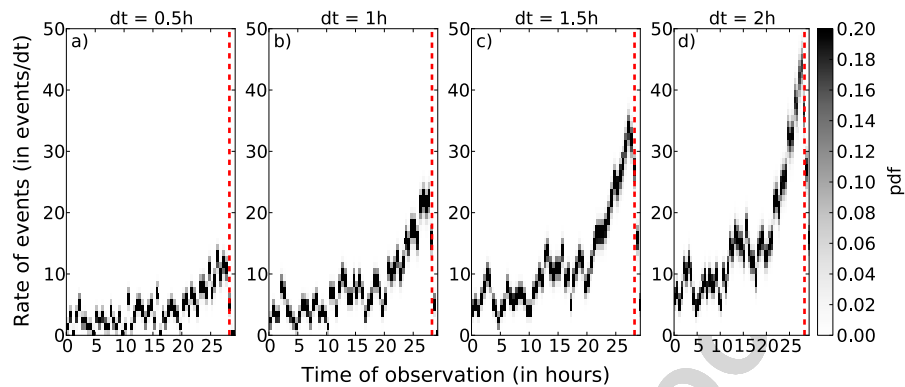


Figure 1. Probability density functions of the rate of events as a function of time for the vulcanian explosion of the 5 June 2005, computed for different window widths Δt . (a) $\Delta t = 0.5$ h, (b) $\Delta t = 1$ h, (c) $\Delta t = 1.5$ h, and (d) $\Delta t = 2$ h. The red dashed line represents the time of explosion.

the VSR as belonging to class j belongs, in fact, (respectively does not belong) to class i . Since the choice of the events within each class may be done independently, the product of these factors must be done as in formula (6). This calculation is repeated for each time window centered around the time of observation $[t_{\text{obs}} - \frac{\Delta t}{2}, t_{\text{obs}} + \frac{\Delta t}{2}]$ where Δt is a window width which has to be defined as discussed in the following.

In practice, the energy and the number of seismic events are calculated for each class of precursor (i.e., VT, LP, or tremor) to identify possible precursory acceleration sequences. In the case of Volcán de Colima, the acceleration behavior of LP numbers is much clearer than that of LP energy. There is no precursory increase of VT activity before explosions for the period of study. We thus used the LP rates as observable, so it is necessary to define a time window width Δt for binning the data, which is a delicate point. The evaluation of $\dot{\Omega}$ at a certain t_{obs} requires a numerical approximation of the time derivative of the number of events Ω at each observation time. Different values of Δt lead to different approximations of $\dot{\Omega}(t_{\text{obs}})$. A too small window Δt could hide a precursory pattern if the signal is dominated by noise fluctuations. On the other hand, a too large window may smooth too much the acceleration pattern. We thus explore a range of reasonable values for Δt , excluding too small values, which do not allow for visual detection of the acceleration sequences to be detected, as well as large values that produce too strong smoothing, in the aim to explore a range of reasonable values for Δt . Figure 1 presents the a priori probability distribution of the rates of LP events as a function of the observation time t_{obs} calculated with four window widths Δt , prior to the major vulcanian explosion of the 5 June 2005. In this case, the precursory LP pattern appears to be clearer for $\Delta t = 1.5$ h and $\Delta t = 2$ h. This observation can be carried out in real time by plotting the data in parallel for different Δt at every new time of observation, as displayed in Figure 1. In practice and if necessary, the prediction results can be computed in parallel for different Δt until the time of eruption. The most stable and accurate results (following the criteria defined in section 2) can be chosen as the time of prediction.

The last methodological point concerns the frequency at which the data have to be updated. In periods of volcanic crisis, hundreds of events can occur everyday, so new data streams can be updated very often. To evaluate the stability criterion in real time, when precursory seismic activity is short, we need to update forecasts as frequently as possible. In this study, we update the calculation of $\dot{\Omega}(t)$ each 30 min to make a new forecast. However, this pragmatic choice may introduce correlations in the data when $\Delta t > 1$ h because the increments will overlap and will result in residual bias in the estimate of the prediction uncertainty. The resulted prediction uncertainties will thus be slightly perturbed, but the proper quantification of this bias is difficult to evaluate due to the nonlinearity of the problem.

Once the a priori probability of the data $P_i(m)$ is determined for each t_{obs} and each Δt , we use a Bayesian approach that yields the a posteriori pdf of the model parameters.

4. A Posteriori Probability Density Function

To compute the pdfs of the FFM parameters, we use the Bayesian approach proposed in *Tarantola* [2005].

In the present case, the data space \mathbb{D} consists of the rates of LP events at n_{obs} observational times before the explosive event. This rate is computed over a time window of a given duration Δt , as explained before. We have also detailed the way to compute the probability of the number of observed LP events, through the VSR, over a centered window. We transform by linear interpolation this discrete probability $P_{\text{LP}}(m)$ into a pdf, ρ_{LP} , over the range $[0, n]$, where n is the total number of events around the given observational time. Beyond the value of n , the probability ρ_{LP} is set to zero. Assuming that the rates of LP events at the different observational times are independent, we finally obtain the a priori data pdf:

$$\rho_{\text{obs}} = \prod_{o=1}^{n_{\text{obs}}} \rho_{\text{LP}}^o. \quad (7)$$

The model space \mathbb{M} consists of the three real numbers k , p , and t_f . In the Bayesian approach, a prior pdf $\rho_{\text{prior}}(k, p, t_f)$ has to be put, at first, over these variables. We assign uniform prior densities for $k \in [0, n]$, for $t_f \geq t_{\text{obs}}$ and for $p \in [0.4, 4]$ based on the relation $p = \frac{1}{\alpha-1}$ and the reported values of α . The choice of a uniform prior is motivated by the lack of knowledge on the model. Consequently, we rely only on the data information. Another possibility could have been to use the posterior pdf obtained at $t_{\text{obs}-1}$ as the prior pdf at t_{obs} , in a data assimilation approach. This has been tested but it appears that using a previous posterior pdf, which is generally poorly constrained due to the consideration of a partial data set, can bias further predictions. At time t_{obs} , the most reliable information is the newest acquired data and it is not consistent to consider older prior information.

Following the Bayesian approach with these uniform prior pdfs and neglecting the error of the theory, the posterior pdf of the model space is given by [*Tarantola*, 2005, equation (1.93), p. 34; *Tarantola and Valette*, 1982, equation (6.9)]:

$$\rho_{\text{post}}(k, p, t_f) \propto \rho_{\text{prior}}(k, p, t_f) \rho_{\text{obs}}(\hat{\Omega}(t)), \quad (8)$$

which expresses that $\rho_{\text{post}}(k, p, t_f)$ is proportional to the a priori uniform pdf of the model multiplied by $\rho_{\text{obs}}(\hat{\Omega}(t))$ (the normalization constant is not explicit). Taking account of expression (7) for ρ_{obs} and of the uniformity of ρ_{prior} , (8) can be rewritten as follows:

$$\rho_{\text{post}}(k, p, t_f) \propto \prod_{o=1}^{n_{\text{obs}}} \rho_{\text{LP}}^o(\hat{\Omega}(t_o)), \quad (9)$$

where $\hat{\Omega}(t_o)$, the theoretical rate of LP event at time t_o , is expressed as a function of k , p , and t_f through equation (4).

Finally, the marginal pdf of t_f is computed as

$$\rho_{\text{post}}(t_f) = \int_k \int_p \rho_{\text{post}}(k, p, t_f) dp dk. \quad (10)$$

The spreading of $\rho_{\text{post}}(t_f)$ can be quantified by the Shannon index [*Shannon*, 1948] at each time of observation:

$$I(t_{\text{obs}}) = - \int_{t_f} \rho_{\text{post}}(t_f) \times \log(\rho_{\text{post}}(t_f)) dt_f. \quad (11)$$

The lower the Shannon index is, the more relevant is the pdf of t_f at the corresponding time of observation.

In a real-time perspective eruption forecast, the maximum likelihood (i.e., the maximum of the a posteriori pdf of t_f) should stabilize with time if there is one single acceleration of the rate of LP events. Stabilization occurs during an accelerating trend because (a) it is consistent with the assumption of equation (4) as the "best fit model" and (b) more data are accrued. Moreover, the prediction should be more precise when approaching the time of eruption as the model becomes more and more constrained, which should be indicated by a decreasing Shannon index related to the narrowing of the pdf. This narrowing of the pdf has already been shown for synthetic data by *Bell et al.* [2013], for a theoretical relation of the form of equation (4). The spread of the a posteriori pdfs can be also evaluated by the 95% and 99% confidence levels.

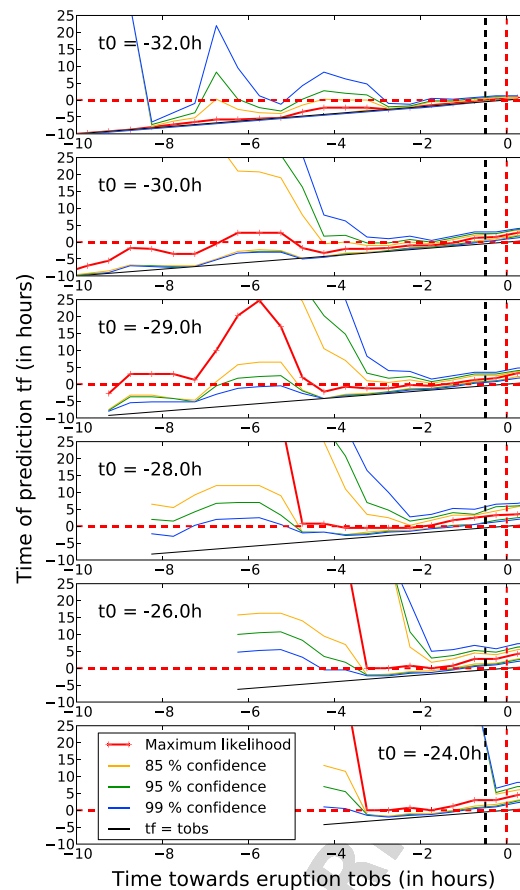


Figure 2. Results of prediction t_f as a function of time for the 5 June 2005 explosion. Each panel represent the results obtained for different starting time t_0 . The red line is the maximum likelihood of the pdf, and the yellow, green, and blue lines indicate the 85%, 95%, and 99% intervals of confidence, respectively. The explosion occurs at $t_{obs}=0$ (dashed red line), and the time of observation corresponds to the number of hours remaining before the explosion occurs.

with a time of eruption at $t_e=28$ h ($t_0=0$). A deceleration of the activity is observed 0.5 h before the explosion. Window sizes $\Delta t=1.5$ h and $\Delta t=2$ h are both suitable for evaluating the LP event rates. Figure 3b represents the prediction t_f as a function of the observation time t_{obs} . The accelerating sequence of LP events starts at $t_{obs}\approx 21$ h, and the first prediction that seems (a posteriori) satisfying when compared with the true eruption time is obtained at $t_{obs}=23$ h, i.e., 5 h before the explosion, but its uncertainty is large (99% confidence intervals range from $t_f=26$ h to $t_f=60$ h). The estimated value of t_f remains quite stable until $t_{obs}=26$ h, while its precision is getting better, as indicated by the Shannon index (Figure 3d). Moreover, the lower bound of the confidence intervals of t_f is equal to the time of observation t_{obs} , and the upper bound of the 99% confidence intervals remains at an almost constant value in a range $t_f=[30, 34]$ h from $t_{obs}=26$ h until the eruption time. Therefore, a prediction could have been made 5 h before the eruption, in an interval between $t_f=t_{obs}$ and $t_f=34$ h, at a confidence level of 99%, with a maximum likelihood around $t_f=28$ h, very close to the real time of eruption. It is important to notice that the maximum likelihood of the p value varies with time and is close but not equal to 1 in the last part of the acceleration (Figure 3b).

5. Results

We propose to represent the results of predictions by displaying the marginal posterior pdf $\rho_{post}(t_f)$ as a function of the time of observation t_{obs} .

For an application in real time, the observer needs to set the beginning time t_0 of the power law to adjust, once the beginning of LP acceleration is noticed. Taking account of requirements discussed in section 2, we propose a practical way of choosing t_0 . Figure 2 shows the results of prediction displayed in parallel for different tested t_0 . The prediction results are similar when a long enough time series is available to constrain the model parameters. Except for the furthest $t_0=-32$ h, all the predictions eventually stabilize around the true time of explosion, but with different uncertainties and stability duration. As expected, the results of prediction obtained with t_0 that are closer to the beginning of the acceleration phase ($t_0=-24$ h in particular) display larger uncertainties and stabilize during a shorter time than other t_0 . Based on the stability and accuracy criteria, the observer could have chosen $t_0=-28$ h, -29 h, or -30 h. Figure 2 thus emphasizes that it is possible to choose t_0 in real time. It also shows that the choice of t_0 is only critical when the chosen value is either very close or very far from the acceleration onset.

The explosion of the 5 June was preceded by a sequence of LP acceleration of about 10 h (Figure 3a)

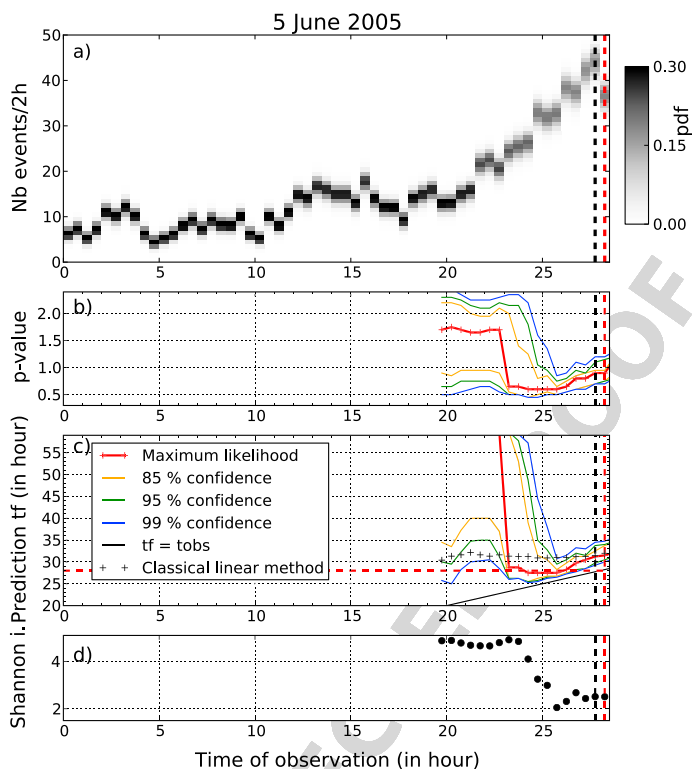


Figure 3. (a) A priori probability density functions on the data for the 5 June 2005 explosion, as a function of the observation time t_{obs} . The true time of eruption is $t_e = 28$ h (red dashed line). The black dashed line indicates the time of deceleration. (b) A posteriori marginal probability density functions of p as a function of the observation time t_{obs} . The red line is the maximum likelihood of the pdf, and the yellow, green, and blue lines indicate the 85%, 95%, and 99% intervals of confidence, respectively. (c) A posteriori marginal probability density functions of the prediction t_f as a function of the observation time t_{obs} . Black crosses represent the prediction t_f obtained for $p = 1$ and k being the maximum likelihood of the a priori pdf of Ω_0 . The red line is the maximum likelihood of the pdf, and the yellow, green, and blue lines indicate the 85%, 95%, and 99% intervals of confidence, respectively. The black line corresponds to $t_f = t_{obs}$. (d) Shannon index of the marginal probability density functions of t_f as a function of the observation time.

In the following, more complex sequences of LP activity composed of multiple acceleration phases interspersed with decreases are analyzed.

The explosive event that occurred on the 29 April 2005 was preceded by a sequence of about 15 h of acceleration, followed by more than 10 h of deceleration (Figure 4a), with the eruption occurring at $t_e = 37$ h. A window width $\Delta t = 2$ h produces more stable and precise t_f distributions than other windows. The predictions are unstable until $t_{obs} = 21$ h and then oscillate in the range $t_f = [35, 40]$ h during 5 h (until $t_{obs} = 26$ h), with the lower and upper 99% of confidence, respectively, around $t_f = 32$ h and $t_f = 40$ h (Figure 4c). After that, t_f becomes unstable during the deceleration part. So in this case we could have made a prediction between $t_f = 32$ h and $t_f = 40$ h with 99% of confidence and a greater probability that it occurs in a range $[35, 40]$ h. Note that the maximum likelihood estimate of the p value is very different from 1 and is not constant (Figure 4b).

An acceleration of the LP seismicity during about 15 h (Figure 5a) occurred before the major vulcanian explosion of the 10 May ($t_e = 37$ h). A window width $\Delta t = 2$ h produces the most stable and precise t_f distributions. As for the 5 June event, a 0.5 h long deceleration occurred before the explosion. Maximum likelihood estimates of the prediction times are unstable until $t_{obs} = 26.5$ h and then stabilize around

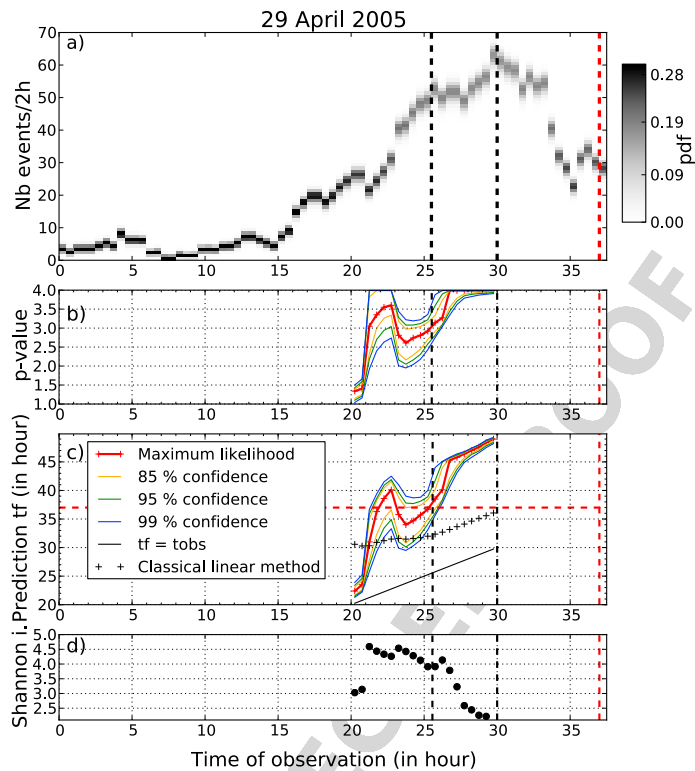


Figure 4. (a) A priori probability density functions on the data for the 29 April 2005 explosion, as a function of the observation time t_{obs} . The true time of eruption is $t_e = 37$ h (red dashed line). The black dashed line indicates the time of deceleration. (b–d) Same as Figures 3b–3d.

$t_f = 29$ h during 3 h, i.e., during the first part of the acceleration (Figure 5c), with a decreasing Shannon index (Figure 5d). The upper 95% of confidence is quite stable around $t_f = 32$ h. Thus, an explosion could have been expected between the observation time and $t_{obs} = 32$ h. However, this sequence is followed by a slight deceleration over 3 h and then by a second acceleration. For times of observation in the interval [29–32] h, i.e., in the short deceleration part, the prediction time t_f is very close to t_{obs} . Even though the Shannon index is relatively low in this interval, the prediction is not reliable due to the instability of t_f with respect to the time of observation. Reliable accurate predictions are obtained since $t_{obs} = 32.5$ h, i.e., 4.5 h before the explosion and give an estimation of $t_f \approx 38$ h. In this case, however, there is probably a bias in the estimations because the fitting interval includes the 3 h long deceleration phase. For the observation times in the interval [32.5, 36] h the maximum likelihood of t_f remains stable between $t_f = 37$ h and $t_f = 38$ h and the pdf of t_f gets more precise until the time of deceleration. Thus, an explosion could be expected to occur at a time between $t_f = 36.5$ h and $t_f = 39$ h at 95% of confidence, with a maximum likelihood of t_f ranging between 37 h and 38 h.

The explosion that occurred on 27 July ($t_e = 72$ h) was preceded by a sequence including three phases of acceleration during more than 70 h in total (Figure 6a). A window width $\Delta t = 4$ h is used here. The first acceleration phase lasted about 30 h and ended at $t_{obs} = 28$ h. It was followed by about 10 h of LP activity decrease until $t_{obs} = 40$ h. Then, another short phase of acceleration and deceleration took place until $t_{obs} = 60$ h. This complicated pattern ended with a sharp increase of the seismicity during 10 h, followed by a decrease of 4 h before the explosion. During the first phase of the acceleration, until $t_{obs} = 30$ h, relatively stable maximum likelihood of t_f are obtained in a range [33, 37] h during 4 h, with upper 99% of confidence

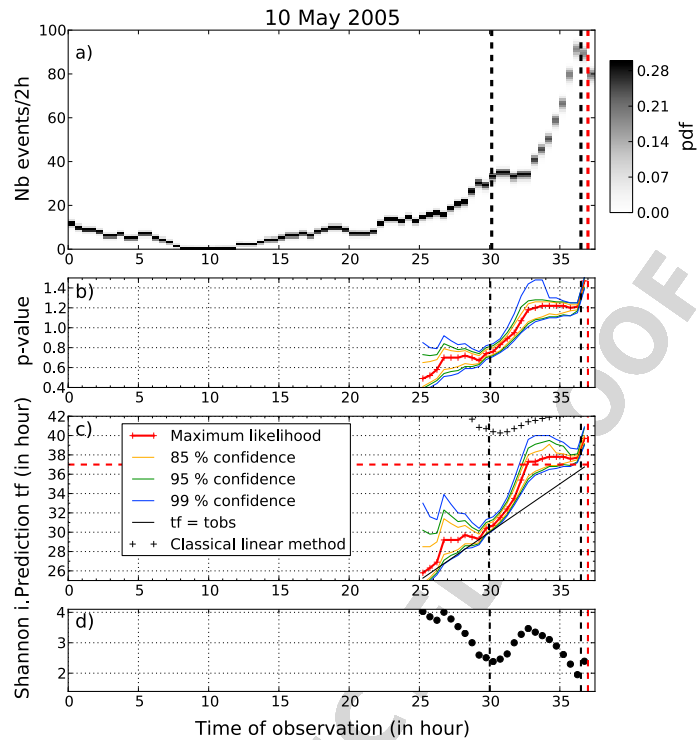


Figure 5. (a) A priori probability density functions on the data for the 10 May 2005, as a function of the observation time t_{obs} . The true time of eruption is $t_e = 37$ h (red dashed line). The black dashed line indicates the time of deceleration. (b–d) Same as Figures 3b–3d.

stabilizing around $t_f = 49$ h (Figure 6c). Figure 6b shows that p values stabilize close to 2. Although the posterior pdf of t_f is very spread (Figure 6d), an eruption could have been expected until $t_f = 50$ h. During the phases of deceleration and fluctuation of the seismicity, the FFM theory is no more valid and thus the results are meaningless. For t_{obs} in the interval [40, 45] h, i.e., when the second phase of acceleration is included, it is difficult to fit a simple power law to the whole complex sequence. A trial was done by setting the origin time t_0 at the beginning of the second phase (i.e., taking $t_0 = 35$ h) and by adjusting the power law to this subsequence only. However, the model is then poorly constrained because the data set is too small in this case. The third accelerating phase is longer than the second one, and predictions can be performed by setting the beginning of the fitting window at $t_0 = 50$ h. Even if the acceleration phase is short, the maximum likelihood of t_f stabilizes around $t_f = 70$ h for t_{obs} ranging from 65.5 to 68 h (Figure 6f), with a decreasing Shannon index (Figure 6g). The method is thus successful as a posteriori analysis, but the stabilization criterion would have been difficult to use in real time because of the short duration of the acceleration phase. Note that the p values are far from the value of $p = 1$ (Figure 6e). In addition, the time lag between the prediction made with the first acceleration part and the true time of eruption is about 35 h, close to the duration of the phases of decrease and fluctuations of seismicity, which appears to have delayed the onset of the eruption. We may speculate that this delay is related to changes in the physical conditions within the magmatic conduit.

The results of predictions obtained with the method proposed in this paper are now compared with predictions made with the classical FFM theory where the value of the exponent is set at $p = 1$ (or $\alpha = 2$) and the value $\hat{\Omega}_0$ is set at the maximum likelihood of the a priori distribution of the data at $t_0 = 0$. The latter results are displayed as black crosses in Figures 3c, 4c, 5c, and 6c. For the examples of 29 April, 10 May,

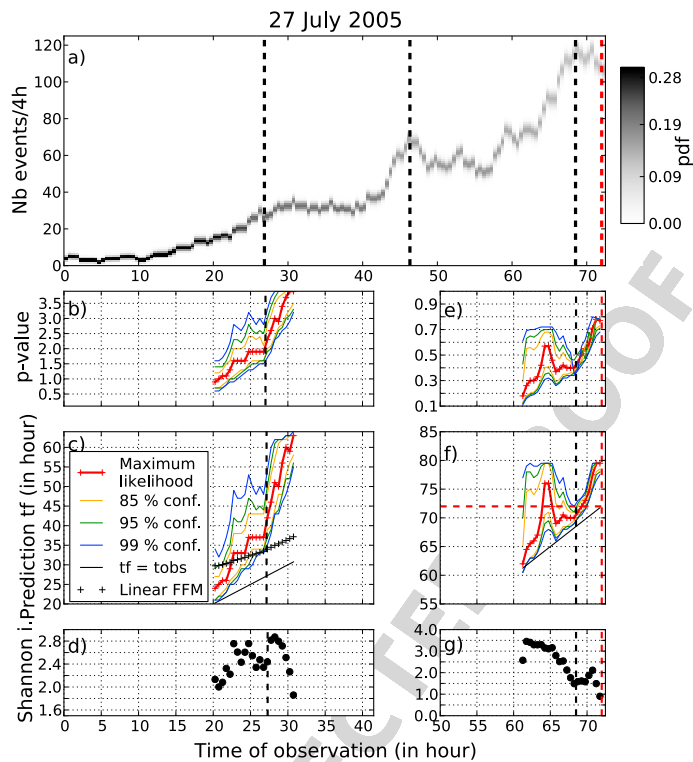


Figure 6. (a) A priori probability density functions on the data for the 27 July 2005 explosion, as a function of the observation time t_{obs} . The true time of eruption is $t_e = 72$ h (red dashed line). The black dashed line indicates the times of deceleration. (b–d) Same as Figures 3b–3d. (e–g) Same as Figures 6b–6d for a beginning of the fitting window at $t_0 = 50$ h.

and 27 July, the predictions made with the classical method always give less accurate forecasts than the method proposed in this paper. Moreover, these predictions never stabilize with the classical method, and no reliable uncertainty can be evaluated on the time of prediction t_f as the uncertainty on the data is not taken into account. It would thus be impossible to obtain reliable and accurate real-time predictions with this method. The predictions made with the classical method on the 5 June are very stable around the time of prediction $t_f = 32$ h during the whole period of analysis. This is probably due to the fact that the value of $p = 1$ is a good estimation of the true p value corresponding to the Ω_0 set. However, the time lag of 4 h between the forecast and the true time of the eruption is explained by an estimated p value slightly smaller than one.

Our results can also be compared with those of *Arámbula-Mendoza et al.* [2011]. They applied the classical FFM, and they used the root-mean-square of the energy of the continuous seismic signal filtered in the range [1, 3] Hz (SSEM) with the whole sequence of acceleration as fitting window. In their study, no prediction could be obtained for the 5 June eruption, while good results are obtained in the present work. For the 10 May event, their prediction is 5 h later than the time of eruption, while our approach provides an excellent forecast (i.e., at $t_f = t_e$) 4 h before the explosion, within a 95% confidence interval comprised between $t_f = 36.5$ h and $t_f = 39$ h. Their prediction for the 27 July is 14 h later than the explosion, whereas our maximum likelihood of t_f is 3 h earlier than the explosion. The prediction made by these authors for the 29 April event is 11 h later than the explosions, while our forecasts oscillate between 2 h before and 3 h after the explosion.

In summary, the proposed method allows for (1) more accurate results than the specific studies cited; i.e., the difference between the forecast t_f and the actual eruption t_e is smaller than the precision at 95% confidence if we are near the eruption time and if the data turn out to fit equation (4); (2) characterizing the true precision of t_f better than those reported in other studies; and (3) making reliable predictions several hours before the time of explosion.

6. Discussion

In this study, we have presented several improvements of the so-called material Failure Forecast Method. First, the seismic events are classified in order to process separately the seismicity of distinct origins and to discard all the signals that do not contain information on the ongoing eruptive processes and are not useful as precursor. It is important to notice that this classification is carried out automatically so the precursory observables can be available in real time, even when hundreds of events are recorded daily. The automatic recognition tool based on Hidden Markov Models is quite efficient for this purpose. However, some discrepancies appear between the results of this system and the manually classified databases, which reflects the inherent difficulty in identifying the type of each event. We take advantage of the statistics on the recognition success rates to calculate probability density functions of the number of counted events which are used in the subsequent procedure.

The second improvement proposed is to use a Bayesian approach to solve the inverse problem that consists of forecasting the eruption time. We use a simple empirical power law which is characterized by three parameters, including the *failure time*, which is supposed to coincide with the eruption onset. The Bayesian approach used to adjust the power law to the observations and to estimate the parameters does not require any hypothesis on the data information. It allows us to evaluate the trade-off between the parameters and to give reliable estimations of their uncertainties. The determination of confidence levels on the estimated eruption times is of special importance for crisis management and decision makers. To simulate real situations, the procedure of data fitting is carried out on observation windows that end at the current time and is repeated at regular intervals assimilating the recently obtained data. This enables us to study the temporal stability of the estimated eruption time. This stability is an important criterion for the estimation of the reliability of the forecast in a real-time situation.

We showed that the assumption of setting the exponent $p=1$ (or $\alpha=2$) is not always relevant in the studied cases, as the values estimated of p can significantly vary from one sequence to another. Up to now, there are few published studies on eruption forecasts in a real-time perspective using FFM with nonfixed exponent (p or α) and addressing the question of uncertainties. *Smith and Kilburn* [2010] and *Smith et al.* [2007] carried out data fitting in a least squares sense, which implies an implicit assumption of a Gaussian distribution of the data. However, they did not quantify the data uncertainties, and consequently, their error in the forecast times are probably not reliable in their examples. Moreover, the forecast times do not stabilize as a function of observation time. *Bell et al.* [2013] assumed that the precursory seismic sequence is distributed according to a nonstationary Poisson process [*Ogata*, 1983], the intensity of which follows a power law of the same form as formula (4). Then, they determined a maximum likelihood estimation of the parameters. They compared their method with a classical least squares approach on several synthetic data sets. They obtained more accurate results than with least squares fitting if the exponent is set to its true value. However, they got large errors when the exponent must be estimated. On real data, and by taking the exponent as unknown parameter, the stability of the forecast time is obtained in the last part of the sequence for only a few study cases.

Figure 7 shows the a priori pdf of the data for the Volcán de Colima explosion of 5 June 2005 at three different observation times. Gaussian and Poisson distributions are adjusted to these pdfs. In this case, it appears that the error structure of the data is much better described by a Gaussian distribution than by a Poisson one. This suggests that a weighted least squares procedure could also be used to perform the inversion. Note that the examples of Volcán de Colima are relatively simple because one type of event predominates the seismic activity (namely, the LP events). In more complex cases characterized by a larger diversity of classes of event, we expect that the pdf of the data, calculated as explained in section 4, would have different patterns and would not be correctly described by a Gaussian distribution. The Bayesian approach can anyway be applied as it does not require any hypothesis on the data information. On the other hand, in cases where the error distribution cannot be correctly determined because of unavailable

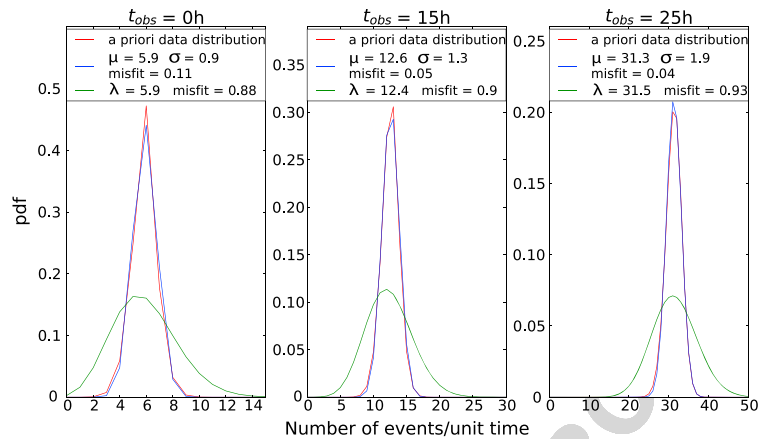


Figure 7. A priori error distribution on the data (red curve) for three different times of observation t_{obs} , for the example of 5 June. Best fits for a Gaussian distribution of mean μ and standard deviation σ (blue curve) and for a Poisson distribution of mean λ (green curve). μ , σ , λ , and misfits are expressed in number of events per unit time. Distributions are adjusted with a L1-norm.

uncertainties on the observable, a Gaussian law could be assumed but a standard deviation on the data should be estimated.

To illustrate the influence of the types of data information on the evaluation of the parameters t_f and p of FFM, we present their a posteriori marginal probabilities in Figure 8. These figures display, for the example of the 5 June event, the marginal pdf of p and t_f which is obtained by integrating $\rho_{post}(k, p, t_f)$ (equation (10)) over k . Results are shown for five different t_{obs} and for the following methods: (1) the Bayesian method of this paper (Figure 8, first row); (2) the Bayesian method with a Gaussian assumption on the data information, with two different standard deviations: $\sigma = 1$ event per unit time (Figure 8, second row) and $\sigma = 3$ events per unit time (Figure 8, third row); and (3) the maximum likelihood estimate of the parameters with the method used in Bell et al. [2013] (nonstationary Poisson process, red dot in each panel).

We first notice that the uncertainty is not reliable in the case of the Gaussian assumption when the value of σ is underestimated ($\sigma = 1$ event per unit time), as the 99% confidence contour almost never contains the time of explosion. A large σ leads to large uncertainties on the parameters because the uncertainty on the data might be overestimated. However, for $t_{obs} = 26$ h, the value of $\sigma = 3$ events per unit time seems to be well adapted since the corresponding uncertainties obtained are comparable to that of our method. The results obtained with the least squares method using $\sigma = 2$ events per unit time are fairly similar to the ones obtained with $\sigma = 3$ events per unit time. The method used in this paper yields to reasonable and rigorous uncertainties on the parameters, with the time of eruption always inside the confidence contours. Furthermore, the maximum likelihoods calculated from the maximum of the posterior distribution are stable around the time of eruption as a function of observation time which is not always the case for the other methods tested. The maximum likelihood estimates of the predictions made with the other methods are similar for observation times greater than $t_{obs} = 24$ h and gives the same values as in this study for $t_{obs} = 25$ h and $t_{obs} = 26$ h. The hypothesis made on the structure of the data is not critical only when enough data are available. The way of defining the a priori data pdf is thus very important to obtain stable results with reliable uncertainties. Consequently, the method proposed in this paper provides the most reliable calculations of uncertainties and the most stable estimation of the eruption time as a function of observation time, at least for the specific examples studied here.

Even if the method is promising, a theoretical problem must be underlined. The data increments used for the numerical approximation of $\dot{\Omega}$ may overlap leading to apparent correlations in the data which we do not consider. Quantifying this approximation is extremely difficult since $\dot{\Omega}(t)$ should be an instantaneous derivative, which is approached, in fact, by a ratio of finite difference. Thus, it is an intrinsic problem of the

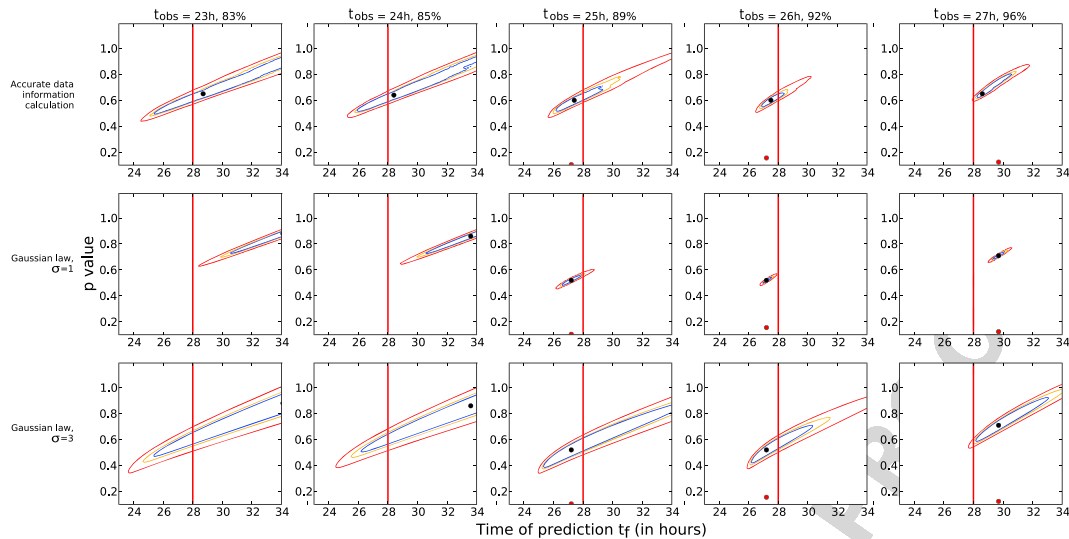


Figure 8. Marginal probability density functions of p and t_f for the 5 June event. (first to third rows) A different hypothesis on the data error structure. (first to fourth columns) The marginal pdfs obtained for a particular time of observation t_{obs} ; the corresponding fraction of accelerating sequence is indicated in percent. Red line represents the time of explosion, the black dot corresponds to the maximum likelihood of each pdf, and the red dot to the maximum likelihood point obtained with the nonstationary Poisson process hypothesis. Blue, orange, and red curves correspond, respectively, to 80%, 90%, and 99% levels of confidence.

theory itself rather than of the data. To avoid this theoretical problem, we should consider cumulative data for which the problem would be then to evaluate the correlation. A way to overcome this alternative could be to consider that the occurrence of earthquakes for each time interval is a Poisson process with a power law intensity to be determined, as assumed in [Ogata, 1983].

In the case of precursory VT activity, the acceleration behavior has been interpreted as due to damaging processes of the solid rock associated with intrusion and possible conduit widening [Voight, 1988; Kilburn, 2003; Budi-Santoso et al., 2013]. On the other hand, similar behavior of LP activity is relatively common as it has been observed prior to vulcanian explosion on other volcanoes such as Galeras (Colombia) [Gil Cruz and Chouet, 1996], Tungurahua (Ecuador) [Molina et al., 2004], Sakurajima (Japan) [Maryanto et al., 2008], or Ubinas (Peru) [Traversa et al., 2011]. In particular, the power law gives also a good representation of the LP activity preceding several eruptions of Volcán de Colima which is the basis of reliable eruption forecasting. From those observations, several questions arise: what is the source mechanism of these LP events and what are the physical processes involved in the acceleration of this type of seismicity? Several source models of LP event, including oscillations of fluid-filled cavities, brittle fractures of magma, or slow ruptures have been proposed [Neuberg et al., 2006; Chouet and Matoza, 2013; Bean et al., 2013]. The most adapted model in a given case probably depends on the type and state of the volcano.

Geological observations [Tuffen et al., 2003; Tuffen and Dingwell, 2005], laboratory experiments [Tuffen et al., 2008; Lavallée et al., 2012], and models of magma conduit [Neuberg et al., 2006; Goto, 1999] suggest that in the case of intrusion of viscous magma, LPs can be generated by brittle fracture of the magma due to large strain rates close to the conduit wall when the magma is ascending. Moreover, Lavallée et al. [2008, 2011], in laboratory experiments on magma coming from Volcán de Colima, showed that complete failure of magma samples can be forecasted using FFM on acoustic emissions. The shear bands that develop close to the conduit wall due to strain localization can produce reduction of the friction between the ascending magma and the solid rock [Hale and Muhlhaus, 2007]. This friction decrease might be involved in a mechanism of acceleration of the magma flow and of the associated seismicity. On the other hand, following the model of Holland et al. [2011], the brittle fractures in the magma might generate network of cracks that are progressively interconnected. An explosion would be triggered when these networks of fractures filled by

01
02
03
04
05
06
07
08
09
10
11
12
13
14
15
16
17
18
19
20
21
22
23
24
25
26
27
28
29
30
31
32
33
34
35
36
37
38
39
40
41
42
43
44
45
46
47
48
49
50
51
52
53
54
55

gas reach the surface producing rapid decompression. Although various processes described above are probably involved in the preruptive phenomena, the exact scenario, describing the interactions between these processes and producing acceleration sequences of LP activity just before eruptions, has still to be modeled. A better understanding of these complex mechanisms would help interpreting the observations and justifying the use of FFM on LP activity for the eruption forecasting. Finally, it could help understand the multiple acceleration patterns of LP, as well as the meaning of the deceleration observed before the explosion and in particular the reason why FFM can give good predictions in this case.

The method proposed in this work is designed for integration in monitoring systems and for producing real-time forecasts of eruptions. However, in operational situations, the role of volcanologists would still be determining in the following tasks: (1) detecting the increases and decreases of activity, setting the initial time t_0 , and eventually, in the case of complex sequences, modifying t_0 ; (2) evaluating the criteria of stability and uncertainty of the forecast times (the Shannon index can be useful for this purpose); and (3) informing the development of policy in setting of alert levels, taking into account the results of the forecasting method together with all the available information.

This paper explores a way of adapting the FFM for real-time forecasting. We propose some tracks for operational use, i.e., how to choose the window width and the starting point t_0 in real time. The statistical evaluation of the success of the method will have to be carried out before testing the method in truly prospective situations. Such a study would require a large amount of data to compute the success rate in a statistically relevant manner and therefore an automatized procedure, although it is very important to keep an eye on the data.

7. Conclusion

In this paper we have presented a new method of volcanic eruption forecasting based on the FFM theory adapted for use in real time. The Bayesian approach used here provides an objective, robust, and flexible way of solving the inverse problem and to estimate the model parameters and their uncertainties from the a priori pdf calculated for the data. The form of the FFM theory we chose (equation (4)) allows a direct estimation of the time of eruption t_r through its a posteriori pdf. These estimations are repeated along the observation time. Thus, the reliability of the forecast can be evaluated along with two criteria: the stability of t_r as a function of time and the uncertainty of its estimation.

We applied our method to two sequences of precursory LP activity at Volcán de Colima characterized by a single phase of acceleration. In these cases, we obtained accurate and reliable forecasts of the eruption time using approximately 80% of the complete sequence of activity, i.e., at times of observation several hours before the eruption onset. This delay is convenient for operational objectives of evacuation on this volcano. We included deliberately in this study more complex patterns of preruptive seismicity, in order to investigate the limits of the method. In the case of sequences including multiple phases of acceleration and deceleration, a simple power law cannot fit correctly the whole series of observations. Thus, the forecast based on these complex sequences are still not reliable. However, when using only the first phase of the acceleration, relatively accurate forecasts are obtained several tens of hours before the explosions.

The success and utility of the methods of eruption forecasting based on precursory seismic activity rely on the following obvious conditions. First, seismic events must occur, and this activity must present acceleration behavior. The reasons why some eruptions are not preceded by earthquakes are not well understood and requires more research. Second, the duration of the seismic unrest and the level of activity must be sufficient for the method to be carried out, and, when an eruption is forecasted, the delay for civil protection to act must be long enough.

Finally, the models proposed to explain the mechanisms of accelerating precursory sequences require further investigations. A better understanding of precursory processes of explosions would be of great help for deterministic eruption forecasts, and also to quantify the size of the future eruptive event. The features and utility of our method of real-time forecasting based on FFM theory have been demonstrated using only four examples from Volcán de Colima. In order to better determine the relevance of our approach, many other preruptive seismic sequences should be analyzed, including predominating VT or LP activity, in various volcanic contexts, and even for the forecasting of landslides for which the method should be well adapted.

Acknowledgments

We are grateful to Raul Arámbula-Mendoza, Carlos Ariel-Ramirez, Alejandro Velasquez-Martinez, and Miguel González-Amueza from RESCO (Red Sísmica del Estado de Colima) for their support in keeping the seismic network working. We thank AXA Research Funds for the PhD fellowship funding. This work has also been partially supported by ECOS-nord program, by the Spanish project Ephestos, CGL2011-470 29499-C02-01, by the EU project EC-FP7 Mediterranean SUPersite Volcanoes (MED471 SUV), and by the APASVO project (TC2012-31551). The continuous seismic data have been provided by RESCO (gard@uocol.mx). We also thank the reviewers for their constructive comments and particularly Ian Main for his detailed corrections.

References

- Arámbula-Mendoza, R., P. Lesage, C. Valdés-González, N. Varley, G. Reyes-Dávila, and C. Navarro (2011), Seismic activity that accompanied the effusive and explosive eruptions during the 2004–2005 period at Volcán de Colima, Mexico, *J. Volcanol. Geotherm. Res.*, *205*, 30–46.
- Bean, C., L. D. Barros, I. Lockmer, J. Métaxian, G. O'Brien, and S. Murphy (2013), Long-period seismicity in the shallow volcanic edifice formed from slow-rupture earthquakes, *Nat. Geosci.*, *7*, 71–75.
- Bell, A. F., J. Greenhough, M. Heap, and I. G. Main (2011), Challenges for forecasting based on accelerating rates of earthquakes at volcanoes and laboratory analogues, *Geophys. J. Int.*, *185*, 718–723.
- Bell, A. F., M. Naylor, and I. G. Main (2013), The limits of predictability of volcanic eruptions from accelerating rates of earthquakes, *Geophys. J. Int.*, *194*(3), 1541–1553.
- Budi-Santoso, A., P. Lesage, S. Dwiyono, P. Jousset, and J.-P. Métaxian (2013), Analysis of the seismic activity associated with the 2010 eruption of Merapi Volcano, Java, *J. Volcanol. Geotherm. Res.*, *261*, 153–170.
- Carniel, R., R. Ortiz, and M. D. Cecca (2006), Spectral and dynamical hints on the time scale of preparation of the 5 April 2003 explosion at Stromboli volcano, *Rev. Can. Sci. Terre*, *43*, 41–55.
- Chastin, S. F. M., and I. G. Main (2003), Statistical analysis of daily seismic event rate as a precursor to volcanic eruptions, *Geophys. Res. Lett.*, *30*(13), 1671, doi:10.1029/2003GL016900.
- Chouet, B. A., and R. S. Matoza (2013), A multi-decadal view of seismic methods for detecting precursors of magma movement and eruption, *J. Volcanol. Geotherm. Res.*, *252*, 108–115.
- Connor, C. B., R. S. J. Sparks, R. M. Mason, C. Bonadonna, and S. R. Young (2003), Exploring links between physical and probabilistic models of volcanic eruptions: The Soufriere Hills Volcano, Montserrat, *Geophys. Res. Lett.*, *30*(13), 1701, doi:10.1029/2003GL017384.
- Cornelius, R., and B. Voight (1994), Seismological aspects of the 1989–1990 eruption at Redoubt Volcano, Alaska: The Materials Failure Forecast Method (FFM) with RSAM and SSAM seismic data, *J. Volcanol. Geotherm. Res.*, *62*, 469–498.
- Cornelius, R., and B. Voight (1995), Graphical and PC-software analysis of volcano eruption precursors according to the Materials Failure Forecast Method (FFM), *J. Volcanol. Geotherm. Res.*, *64*, 295–320.
- Cornelius, R. R., and P. A. Scott (1993), A materials failure relation of accelerating creep as empirical description of damage accumulation, *Rock Mech. Rock Eng.*, *26*, 233–252.
- Cortés, G., L. García, I. Álvarez, C. Benítez, Á. de la Torre, and J. Ibáñez (2014), Parallel system architecture (PSA): An efficient approach for automatic recognition of volcano-seismic events, *J. Volcanol. Geotherm. Res.*, *271*, 1–10.
- De La Cruz-Reyna, S., and G. Reyes-Dávila (2001), A model to describe precursory material failure phenomena: Application to short-term forecasting at Colima Volcano, Mexico, *Bull. Volcanol.*, *63*, 297–308.
- Endo, E., and T. Murray (1991), Real-time Seismic Amplitude Measurement (RSAM): A volcano monitoring and prediction tool, *Bull. Volcanol.*, *53*, 533–545.
- Fukuzuno, T. (1985), A method to predict the time of slope failure caused by rainfall using the inverse number of velocity of surface displacement, *J. Jpn. Landslide Soc.*, *22*(2), 8–14.
- Gil Cruz, F., and B. A. Chouet (1996), Long period events, the most characteristic seismicity accompanying the emplacement and extrusion of a lava dome in Galeras Volcano, Columbia, in 1991, *J. Volcanol. Geotherm. Res.*, *77*, 121–158.
- Gonzalez, M. B., J. Ramirez, and C. Navarron (2002), Summary of the historical eruptive activity of Volcán de Colima, Mexico 1519–2000, *J. Volcanol. Geotherm. Res.*, *117*, 21–46.
- Goto, A. (1999), A new model for volcanic earthquake at Unzen Volcano: Melt rupture model, *Geophys. Res. Lett.*, *26*, 2541–2544.
- Greenhough, J., and I. G. Main (2008), A Poisson model for earthquake frequency uncertainties in seismic hazard analysis, *Geophys. Res. Lett.*, *35*, L19313, doi:10.1029/2008GL035353.
- Greenhough, J., A. Bell, and I. G. Main (2009), Comment on “Relationship between accelerating seismicity and quiescence, two precursors to large earthquakes” by Arnaud Mignan and Rita Di Giovambattista, *Geophys. Res. Lett.*, *36*, L17303, doi:10.1029/2009GL039846.
- Hale, A. J., and H.-B. Muhlhaus (2007), Modelling shear bands in a volcanic conduit: Implication for over-pressures and extrusion rates, *Earth Planet. Sci. Lett.*, *263*, 74–87.
- Hardebeck, J., K. Felzer, and A. Michael (2008), Improved tests reveal that the accelerating moment release hypothesis is statistical insignificant, *J. Geophys. Res.*, *113*, B08310, doi:10.1029/2007JB005410.
- Helmstetter, A., D. Sornette, J.-R. Grasso, J. Andersen, S. Gluzman, and V. Pisarenko (2004), Slider block friction model for landslides: Application to Vaiont and la Clapière landslides, *J. Geophys. Res.*, *109*, B02409, doi:10.1029/2002JB002160.
- Holland, A. P., I. M. Watson, J. C. Phillips, L. Caricchi, and M. P. Dalton (2011), Degassing process during lava dome growth: Insight from Santiaguito lava dome, Guatemala, *J. Volcanol. Geotherm. Res.*, *202*, 153–166.
- Kilburn, C. (2003), Multiscale fracturing as a key to eruption forecasting, *J. Volcanol. Geotherm. Res.*, *125*, 271–289.
- Kilburn, C. (2012), Precursory deformation and fracture before brittle rock failure and potential application to volcanic unrest, *J. Geophys. Res.*, *117*, B02211, doi:10.1029/2011JB008703.
- Kilburn, C., and B. Voight (1998), Slow rock fracture as eruption precursor at Soufriere Hills volcano, Montserrat, *Geophys. Res. Lett.*, *25*, 3665–3668.
- Lavallée, Y., P. Meredith, D. Dingwell, K. Hess, J. Wassermann, B. Cordonnier, A. Gerik, and J. Kruhl (2008), Seismogenic lavas and explosive eruption forecasting, *Nature*, *453*, 507–510.
- Lavallée, Y., N. Varley, A. Alatorre-Ibargiengoitia, K. Hess, U. Kueppers, S. Mueller, D. Richards, B. Scheu, O. Spieler, and D. Dingwell (2011), Magma architecture of dome building eruptions at Volcán de Colima, Mexico, *Bull. Volcanol.*, *74*(1), 249–260.
- Lavallée, Y., B. Benson, M. Heap, A. Flaw, K. Hess, and D. Dingwell (2012), Volcanic conduit failure as a trigger to magma fragmentation, *Bull. Volcanol.*, *74*, 11–13.
- Main, I. G. (1999), Applicability of time-to-failure analysis to accelerated strain before earthquakes and volcanic eruptions, *Geophys. J. Int.*, *139*, F1–F6.
- Marsan, D., and S. S. Nalbant (2005), Methods for measuring seismicity rate changes: A review and a study of how the Mw7.3 Landers earthquake affected the aftershock sequence of the Mw6.1 Joshua Tree earthquake, *Pure Appl. Geophys.*, *162*, 1151–1185.
- Maryanto, S., M. Iguchi, and T. Tameguri (2008), Constraints on the source mechanism of harmonic tremors based on seismological, ground deformation, and visual observations at Sakurajima Volcano, Japan, *J. Volcanol. Geotherm. Res.*, *170*, 193–217.
- Marzocchi, W., and M. Bebbington (2012), Probabilistic eruption forecasting at short and long time scales, *Bull. Volcanol.*, *74*, 1777–1805.
- McNutt, S. (1996), Seismic monitoring and eruption forecasting of volcanoes: A review of the state-of-the-art and case of studies, in *Monitoring and Mitigation of Volcano Hazard*, edited by R. Scarpa, and R. Tilling, chap. 3, pp. 99–146, Springer, Berlin, Heidelberg.
- Molina, I., H. Kumagai, and H. Yepes (2004), Resonances of a volcanic conduit trigger by repetitive injections of an ash-laden gas, *Geophys. Res. Lett.*, *31*, L03603, doi:10.1029/2003GL018934.



- Murray, J., and J. Ramirez Ruiz (2002), Long-term predictions of the time of eruptions using remote distance measurement at Volcán de Colima, Mexico, *J. Volcanol. Geotherm. Res.*, *117*, 79–89. 01
- Neuberg, J., H. Tuffen, L. Collier, D. Green, T. Powell, and D. Dingwell (2006), The trigger mechanism of low-frequency earthquakes on Montserrat, *J. Volcanol. Geotherm. Res.*, *153*, 37–50. 02
- Ogata, Y. (1983), Estimation of the parameters in the modified Omori formula for aftershock frequencies by the maximum likelihood procedure, *J. Phys. Earth*, *31*, 115–124. 03
- Ortiz, R., H. Moreno, A. Garcia, G. Garcia, M. Astiz, P. Pena, N. Sanchez, and M. Tarraga (2003), Villarica volcano (Chile): Characteristic of the volcanic tremor and forecasting of small explosions by means of a material Failure Forecast Method, *J. Volcanol. Geotherm. Res.*, *128*, 247–259. 04
- Schmid, A., J. R. Grasso, D. Clarke, V. Ferrazzini, P. Bachelery, and T. Staudacher (2012), Eruption forerunners from multiparameter monitoring and application for eruptions time predictability (Piton de la Fournaise), *J. Geophys. Res.*, *117*, B11203, doi:10.1029/2012JB009167. 05
- Shannon, C. (1948), A mathematical theory of communication, *Bell Syst. Tech. J.*, *27*, 379–423. 06
- Smith, R., and C. Kilburn (2010), Forecasting eruptions after long repose intervals from accelerating rates of rock fracture: The June 1991 eruption of Mount Pinatubo, Philippines, *J. Volcanol. Geotherm. Res.*, *191*, 129–136. 07
- Smith, R., C. Kilburn, and P. Sammonds (2007), Rock fracture as a precursor to lava dome eruptions at Mount St Helens from June 1980 to October 1986, *Bull. Volcanol.*, *69*, 681–693. 08
- Stephens, C., B. Chouet, R. Page, J. Lahr, and J. Power (1994), Seismological aspects of the 1989–1990 eruptions at Redoubt volcano, Alaska: The SSAM perspective, *J. Volcanol. Geotherm. Res.*, *62*, 153–182. 09
- Tarantola, A. (2005), *Inverse Problem Theory and Methods for Model Parameter Estimation*, SIAM, Philadelphia, Pa. 10
- Tarantola, A., and B. Valette (1982), Inverse problems = Quest for information, *J. Geophys.*, *50*, 159–170. 11
- Tarraga, M., R. Carniel, R. Ortiz, J. Marrero, and A. Garcia (2006), On the predictability of volcano-tectonic events by low frequency seismic noise analysis at Teide-Pico Viejo volcanic complex, Canary Islands, *Nat. Hazards Earth Syst. Sci.*, *6*, 365–376. 12
- Traversa, P., O. Lengliné, O. Macedo, J. P. Métaxian, J. R. Grasso, A. Inza, and E. Taïpe (2011), Short term forecasting of explosions at Ubinas volcano, Perú, *J. Geophys. Res.*, *116*, B11301, doi:10.1029/2010JB008180. 13
- Tuffen, H., and D. Dingwell (2005), Fault textures in volcanic conduit: Evidence for seismic trigger mechanism during silicic eruptions, *Bull. Volcanol.*, *67*, 370–387. 14
- Tuffen, H., D. Dingwell, and H. Pinkerton (2003), Repeated fracture and healing of silicic magma generate flow banding and earthquakes, *Geol. Soc. Am.*, *31*, 1089–1092. 15
- Tuffen, H., R. Smith, and P. Sammonds (2008), Evidence for seismogenic fracture of silicic magma, *Nature*, *453*, 511–514. 16
- Varley, N., R. Arambula-Mendoza, G. Reyes, R. Sanderson, and J. Stevenson (2010a), Generation of Vulcanian activity and long-period seismicity at Volcán de Colima, Mexico, *J. Volcanol. Geotherm. Res.*, *198*, 45–56. 17
- Varley, N. R., R. Arambula-Mendoza, G. Reyes-Davila, J. Stevenson, and R. Harwood (2010b), Long-period seismicity during magma movement at Volcán de Colima, *Bull. Volcanol.*, *72*, 1093–1107. 18
- Voight, B. (1988), A method for prediction of volcanic eruptions, *Nature*, *332*, 125–130. 19
- Voight, B. (1989), A relation to describe rate-dependant material failure, *Science*, *243*, 200–203. 20
- Voight, B., and R. R. Cornelius (1991), Prospects for eruption prediction in near real-time, *Nature*, *350*, 695–698. 21
- Young, S. J., G. Evermann, M. J. F. Gales, T. Hain, D. Kershaw, G. Moore, J. Odell, D. Ollason, D. Povey, V. Valtchev, and P. C. Woodland (2006), *The HTK Book (for HTK Version 3.4)*. Cambridge University Engineering Department. 22

Bibliography

- Alidibirov, M. and Dingwell, D. (1996). Magma fragmentation by rapid decompression. Nature, 380:146–148.
- Alvarez, I., Cortes, G., de la Torre, A., Benitez, C., Garcia, L., Lesage, P., Arambula, R., and Gonzalez, M. (2009). Improving feature extraction in the automatic classification of seismic events. Application to Colima and Arenal volcano. Geoscience and Remote Sensing Symposium, 2009 IEEE International, IGARSS, 4.
- Alvarez, I., Garcia, L., Cortes, G., Benitez, C., and De la Torre, A. (2012). Discriminative feature selection for automatic classification of volcano-seismic signals. Geoscience and Remote Sensing Letters, IEEE, 9:151–155.
- Amitrano, D. and Helmstetter, A. (2006). Brittle creep, damage, and time to failure in rocks. Journal of Geophysical Research, 111.
- Anderson, O. L. and Grew, P. C. (1977). Stress corrosion theory of crack propagation with applications to geophysics. Review of Geophysics, 15:77–104.
- Arámbula, R. (2011). Clasificación automática de eventos sísmicos volcánicos y análisis de la actividad sísmica reciente en el Volcán de Colima. PhD thesis, Universidad nacional autonoma de Mexico.
- Arámbula-Mendoza, R., Lesage, P., Valdés-González, C., Varley, N., Reyes-Dávila, G., and Navarro, C. (2011). Seismic activity that accompanied the effusive and explosive eruptions during the 2004-2005 period at Volcán de Colima, Mexico. Journal of Volcanology and Geothermal Research, 205:30–46.
- Atkinson, B. K. (1984). Subcritical crack growth in geological materials. Journal of Geophysical Research, 89:4077–4114.
- Atkinson, B. K. and Meredith, P. G. (1987). The theory of subcritical crack growth with applications to minerals and rocks. in Fracture Mechanics of Rock, edited by B. K. Atkinson, Academic Press, London:111–166.
- Bahl, L., Jelinek, F., and Mercer, R. (1983). A maximum likelihood approach to continuous speech recognition. IEEE Transactions on Pattern Analysis and Machine Intelligence, PAMI-5:179–190.
- Baud, P. and Meredith, P. G. (1997). Damage accumulation during triaxial creep of darley dale sandstone from pore volumetry and acoustic emission. International Journal of Rock Mechanics and Mining Sciences, 34:2–3.

BIBLIOGRAPHY

- Baum, L., Petrie, T., Soules, G., and Weiss, N. (1970). A maximization technique occurring in the statistical analysis of probabilistic functions of Markov chains. Annals of Mathematical Statistics, 41:164–171.
- Bean, C., Barros, L. D., Lockmer, I., Métaixian, J., O'Brien, G., and Murphy, S. (2013). Long-period seismicity in the shallow volcanic edifice formed from slow-rupture earthquakes. Nature Geoscience, 7:71–75.
- Bean, C., Lokmer, I., and O'Brien, G. (2008). Influence of near-surface volcanic structure on long-period seismic signals and on moment tensor inversions: Simulated examples from mount etna. Journal of Geophysical Research, 113:B08308, doi:10.1029/2007JB005468.
- Beauducel, F., Cornet, F., Suhanto, E., Duquesnoy, T., and Kasser, M. (2000). Constraints on magma flux from displacements data at Merapi volcano,Java. Journal of Geophysical Research, 105 :B4:8193–8204.
- Beauducel, F., Nandaka, M. A., Cornet, F., and Diament, M. (2006). Mechanical discontinuities monitoring at Merapi volcano using kinematic GPS. Journal of Volcanology and Geothermal Research, 150:300–312.
- Bell, A. F., Greenhough, J., Heap, M., and Main, I. G. (2011). Challenges for forecasting based on accelerating rates of earthquakes at volcanoes and laboratory analogues. Geophysical Journal International, 185:718–723.
- Bell, A. F., Naylor, M., and Main, I. G. (2013). The limits of predictability of volcanic eruptions from accelerating rates of earthquakes. Geophysical Journal International, 201:1541–1553.
- Belousov, A., Voight, B., Belousova, M., and Petukhin, A. (2002). Pyroclastic surges and flows from the 8-10 may 1997 explosive eruption of Bezymianny volcano, Kamchatka, Russia. Bulletin of Volcanology, 64:455–471.
- Benítez, C., Ramírez, J., Segura, J., Ibáñez, J., Almendros, J., García-Yeguas, A., and Cortés, G. (2007). Continuous HMM-based seismic event classification at Deception Island, Antarctica. IEEE Transactions on Geoscience Remote Sensing, 45:138–147.
- Benson, M., Vinciguerra, S., Meredith, P., and Paul Young, R. (2010). Spatio-temporal evolution of volcano seismicity : a laboratory study. Earth and Planetary Science Letters, 297:315–323.
- Benson, P., Vinciguerra, S., Meredith, P., and Paul Young, R. (2008). Laboratory simulation of volcano seismicity. Science, 322:249–252.
- Berlo, K., Blundy, J., Turner, S., Cashman, K., Hawkesworth, C., and Black, S. (2004). Geochemical precursors to volcanic activity at Mount St. Helens, USA. Science, 306:1167–1169.
- Brenguier, F., Shapiro, N. M., Campillo, M., Ferrazzini, V., Duputel, Z., Coutant, O., and Necessian, A. (2008). Towards forecasting volcanic eruptions using seismic noise. Nature Geoscience, 1:2:126–130.
- Budi-Santoso, A., Lesage, P., Dwiyono, S., Jousset, P., and Metaxian, J.-P. (2013). Analysis of the seismic activity associated with the 2010 eruption of Merapi Volcano, Java. Journal of Volcanology and Geothermal Research, 261:153–170.

- Carbone, D. and Greco, F. (2007). Review of microgravity observations at mt. etna: A powerful tool to monitor and study active volcanoes. Pure Applied Geophysics, 164:769–790.
- Carniel, R., Ortiz, R., and Cecca, M. D. (2006). Spectral and dynamical hints on the time scale of preparation of the 5 april 2003 explosion at Stromboli volcano. Revue canadienne des sciences de la Terre, 43:41–55.
- Carrier, A., Got, J.-L., Peltier, A., Ferrazzini, V., Staudacher, T., Kowalski, P., and Boissier, P. (2015). A damage model for volcanic edifices: Implications for edifice strength, magma pressure, and eruptive processes. Journal of Geophysical Research, 120:567–583.
- Cashman, K., Sturtevant, B., Papale, P., and Navon, O. (2000). Encyclopedia of Volcanoes, Magmatic fragmentation. Academic Press, San Diego.
- Cashman, K. V. and McConnell, S. M. (2005). Multiple levels of magma storage during the 1980 summer eruptions of Mount St. Helens, WA. Bulletin of Volcanology, 68:57–75.
- Cervelli, P., Fournier, T., Freymueller, J., and Power, J. A. (2006). Ground deformation associated with the precursory unrest and early phases of the January 2006 eruption of Augustine volcano, Alaska. Geophysical Research Letters, 33:L18304.
- Charles, R. J. (1958). Static fatigue of glass. Journal of Applied Physics, 29:1549–1560.
- Chastin, S. F. M. and Main, I. G. (2003). Statistical analysis of daily seismic event rate as a precursor to volcanic eruptions. Geophysical Research Letters, 30:1671.
- Chaussard, E., Amelung, F., and Aoki, Y. (2013). Characterization of open and closed volcanic systems in Indonesia and Mexico using InSAR time series. Journal of Geophysical Research, 118:3957–3969.
- Chouet, B. (1985). Excitation of a buried magmatic pipe: A seismic source model for volcanic tremor. Journal of Geophysical Research, 90:1881–1893.
- Chouet, B. (1986). Dynamics of a fluid-driven crack in three dimensions by the finite difference method. Journal of Geophysical Research, 91:13967–13992.
- Chouet, B. (1988). Resonance of fluid-driven crack: radiation properties and implications for the source of long-period events and harmonic tremor. Journal of Geophysical Research, 93:4375–4400.
- Chouet, B. (1992). A Seismic Model for the Source of Long-Period Events and Harmonic Tremor. Springer-Verlag.
- Chouet, B. A. (1996). Long-period volcano seismicity: its source and use in eruption forecasting. Nature, 380:309 – 316.
- Chouet, B. A. and Matoza, R. S. (2013). A multi-decadal view of seismic methods for detecting precursors of magma movement and eruption. Journal of Volcanology and Geothermal Research, 252:108–175.
- Chouet, B. A., Page, R. A., Stephens, C. D., Lahr, J. C., and Power, J. A. (1994). Precursory swarms of long-period events at Redoubt volcano (1989-1990), Alaska: Their origin and use as a forecasting tool. Journal of Volcanology and Geothermal Research, 62:95–135.

BIBLIOGRAPHY

- Collombet, M., Grasso, J.-R., and Ferrazzini, V. (2003). Seismicity rate before eruptions on Piton de la Fournaise volcano: Implications for eruption dynamics. Geophysical Research Letters, 30.
- Connor, C. B., Sparks, R. S. J., Mason, R. M., Bonadonna, C., and Young, S. R. (2003). Exploring links between physical and probabilistic models of volcanic eruptions: The Soufriere Hills Volcano, Montserrat. Geophysical Research Letters, 30.
- Cornelius, R. and Voight, B. (1994). Seismological aspects of the 1989-1990 eruption at Redoubt Volcano, Alaska: the Materials Failure Forecast Method (FFM) with RSAM and SSAM seismic data. Journal of Volcanology and Geothermal Research, 62:469–498.
- Cornelius, R. and Voight, B. (1995). Graphical and PC-software analysis of volcano eruption precursors according to the Materials Failure Forecast Method (FFM). Journal of Volcanology and Geothermal Research, 64:295–320.
- Cornelius, R. R. and Scott, P. A. (1993). A materials failure relation of accelerating creep as empirical description of damage accumulation. Rock Mechanics and Rock Engineering, 26:233–252.
- Cornelius, R. R. and Voight, B. (1996). Real-time seismic amplitude measurement (RSAM) and seismic spectral amplitude measurement (SSAM) analyses with the Materials Failure Forecast Method (FFM), June 1991 explosive eruption at Mount Pinatubo. University of Washington Press, Seattle; PHIVOLCS, Quezon City.
- Cortés, G., Arámbula, R., Álvarez, I., Benítez, C., Ibáñez, J., Lesage, P., González-Amézcuca, M., and Reyes-Dávila, G. (2009). Analysis of Colima, Popocatepetl and Arenal volcanic seismicity using an automatic Continuous Hidden Markov Models-based recognition system. In Bean, C. B. A. and 6th Framework, E. C. P., editors, VOLUME Project: VOLcanoes, Understanding Subsurface Mass MoveMent, pages 150–160. Bean, C.J., Braiden, A.K., Lokmer, I., Martini, F. and O'Brien, G.S, School of Geological Sciences, University College Dublin.
- Cortés, G., García, L., Álvarez, I., Benítez, C., de la Torre, Á., and Ibáñez, J. (2014). Parallel System Architecture (PSA): An efficient approach for automatic recognition of volcano-seismic events. Journal of Volcanology and Geothermal Research, 271:1–10.
- Costin (1987). Fracture Mechanics of Rock, chapter Time-dependent deformation and failure, pages 167–216. Academic Press, London.
- Courtillot, V., Besse, J., Vandamme, D., Jaegger, J., and Montigny, R. (1986). Deccan trap volcanism as a cause of biologic extinctions at the cretaceous-tertiary boundary? Comptes rendus de l'Académie des sciences, 303:863–868.
- Cruden, D. M. (1973). Static fatigue of brittle rock under uniaxial compression. International Journal of Rock Mechanics and Mining Sciences, 11:67–73.
- Cruz, F. G. and Chouet, B. A. (1997). Long-period events, the most characteristic seismicity accompanying the emplacement and extrusion of a lava dome in Galeras volcano, Colombia, in 1991. Journal of Volcanology and Geothermal Research, 77:121–158.
- De La Cruz-Reyna, S. and Reyes-Davila, G. (2001). A model to describe precursory material failure

- phenomena: application to short-term forecasting at Colima volcano, Mexico. Bulletin of Volcanology, 63:297–308.
- Del Pezzo, E., Esposito, A., Giudicepietro, F., Marinaro, M., Martini, M., and Scarpetta, S. (2003). Discrimination of earthquakes and underwater explosions using neural networks. Bulletin of the Seismological Society of America, 93:215–223.
- Denlinger, R. P. and Hoblitt, R. P. (1999). Cyclic eruptive behavior of silicic volcanoes. Geology, 27:459–462.
- Dieterich, J. (1994). A constitutive law for rate of earthquake production and its application to earthquake clustering. Journal of Geophysical Research, 99:2601–2618.
- Dmitrieva, K., Hotovec-Ellis, A., Prejean, S., and Dunham, E. (2013). Frictional-faulting model for harmonic tremor before redoubt volcano eruptions. Nature Geoscience, 6:652–656.
- Doocy, S., Daniels, A., Dooling, S., and Gorokhovich, Y. (2013). The human impact of volcanoes: a historical review of events 1900-2009 and systematic literature review. PLOS Currents Disasters.
- Druitt, T. H., Young, S. R., Baptie, B., Bonadonna, C., Calder, E. S., Clarke, A. B., Cole, P. D., Harford, C. L., Herd, R. A., Luckett, R., Ryan, G., and Voight, B. (2002). Episodes of cyclic vulcanian explosive activity with fountain collapse at Soufrière Hills volcano, Montserrat. Geological Society, London, Memoirs, 21:281–306.
- Duncan, R. A. (1990). The volcanic record of Réunion hotspot. Proc. ODP Sci. Res., 115:3–10.
- Dunham, E. M. and Ogden, D. E. (2012). Guided waves along fluid-filled cracks in elastic solids and instability at high flow rates. Journal of Applied Mechanics, 79(3):031020.
- Duputel, Z., Ferrazzini, V., Brenguier, F., Shapiro, N. M., Campillo, M., and Nercessian, A. (2009). Real time monitoring of relative velocity changes using ambient seismic noise on the Piton de la Fournaise volcano (La Réunion) from January 2006 to June 2007. Journal of Volcanology and Geothermal Research, 184:164–173.
- Dzierma, Y. and Wehrmann, H. (2010). Statistical eruption forecast for the Chilean Southern Volcanic Zone: typical probabilities of volcanic eruptions as baseline for possibly enhanced activity following the large 2010 Concepción earthquake. Natural Hazards and Earth System Sciences, 10:2093–2108.
- Eggers, A. (1983). Temporal gravity and elevation changes at Pacaya volcano, Guatemala. Journal of Volcanology and Geothermal Research, 19:223–227.
- Endo, E. and Murray, T. (1991). Real-time Seismic Amplitude Measurement (RSAM): a volcano monitoring and prediction tool. Bulletin of Volcanology, 53:533–545.
- Esposito, A., Giudicepietro, F., D’Auria, L., Scarpetta, S., Martini, M., Coltelli, M., and Marinaro, M. (2008). Unsupervised neural analysis of very long period events at stromboli volcano using the self-organizing maps. Bulletin of the Seismological Society of America, 98:2449–2459.
- Fayyad, U., Piatetsky-Shapiro, G., and Smyth, P. (1996). From data mining to knowledge discovery in databases. American Association for Artificial Intelligence, 17:37–55.

BIBLIOGRAPHY

- Fukuzuno, T. (1985). A method to predict the time of slope failure caused by rainfall using the increase number of velocity of surface displacement. Journal of Japan Landslide Society, 22-2:8–14.
- Gambino, S., Falzone, G., Ferro, A., and Laudani, G. (2014). Volcanic processes detected by tiltmeters: A review of experience on Sicilian volcanoes. Journal of Volcanology and Geothermal Research, 271:43–54.
- Gasparini, P., Scarpa, R., and (Eds.), K. A., editors (1992). Volcanic Seismology. Springer-Verlag.
- Gil Cruz, F. and Chouet, B. A. (1996). Long period events, the most characteristic seismicity accompanying the emplacement and extrusion of a lava dome in Galeras Volcano, Columbia, in 1991. Journal of Volcanology and Geothermal Research, 77:121–158.
- Gilbert, J. and Sparks, R., editors (1998). The Physics of Explosive Volcanism. Special Publication of the Geological Society of London.
- Gonnermann, H. and Manga, M. (2012). Modeling volcanic prprocess: the physics and mathematics of volcanism. Cambridge College University.
- Gonzalez, M. B., Ramirez, J., and Navarron, C. (2002). Summary of the historical eruptive activity of Volcán Colima, Mexico 1519-2000. Journal of Volcanology and Geothermal Research, 117:21–46.
- Goto, A. (1999). A new model for volcanic earthquake Volcano' Melt rupture model at Unzen. Geophysical Research Letters, 26:2541–254.
- Grasso, J. and Bachèlery, P. (1995). Hierarchical organisation as diagnostic approach to volcano mechanics : Validation on Piton de la Fournaise volcano. Geophysical Research Letters, 22(21):2897–2900.
- Grasso, J. and Zialapin, I. (2004). Predictability of volcano eruption: Lessons from a basaltic effusive volcano. Geophysical Research Letters, 31:L05602.
- Greenhough, J., Bell, A., and Main, I. (2009). Comment on "relationship between accelerating seismicity and quiescence, two precursors to large earthquakes" by Arnaud Mignan and Rita Di Giovambatista. Geophysical Research Letters, 36:10.1029/2009GL039846.
- Greenhough, J. and Main, I. G. (2008). A poisson model for earthquake frequency uncertainties in seismic hazard analysis. Geophysical Research Letters, 35:L19313.
- Gutenberg, B. and Richter, C. F. (1944). Frequency of earthquakes in California. Bulletin of the Seismological Society of America, 34:164–176.
- Hale, A. J. and Muhlhaus, H.-B. (2007). Modelling shear bands in a volcanic conduit: Implication for over-pressures and extrusion rates. Earth and Planetary Science Letters, 263:74–87.
- Hammer, J., Cashman, K., Hoblitt, R., and Newman, S. (1999). Degassing and microlite crystallization during pre-climactic events of the 1991 eruption of Mt. Pinatubo, Philippines. Bulletin of Volcanology, 60:355–380.
- Hardebeck, J., Felzer, K., and Michael, A. (2008). Improved tests reveal that the accelerating moment release hypothesis is ststatistically insignificant. Journal of Geophysical Research, 113:B08310, doi:10.1029/2007JB005410.

- Heap, M. J. and Faulkner, D. R. (2008). Quantifying the evolution of static elastic properties as crystalline rock approaches failure. International Journal of Rock Mechanics and Mining Sciences, 45:564–573.
- Hidayat, D., Voight, B., Langston, C., Ratdomopurbo, A., and Ebeling, C. (2000). Broadband seismic experiment at Merapi volcano, Java, Indonesia: very-long-period pulses embedded in multiphase earthquakes. Journal of Volcanology and Geothermal Research, 100:215–231.
- Hill, D., Pollitz, F., and Newhall, C. (2002). Earthquake-volcano interactions. Physics Today, 55(11):41–47.
- Hirata, T., Satoh, T., and Ito, K. (1987). Fractal structure of spatial distribution of microfracturing in rock. Geophysical Journal International, 90:369–374.
- Holland, A. P., Watson, I. M., Phillips, J. C., Caricchi, L., and Dalton, M. P. (2011). Degassing process during lava dome growth: Insight from Santiaguito lava dome, Guatemala. Journal of Volcanology and Geothermal Research, 202:153–166.
- Ibanez, J., Benítez, C., Gutiérrez, L. A., Cortés, G., García-Yeguasa, A., and Alguacila, G. (2009). The classification of seismo-volcanic signals using Hidden Markov Models as applied to the Stromboli and Etna volcanoes. Journal of Volcanology and Geothermal Research, 187:218–226.
- Iverson, R. M., Dzurisin, D., Gardner, C. A., Gerlach, T. M., LaHusen, R. G., Lisowski, M., Major, J. J., Malone, S. D., Messerich, J. A., Moran, S. C., Pallister, J. S., Qamar, A. I., Schilling, S. P., and Vallance, J. W. (2006). Dynamic of seismogenic extrusion at Mount St Helens in 2004-2005. Nature, 444:439–443.
- Jousset, P., Neuberg, J., and Sturton, S. (2003). Modelling the time-dependent frequency content of low-frequency volcanic earthquakes. Journal of Volcanology and Geothermal Research, 128:201–223.
- Juang, B. and Rabiner, L. (1991). Hidden Markov Models for speech recognition. Technometrics, 33:251–272.
- Julian, B. R. (1994). Volcanic tremor: non-linear excitation of fluid flow. Journal of Geophysical Research, 99:11,859–11,87.
- Kedar, S., Sturtevant, B., and Kanamori, H. (1996). The origin of harmonic tremor at Old Faithful geyser. Nature, 379:708–711.
- Kedar, S., Sturtevant, B., and Kanamori, H. (1998). Bubble collapse as the source of tremor at Old Faithful Geyser. Journal of Geophysical Research, 103:24,283–24,29.
- Kieffer, S. W. (1984). Seismicity at old faithful geyser: an isolated source of geothermal noise and possible analogue of volcanic seismicity. Journal of Volcanology and Geothermal Research, 22:59–95.
- Kilburn, C. (2003). Multiscale fracturing as a key to eruption forecasting. Journal of Volcanology and Geothermal Research, 125:271–289.
- Kilburn, C. (2012). Precursory deformation and fracture before brittle rock failure and potential application to volcanic unrest. Journal of Geophysical Research, 117:1–12.

BIBLIOGRAPHY

- Kilburn, C. and Voight, B. (1998). Slow rock fracture as eruption precursor at Soufriere Hills volcano, Montserrat. Geophysical Research Letters, 25:3665–3668.
- Kumagai, H., Chouet, B. A., and Dawson, P. (1995). Source process of a long-period event at Kilauea volcano, Hawaii. Geophysical Journal International, 161:243–254.
- Lahr, J., Chouet, B., Stephens, C., Power, J., and Page, R. (1994). Earthquake classification, location, and error analysis in a volcanic environment: implications for the magmatic system of the 1989-1990 eruptions at Redoubt volcano, Alaska. Journal of Volcanology and Geothermal Research, 62:137–151.
- Langer, H. and Falsaperla, S. (2003). Seismic monitoring at Stromboli Volcano (Italy): a case study for data reduction and parameter extraction. Journal of Volcanology and Geothermal Research, 128:233–245.
- Lavallée, Y., Benson, B., Heap, M., Flaw, A., Hess, K., and Dingwell, D. (2012). Volcanic conduit failure as a trigger to magma fragmentation. Bulletin of volcanology, 74:11–13.
- Lavallée, Y., Meredith, P., Dingwell, D., Hess, K., WaHess, K., J., Cordonnier, B., Gerik, A., and Kruhl, J. (2008). Seismogenic lava and explosive eruption forecasting. Nature, 453:507–510.
- Lavallée, Y., Varley, N., Alatorre-Ibargiengoitia, A., Hess, K., Kueppers, U., Mueller, S., Richards, D., Scheu, B., Spieler, O., and Dingwell, D. (2011). Magma architecture of dome building eruptions at Volcán de Colima, Mexico. Bulletin of volcanology.
- Leet, R. C. (1988). Saturated and subcooled hydrothermal boiling in groundwater flow channels as a source of harmonic tremor. Journal of Geophysical Research, 93:4835–4849.
- Lénat, J. and Bachèlery, P. (1990). Structure and dynamics of the central zone of Piton de la Fournaise volcano, in Le Volcanisme de la Réunion. Monographie : Centre de Recherche en Volcanologie. Clermont-Ferrand, France.
- Lesage, P., Mora, M. M., Alvarado, G. E., Pacheco, J., and Métaxian, J.-P. (2006). Complex behavior and source model of the tremor at Arenal volcano, Costa Rica. Journal of Volcanology and Geothermal Research, 157:49–59.
- Lesage, P. and Surono (1995). Seismic precursors of the february 10, 1990 eruption of Kelut volcano, java. Journal of Volcanology and Geothermal Research, 65:135–146.
- Lister, J. (1990a). Buoyancy-driven fluid fracture: similarity solutions for the horizontal and vertical propagation of fluid-filled cracks. Journal of Fluid Mechanics, 217:213–239.
- Lister, J. (1990b). Buoyancy-driven fluid fracture: the effects of material toughness and of highly viscous fluids. Journal of Fluid Mechanics, 210:263–280.
- Lockner, D. (1993). Room temperature creep in saturated granite. Journal of Geophysical Research, 98:475–487.
- Lockner, D. and Byerlee, J. (1975). Acoustic emission and creep in rock at high confining pressure and differential stress. Bulletin of the Seismological Society of America, 67:247–258.
- Luhr, J. (2002). Petrology and geochemistry of the 1991 and 1998-1999 lava flows from Volcán de Colima,

- Mexico: implications for the end of the current eruptive cycle. Journal of Volcanology and Geothermal Research, 117:169–194.
- Luhr, J. F. and Carmichael, I. S. E. (1980). The colima volcanic complex, Mexico. Contributions to Mineralogy and Petrology, 71:343–372.
- Mader, H. (1998). The Physics of Explosive Volcanic Eruptions, Conduit flow and fragmentation. Geological Society, London.
- Main, I. (2000). A damage mechanics model for power-law creep and earthquake aftershock and foreshock sequences. Geophysical Journal International, 142:151–161.
- Main, I. G. (1999). Applicability of time-to-failure analysis to accelerated strain before earthquakes and volcanic eruptions. Geophysical Journal International, 139:F1–F6.
- Marchese, F., Lacava, T., Pergola, N., Hattori, K., Miraglia, E., and Tramutoli, V. (2012). Inferring phases of thermal unrest at Mt. Asama (Japan) from infrared satellite observations. Journal of Volcanology and Geothermal Research, 237-238:10–18.
- Marsan, D. and Daniel, G. (2007). Measuring the heterogeneity of the coseismic stress change following the 1999 Mw7.6 Chi-Chi earthquake. Journal of Geophysical Research, 112:B07305.
- Maryanto, S., Iguchi, M., and Tameguri, T. (2008). Constraints on the source mechanism of harmonic tremors based on seismological, ground deformation, and visual observations at Sakurajima Volcano, Japan. Journal of Volcanology and Geothermal Research, 170:193–217.
- Marzocchi, W. and Bebbington, M. (2012). Probabilistic eruption forecasting at short and long time scales. Bulletin of volcanology, 74:1777–1805.
- Marzocchi, W., Sandri, L., and Selva, J. (2008). BET-EF: a probabilistic tool for long and short term eruption forecasting. Bulletin of Volcanology, 70:623–632.
- Matoza, R. and Chouet, B. (2010). Subevents of long-period seismicity: Implications for hydrothermal dynamics during the 2004-2008 eruption of Mount St. Helens. Journal of Geophysical Research, 115:B12206.
- McGuire, W. J. and Kilburn, C. R. J. (1997). Forecasting volcanic events: some contemporary issues. International Journal of Earth Sciences, 86:439–445.
- McNutt, S. (1996). Seismic monitoring and eruption forecasting of volcanoes: a review of the state-of-the-art and case of studies. Monitoring and mitigation of volcano hazard.
- Melnik, O., Barmin, A., and Sparks, R. S. J. (2005). Dynamic magma flow inside volcanic conduits with bubble overpressure buildup and gas loss through permeable magma. Journal of Volcanology and Geothermal Research, 06269:16–32.
- Melnik, O. and Sparks, S. (1999). Nonlinear dynamics of lava dome extrusion. Nature, 402:37–41.
- Mogi, K. (1958). Relations between the eruptions of various volcanoes and the deformations of the ground surface around them. Bulletin of the Earthquake Research Institute of Tokyo, 36:99–134.

BIBLIOGRAPHY

- Molina, I., Kumagai, H., and Yepes, H. (2004). Resonances of a volcanic conduit trigger by repetitive injections of an ash-laden gas. Geophysical Research Letters, 31.
- Morrissey, M. M. and Chouet, B. A. (1997). A numerical investigation of choked flow dynamics and its application to the triggering mechanism of long-period events at Redoubt volcano, Alaska. Journal of Geophysical Research, 102:7965–7983.
- Mulargia, F., Gasperini, P., and Marzocchi, W. (1991). Pattern recognition applied to volcanic activity: Identification of precursory papatterns Etna recent flank eruptions and periods of unrest. Journal of Volcanology and Geothermal Research, 45:187–196.
- Mulargia, F., Marzocchi, W., and Gasperini, P. (1992). Statistical identification of physical patterns to Etna recent flank eruptions and periods of unrest. Journal of Volcanology and Geothermal Research, 53:289–296.
- Murphy, S., Wright, R., Oppenheimer, and Filho, C. S. (2013). MODIS and ASTER synergy for characterizing thermal volcanic activity. Remote Sensing of the Environment, 131:195–205.
- Murray, J. and Ramirez Ruiz, J. (2002). Long-term predictions of the time of eruptions using remote distance measurement at Volcán de Colima, Mexico. Journal of Volcanology and Geothermal Research, 117:79–89.
- Navarro-Ochoa, C., J.C., G.-R., and Cortes-Cortes, A. (2002). Movement and emplacement of lava flows at Volcán de Colima, Mexico: November 1998-February 1999. Journal of Volcanology and Geothermal Research, 117:155–167.
- Nercessian, A., Him, A., Lépine, J.-C., , and Sapin, M. (1996). Internal structure of Piton de la Fournaise volcano from seismic wave propagation and earthquake distribution. Journal of Volcanology and Geothermal Research, 70(3-4):123–143.
- Neuberg, J., Luckett, R., Baptie, B., and Olsen, K. (2000). Models of tremor and low-frequency earthquake swarms on Montserrat. Journal of Volcanology and Geothermal Research, 101:83–104.
- Neuberg, J., Tuffen, H., Collier, L., Green, D., Powell, T., and Dingwell, D. (2006). The trigger mechanism of low-frequency earthquakes on Montserrat. Journal of Volcanology and Geothermal Research, 153:37–50.
- Newhall, C. and Hobblitt, R. (2002). Constructing event trees for volcanic crises. Bulletin of Volcanology, 64:2–20.
- Newhall, C. and Self, S. (1982). The volcanic explosivity index (VEI): an estimate of explosive magnitude for historical volcanism. Journal of Geophysical Research, 87:1231–1238.
- Nishizawa, O. and Noro, H. (1990). Self-exciting process of acoustic emission occurrence in steady creep of granite under uniaxial stress. Journal of Geophysical Research, 17:1521–1524.
- Ogata, Y. (1983). Estimation of the parameters in the modified omori formula for aftershock frequencies by the maximum likelihood procedure. Journal of Physics of the Earth, 31:115–124.
- Ohnaka, M. (1983). Acoustic emission during creep of brittle rock. International Journal of Rock Mechanics and Mining Sciences, 20:121–134.

- Orhnberger, M. (2001). Continuous automatic classification of seismic signals of volcanic origin at Mt Merapi, Java, Indonesia. PhD thesis, Mathematisch-Naturwissenschaftlichen Facultat der Universitat Potsdam.
- Ortiz, R., Moreno, H., Garcia, A., Garcia, A., G., Astiz, M., Pena, P., Sanchez, N., and Tarraga, M. (2003). Villarica volcano (Chile): characteristic of the volcanic tremor and forecasting of small explosions by means of a material Failure Forecast Method. Journal of Volcanology and Geothermal Research, 128:247–259.
- Papale, P. (1999). Strain-induced magma fragmentation in explosive eruptions. Nature, 397:425–428.
- Paterson, M. (1958). Experimental deformation and faulting in wombeyan marble. Bulletin of the Seismological Society of America, 69:465–475.
- Peltier, A. (2007). Suivi, modélisation et évolution des processus d'injections magmatiques au Piton de La Fournaise (Réunion). PhD thesis, Institut de Physique du Globe de Paris, St Denis, France.
- Peltier, A., Bachèlery, P., and Staudacher, T. (2011). Early detection of large eruptions at Piton de la Fournaise volcano (La Réunion island): contribution of a distant tiltmeter station. Journal of Volcanology and Geothermal Research, 199:96–104.
- Peltier, A., Bachèlery, P., and Staudacher, T. (2009). Magma transport and storage at Piton de la Fournaise (La Réunion) between 1972 and 2007: a review of geophysical and geochemical data. Journal of Volcanology and Geothermal Research, 184:93–108.
- Peltier, A., Ferrazzini, V., Staudacher, T., and Bachèlery, P. (2005). Imaging the dynamics of dyke propagation prior to the 2000-2003 flank eruptions at Piton de La Fournaise, Réunion Island. Geophysical Research Letters, 32:L22302.
- Pinel, V., Poland, M., and A.Hooper (2014). Volcanology: Lessons learned from Synthetic Aperture Radar imagery. Journal of Volcanology and Geothermal Research, 289:81–113.
- P.W. Lipman, D. M. E., editor (1981). The 1980 Eruptions of Mount St. Helens, Washington. USGS, Washington, D.C.
- Quezada-Reyes, A., Lesage, P., C., V.-G., and Perrier, L. (2013). An analysis of the seismic activity of Popocatepetl volcano, Mexico, associated with the eruptive period of December 2002 to February 2003: looking for precursors. Geological Society of America, 498:89–106.
- Rabiner, L. (1989). A tutorial on Hidden Markov models and selected applications in speech recognition. Proceedings of the IEEE, 77:257–285.
- Ratdomopurbo, A. and Poupinet, G. (2000). An overview of the seismicity of Merapi volcano, (Java, Indonesia), 1983-1995. Journal of Volcanology and Geothermal Research, 100:193–214.
- Reches, Z. and Lockner, D. (1994). Nucleation and growth of faults in brittle rocks. Journal of Geophysical Research, 99, No. B9:18159–18173.
- Roult, G., Peltier, A., Taisne, B., Staudacher, T., Muro, V. F. F. D., and the OVPF Team (2012). A new comprehensive classification of the Piton de la Fournaise activity spanning the 1985-2010

BIBLIOGRAPHY

- period. search and analysis of short-term precursors from broad-band seismological station. Journal of Volcanology and Geothermal Research, 241-242:78–104.
- Rubin, A. (1995). Propagation of Magma-Filled Cracks. Annual Review of Earth and Planetary Sciences, 23(1):287–336.
- Ruina, A. (1983). Slip instability and state variable friction laws. Journal of Geophysical Research, 88:10359–10370.
- Rust, A. C., Balmforth, N. J., and Mandre, S. (2008). The feasibility of generating low-frequency volcano seismicity by flow through a deformable channel. Geological Society, London, Special, 307:45–56.
- Rydelek, P. A. and Sacks, I. S. (1989). Testing the completeness of earthquake catalogues and the hypothesis of self-similarity. Nature, 337:251–253.
- Rymer, H. and Brown, G. (1984). Periodic gravity changes at Poás volcano, Costa Rica. Nature, 311:243–245.
- Sainz-Maza, S., Arnosó, J., Montesinos, F. G., and J.Marti (2014). Volcanic signatures in time gravity variations during the volcanic unrest on el hierro (canary islands). Journal of Geophysical Research, 119:5033–5051.
- Scarpetta, S., Giudicepietro, F., Ezin, E., Petrosino, S., Del Pezzo, E., Martini, M., and Marinaro, M. (2005). Automatic classification of seismic signals at Mt. Vesuvius volcano, Italy, using neural networks. Bulletin of the Seismological Society of America, 95:185–196.
- Schmid, A., Grasso, J. R., Clarke, D., Ferrazzini, V., Bachelery, P., and Staudacher, T. (2012). Eruption forerunners from multiparameter monitoring and application for eruptions time predictability (Piton de la Fournaise). Journal of Volcanology and Geothermal Research, 117.
- Segall, P. (2010). Earthquake and Volcano deformation. Princeton University Press,.
- Segall, P. (2013). Volcano deformation and eruption forecasting. Geological Society, London, Special publications, 380.
- Shannon, C. (1948). A mathematical theory of communication. The Bell System Technical Journal, 27:379–423.
- Sigurdsson, H., Houghton, B. F., McNutt, S. R., Rymer, H., and Stix, J., editors (2000). Encyclopedia of Volcanoes, 1st Edition. ACADEMIC PRESS.
- Simkin, T. and Siebert, L. (1994). Volcanoes of the world. Geoscience Press in association with the Smithsonian Institution Global Volcanism Program, 2nd edition.
- Smith, R. and Kilburn, C. (2010). Forecasting eruptions after long repose intervals from accelerating rates of rock fracture: The June 1991 eruption of Mount Pinatubo, Philippines. Journal of Volcanology and Geothermal Research, 191:129–136.
- Smith, R., Kilburn, C., and Sammonds, P. (2007). Rock fracture as a precursor to lava dome eruptions at Mount St Helens from June 1980 to October 1986. Bulletin of Volcanology, 69:681–693.

- Sobradelo, R., Bartolini, S., and Martí, J. (2014). HASSET: a probability event tree tool to evaluate future volcanic scenarios using Bayesian inference. Bulletin of Volcanology, 76:770.
- Sparks, R. (1978). The dynamics of bubble formation and growth in magmas: a review and analysis. Journal of Volcanology and Geothermal Research, 3:1–37.
- Sparks, S. (2003). Dynamics of magma degassing. Geological Society, London, Special, 213:5–22.
- Stephens, C., Chouet, B., Page, R., Lahr, J., and Power, J. (1994). Seismological aspects of the 1989–1990 eruptions at Redoubt volcano, Alaska: the SSAM perspective. Journal of Volcanology and Geothermal Research, 62:153–182.
- Surono, P., J., Pallister, J., Boichu, M., Buongiorno, M., Budi-Santoso, A., Costa, F., Andreastuti, S., Prata, F., D., S., Clarisse, L., Humaida, H., Sumarti, S., Bignami, C., Griswold, J., Carn, S., and Oppenheimer, C. (2012). The 2010 explosive eruption of Java’s Merapi volcano - a ‘hundred-year’ event. Journal of Volcanology and Geothermal Research, 241–242:121–135.
- Symonds, R. B., Gerlach, T. M., and Reed, M. H. (2001). Magmatic gas scrubbing: Implications for volcano monitoring. Journal of Volcanology and Geothermal Research, 108:303–341.
- Taddeucci, J., Spieler, O., Kennedy, B., Pompilio, M., Dingwell, D. B., and Scarlato, P. (2004). Experimental and analytical modeling of basaltic ash explosions at Mount Etna, Italy, 2001. Journal of Geophysical Research, 109:B08203.
- Taisne, B., Brenguier, F., Shapiro, N., and Ferrazzini, V. (2011). Imaging the dynamics of magma propagation using radiated seismic intensity. Geophysical Research Letters, 38:L04304.
- Tarantola, A. and Valette, B. (1982a). Generalized nonlinear inverse problems solved using the least squares criterion. Review of Geophysics, 20:219–332.
- Tarantola, A. and Valette, B. (1982b). Inverse problems = quest for information. Journal of Geophysics, 50:159–170.
- Tarraga, M., Carniel, R., Ortiz, R., Marrero, J., and Garcia, A. (2006). On the predictability of volcano-tectonic events by low frequency seismic noise analysis at Teide-Pico Viejo volcanic complex, Canary Islands. Natural Hazards and Earth System Sciences, 6:365–376.
- Traversa, P., Lengliné, O., Macedo, O., Metaxian, J. P., Grasso, J. R., Inza, A., and Taipei, E. (2011). Short term forecasting of explosions at Ubinas volcano, Perú. Journal of Geophysical Research, 116.
- Tuffen, H. and Dingwell, D. (2005). Fault textures in volcanic conduit: evidence for seismic trigger mechanism during silicic eruptions. Bulletin of Volcanology, 67:370–387.
- Tuffen, H., Dingwell, D., and Pinkerton, H. (2003). Repeated fracture and healing of silicic magma generate flow banding and earthquakes. Geological Society of America, 31:1089–1092.
- Tuffen, H., Smith, R., and Sammonds, P. (2008). Evidence for seismogenic fracture of silicic magma. Nature, 453:511–514.
- Turcotte, D. L., Newman, W. I., and Shcherbakov, R. (2003). Micro and macroscopic models of rock fracture. Geophysical Journal International, 152:718–728.

BIBLIOGRAPHY

- Utsu, T., Ogata, Y., and Matsu'ura, R. S. (1995). The centenary of the omori formula for a decay law of aftershock. Journal of Physics of the Earth, 43:1â€”33.
- Varley, N., Arambula-Mendoza, R., Reyes, G., Sanderson, R., and Stevenson, J. (2010a). Generation of Vulcanian activity and Long-period seismicity at Volcán de Colima, Mexico. Journal of Volcanology and Geothermal Research, 198:45–56.
- Varley, N. R., Arambula-Mendoza, R., Reyes-Davila, G., Stevenson, J., and Harwood, R. (2010b). Long-period seismicity during magma movement at Volcán de Colima. Bulletin of Volcanology, 72:1093–1107.
- Viterbi, A. (1967). Error bounds for convolutional codes and an asymptotically optimum decoding algorithm. IEEE Transactions on Information Theory, 13:260–269.
- Voight, B. (1988). A method for prediction of volcanic eruptions. Nature, 332:125–130.
- Voight, B. (1989). A relation to describe rate-dependant material failure. Science, 243:200–203.
- Voight, B., Constantine, E., Sismowidjoyo, S., and Torley, R. (2000). Historical eruptions of Merapi volcano, Central Java, indonesia, 1768-1998. Journal of Volcanology and Geothermal Research, 100:69–138.
- Voight, B. and Cornelius, R. R. (1991). Prospects for eruption prediction in near real-time. Nature, 350:695–698.
- Watt, S., Mather, T., and Pyle, D. (2007). Vulcanian explosion cycles: patterns and predictability. The Geological Society of America, 9:839–842.
- Werner, C., Doukas, M., and Kelly, P. (2011). Gas emissions from failed and actual eruptions from Cook Inlet Volcanoes, Alaska, 1989â€”2006. Bulletin of Volcanology, 73:155–173.
- Werner, C., Evans, W. C., Kelly, P. J., McGimsey, R., Pfeffer, M., Doukas, M., and Neal, C. (2012). Deep magmatic degassing versus scrubbing: Elevated CO₂ emissions and c/s in the lead-up to the 2009 eruption of Redoubt Volcano, Alaska. Geochemistry, Geophysics, Geosystems, 13:1–18.
- Williams-Jones, G. and Rymer, H. (2002). Detecting volcanic eruption precursors: a new method using gravity and deformation measurements. Journal of Volcanology and Geothermal Research, 13:379–389.
- Wilson, L. and Head, J. (1981). Ascent and eruption of basaltic magma on the earth and moon. Journal of Geophysical Research, 86:2971–3001.
- Withers, M. e. a. (1998). A comparison of select trigger algorithms for automated global seismic phase and event detection. Bulletin of the Seismological Society of America, 88:95–106.
- Wu, F. J. and Thomsen, L. (1975). Microfracturing and deformation of westerly granite under creep condition. International Journal of Rock Mechanics and Mining Sciences., 12:167–173.
- Yanagidani, T., Ehara, S., Nishizawa, O., Kusunose, K., and Terada, M. (1985). Localization of dilatancy in ohshima granite under constant uniaxial stress. Journal of Geophysical Research, 94:6840–6858.

- Yokoyama, I. (1989). Microgravity and height changes caused by volcanic activity: Four Japanese examples. Bulletin of Volcanology, 51:333–345.
- Young, S. J., Evermann, G., Gales, M. J. F., Hain, T., Kershaw, D., Moore, G., Odell, J., Ollason, D., Povey, D., Valtchev, V., and Woodland, P. C. (2006). The HTK book. Cambridge University Engineering Department.
- Zobin, V., Luhr, J., Taran, Y., Breton, M., Cortes, A., Cruz-Reyna, S. D. L., Dominguez, T., Galindo, I., Gavilanes, J., Muniz, J., Navarro, C., Ramirez, J., Reyes, G., Ursua, M., Velasco, J., and E Alatorre, H. S. (2002). Overview of the 1997-2000 activity of Volcan de Colima, Mexico. Journal of Volcanology and Geothermal Research, 117:1–19.
- Zobin, V. M., Varley, N. R., González, M., Orozco, J., Reyes, G. A., Navarro, C., and Bretón, M. (2008). Monitoring the 2004 andesitic block-lava extrusion at Volcán de Colima, Mexico from seismic activity and SO₂ emission. Journal of Volcanology and Geothermal Research, 117:367–377.
- Zuniga, F. and Wyss, M. (1995). Inadvertent changes in magnitude reported in earthquake catalogs: their evaluation through b-value estimates. Bulletin of the Seismological Society of America, 85:1858–1866.

